Università degli Studi di Napoli Federico II
Facoltà di Ingegneria

Antonio Bilotta

BEHAVIOUR OF FRP-TO-CONCRETE INTERFACE: THEORETICAL MODELS AND EXPERIMENTAL RESULTS

Tesi di Dottorato
XXIII ciclo

Il Coordinatore
Prof. Ing. Federico M. MAZZOLANI

Il Tutor
Prof. Ing. Emidio Nigro

Dottorato di Ricerca in Ingegneria delle Costruzioni

Acknowledgements

My research activity has been carried out under the guidance of Prof Emidio Nigro, who proposed to me the topic to study. I am particularly indebted to him: in many occasions he stimulated my curiosity, encouraged my initiatives and gave me the right measure of things to do. Thanks to his support, the strong feeling of freedom in my work has always been tied to an agreeable sense of security.

I have carried out part of my research in the DIST laboratory: I strongly wish to acknowledge all the technical staff for their patience and help. In particular I wish to thank Pino Campanella and Emanuele Scaiella for their precious contribution in carrying out the tests.

My thanks also go to Dr Marco Di Ludovico and Dr Francesca Ceroni as they have always supported me with their brilliance, experience, competence.

I would like to give special thanks to Dr Enzo Martinelli for the enthusiasm, kindness and proficiency shown in our discussions.

I wish to thank Prof Ciro Faella of the University of Salerno and Prof Maria Rosaria Pecce of the University of Sannio for the interest they have shown for my research activity and their useful suggestions.

Moreover I am grateful to Prof. Gaetano Manfredi and Prof. Edoardo Cosenza for the scientific support received over the years, making me proud to be part of a team.

Finally I particularly wish to remember the friendly support I have received at the Department of Structural Engineering of the University of Naples and the long time I spent there with my friend and colleague Giuseppe Cefarelli.

I thank my family who has always supported me and my choices.

The experimental tests were carried out in the framework of the activities of the Laboratories University Network of seismic engineering (ReLUIS) supported by the Department of the Civil Protection (Reluis 2005 Grant – Task 8: Innovative materials for the vulnerability mitigation of existing structures) and within the Round Robin Tests organized by the European Network for Composite Reinforcement supported by the *fib* Task Group 9.3.

mai e sempre

jtm

volli, sempre volli, fortissimamente volli

a Papà

I n d e x

Preface

Fiber-reinforced polymers (FRP) are more and more commonly employed for structural strengthening existing structures of both reinforced concrete (RC) and masonry. Since FRP are externally bonded on a concrete or masonry substrate, the issue of adhesion on those materials generally controls the effectiveness of strengthening in members stressed either in bending or shear.

Understanding the behaviour of FRP-to-concrete joints tested under pull-out actions is of paramount importance for describing the key mechanical properties of the adhesive interface between FRP and concrete, which plays a key role in the possible debonding failure of externally strengthened beams.

With this aim the present dissertation deals with the theoretical models and the experimental results related to the behaviour of the FRP-to-concrete adhesive interface. It consists of eight chapters:

The **first chapter** introduces the topic of the use of fiber-reinforced polymer (FRP) for the design and the construction of Externally Bonded FRP Systems for Strengthening Existing Structures. Particular attention is paid to the issue of the adhesion of external FRP reinforcement applied to concrete elements. A brief state of the art referring to national and international literature is also reported. The aims and the outline of this doctoral thesis are clarified.

In the **second chapter** an analytical model will be firstly presented for determining both shear and normal stresses throughout the adhesive interface in the linear range. The main parameters that govern the phenomenon of adhesion will be analyzed. The nonlinear behaviour of the FRP-to-concrete interface will be also addressed by discussing the ultimate bearing capacity of FRP laminates bonded on concrete members.

The **third chapter** presents the experimental program that was conducted to compare the interface behavior, under monotonic and cyclic actions, of two main types of commercial external FRP reinforcement, namely sheets and plates. In particular, the set-up designed to perform the 58 bond tests is accurately described and the main results obtained, with particular reference to the strains recorded on each reinforcement during the test, are reported and discussed.

The **fourth chapter** presents two alternative methods of identification of interface laws defined respectively direct method (DirIM) and indirect method (IndIM). The comparison between the bilinear bond laws obtained by both methods showed the greater effectiveness of IndIM method than the DirIM one. Moreover, an extensive interpretation of the experimental readings made by the method IndIM allowed to obtain useful results to define a proposal for updating the instructions CNR-DT200/2004.

The **fifth chapter** describes the intermediate debonding phenomenon, due to the detachment of the reinforcement between the cracks in the concrete member. The main contributions from the national and international literature, related to both the theoretical interpretative models and the results of tests performed on full-scale member, are collected. A comparison between theoretical and experimental results highlights that it is necessary to continue with further investigations on the geometric and mechanical parameters governing the phenomenon, and, at the same time, to validate the design formulas currently in use on the basis of the latest experimental results.

In the **sixth chapter** a statistical procedure for the Calibration of resistance models from experimental data, in accordance with the guidelines provided in Eurocode 0 is presented. The procedure has been implemented on the basis of the results of the bond tests carried out and analyzed in the third and fourth chapters, and based on the results of tests on full-scale members found in literature and discussed in the fifth chapter. The application of the procedure allowed a proposal for updating the design formulae provided in the Instructions CNR-DT200 (2004) to be formulated.

In the **seventh chapter**, the results obtained by applying the IndIM procedure to obtain simplified bond laws and the statistical procedure calibrating the bond strength relationships were summarized and integrated, in order to prepare an updating proposal for instructions CNR-DT200 (2004).

In the **eighth chapter** the conclusions of the dissertation were summarized as well as the expected future developments downstream of the activity.

Chapter 1 - Introduction

The job of the engineer is to design a durable and economical construction, which, once erected, however begins to deteriorate under environmental and user influences. At times the deterioration is excessive due to human mistakes at the designing stage or execution errors during construction. After a certain time, the construction will not be able anymore to fulfil its function. To enlarge the lifetime of a construction, maintenance, repair and retrofitting, and sometimes more structural interventions and strengthening are required.

For these purposes, several different techniques, some deduced from practical experience, some based on scientific research, were developed. One of these techniques is the externally bonding of reinforcements, which is a versatile and reversible technique based on the principles of minimize resource consumption.

The basic principle of externally bonded reinforcement is very simple. Additional reinforcement, in most cases for carrying tensile forces, is added to the structure by bonding it onto the structures elements. Several material families can be used: not only classical steel plates, but also new high grade Fibre Reinforced Polymers (FRP). These materials consist of fibres embedded in a resin matrix. Different fibre types can be used, but most commonly carbon, glass or basalt are applied. The corresponding composites are indicated as CFRP, GFRP or BFRP.

This chapter introduces a brief state of the art on the use of FRP for the design and the construction of Externally Bonded FRP Systems for strengthening existing structures.

1.1 GENERAL REMARKS

In this section the causes leading to strengthening intervention on structures are catalogued, some research activities on composites materials are briefly mentioned and the main codes available for the strengthening techniques with FRP are recalled. Furthermore, the main strengthening systems and interventions are classified. Finally interesting applications of externally bonded FRP for seismic retrofit is cited.

1.1.1 The causes of strengthening interventions

Three main groups of causes may lead to the use of externally bonded reinforcement:

- users,
- constructors
- environmental conditions and disasters.

The increase of the bearing capacity or the change in utilization are typical examples of causes induced by the users (e.g. increase in traffic load and volume on bridges, changing in usage of buildings, etc). Also bad maintenance or protection by the user often lead to additional repairing works, which might be done by externally bonded reinforcement.

The second group of causes is linked with mistakes or faults by the constructors. As examples can be given lacks in: structural design and details; execution methods and workmanship; soil investigation and foundation; quality of the used materials.

The third group of causes contains the damage introduced by aggressive environmental conditions (e.g. severe corrosion) or disasters. (e.g. damage due to fire, explosions and earthquakes).

Externally bonded reinforcement can be used for strengthening, repairing and stiffening and all types of structures can be treated: evidently concrete structures, but also masonry and wooden structures. However, up to now, mainly concrete structures have been dealt with. A lot of scientific research has already been done in that area, combined with practical experience gathered from worldwide applications.

1.1.2 Research activities composite materials

The use of composite materials for structural strengthening of civil structures and infrastructures began with some pioneering application at the middle of the '80s (Meier, 1987) of the past century.

Plenty of experimental work and theoretical investigations have been carried out in the following years with the aim of demonstrating the feasibility of strengthening civil structures by means of composite materials (Swamy et al., 1987; Meier, 1995). However, composite materials were already widely used in other fields of structural engineering, such as aerospace (Hart-Smith, 1973), aeronautics and, later, and automotive. Thus, the initial research activities about the possible use of composites in civil structures were not mainly focused on the behavior of composites themselves. They were rather intended at addressing two main issues regarding, on the one hand, the different behavior of composites with respect to more traditional materials (basically, steel) commonly used as a reinforcement in civil structures (Arduini & Nanni, 1997; Naaman et al., 2001; Triantafillou et al., 2001) and, on the other hand, the aspects related to the adhesive connection of the FRP laminates to the concrete (or masonry) substrate (Täljsten, 1997; Neubauer & Rostasy, 1997). Indeed, since FRP laminates are externally bonded on a concrete or masonry substrate, the issue of adhesion on those materials generally controls the effectiveness of strengthening in members stressed either in bending or shear (Motavalli & Czaderski, 2007).

The main findings of the research activities carried out in the '90s have been contributed to guidelines (ACI 440-2R-02, 2002 updated in 2008; fib bulletin 14, 2001 in updating stage; CNR-DT200, 2004 in updating stage) for designing FRP-based strengthening intervention of RC and masonry members.

1.1.3 FRP strengthening systems and interventions

The FRP systems suitable for external strengthening of structures may be mainly classified as:

- Pre-cured systems, which are manufactured in various shapes, by pultrusion or lamination. They are directly bonded to the structural member to be strengthened.

- Wet lay-up systems which are manufactured with fibers lying in one or more directions, as FRP sheets or fabrics. They are impregnated with resin at the job site and simultaneously applied to the support.

This classification is significant for practical applications but also for some aspects that will be analyzed and discussed in this Thesis. Therefore, two FRP reinforcement systems will be briefly called *plates* and *sheets* respectively.

A stated above all kinds of elements can be strengthened: concrete beams, concrete slabs, masonry walls (Velazquez et. al., 2000), wooden beams (Triantafillou, 1998). Clearly, the designer must be aware of the specific properties and characteristics of the materials involved.

As concerns the concrete reinforced (RC) structures, externally bonded reinforcement can be mainly used for bending and shear strengthening of beams and columns. Moreover very good results can be obtained for the confinement of the columns.

From the seismic standpoint, the driving principles of the FRP intervention strategies should be to increase the strength and the ductility of the structure, keeping in mind that stiffness irregularities cannot be solved by applying FRP.

The FRP strengthening may be regarded as a selective intervention technique that could allow:

- increasing the flexural capacity of deficient members, with and without axial load, through the application of composites with the fibers placed parallel to the element axis;
- increasing the shear strength through the application of composites with the fibers placed transversely to the element axis;
- increasing the ductility (or the chord rotation capacity) of critical zones of beams and columns through FRP wrapping (confinement);
- improving the efficiency of lap splice zones, through FRP wrapping;
- preventing buckling of longitudinal rebars under compression through FRP wrapping;
- increasing the tensile strength of the panels of partially confined beam-column joints through the application of composites with the fibers placed along the principal tensile stresses.

In the following applications of externally bonded FRP for seismic retrofit are briefly cited.

1.1.4 Seismic retrofit

An important field of application of externally bonded CFRP is the seismic retrofit of concrete columns and piles. After the great Hanshin-Awaji Earthquake in January 1995 in the region of Kobe, Japan, the use of CFRP laminates for seismic upgrading of existing structures noticeably increased. Many buildings and structures were destroyed by the strong earthquake due to a lack of ductility and shear capacity in the horizontal direction. The magnitude of the earthquake and the extent of the damage was much heavier than foreseen in the Japanese standards at that moment, which made the engineers aware of the need of seismic retrofitting of existing similar structures. Attention was focused on the improvement of the shear capacity and the ductility of columns and piers (Katsumata et. al., 1998; Horii et. al., 1998). Also in other earthquake sensitive regions, e.g. California, USA, research is going on (Chaallal & Shahawy, 2000; Emmons et. al., 1998a, 1998b).

By wrapping CFRP sheets around columns and piers, the ductility and the shear capacity of the system can be increased significantly (Mutsuyoshi et. al., 1999; Saadatmanesh et. al., 1996; Saadatmanesh et. al., 1997a). Especially circular cross sections can easily be wrapped with the flexible CFRP sheets, but with the appropriate preparation, i.e. rounding of the corners, also rectangular cross sections can be treated. The great advantage of the system is the fact that the strengthening works can be done while the structure or the building remains in operation and that only minor changes to the geometry are required.

Similar strengthening interventions were recently performed in L'Aquila (Italy), after the fatal earthquake occurred in April 2009. In particular, such interventions (see www.reluis.it) were performed on RC structures in order to increase the shear resistance of the ends of beams and columns as well as the ductility of the beam-column node where the greatest requirements of ductility occur due to combined compression and flexure. Some schemes of the strengthening intervention are reported in Figure 1.1 and an example is showed in Figure 1.2.

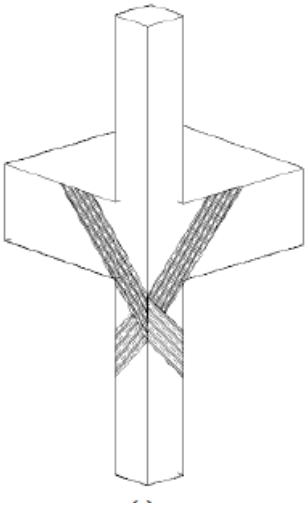

(a) Wrap diagonally with unidirectional sheets on corner node

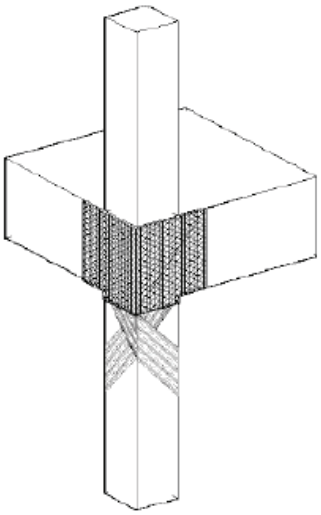

(b) Biaxial carbon fiber sheet centered on the face of the corner node

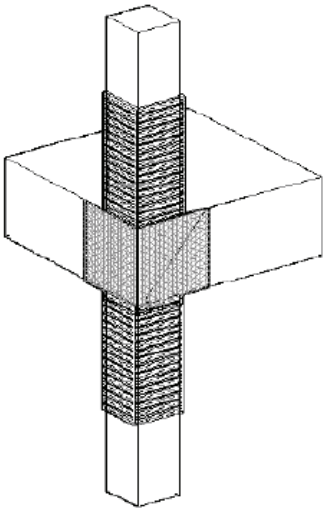

(c) Confinement of the column in a corner node

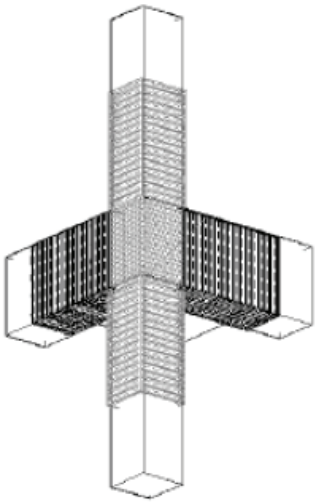

(d) Shear reinforcement in U shape at the end of the beams in the corner node

Figure 1.1 - FRP strengthening interventions for seismic retrofit (www.reluis.it)

Figure 1.2 - FRP strengthening intervention for a beam column node
(Picture by courtesy of M. Di Ludovico)

1.2 THE DEBONDING MECHANISMS

When strengthening reinforced concrete members with FRP composites, the role of bond between concrete and FRP is of great relevance due to the brittleness of the failure mechanism by debonding (loss of adhesion). According to the capacity design criterion, such a failure mechanism shall not precede flexural or shear failure of the strengthened member.

The loss of adhesion between FRP and concrete may concern both laminates or sheets applied to reinforced concrete beams as flexural and/or shear strengthening. As shown in Figure 1.3, debonding may take place within the adhesive, between concrete and adhesive, in the concrete itself, or within the FRP reinforcement (e.g. at the inteface between two adjacent layers bonded each other) with different fiber inclination angles. When proper installation is performed, because the adhesive strength is typically much higher than the concrete tensile strength, debonding always takes place within the concrete itself with the removal of a layer of material, whose thickness may range from few millimeters to the whole concrete cover.

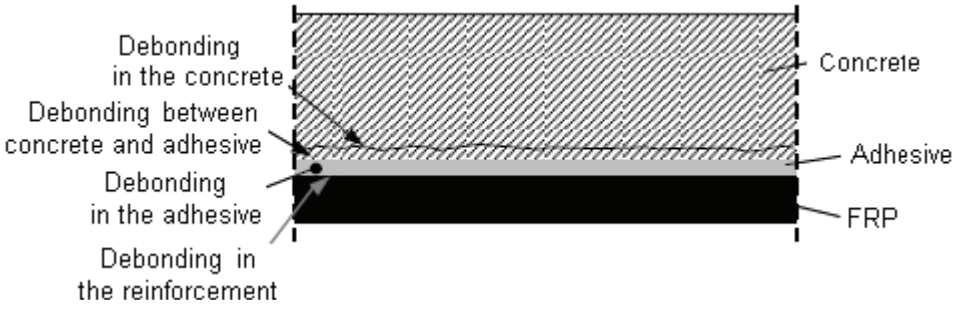

Figure 1.3 - Debonding between FRP and concrete (CNR-DT200/2004).

1.2.1 The debonding failure mode

Bonding between FRP laminates and concrete emerged as a cutting-edge issue from the first decade of research activities on composite materials for civil structures. In particular, several failure modes due to loss of adhesion between the externally bonded FRP element and the concrete substrate have

been observed experimentally and recognized as specific features of this kind of members (Meier, 1995; Bonacci, 1996).

As a matter of principle, the following seven failure modes have been defined in the scientific literature (Teng et al., 2002):

a) flexural failure by FRP rupture;
b) flexural failure by crushing of compressive concrete;
c) shear failure;
d) concrete cover separation;
e) plate end interfacial debonding;
f) intermediate flexural crack induced interfacial debonding;
g) intermediate flexural-shear crack induced interfacial debonding.

The last three failure modes are actually related to debonding failure of the FRP laminate from the concrete substrate. Local failure possibly induced by irregularities in the substrate surface can be also observed. Figure 1.4 represents those failure modes pointing their typical position throughout the FRP-to-composite adhesive interface.

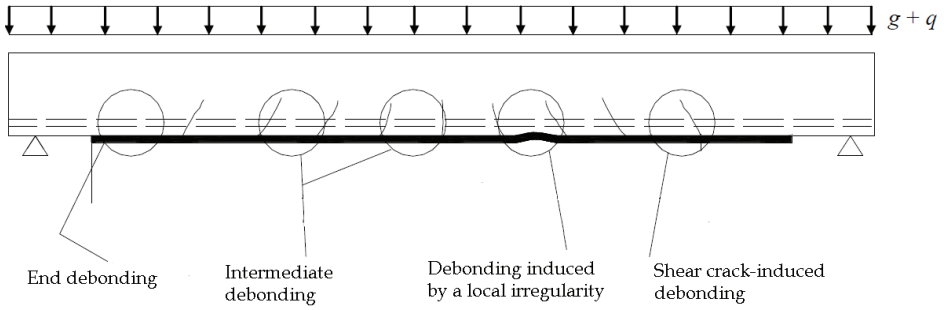

Figure 1.4 - Possible debonding failure modes in RC beams externally strengthened by FRP

1.3 RESEARCH ACTIVITIES ON BOND

In this section some analytical studies on bond laws and theoretical bond strength models are recalled. Some experimental works are also cited.

These three issues represent the main topics examined and discussed in this Thesis. Thus, additional details are reported within each chapter of the Thesis, specific to the corresponding topic, in order to better contextualize the contents of the research activities studied and analyzed.

1.3.1 Analytical studies on bond laws

Analytical studies have been carried out for determining the actual distribution of stresses throughout the adhesive interface. In particular, well-established elastic models, already used within the framework of structural mechanics, have been proposed as simplified practical methods for determining both shear and normal (peeling) stresses at the FRP-to-concrete interface (Roberts, 1989; Malek et al., 1998; Rabinovich & Frostig, 2000). However, those simplified methods were generally based on the assumption of an elastic behaviour of the above mentioned interface. Although this assumption can be considered under service loads, it cannot be generally accepted for the load values close to the onset of debonding. Micro-cracking phenomena develop as the levels of the interface stresses cannot be resisted by concrete, resulting in a highly nonlinear behaviour for the FRP-to-concrete interface which can be modelled by means of several possible relationships between interface stresses and displacements (Lu et al, 2005). Consequently, more advanced numerical models have been also proposed for simulating the actual distribution of stresses looking after the various fracture phenomena developing in concrete beneath the adhesive interface (Rabinovich & Frostig, 2000; Faella et al., 2008a).

1.3.2 Theoretical bond strength models

More recently, several models have been proposed in the scientific literature for predicting the strength of beams against both plate end debonding and intermediate-debonding (Smith & Teng, 2001; Teng et al.,

2003). They generally derive by mechanical observations carried out on the behaviour of FRP laminates glued on concrete blocks (Täljsten, 1996) and tested in pullout with the aim of measuring some relevant quantities like the ultimate strength at debonding and the axial strain distribution throughout the FRP bonded length (Chajes et al., 1996).

1.3.3 Experimental results analysis and understanding

Understanding the behaviour of FRP-to-concrete joints tested under pull-out actions is of paramount importance for describing the key mechanical properties of the adhesive interface between FRP and concrete, which plays a key role in the possible debonding failure of externally strengthened beams. Thus, advanced testing and monitoring techniques have been also used for a deeper investigation of the behaviour of those joints (Czaderski et al., 2010). The experimental results obtained by the mentioned pull-out tests can be considered for identifying the non-linear relationships connecting interface stresses and displacements (Faella et al., 2009a). In particular, a bilinear elastic-softening relationship between the interface shear stress and the corresponding displacements is often used for the FRP-to-concrete interface. The elastic branch of that stress-strain relationship results from the elastic behaviour of both the adhesive layer and the concrete substrate, mainly stressed in shear. The slope of such an elastic branch (namely, the slip modulus according to Lee et al, 1999) is generally much smaller than the value corresponding to the ratio between the shear modulus of the resin and its thickness, as it would be determined by assuming a fully stiff behaviour of the concrete block (Faella et al., 2002c).

A closed-form analytical solution has been derived in Faella et al. (2002c) for the distribution of both shear stresses and relative slips in FRP-to-concrete joints with a bilinear adhesive interface. Further advances have been proposed by Lu et al. (2005), while the influence of different assumptions on the shape of the stress-slip relationship (i.e. bilinear, linearly softening, rigid-plastic, and so on) is discussed in both Chen & Teng (2001b) and Wu et al. (2002). However, the fracture energy G_F (Täljsten, 1996) is the key parameter characterizing any various shear-stress-interface-slip relationship. The ultimate pull-out strength of the FRP-to-concrete joints is controlled by that parameter as well as the axial stiffness of the plate and the bonding length. A

limit value of the bonding length beyond which no further increases of the ultimate pull-out force can be observed; it is generally referred as “transfer length” (Bizindavyi & Neale, 1999). Some concepts of Fracture Mechanics are more and more employed in modelling the overall behaviour of both FRP laminates connected to concrete blocks (Yuan et al., 2007) and RC beams externally strengthened by FRP (Rabinovitch & Frostig, 2001; Achintha & Burgoygne, 2008; Faella et al. 2007a,b,c,d).

Chapter 2 - Theoretical models

An analytical formulation for modelling the behaviour of the FRP-to-concrete adhesive interfaces is presented and discussed in the present section. The general analytical model will be firstly presented for determining both shear and normal stresses throughout the adhesive interface in the linear range. The main parameters that govern the phenomenon of adhesion will be analyzed. The nonlinear behaviour of the FRP-to-concrete interface will be also addressed by discussing the ultimate bearing capacity of FRP laminates bonded on concrete members. The behaviour of FRP-to-concrete joints in the linear range is examined in the first subsection. Then, the aspects more directly related at the ultimate behaviour are addressed in the second one.

2.1 FORMULATION IN THE LINEAR RANGE

2.1.1 A general analytical model

A simplified model (Martinelli et al., 2011) is formulated in the present section with the aim of simulating the behaviour of FRP plates bonded on concrete and tested in pull-out, simulating how both the in-plane (namely, "slip") and out-of-plane displacement components develop throughout the FRP length. It is based on the following assumptions:

- the FRP laminate is simulated as a Bernoulli beam;

- the adhesive layer is modelled as a bi-dimensional elastic domain in plane deformations.

The generalized forces N, V, M applied on the transverse section of the laminate at the abscissa z and the interface stresses (shear τ and normal σ, respectively) are represented in Figure 2.1. The following equilibrium equations can be stated between those force and stress components:

$$\frac{dN}{dz} + \tau_f b_f = 0 \ , \qquad (2.1)$$

$$\frac{dV}{dz} = -b_f \sigma_y \ , \qquad (2.2)$$

$$\frac{dM}{dz} + \tau_f \frac{b_f t_f}{2} - V = 0 \ . \qquad (2.3)$$

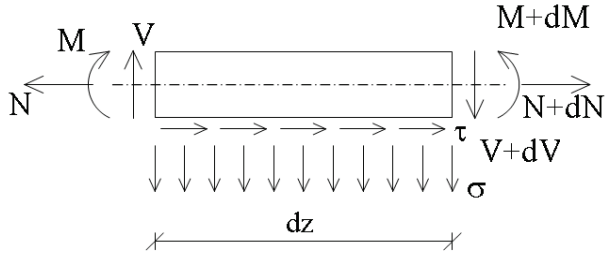

Figure 2.1. - Forces on the segmental FRP laminate element

The parameters v, w and φ completely describe the displacement field of the laminate and the following compatibility equations relate them to the axial strain ε and the curvature χ (Figure - 2.2):

$$\varepsilon = \frac{dw}{dz} \ , \qquad (2.4)$$

$$\chi = \frac{d\varphi}{dz} \ , \qquad (2.5)$$

$$\varphi = -\frac{dv}{dz} \ . \qquad (2.6)$$

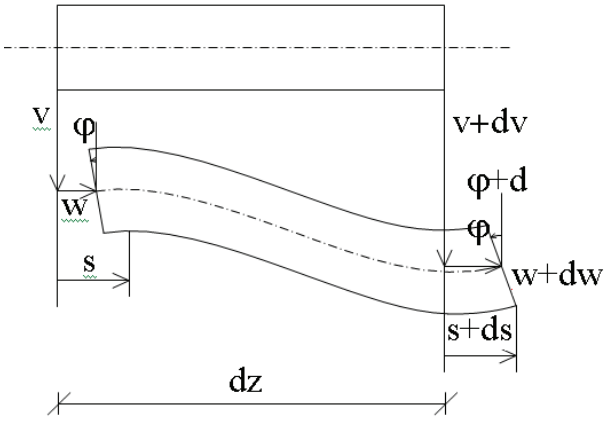

Figure - 2.2. Displacements components of the segmental element

The interface slip s, namely the axial displacement at the bottom chord of the laminate transverse section, can be also related to the displacement components represented in Figure - 2.2:

$$s = w + \frac{t_f}{2} \cdot \varphi \ . \tag{2.7}$$

Finally, the usual (generalized) stress-strain relationships can be introduced for the laminate modelled as a Bernoulli beam:

$$N = EA_f \varepsilon = E_f b_f t_f \varepsilon \ , \tag{2.8}$$

$$M = EI_f \chi = E_f \frac{b_f t_f^{\,3}}{12} \chi \ , \tag{2.9}$$

where EA_f and EI_f are respectively the axial and flexural stiffnesses which can be assumed for the laminate transverse section. Based on the second assumptions reported at the beginning of this section, The following equilibrium equations can be written for the infinitesimal 2D element of resin within the adhesive layer (Figure 2.3):

$$\begin{cases} \dfrac{\partial \sigma_{yy}}{\partial y_a} + \dfrac{\partial \tau_{yz}}{\partial z_a} = 0 \\ \dfrac{\partial \tau_{yz}}{\partial y_a} + \dfrac{\partial \sigma_{zz}}{\partial z_a} = 0 \end{cases}, \tag{2.10}$$

where y_a and z_a are the Cartesian coordinates of the infinitesimal areal element of resin.

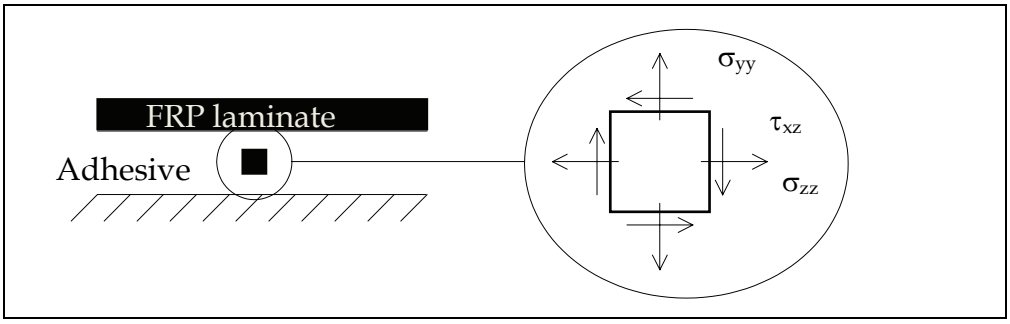

Figure 2.3. - General plane stress-state for an infinitesimal element of the adhesive layer

The corresponding strain measures can be expressed as functions of the displacement field $v_a(y_a,z_a)$ e $w_a(y_a,z_a)$ within the adhesive layer:

$$\begin{cases} \varepsilon_{yy} = \dfrac{\partial v_a}{\partial y_a} \\ \varepsilon_{zz} = \dfrac{\partial w_a}{\partial z_a} \\ \gamma_{yz} = \dfrac{\partial v_a}{\partial z_a} + \dfrac{\partial w_a}{\partial y_a} \end{cases} \tag{2.11}$$

where y_a and z_a are the Cartesian coordinates of the infinitesimal areal element of resin. Finally, the following elastic relationships can be stated between stresses and strains:

$$\begin{cases} \varepsilon_{yy} = \dfrac{1}{E_a} \cdot \left[\sigma_{yy} - \nu_a \cdot \sigma_{zz} \right] \\ \varepsilon_{zz} = \dfrac{1}{E_a} \cdot \left[\sigma_{zz} - \nu_a \cdot \sigma_{yy} \right] \\ \gamma_{yz} = \dfrac{\tau_{xy}}{G_a} = 2 \cdot \left(1 + \nu_a\right) \cdot \dfrac{\tau_{xy}}{E_a} \end{cases} \tag{2.12}$$

where E_a and G_a are the elastic properties of the adhesive layer. In this formulation, it connects the FRP reinforcement to a stiff substrate representing the concrete element. The upper bound of this layer is connected to that reinforcement and some compatibility equations should be written for introducing this physical constraint into the mathematical model. Thus, the three equations (2.10)-(2.12) can be worked out for deriving a relationship between the displacement components $v_a(0,z_a)$ and $w_a(0,z_a)$ and the corresponding stress components $\sigma_{yy}(0,z_a)$ and $\tau_{xy}(0,z_a)$. A key assumption can be introduced for simplifying the analytical expressions of the interface stresses, considering a constant value of the shear stress throughout the adhesive thickness (Rabinovich & Frostig, 2000):

$$\tau_{yz} = \tau_a(z_a) = \tau_a(z)\,, \tag{2.13}$$

Consequently, the second one of the two equations in (2.10) leads to the following simplification in terms of the normal stress in longitudinal direction:

$$\frac{\partial \sigma_{zz}}{\partial z_a} = 0 \Rightarrow \sigma_{zz} = f_1\left(y_a\right) \Rightarrow \sigma_{zz} = 0\ . \tag{2.14}$$

The last implication derives by the assumption of zero axial stress on the initial section of the layer adhesive.

Further simplifications can be introduced looking after the first equations in (2.10) and introducing therein the stress-strain relationship and the compatibility equation within the adhesive layer:

$$\sigma_{yy}\left(y_a, z_a\right) = -\int \frac{d\tau_a}{dz} dy + g_1\left(z_a\right) = -\frac{d\tau_a}{dz} y_a + g_1\left(z_a\right), \tag{2.15}$$

and

$$\varepsilon_{yy}\left(y_a, z_a\right) = \frac{\sigma_{yy}\left(y_a, z_a\right)}{E_a} = -\frac{1}{E_a} \cdot \frac{d\tau_a}{dz} y_a + \frac{g_1\left(z_a\right)}{E_a}. \tag{2.16}$$

The transverse component of the displacement field can be derived by further integration:

$$\begin{aligned} v_a\left(y_a, z_a\right) &= v\left(z_a\right) + \int \varepsilon_{yy} dy = v\left(z_a\right) + \int \left(-\frac{1}{E_a} \cdot \frac{d\tau_a}{dz} y_a + \frac{g_1\left(z_a\right)}{E_a} \right) dy = \\ &= v\left(z_a\right) - \frac{1}{E_a} \cdot \frac{d\tau_a}{dz} \frac{{y_a}^2}{2} + \frac{g_1\left(z_a\right)}{E_a} y_a \end{aligned} \tag{2.17}$$

and the value of the unknown function g_1 can be finally derived by imposing zero value to the displacement at the bottom interface ($y_a=t_a$):

$$v\left(z_a\right) - \frac{1}{E_a} \cdot \frac{d\tau_a}{dz} \frac{{t_a}^2}{2} + \frac{g_1\left(z_a\right)}{E_a} t_a = 0 \ , \tag{2.18}$$

$$g_1\left(z_a\right) = -\frac{E_a}{t_a} \cdot v\left(z_a\right) + \frac{d\tau_a}{dz} \frac{t_a}{2} \ . \tag{2.19}$$

Consequently, the following explicit expressions can be written for σ_{yy}, ε_{yy} and v_a described in (2.15), (2.16) and (2.17), by introducing the expression of g_1 given by equation (2.19):

$$\varepsilon_{yy}\left(y_a, z_a\right) = \frac{d\tau_a}{dz} \cdot \left(\frac{t_a - 2y_a}{2 \cdot E_a} \right) - \frac{v\left(z_a\right)}{t_a}, \tag{2.20}$$

$$\sigma_{yy}\left(y_a,z_a\right)=E_a\cdot\varepsilon_{yy}\left(y_a,z_a\right)=\frac{d\tau_a}{dz}\cdot\left(\frac{t_a-2y_a}{2}\right)-\frac{E_a}{t_a}v\left(z_a\right), \tag{2.21}$$

$$v_a\left(y_a,z_a\right)=v\left(z_a\right)\cdot\left(1-\frac{y_a}{t_a}\right)+\frac{d\tau_a}{dz}\cdot\left(\frac{t_a-y_a}{2E_a}\right)y_a. \tag{2.22}$$

Shear strain and stress can be related according to the following relationship:

$$\gamma_{yz}\left(z_a\right)=\frac{\tau_a\left(z_a\right)}{G_a} \tag{2.23}$$

and, considering the compatibility equation involving shear strains, further transformations can be carried out by introducing the compatibility equation in (2.11):

$$\gamma_{yz}\left(z_a\right)=\frac{\partial v_a}{\partial z_a}+\frac{\partial w_a}{\partial y_a} \tag{2.24}$$

The first derivative of the longitudinal displacement w_a of the inside the adhesive layer can be written as follows:

$$\frac{\partial w_a}{\partial y_a}=\gamma_{yz}\left(z_a\right)-\frac{\partial v_a}{\partial z_a}=\frac{\tau_a\left(z_a\right)}{G_a}-\frac{dv}{dz}\cdot\left(1-\frac{y_a}{t_a}\right)-\frac{d^2\tau_a}{dz^2}\cdot\left(\frac{t_a-y_a}{2E_a}\right)y_a \tag{2.25}$$

and the corresponding function w_a can be derived by integrating eq. (2.25) and introducing a zero-displacement condition for $y_a=t_a$ (namely, at the bottom of the adhesive layer):

$$\begin{aligned}w_a\left(y_a,z_a\right)=&-\frac{\tau_a\left(z_a\right)}{G_a}\left(t_a-y_a\right)+\frac{dv}{dz}\cdot\left(\frac{t_a}{2}-y_a+\frac{{y_a}^2}{2t_a}\right)+\\&+\frac{d^2\tau_a}{dz^2}\cdot\left(\frac{{t_a}^3}{12E_a}-\frac{t_a{y_a}^2}{4E_a}+\frac{{y_a}^3}{6E_a}\right)\end{aligned} \tag{2.26}$$

The above relationship can be utilized for deriving the expression of the axial displacements beneath the laminate (y_a=0):

$$w_a(0,z_a)=s(z)=-\frac{t_a}{G_a}\cdot\tau_a+\frac{{t_a}^3}{12E_a}\cdot\frac{d^2\tau_a}{dz^2}+\frac{t_a}{2}\cdot\frac{dv}{dz} \tag{2.27}$$

as well as equation (2.22) can be utilized for recognizing that the corresponding transverse component $v_a(0,z_a=z)$ is equal to v(z).

$$\sigma_{yy}\left(y_a,z_a\right)=E_a\cdot\varepsilon_{yy}\left(y_a,z_a\right)=E_a\cdot\left[\frac{d\tau_a}{dz}\cdot\left(\frac{t_a-2y_a}{2\cdot E_a}\right)-\frac{v\left(z_a\right)}{t_a}\right] \tag{2.28}$$

$$\sigma_y\left(z\right)=\sigma_{yy}\left(0,z_a\right)=-v\left(z_a\right)\cdot\frac{E_a}{t_a}+\frac{t_a}{2}\cdot\frac{d\tau_a}{dz} \tag{2.29}$$

The rotation field φ(z) of the laminate element can be then easily defined through equation (2.6) and the generalized strain fields can be determined by means of equation (2.4) and (2.5).

The above equations can be finally combined for deriving a unique differential equation in terms of interface shear stresses. A first equation can be obtained by differentiating eq. (2.7) and introducing (2.4), (2.6) and (2.8). After a further differentiation and introducing the definition of interface slip provided by eq. (2.27), the following differential relationship between the shear stress and the transverse displacements can be obtained:

$$\frac{G_a}{E_f t_f t_a}\cdot\tau_a-\frac{d^2\tau_a}{dz^2}+\frac{G_a}{2}\cdot\frac{d^3v}{dz^3}+\frac{G_a}{12E_a}\cdot{t_a}^2\cdot\frac{d^4\tau_a}{dz^4}=0 \tag{2.30}$$

Another relationship is obtained by differentiating equation (2.3) and introducing equation (2.2), (2.4), (2.5) and (2.9) for expressing both the bending moment and the shear force in terms of transverse displacements and interface (shear and normal) stresses. The final expression of an equation in terms of t_f and v (and their derivatives) can be obtained introducing equation (2.29):

$$\frac{b_f\left(t_f+t_a\right)}{2}\cdot\frac{d\tau_a}{dz}-\frac{E_f b_f {t_f}^3}{12}\cdot\frac{d^4v}{dz^4}-\frac{E_a b_f}{t_a}\cdot v=0 \tag{2.31}$$

The two equations (2.30) and (2.31) can be easily combined for deriving the following eighth-order differential equation in terms of interface shear stresses:

$$\begin{aligned}&\frac{G_a}{E_f t_f t_a}\cdot\tau_a-\frac{d^2\tau_a}{dz^2}+\left(\frac{{t_a}^2}{3}+\frac{t_a t_f}{6}+\frac{{t_f}^2}{12}\right)\cdot\frac{G_a}{E_a}\cdot\frac{d^4\tau_a}{dz^4}+\\&-\frac{E_f t_a {t_f}^3}{12\cdot E_a}\cdot\frac{d^6\tau_a}{dz^6}+\frac{E_f G_a {t_a}^3 {t_f}^3}{144\cdot {E_a}^2}\cdot\frac{d^8\tau_a}{dz^8}=0\end{aligned} \tag{2.32}$$

Finally, an expression of the displacement function v as a function of the interface shear stresses can be derived by solving equation (2.31) and introducing the (2.30):

$$v=\frac{3\cdot {t_a}^2+3\cdot t_a t_f+{t_f}^2}{6E_a}\cdot\frac{d\tau_a}{dz}-\frac{E_f t_a {t_f}^3}{6E_a G_a}\cdot\frac{d^3\tau_a}{dz^3}+\frac{E_f {t_a}^3 {t_f}^3}{72\cdot {E_a}^2}\cdot\frac{d^5\tau_a}{dz^5} \tag{2.33}$$

Eight boundary conditions are needed for the problem at hand and they can be symbolically written as follows:

$$\tau_a\big|_{z=0}=0\ , \qquad \tau_a\big|_{z=L}=0\ , \tag{2.34}$$

$$\varepsilon\big|_{z=0}=-\frac{N(0)}{E_f A_f}\ , \qquad \varepsilon\big|_{z=L}=\frac{N(L)}{E_f A_f}\ , \tag{2.35}$$

$$M\big|_{z=0}=0\ , \qquad M\big|_{z=L}=0\ , \tag{2.36}$$

$$V\big|_{z=0}=0\ , \qquad V\big|_{z=L}=0\ . \tag{2.37}$$

The results of the analysis carried out by means of this model are completely controlled by the following non-dimensional parameters:

$$\omega L \ , \tag{2.38}$$

$$\omega t_f = \sqrt{\frac{G_a t_f}{E_f t_a}} = \sqrt{\frac{k_{s,a} t_f}{E_a}} \ , \tag{2.39}$$

$$\frac{G_a}{E_a} = \frac{k_{s,a}}{k_{v,a}} \ , \tag{2.40}$$

$$\frac{t_a}{t_f} . \tag{2.41}$$

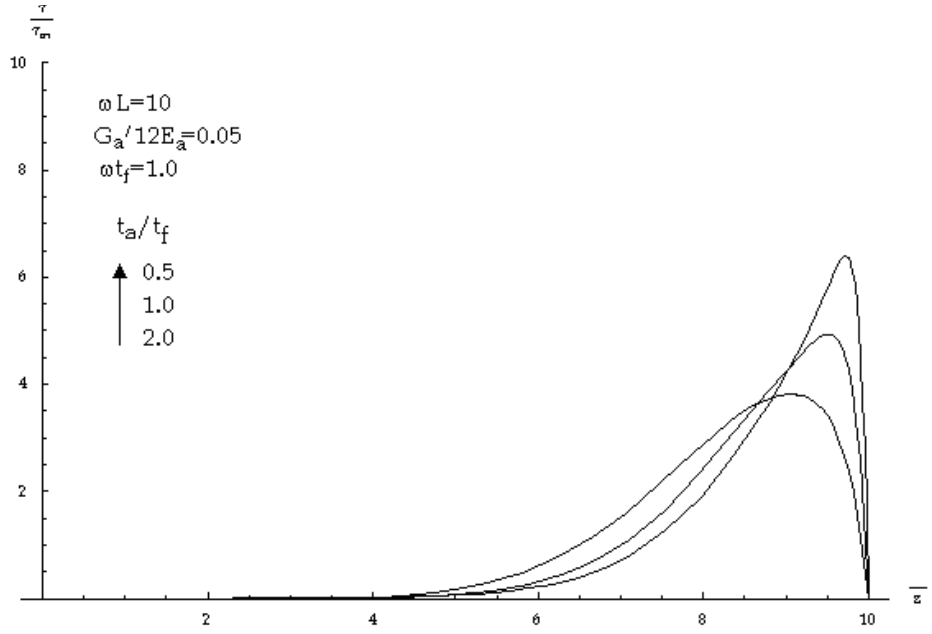

Figure 2.4 - Possible distributions of interface shear stresses throughout the adhesive interface

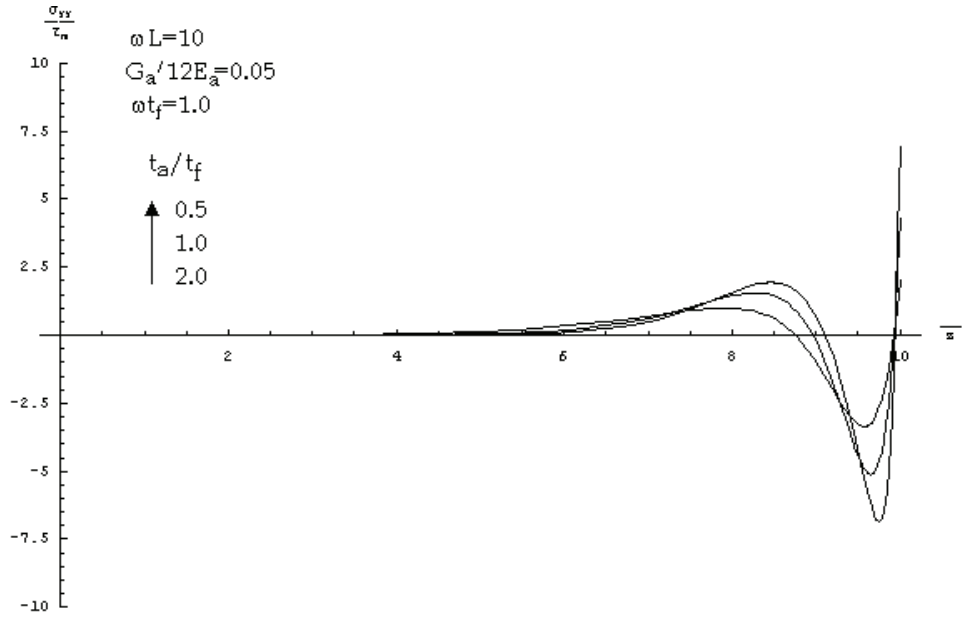

Figure 2.5 - Possible distributions of interface normal stresses throughout the adhesive interface

2.1.2 Possible simplifications of the general model

The general model formulated in the previous section can be simplified considering further assumptions about the geometric and mechanical assumptions.

In particular, a key simplification derives in the case of negligible thickness t_f of the FRP laminate, if compared, for instance, with a suitable reference value of the length. In particular, it is possible to demonstrate that the six-order equation (2.32) can be reduced by uncoupling the equations (2.30) and (2.31):

$$\frac{d^2\tau_a}{dz^2} + \omega^2 \tau_a = 0 \ , \tag{2.42}$$

$$\frac{d^4 v}{dz^4} + 12 \cdot \frac{E_a}{t_a t_f^{\ 3}} v = 0 \, , \tag{2.43}$$

Under the mathematical point of view, the above simplification derives from the condition $\omega t_f \to 0$ for which ever value of the non dimensional parameters listed at the end of section 2.1. It means that the thickness of the FRP laminate is much smaller than the characteristic length of the problem ω, which is the main argument of the solutions of the general equation (2.32). The uncoupled boundary conditions for eq. (2.42) simplify as a consequence of the condition $\omega t_f \to 0$, turning in a completely uncoupled expressions:

$$\varepsilon\big|_{z=0} = -\frac{N(0)}{E_f b_f t_f} = \left.\frac{ds}{dz}\right|_{z=0} \qquad \varepsilon\big|_{z=L} = \frac{N(L)}{E_f b_f t_f} = \left.\frac{ds}{dz}\right|_{z=L} \tag{2.44}$$

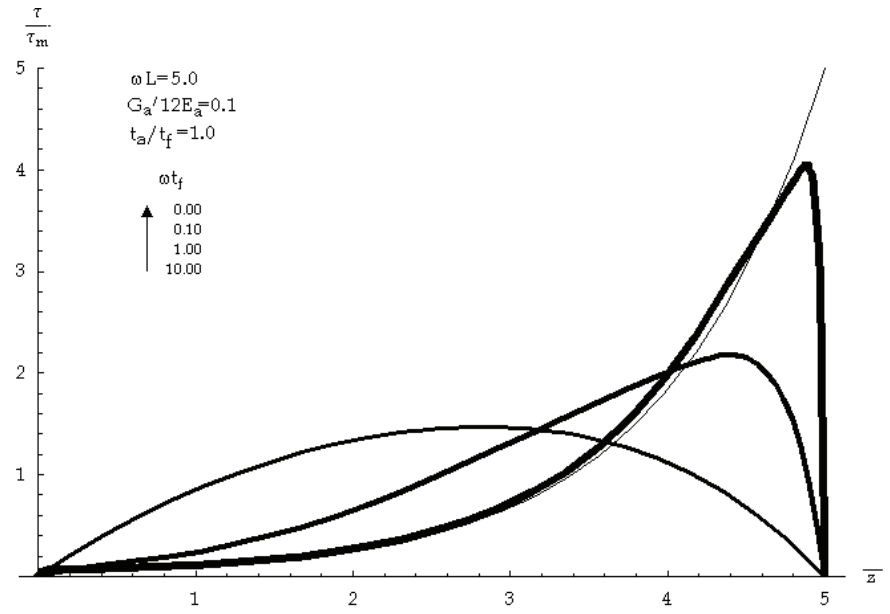

Figure 2.6 - Interface shear stress for a thin FRP laminate

A sound demonstration about how equation (2.32) reduces to (2.42)-(2.43) in the case of $\omega t_f \to 0$, can be obtained by means of some mathematical transformations of both the equation (2.32) and the boundary conditions (2.34)-(2.37) in dimensionless form. These transformations, as well as the discussion of the slight modifications in the out-of-plane stress regime, are omitted herein for the sake of brevity.

2.2 SOLUTIONS IN THE NONLINEAR RANGE

The assumption introduced in the subsection 2.1.2 for simplifying the general eighth-order equation formulated in subsection 2.1.1 can be generally assumed as a reasonable trade-off between the (good) accuracy of the obtained model and the (higher) simplicity of its equations. The approximation introduced by the supplementary assumption is generally accepted especially in the nonlinear range, as further uncertainties are introduced by the fracture behaviour of concrete which cannot be covered by the complex assumptions leading to equation (2.32).

Thus, the nonlinear response of FRP-to-concrete joints under pull-out actions can be analyzed by assuming the problem described by equation (2.42) with the boundary conditions in (2.44). Since the nonlinear response is now of interest, equation (2.42) can be slightly modified for considering the possibility of a nonlinear relationship $\tau_a=\tau(s)$. Moreover, eq. (*2.1)* can be written in terms of axial strains ε in the FRP laminate by introducing equation (2.8):

$$\frac{d\varepsilon}{dz}+\frac{\tau(s)}{E_f t_f}=0 \ . \tag{2.45}$$

and, considering the relationship between axial strains and interface slip derided at the end of the subsection 2.1.2 , the following relationship can be written for generalizing eq. (2.42) to the nonlinear range:

$$\frac{d^2 s}{dz^2}+\frac{\tau(s)}{E_f t_f}=0 \ . \tag{2.46}$$

The bilinear shear-stress-interface-slip relationship is considered herein as a general relationship for the nonlinear response of the interface between FRP and concrete:

$$\tau(s)=\begin{cases} -k_{el}\cdot s & |s|\le s_{el} \\ -k_u\cdot(s_u-|s|)\cdot sign(s) & s_{el}<|s|\le s_u \\ 0 & |s|>s_u \end{cases} \tag{2.47}$$

where all symbols are represented in Figure 2.7. For the sake of simplicity, only the monotonic behaviour with $s\ge 0$ will be considered in the following elaborations.

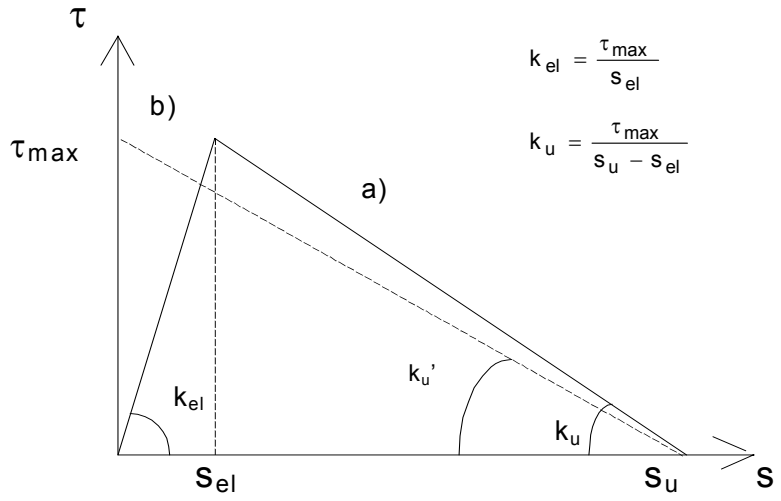

Figure 2.7 - Bilinear shear-stress-interface-slip relationship (fib - bulletin 14, 2001)

Consequently, two second order differential equations can be obtained by introducing the two nonzero branches of the relationship (2.47) within the general equation (2.46). In particular, under low load levels, the condition $0 \le s \le s_{el}$ yields throughout all the bonding length and the equation (2.46) can be written in the following form in terms of interface slips s:

$$\frac{d^2 s}{dz^2} - \omega^2 \cdot s = 0 \ . \tag{2.48}$$

Considering a pull-out force P applied at the end (z=L) of the bonding length, the following boundary conditions can be written after eq. (2.44):

$$\varepsilon\big|_{z=0} = \left.\frac{ds}{dz}\right|_{z=0} = 0 \qquad \varepsilon\big|_{z=L} = \left.\frac{ds}{dz}\right|_{z=L} = \frac{P}{E_f b_f t_f} \ . \tag{2.49}$$

Simple mathematical transformations (whose details are omitted herein) lead to the following solution in terms of interface shear stresses:

$$\tau = -\omega \cdot \frac{P}{b_f} \cdot \frac{\cosh\left[\omega \cdot z\right]}{\sinh\left(\omega L\right)} \ , \tag{2.50}$$

which can be easily turned in terms of interface slips s considering the expression describing the linear elastic branch in eq. (2.47). This solution can be accepted for values of the shear strength $|\tau| \le \tau_{max}$ or, in order words, for pull-out forces lower than P_{el}:

$$F_{el} = \frac{\tau_{\max}}{\omega} \cdot b_f \ . \tag{2.51}$$

leading to an interface slip $s=s_{el}$ in $z=L$. As $P>P_{el}$, two different parts of the adhesive interface can be recognized. In the first part, namely for $0 \le z \le z_{el} < L$, the values of the interface slips s keep smaller than the elastic threshold s_{el}. In the second part, for $z_{el} < z \le L$, the interface slips s are in the range (s_{el}, s_u), and the following solution can be derived by integrating the two differential equations:

$$\frac{d^2 s_1}{dz^2} - \omega \cdot s_1 = 0 \qquad \text{for} \quad 0 \le z \le z_{el} < L, \tag{2.52}$$

$$\frac{d^2 s_2}{dz^2} + \frac{k_{in}}{E_f t_f} \cdot s_2 = \frac{k_{in}}{E_f t_f} \cdot s_u \qquad \text{for} \qquad z_{el} < z \le L. \tag{2.53}$$

with the following boundary conditions:

$$\varepsilon\big|_{z=0} = \left.\frac{ds_1}{dz}\right|_{z=0} = 0 \qquad s_1\big|_{z=z_{el}} = s_{el} \tag{2.54}$$

$$s_1\big|_{z=z_{el}} = s_1\big|_{z=z_{el}} \qquad \left.\frac{ds_1}{dz}\right|_{z=z_{el}} = \left.\frac{ds_2}{dz}\right|_{z=z_{el}} \tag{2.55}$$

The following solution in terms of interface shear stress τ involves the parameter $z_{el} < L$, describing the length of the elastic part of the bonding length:

$$|\tau| = \begin{cases} \tau_{\max} \dfrac{\cosh\left[\omega \cdot z\right]}{\cosh\left[\omega \cdot z_{el}\right]} & 0 \le z \le z_{el} \\ \tau_{\max} \left\{ \begin{array}{l} \cos\left[\omega_{in}\left(z - z_{el}\right)\right] + \\ -\dfrac{\omega_{in}}{\omega} \cdot \sin\left[\omega_{in}\left(z - z_{el}\right)\right] \cdot \tanh\left[\omega z_{el}\right] \end{array} \right\} & z_{el} < z \le L \end{cases} \tag{2.56}$$

where

$$\omega_{in} = \sqrt{\frac{\tau_{\max} / \left(s_u - s_{el}\right)}{E_f t_f}} = \sqrt{\frac{k_{in}}{E_f t_f}} \quad . \tag{2.57}$$

Figure 2.8 shows two typical distributions of shear stresses in the a) linear and b) nonlinear range of the behaviour of the adhesive interface described by the bilinear relationship in eq. (2.47).

It is worth noting that z_{el} can actually range in the interval [$z_{el,min}$, L):

$$z_{el,\min} = \max\left\{0; z_{el,deb}\right\} \tag{2.58}$$

in which $z_{el,deb}$ is the value of z_{el} leading to $\tau(L)=0$ (or $s(L)=s_u$):

$$\cos\left[\omega_{in}\left(L - z_{el,deb}\right)\right] - \sqrt{\frac{k_{in}}{k}} \cdot \sin\left[\omega_{in}\left(L - z_{el,deb}\right)\right] \cdot \tanh\left[\omega \cdot z_{el,deb}\right] = 0 \tag{2.59}$$

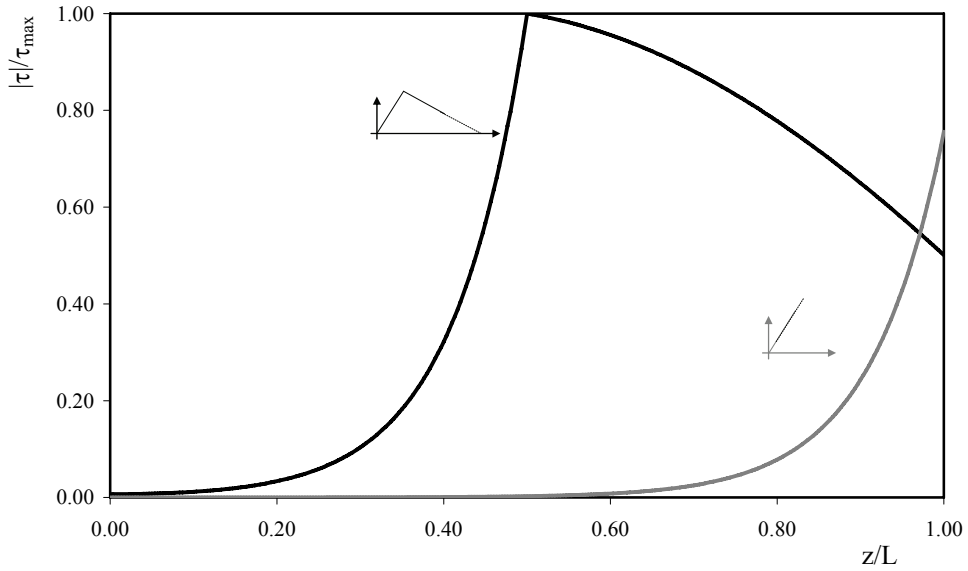

Figure 2.8 - Typical distribution of interface shear-strength in the linear and nonlinear range

2.2.1 Key parameters related to the ultimate strength

The case of $z_{el,deb}=0$ is of particular relevance, as it represents the condition of debonding initiation (namely, $s(L)=s_u$) with $\tau(0)=\tau_{max}$. A characteristic length L_{eff} can be defined in that case by means of equation (2.59):

$$\cos\left[\omega_{in} L_{eff}\right] = 0 \;\Rightarrow\; L_{eff} = \frac{\pi}{2}\cdot\sqrt{\frac{E_f t_f}{k_{in}}} \tag{2.60}$$

Under the mechanical standpoint, this characteristic value has a paramount conceptual meaning. It represents the border between "short" and "long" anchorage length. In particular, the general expression of the force $F>F_{el}$ corresponding to a given position of z_{el} can be derived by integrating the shear stresses in equation (2.56):

$$F = \tau_{\max} b_f \cdot \left\{ \frac{\sin\omega_{in}\left(L - z_{el}\right)}{\omega_{in}} + \frac{\cos\omega_{in}\left(L - z_{el}\right)\cdot\tanh\omega z_{el}}{\omega} \right\} \tag{2.61}$$

It can be applied if and only if $z_{el} \in [z_{el,min}, L)$ (namely, the interface slip s is $s_{el} \leq s \leq s_u$). In the case of $z_{el}=L$ equation (2.61) reduces to (2.51). On the contrary, when $z_{el}=z_{el,deb}=0$ the following expression can be derived for the pull-out force:

$$F_{deb} = \tau_{\max} b_f \cdot \frac{\sin\omega_{in} L_{eff}}{\omega_{in}} = \frac{\tau_{\max} b_f}{\omega_{in}} = b_f \cdot \sqrt{\tau_{\max}\cdot\left(s_u - s_{el}\right)\cdot E_f t_f} \tag{2.62}$$

Since generally $s_u >> s_{el}$ the value F_{deb} is only slightly lower than the maximum strength F_{max} which can be evaluated by applying the theory of Fracture Mechanics (Täljsten, 1996) (or either as a maximum on z_{el} of the for F in eq.(2.61)):

$$F_{\max} = b_f \cdot \sqrt{2G_F \cdot E_f t_f} = b_f \cdot \sqrt{\tau_{\max}\cdot s_u \cdot E_f t_f} \quad . \tag{2.63}$$

They can be assumed as coincident in the approximation of rigid-softening behaviour in considered Figure 2.8.

Note that equation (2.63) can be applied only if $L_b \geq L_{eff}$ being L_{eff}, the effective transfer length. If $L_b < L_{eff}$ a smaller value of the ultimate force has to be expected according to the following relationship:

$$F_{deb} = \sqrt{2G_F E_f t_f} \cdot b_f \cdot \left[\frac{L_b}{L_{eff}} \cdot \left(2 - \frac{L_b}{L_{eff}} \right) \right] \tag{2.64}$$

2.2.2 Energy approach for the bond strength model

It is worth summarize the main steps showed by Täljsten (1994) to obtain the equation (2.63) through the theory of Fracture Mechanics

The maximum transferable load for bonded connections subjected to pure shear can also be determined by using an energy approach (Täljsten, 1994; Browsens 2001).

Figure 2.9 shows a bonded connection subjected to pure shear. A crack with length *a* is present in the concrete. The energy required for crack growth must be delivered as release of elastic energy U_e. If the adherents are free to move during crack propagation, work A_F is done by the external load *F*.

Crack growth is initiated when

$$\frac{1}{b_l}\frac{d}{da}\left(A_F - U_e\right) = \frac{1}{b_l}\frac{dW}{da} = G_f \ , \tag{2.65}$$

where

U_e is the Elastic energy stored in the structure (Nm)
A_F is the Potential energy of the external load (Nm)
W is the Energy for crack propagation (Nm)
b_l is the Width of the laminate (m)
da is the Infinitesimal crack length (m)
G_F is the Fracture energy (Nm/m^2)

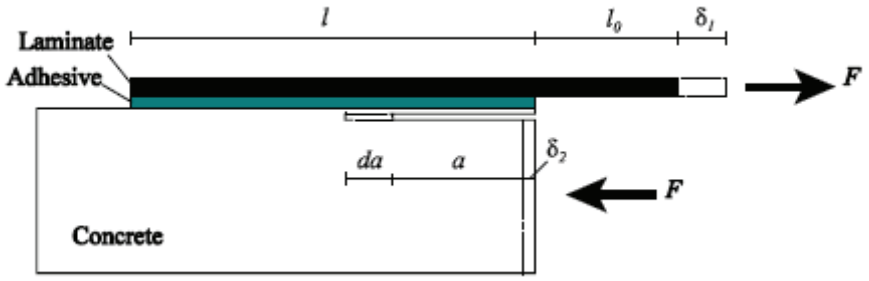

Figure 2.9 - Pure shear case (Täljsten, 1994)

The fracture energy $_{GF}$ is defined as the energy per area unit to bring a connection into complete failure. During the action of the load F, the load application points undergo a relative displacement $\delta = \delta_1 + \delta_2$. When the crack length increases with da, this displacement will increase with $d\delta$. The work A_F, done by the external force is $Fd\delta$.

Expression (2.27) can be rewritten as

$$G_f = \frac{1}{b_l}\frac{d}{da}\left(A_F - U_e\right) = \frac{1}{b_l}\left(F\frac{d\delta}{da} - \frac{dU_e}{da}\right), \tag{2.66}$$

The deformations are elastic and as long as there is no crack growth, the displacement δ is proportional to the load, $\delta = FC$, (see Figure 2.10). C is the compliance (inverse of the stiffness) of the structure. The elastic energy stored in the structure is

$$U_e = \frac{1}{2}\cdot F\cdot\delta = \frac{1}{2}\cdot F^2\cdot C\ , \tag{2.67}$$

Using (2.67) in (2.66) leads to

$$G_f = \frac{1}{b_l}\left(F^2\frac{\partial C}{\partial a} + FC\frac{dF}{da} - \frac{1}{2}F^2\frac{\partial C}{\partial a} - FC\frac{dF}{da}\right) = \frac{F^2\partial C}{2b_l\partial a}\ , \tag{2.68}$$

and thus:

$$F = \sqrt{\frac{2b_l G_f}{\frac{\partial C}{\partial a}}} \ , \tag{2.69}$$

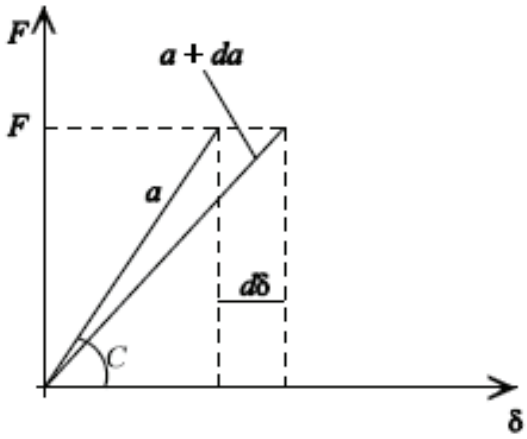

Figure 2.10 - Load - displacement relationship [Browsens, 2001]

Under the hypothesis that the concrete member has a stiffness much larger than the reinforcement the compliance C can be written as

$$C = \frac{l_0 + a}{E_f A_f} \ , \tag{2.70}$$

and

$$\frac{\partial C}{\partial a} \approx \frac{1}{E_f A_f} \ , \tag{2.71}$$

Using (2.71) in (2.69) the maximum force before debonding can be expresses as:

$$F_{deb} = b_l \sqrt{2 E_f t_f G_f} \ , \tag{2.72}$$

which coincides with the formula mentioned in (2.63).

Chapter 3 - Experimental testing and results

The effectiveness of externally bonded fibre reinforced polymer (FRP) laminates for strengthening existing reinforced concrete (RC) structures is strictly related to the bond of FRP reinforcement to the concrete substrate that, as stated in the previous chapter, depends on the mechanical and geometrical properties of the materials.

Although numerous experimental works have been carried out to investigate this aspect, experimental data concerning cyclic tests on both FRP sheets and plates applied on concrete specimens are still lacking. Thus a first series of single shear tests (SSTs) under both monotonic and cyclic actions, without inversion of sign, were performed on concrete prismatic specimens reinforced with CFRP sheets or plates. A further set of bond tests has been performed on concrete specimens reinforced with CFRP plates under monotonic actions, in order to significantly enrich the existing database of tests on EBR carbon plates.

In order to evaluate and compare the influence of cyclic external actions on the bonding behavior of sheets and plate reinforcements, the results provided by monotonic and cyclic tests are reported and discussed in this chapter. In particular, force-displacement relationships as well as axial strains and shear stresses recorded along the FRP reinforcement are reported; the influence of the load path on the FRP debonding behavior is also examined.

In the first section an overview of most common bond test techniques is reported and discussed; in the second section the experimental program is summarized; the most significant results achieved by bond tests performed are showed and discussed in the last two sections.

3.1 OVERVIEW OF TESTING TECHNIQUES

Yao et al. (2005) classified the existing test set-ups into the following types: (a) double-shear pull tests; (b) double-shear push tests; (c) single-shear pull tests; (d) single-shear push tests; and (e) beam (or bending) tests. These arrangements are based on the definition of the loading condition of the element and on the symmetry of the system (a double or single test refers to the contemporaneous loading of two or one FRP reinforcement applied on the specimen sides). Collectively, the first four test methods, may also be referred to as pull tests, as the plate is always directly pulled by a tensile force. Pull-pull (a) and push-pull (d) test set-up have been the most popular test methods. In the plate end debonding failures in FRP flexural- strengthened RC beams with longitudinal plates as well as debonding failures in FRP shear-strengthened RC beams with transverse plates, the bond strength model developed from pull tests is directly applicable. Furthermore, in intermediate crack-induced debonding failures in FRP flexural- strengthened RC beams with longitudinal plates, the stress state in the critical region of the beam is also closely similar to that of the concrete prism in a single-shear pull test.

In order to extend the results of bond tests to various types of strengthening (flexural, shear, torsion), the pull-pull test set-up (a and c) are probably the configuration giving the loading condition more similar to the actual one in RC elements, but it is also the most difficult to realize with a reliable set-up. Furthermore the test setup (a), as well as (b) could lead to underestimate the bond strength due to the influence of detailing (Blontrock et al., 2002; Ceroni et al., 2008). On the contrary, the push-pull test (d), where the concrete is in compression, is more simple to realize; moreover it gives comparable predictions of the bond strength, if the pushing force is applied on the concrete block sufficiently far from the external reinforcement (Yao et al., 2005). Indeed, if the compressed area of concrete is too extended, the volume of material involved in the debonding failure can be lower and, thus, the related fracture energy decreases.

Asymmetrical schemes (c and d) are in general preferable to the symmetrical ones (a and b) mainly because the latter are more influenced by the alignment detailing of the two strengthened sides. Moreover the specimen symmetry is however lost when the debonding starts on one side and prevents from following correctly the post-peak behaviour.

Asymmetrical push-pull test set-ups (d) are commonly realized by positioning a single concrete block in a stiff steel frame with an upper plate compressing the specimen, while the end of the FRP reinforcement, glued on one side, is clamped in the grips of a tensile machine (Nigro et al., 2008c; Savoia et al. 2009; Ceroni and Pecce, 2010). An alternative configuration can be also realized by fixing the end of the concrete block, placed horizontally, and applying tension to the FRP reinforcement with an hydraulic jack (Yao et al., 2005; Mazzotti et al., 2009). Asymmetrical pull-pull test set-ups (c) can be realized by installing metallic threaded rods inside the concrete specimen which can be clamped in the testing machine grips (Bilotta et al. 2011a).

Therefore asymmetrical single-shear test setup (c or d) appear to be promising candidate as a standard set-up for determining the FRP-to-concrete bond strength and were therefore adopted in the experimental results presented in the following sections.

3.2 EXPERIMENTAL PROGRAM

In this section the experimental program is only briefly summarized to provide an overview of the experimental activities carried out.

A total of 58 SST tests in four sets (i.e. I-12 tests, II-16 tests, III-12 tests, IV-18 tests) were performed on CFRP plates (38) and sheets (20) applied on two opposite longitudinal faces of 29 concrete prisms.

Concrete mix was specifically designed to obtain low compressive concrete strength to simulate the FRP application on existing concrete. Compressive tests were performed at 28 days after casting: the cylinder mean strength, f_{cm}, was equal to 23.82 MPa, 21.46 MPa, 26.00 MPa and 19.00 MPa for set I, II, III and IV respectively.

CFRP Young's moduli, E_f, were obtained by means of tensile flat coupon tests: their mean values were between 110-220 GPa for plates and 170-240 GPa for sheets.

Prior to FRP installation, the concrete surface was treated by sand paper (sets I, II, III) or by bush hammering (set IV), in order to eliminate the mortar till the aggregate became clear. Primer was always used to consolidate the concrete surface except for specimens of set VI.

The main parameter of experimental tests as the concrete compressive strength; the specimen width; the FRP type, geometry and mechanical properties are summarized in Table 3.1. As concerns the FRP Young modulus in Table 3.1 is reported the average of the values obtained by means of 5 tensile tests for each type of FRP; hence in brackets the coefficient of variation is reported.

Further details related to experimental tests of each set can be founded in the following two sections of this chapter and in Nigro et al. (2008c), Savoia et al. (2009), Bilotta et al. (2009a), Bilotta et al. (2011a).

Table 3.1 - Experimental debonding load values (58 SST tests).

58 SST test *cyclic test		CONCRETE Cylinder mean strength	Prism width	FRP Fiber type	Young modulus	Width	Thickness	Bond length
Set	**Labels**	f_{cm} [*Mpa*]	b_c [*mm*]		E_f [G*pa*]	b_f [*mm*]	t_f [*mm*]	L_b [*mm*]
Set I 12 tests *Nigro et al. (2008c)*	PM1-2-3 | PC*4-5-6	23.82	150	Plate	$171_{(5\%)}$	50	1.4	400
	SM1-2-3 | SC*4-5-6	23.82	150	Sheet	$216_{(7\%)}$	100	0.166	
Set II 16 tests *Bilotta et al. (2009a)*	PM7-8-9 | PC*10	21.46	150	Plate	$171_{(5\%)}$	50	1.4	250
	PM13-14-15 | PC*16							125
	SM7-8-9 | SC*10	21.46	150	Sheet	$216_{(7\%)}$	100	0.166	100
	SM13-14-15 | SC*16							50
Set III 12 tests *Savoia et al. (2009)*	V1a-2a-3a	26.00	150	Plate	180	80	1.2	400
	V1b-2b-3b							100
	V18a-19a-20a	26.00	150	Sheet	241	100	0.166	400
	V18b-19b-20b							100
Set IV 18 tests *Bilotta et al. (2010a)*	C-1.25x100-1-2-3	19.00	160	Plate	$171_{(2\%)}$	100	1.25	300
	C-1.40X100-1-2-3				$221_{(4\%)}$	100	1.4	
	C-1.30X60-1-2-3				$175_{(1\%)}$	60	1.3	
	C-1.60X100-1-2-3				$109_{(15\%)}$	100	1.6	
	C-1.20X100-1-2-3				$166_{(4\%)}$	100	1.2	
	C-1.70X100-1-2-3				$141_{(1\%)}$	100	1.7	

Note that the test set-up adopted for the set VI is different from that adopted for other sets. In particular with regard to the classification given in Yao et al (2005) test set-up of the sets I, II and III is of type SST near end supported (NES – i.e. test setup d, see 3.1), while for the set VI the type SST far end supported (FES – i.e. test setup c, see 3.1) was adopted. From a theoretical point of view the differences should be negligible due to the high stiffness of the concrete block (Browsens, 2001).

Finally it is worth noting that several strain gauges were applied along the FRP laminates in order to measure axial strains during the bond test (see Figure 3.1b,c). These experimental readings allow theoretical models of the adhesion laws to be to verified or calibrated, as detailed showed in the chapter 4.

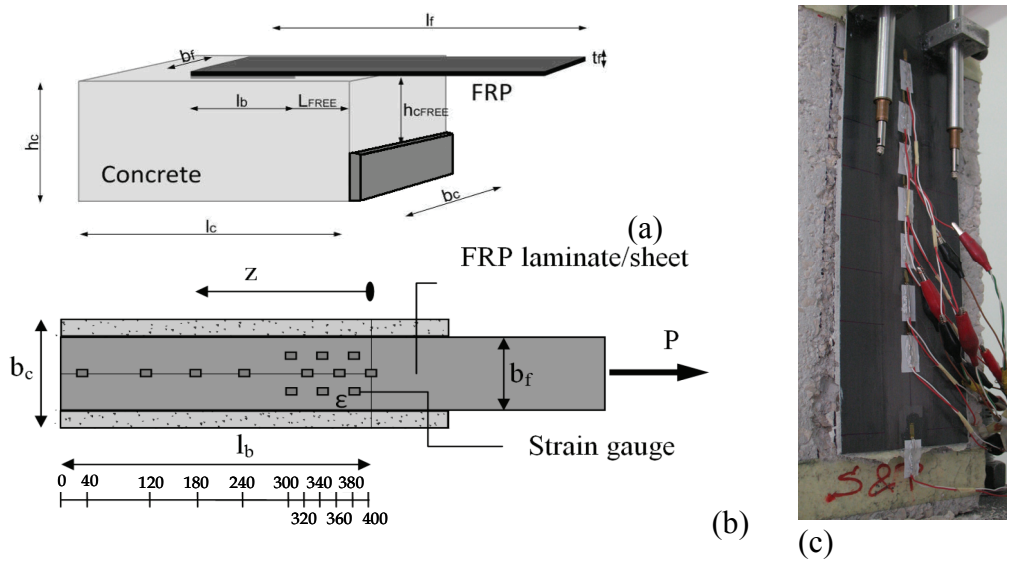

Figure 3.1 - Test set-up scheme (a) – strain gauges distributions: scheme (b) and photo (c)

3.3 BOND TESTS ON FRPS UNDER MONOTONIC AND CYCLIC ACTIONS

The flexural strength of reinforced concrete (RC) members can be significantly increased by externally bonded fiber reinforced polymer (FRP) sheets and plates (referred to in the following as "laminates" for brevity). This strengthening method has become very popular worldwide in the past decade, due to the well-known advantages of FRP composites over other materials such as their high strength/stiffness-to-weight ratio and excellent corrosion resistance (ACI 440.2R-08 2008).

Ideally, RC members strengthened with externally bonded FRP laminates could fail either under compressive concrete crushing or FRP tensile rupture. In reality, debonding of FRP laminates from concrete substrate controls the FRP failure in most cases, unless appropriate local measures are taken to prevent it. In order to avoid debonding failure, which is brittle, a fundamental understanding of FRP bonding behavior is essential: several theoretical scientific contributions have been proposed by researchers in recent years concerning both the behavior of the FRP-to-concrete interface and the evaluation of the interface stresses (Ueda and Dai 2005; Dai et al. 2005a). Moreover, many experimental tests have been carried out to evaluate both bond strength and effective bonding length (Chajes et al. 1996; Bizindavyi et al. 1999; Brosens et al. 2001; Yao et al. 2005). In particular, the influence of FRP stiffness, width and bond length as well as concrete compressive strength and surface treatments has been investigated in depth (Brosens et al. 2001; De Lorenzis et al. 2001; Faella et al. 2002a,b; Savoia et al. 2003; Guo et al. 2005; Lu et al. 2005; Faella et al. 2007e; Nigro et al. 2008c). Both theoretical and experimental contributions have led to the development of design guidelines and codes (ACI 440.2R-08 2008; CNR-DT200/2004 2004; fib bulletin 14 2001). Such guidelines are mainly based on the results of monotonic bond tests, while many strengthened structures are subjected to fatigue loads (i.e. roads and railways bridges) or to shorter but more intense cyclic actions such as seisms. In particular, in these cases the FRP-concrete interface is subject to cyclic stresses which could lead to premature debonding failure.

Thus some researchers have recently begun to investigate the fatigue performance of the FRP-concrete interface (Kobayashi et al. 2003; Dai et al. 2005b; Bizindavyi et al. 2003; Diab et al. 2007). Nevertheless, at present, bond tests under cyclic actions performed on CFRP sheets applied on concrete blocks are not as numerous as monotonic ones, and particularly lacking are the cyclic tests performed on CFRP plates. Furthermore, few studies are available on debonding phenomena under few cycles at very high force levels, typical occurring during earthquakes. During seisms, FRP instability in compression may start before debonding; however in some cases (i.e. statically determinate bridge beams and slabs), FRP laminates may be always in tension. Ko and Sato (2007) showed that the load-displacement curves recorded during cyclic tests basically traced the load-displacement curves related to monotonic counterpart tests even if plastic displacements and stiffness reduction were observed due to the partial debonding imposed by the repeated unload/reload cycles. Finally, they showed that partial debonding under cyclic loads does not affect the FRP reinforcement debonding force if adequate bond length is provided.

The present section focuses on the influence of cyclic actions on bond behavior of FRP reinforcement in tension. In particular, the effects exerted on FRP reinforcement by seismic actions of different magnitudes (i.e. a few cycles at different load levels) were investigated by a series of Single Shear Tests (SSTs). Monotonic tests were also performed to compare the bonding behavior of FRP sheets and plates under monotonic and cyclic actions. The influence of FRP bond length is also discussed.

3.3.1 Experimental program for cyclic bond tests

As stated above, various experimental set-ups were previously used to determine FRP-to-concrete bond strength (Yao et al. 2005). Both numerical (Chen et al. 2001a) and experimental studies have shown that different test set-ups can significantly change the experimental results. Nevertheless, at present no consensus on a standard test procedure has been still reached. The experimental results obtained by SST have shown a minor data scattering procedure (Yao et al. 2005, Savoia et al. 2008, 2009). The SST procedure was adopted in the present study for the bond tests. In particular, 28 SST tests were

performed on CFRP sheets and plates applied on two opposite longitudinal faces of 14 concrete prisms made up with the same nominal dimensions: width b_c = 150 mm, height h_c = 200 mm and length l_c = 500 mm. Further geometrical dimensions of the specimens are reported in Figure 3.2: h_{cFREE} = 50 mm is the height of the concrete free edge ($h_{cFREE} = h_c - h_b$ where h_c is the concrete prism height and h_b is the height of the support block), l_b is the bond length, L_{FREE} = 100mm is the un-bonded length of FRP, b_f = 100 mm and b_f = 50mm are the FRP widths of sheets and plates respectively, t_f = 0.166 mm and t_f = 1.4 mm are the corresponding thicknesses. Sheets and plates were specifically selected to investigate the performance of reinforcements with a low or high value of axial stiffness. The un-bonded length L_{FREE} = 100mm was adopted to avoid anomalous failure mode such as cracking in the concrete prism (Yao et al. 2005).

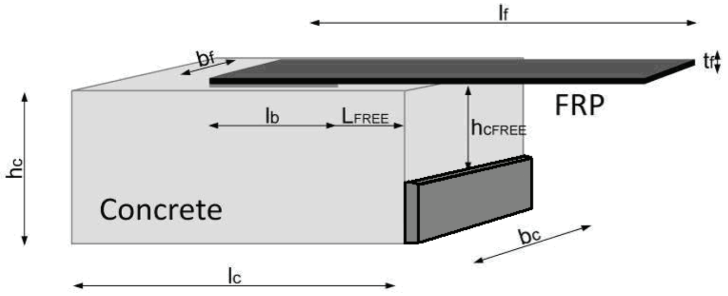

Figure 3.2 - Specimen dimensions

The concrete aggregates were characterized by a maximum diameter D_{max} = 31.5 mm and consistency class S.3 (according to BS EN 206-1:2000). Concrete mix design was specifically designed to obtain low compressive concrete strength to better simulate the FRP application on existing structural members that need to be strengthened. Compressive tests were performed at 28 days after casting: cylinder mean strength relating to two batches was f_{cm} = 22.5 MPa.

CFRP Young's modulus were obtained by means of tensile flat coupon tests on CFRP sheets and plates respectively: their mean values were $E_{f,S}$ = 216 GPa and $E_{f,P}$ = 171 GPa for sheets and plates respectively; the ultimate mean strains were ε_u = 1.5% for sheets and ε_u = 1.2% for plates;_ultimate

strength mean values were $f_{fu,S}$ = 3240MPa for sheets and $f_{fu,P}$ = 2052 MPa for plates. Prior to FRP installation, the concrete surface was treated by both sand paper to eliminate the mortar till the aggregate became clear, and primer to consolidate the concrete surface.

As illustrated in the setup scheme (Figure 3.3), tests were carried out with a servo-hydraulic testing machine (MTS810). Metallic tabs were installed at the end of FRP reinforcement in order to ensure adequate clamping in the test machine grip. To block the specimen in the machine a steel frame was designed. Several strain gauges were applied along the FRP laminates in order to measure axial strains during the bond test (see Figure 3.4). Each test is identified by a label "XY_n": X indicates the type of reinforcement (P=Plate; S=Sheet), Y the type of action (M=Monotonic; C=Cyclic), n is the progressive test number.

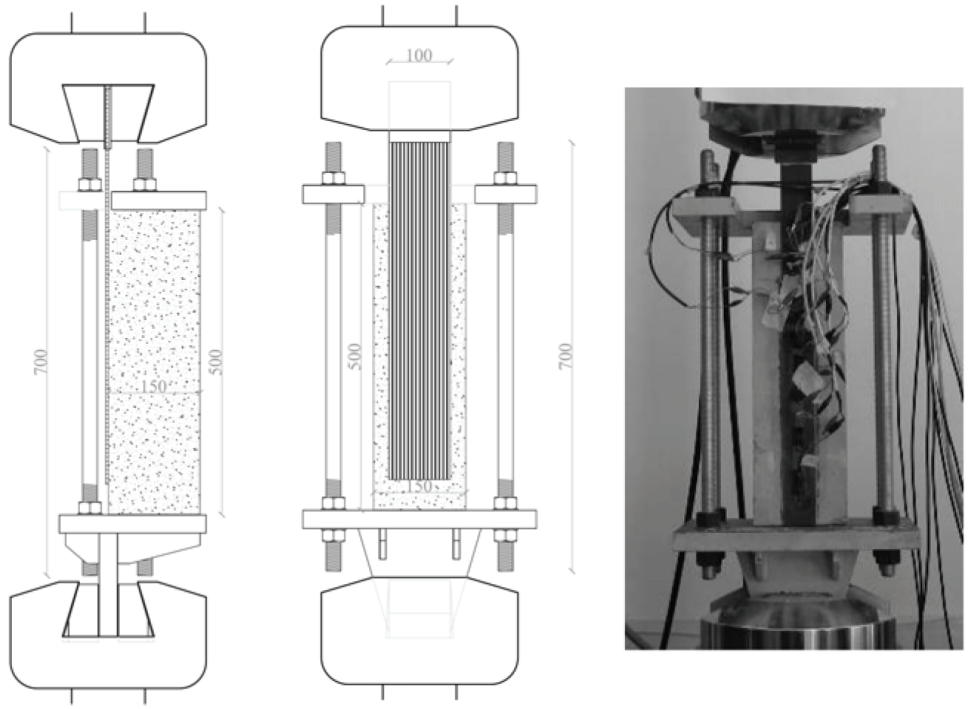

Figure 3.3 - Test setup layout.

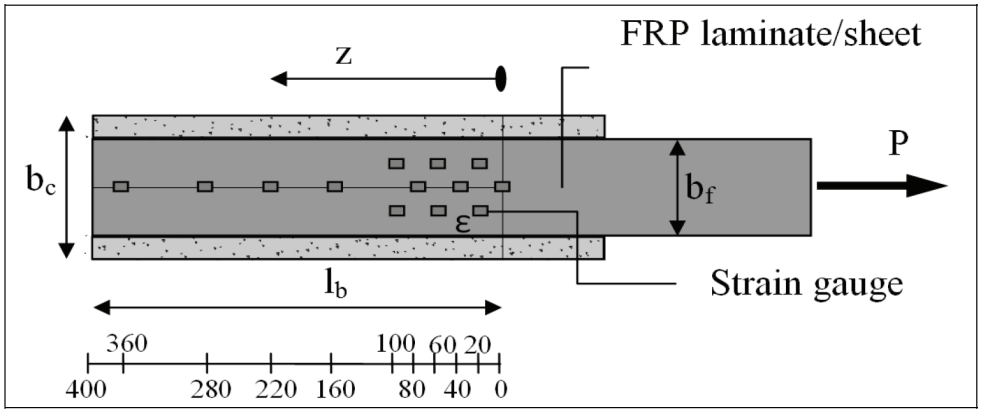

Figure 3.4 - Strain gauges (tests on sheets)

To investigate the influence of the reinforcement bond length, l_b, on the interface behavior under cyclic actions, different l_b values were assumed in the experimental program. In particular, effective bond lengths, $l_{eff,CNR}$, were first computed for both sheets and plates according to relationships suggested by CNR-DT200 (2004) (i.e. 106mm and 262mm, for sheets and plates, respectively). Three different values were adopted for plates and sheets: 400mm, 250mm, and 125mm (i.e. higher, about equal to, and lower than $l_{eff,CNR}$, respectively) for plates; and 400mm, 100mm and 50mm for sheets. In all, 18 monotonic tests on CFRP reinforced concrete specimens were performed under displacement control as reported in Table 3.1. Monotonic tests were performed with different test speeds (0.001mm/s, and 0.003mm/s for plates and sheets, respectively) since plates and sheets are characterized by different stiffness; thus similar load speeds were adopted in the tests (about 10 N/sec).

Once the mean debonding load value, $P_{max,M}$, had been determined through monotonic tests, a total of 10 cyclic tests were performed. Three different cyclic load paths were adopted in the experimental program (see Table 3.2):

One test (PC_4) was performed with three series of five cycles of load-unload starting from 15% of $P_{max,M}$ up to 30%, 50% and 70% of $P_{max,M}$, respectively.

Eight tests (PC_5, PC_6, PC_10, PC_16 and SC_4, SC_5, SC_10, SC_16) were performed with four series of ten cycles of load-unload starting from 15% of $P_{max,M}$ up to 30%, 50%, 70% and 90% of $P_{max,M}$ respectively.

One test (SC_6) was performed with 300 cycles of load-unload between 70% and 90% of $P_{max,M}$.

Table 3.2 - Test load paths

	Actions	Cycle details	Test	L_b [*mm*]	f_{cm} [*MPa*]
PLATES	Monotonic up to failure (v = 0.001 mm/s)	-	PM_1 PM_2 PM_3	400	23.82
			PM_7 PM_8 PM_9	250	21.23
			PM_13 PM_14 PM_15	125	21.23
	15 cycles up to 70% $P_{max,M}$ (v = 0.1 kN/s) + monotonic reloading (v = 0.001 mm/s)	5 cycles: 15 - 30% of $P_{max,M}$ 5 cycles: 15 - 50% of $P_{max,M}$ 5 cycles: 15 - 70% of $P_{max,M}$ + 15% of $P_{max,M}$ - failure	PC_4	400	23.82
	40 cycles up to 90% $P_{max,M}$ (v = 0.1 kN/s) + monotonic reloading (v = 0.001 mm/s)	10 cycles: 15 - 30% of $P_{max,M}$ 10 cycles: 15 - 50% of $P_{max,M}$ 10 cycles: 15 - 70% of $P_{max,M}$ 10 cycles: 15 - 90% of $P_{max,M}$ + 15% of $P_{max,M}$ - failure	PC_5 PC_6	400	23.82
			PC_10	250	21.23
			PC_16	125	21.23
SHEETS	Monotonic up to failure (v = 0.003 mm/s)	-	SM_1 SM_2 SM_3	400	23.82
			SM_7 SM_8 SM_9	100	21.23
			SM_13 SM_14 SM_15	50	21.23
	40 cycles up to 90% $P_{max,M}$ (v = 0.1 kN/s) + monotonic reloading (v = 0.003 mm/s)	10 cycles: 15 - 30% of $P_{max,M}$ 10 cycles: 15 - 50% of $P_{max,M}$ 10 cycles: 15 - 70% of $P_{max,M}$ 10 cycles: 15 - 90% of $P_{max,M}$ + 15% of $P_{max,M}$ - failure	SC_4 SC_5	400	23.82
			SC_10	100	21.23
			SC_16	50	21.23
	300 cycles up to 90% $P_{max,M}$ (v = 0.1 kN/s) + monotonic reloading (v = 0.003 mm/s)	300 cycles: 70 - 90% of $P_{max,M}$ + 15% of $P_{max,M}$ - failure	SC_6	400	23.82

Cyclic load paths “a” and “b” were adopted to simulate a seismic event (low number of cycles) of different intensity; cyclic load path “c” was adopted to evaluate the extent of the influence of cycle number on bond behavior. Cyclic actions were provided in a force control (i.e. 100 N/sec); each cyclic test ended with a monotonic reloading stage starting from 15% of $P_{max,M}$ up to failure under displacement control.

3.3.2 Load - displacement behavior

The main experimental results are herein reported with reference to both monotonic and cyclic tests performed on specimens with FRP bond length l_b = 400 mm. Results of tests performed on specimens with FRP bond length lower than 400 mm are given in the section related to the comparisons between different bond lengths. For each test we report the first debonding load, P_{fd}, that identified the beginning of debonding, the maximum load recorded during the test, P_{max}, and the mean load value P_{dm} obtained as the average of local peak load values recorded after P_{fd}. Furthermore, we examine the displacement corresponding to the first debonding load, w_{fd}, the ultimate displacement w_u, and mean values of w_u for identical monotonic tests, $w_{u,M}$.

3.3.2.1 Monotonic tests on plates and sheets with l_b = 400mm

The experimental load-displacement relationships related to FRP plates and sheets reinforced specimens are shown in Figure 3.5a,b; the displacements, w, were computed with reference to the loaded end of the CFRP laminate (by integrating the strain recorded along the reinforcement). Three LVDTs were installed (see Figure 3.6a); from experimental records it results that no significant differences were observed on integrating the strain recorded along the reinforcement or using data from LVDTs, as shown in Figure 3.6b.

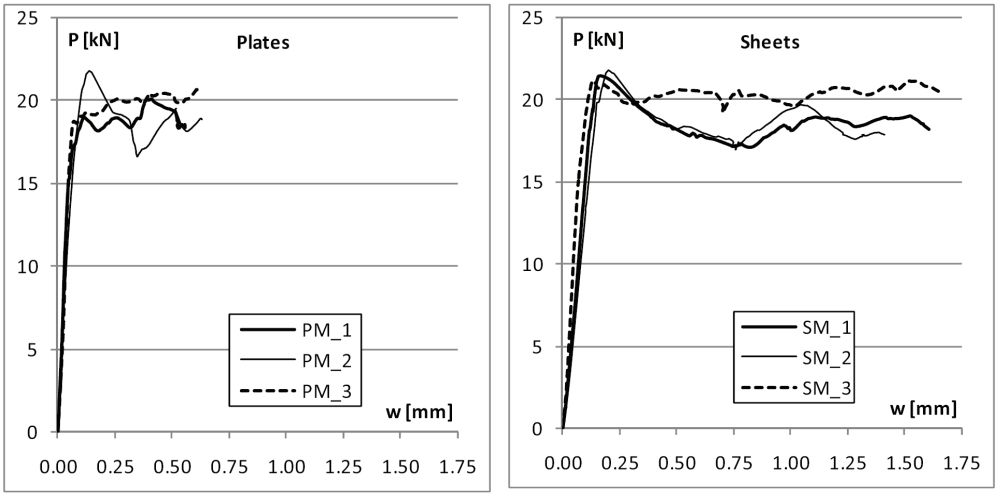

(a) Plates (b) Sheets

Figure 3.5 - Experimental load-displacement relationships

Plate-reinforced specimens showed a substantially equal slope of the load-displacement curves up to the first debonding load value P_{fd}: on specimen PM_2 the maximum first debonding load value of P_{fd} = 21.78 kN was recorded, slightly higher than those recorded on the other two specimens, P_{fd} = 18.99 kN and P_{fd} = 19.18 kN for PM_1 and PM_3, respectively. The displacement corresponding to the debonding load, w_{fd}, was about 0.11mm, 0.14mm and 0.12mm for PM_1, PM_2 and PM_3, respectively.

Sheet-reinforced specimens also showed a substantially equal slope of the load displacement curves up to P_{fd} which were on average about 21.5 kN. The displacements corresponding to the debonding load, w_{fd}, achieved a mean value of about 0.14mm.

Once P_{fd} was achieved, both on plates and sheets, the *P*-*w* relationships showed a pseudo-constant trend up to the ultimate displacement w_u: the mean values were $w_{u,M}$ = 0.60mm and $w_{u,M}$ = 1.56mm for plates and sheets, respectively; the significant difference between these values is due to the lower strain values achieved by plates at debonding than those achieved by sheets. In the range w_{fd}-w_u the load achieved different peak values due to the transfer of the effective bond length along the wide bonded zone of FRP. The mean loads, P_{dm}, were 19.76 kN and 19.84 kN on average for plates and sheets

respectively; the maximum peak loads, P_{max}, were 20.86 kN and 21.49 kN. The main experimental results are summarized in Table 3.3.

Finally, it is noted that all tested specimens failed due to debonding in concrete (DB-C) referring to failure type classification reported in Yao et al. (2005) (see Figure 3.7 and Figure 3.8).

(a) LVDTs location

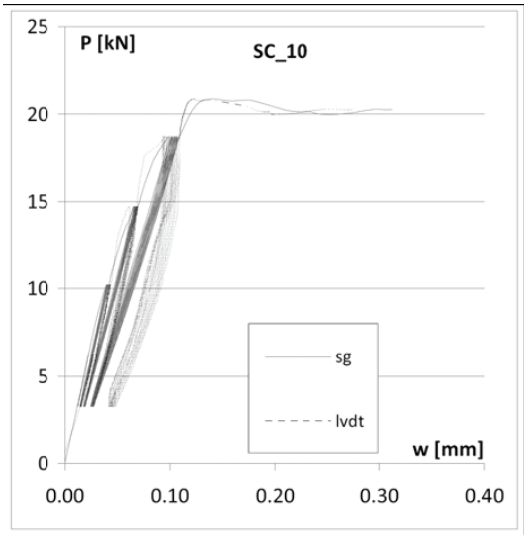

(b) Displacements comparison

Figure 3.6.

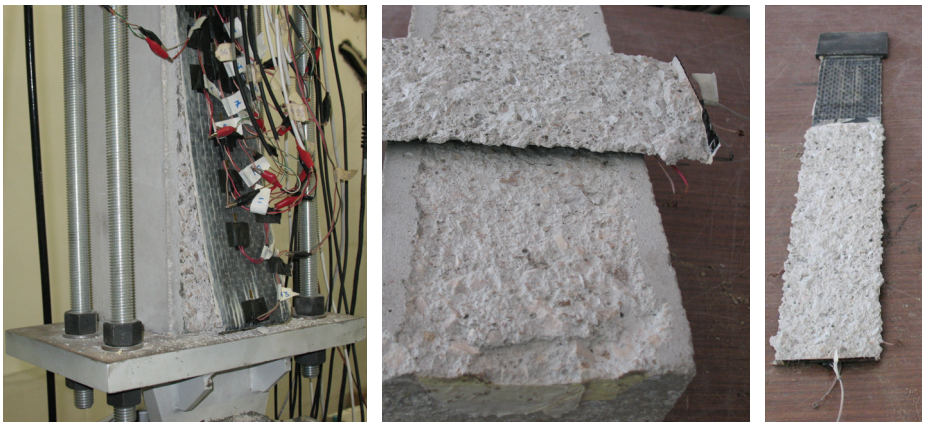

Figure 3.7 - Specimen after test and typical failure mode

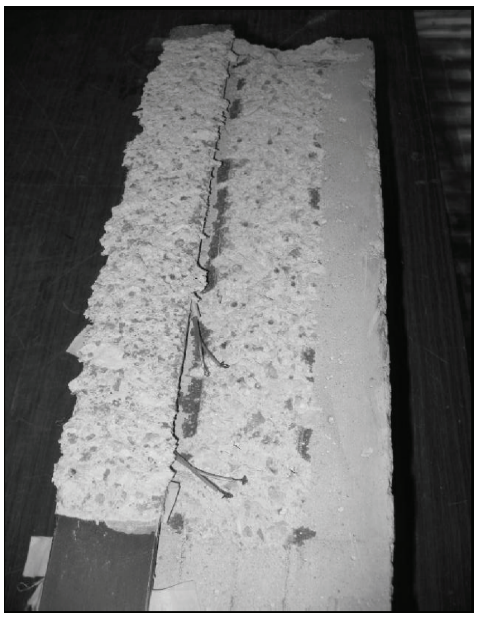

Figure 3.8 - Failure mode: debonding in concrete (DB-C)

Table 3.3 - Monotonic test results

FRP Type	l_b [mm]	f_{cm} [MPa]	Label	P_{fd} [kN]	$P_{fd,M}$ [kN]	P_{max} [kN]	$P_{max,M}$ [kN]	P_{dm} [kN]	$P_{dm,M}$ [kN]	w_{fd} [mm]	$w_{fd,M}$ [mm]	w_u [mm]	$w_{u,M}$ [mm]
Plates			PM_1	18.99		20.10		19.40		0.11		0.56	
t_f = 1.4 mm	400	23.82	PM_2	21.78	19.98	21.78	20.86	19.79	19.76	0.14	0.12	0.63	0.60
b_f= 50 mm			PM_3	19.18		20.71		20.09		0.12		0.61	
Sheets			SM_1	19.18		21.41		19.30		0.10		1.61	
t_f = 0.166 mm	400	23.82	SM_2	21.81	21.49	21.81	21.49	19.45	19.84	0.20	0.14	1.42	1.56
b_f = 100mm			SM_3	21.24		21.24		20.78		0.13		1.65	

3.3.2.2 Cyclic tests on plates with l_b = 400mm

The first test under cyclic actions, PC_4, was performed with an initial series of five cycles between 3kN and 7kN (respectively about 15% and 30% of $P_{max,M}$). The *P*-*w* curve is reported in Figure 3.9 (bold curve) and compared with those related to monotonic tests PM_1, PM_2 and PM_3.

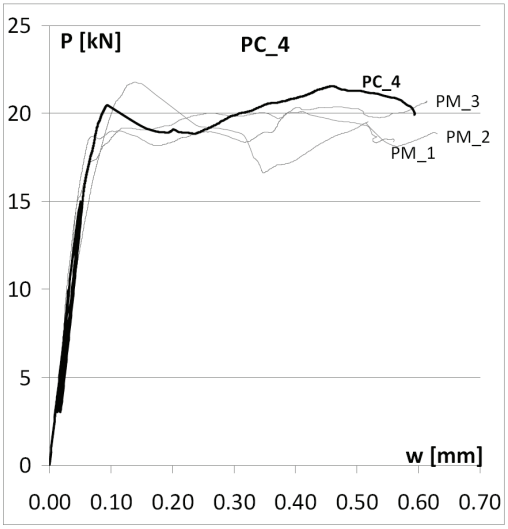

Figure 3.9 - Experimental load-displacement relationships: Test PC_4

The *P*-*w* curve shows that FRP-concrete interface behavior was still elastic between 15% and 30% of $P_{max,M}$ even if negligible residual displacements, Δ, were recorded after load-unload cycles (see Table 3.4). The residual displacements are computed as the difference between displacements before and after cycles at the same load; they indicate the damage of the interface between concrete and FRP (e.g. the higher the residual displacement, the lower is the stress transfer). A second series of five load cycles between 3kN and 10kN (i.e. up to 50% of $P_{max,M}$) and between 3kN and 15 kN (i.e. up to 70% of $P_{max,M}$) were then performed. For these cycles larger residual displacements were recorded, ranging between 0.0025 mm and 0.0050 mm (i.e. 0.42% and 0.83% of the mean ultimate displacement $w_{u,M}$ = 0.60 mm achieved during monotonic tests). The test ended with a monotonic load path starting from a load of 3kN (i.e. 15% of $P_{max,M}$) up to the failure load. During this step the bonding behavior was very similar to that observed during the monotonic tests. This was clearly due to the low number and maximum load of cycles (i.e. 5 cycles and 70% of $P_{max,M}$). The first debonding load was unaffected by cyclic actions; its value, P_{fd} = 20.01 kN, was very similar to the mean value, $P_{fd,M}$ = 19.98 kN, recorded during monotonic tests. Maximum load, P_{max}, and the ultimate displacement, w_u, were also slightly affected by cyclic actions (see Table 3.5). Based on such results, we performed two

further tests, PC_5 and PC_6 (see Figure 3.10a,b) with the same load path (see Table 3.2): 10 instead of 5 was the number of cycles for each series and 90% $P_{max,M}$ instead of 70% $P_{max,M}$ the maximum load reached during the cyclic test phase.

Table 3.4 - Residual displacements Δ after load-unload cycles

Test	Cycle details	Δ [mm]	% $w_{u,M}$
PC_4	5 cycles: 15 - 30% $P_{max,M}$	---	---
	5 cycles: 15 - 50% $P_{max,M}$	0.0025	0.42%
	5 cycles: 15 - 70% $P_{max,M}$	0.0050	0.83%
PC_5	10 cycles: 15 - 30% $P_{max,M}$	---	---
	10 cycles: 15 - 50% $P_{max,M}$	0.0038	0.63%
	10 cycles: 15 - 70% $P_{max,M}$	0.0045	0.75%
	10 cycles: 15 - 90% $P_{max,M}$	0.0607	10.12%
PC_6	10 cycles: 15 - 30% $P_{max,M}$	---	---
	10 cycles: 15 - 50% $P_{max,M}$	0.0003	0.05%
	10 cycles: 15 - 70% $P_{max,M}$	0.0062	1.03%
	10 cycles: 15 - 90% $P_{max,M}$	0.0822	13.70%
SC_4	10 cycles: 15 - 30% $P_{max,M}$	---	---
	10 cycles: 15 - 50% $P_{max,M}$	---	---
	10 cycles: 15 - 70% $P_{max,M}$	0.0051	0.33%
	10 cycles: 15 - 90% $P_{max,M}$	0.0129	0.83%
SC_5	10 cycles: 15 - 30% $P_{max,M}$	---	---
	10 cycles: 15 - 50% $P_{max,M}$	---	---
	10 cycles: 15 - 70% $P_{max,M}$	0.0024	0.15%
	10 cycles: 15 - 90% $P_{max,M}$	0.0225	1.44%
SC_6	300 cycles: 70 - 90% $P_{max,M}$	0.0910	5.83%

The first series of 10 load-unload cycles was between 3 kN and 7 kN, approximately 15% and 30% of $P_{max,M}$, respectively. For these load levels the FRP-concrete interface behavior was elastic and the residual displacements were negligible. No visible cracks were observed during cyclic series between 15% and 50% of $P_{max,M}$ or between 15% and 70% of $P_{max,M}$. By contrast, significant residual displacements, Δ, were recorded after the load-unload cycles (see Table 3.4). During the last series of 10 load-unload cycles between 3 kN and 19 kN (i.e. 90% of $P_{max,M}$) the large displacements at the FRP-concrete interface denoted the beginning of the debonding phenomenon. Debonding was also highlighted by the formation of cracks, visible to the naked eye, along the lateral edges of FRP plates.

Table 3.5 - Cyclic test results

FRP Type	l_b [mm]	f_{cm} [MPa]	Label	*Total no. of cycles*	P_{fd} [kN]	P_{max} [kN]	P_{dm} [kN]	w_{fd} [mm]	w_u [mm]
Plates			PC_4	15	20.01	21.55	20.50	0.06	0.56
t_f = 1.4 mm	400	23.82	PC_5	40	19.00	19.49	19.00	0.35	0.63
b_f= 50 mm			PC_6	40	18.47	19.01	18.68	0.39	0.52
Sheets			SC_4	40	20.96	21.69	20.64	0.21	1.86
t_f = 0.166 mm	400	23.82	SC_5	40	20.45	20.74	20.16	0.20	1.75
b_f= 100mm			SC_6	300	20.14	22.11	20.72	0.42	1.81

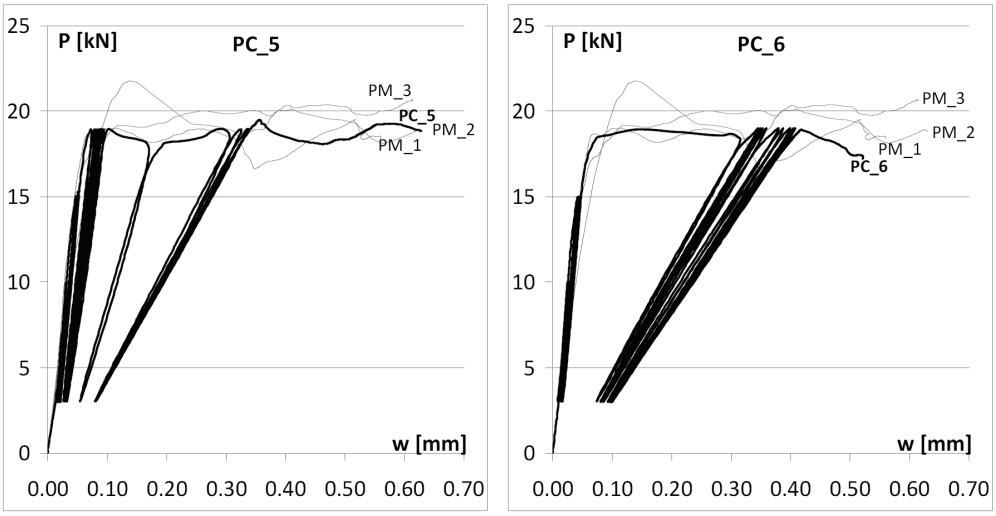

(a) Test PC_5 (b) Test PC_6

Figure 3.10 - Experimental load-displacement relationships

Note that the debonding phenomenon started in each case during the last series of cycles. Comparison with the counterpart monotonic tests (Table 3.3) shows that the cyclic actions reduced the debonding load by about 10%. Such a reduction in load probably corresponds to a reduction in the reinforcement bond length due to partial debonding of reinforcement during the load cycles, as better shown by profiles of strain and shear stresses reported in the following sections. By contrast, ultimate displacements recorded in monotonic and cyclic tests seemed approximately equal because they are the result of different strain profiles.

3.3.2.3 Cyclic tests on sheets with lb = 400mm

In order to compare the experimental results between plates and sheets, two tests on sheets (SC_4 and SC_5) were performed, adopting the same load path followed during tests PC_5 and PC_6 (see Table 3.2). The *P*-*w* relationships are reported in bold and compared to monotonic counterparts SM_1, SM_2 and SM_3 in Figure 3.11a,b: negligible residual displacements at the FRP-to-concrete interface were recorded after load-unload cycles up to 70% of $P_{max,M}$. On the other hand, residual displacements recorded during the last series of cycles were more meaningful (the mean value of the two tests was about 0.0177mm – 1.13% of $w_{u,M}$) but lower than the counterpart recorded on plates. Tests ended with a monotonic reloading path from 3kN up to failure. The first debonding was observed during this phase and the P_{fd} load value was slightly lower than those recorded during monotonic tests (SM_1, SM_2 and SM_3). As opposed to the experimental outcomes of tests on plates (PC_5 and PC_6) neither values of P_{dm} and P_{max} nor ultimate displacements, w_u, were significantly affected by cyclic actions on sheet-reinforced specimens (see Table 3.5).

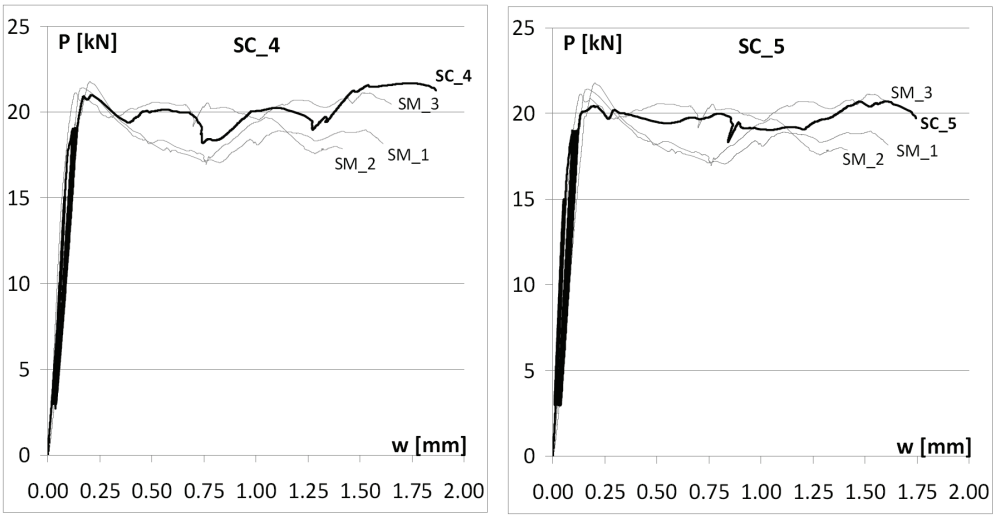

(a) Test SC_4 (b) Test SC_5

Figure 3.11 - Experimental load-displacement relationships

In order to evaluate the extent of the influence of cycle number at high load level on bond behavior, the load path of the SC_6 test (see Table 3.2) was

substantially different from the other cyclic tests: 300 load-unload cycles between 15 kN (about 70% of $P_{max,M}$) and 19 kN (about 90% of $P_{max,M}$). The test ended with a monotonic reloading path from 15% of $P_{max,M}$ up to failure. In this stage the maximum load (P_{max}) was 22.11 kN and the ultimate displacement (w_u) 1.81 mm (Figure 3.12).

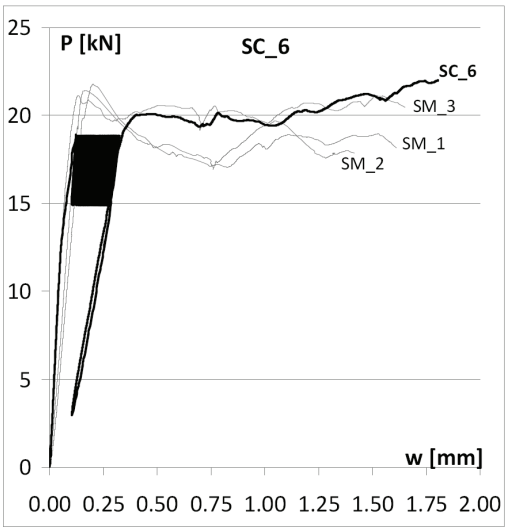

Figure 3.12 - Experimental load-displacement relationships: Test SC_6

After each load-unload cycle, residual displacements Δ were recorded. After 300 cycles the residual displacement was 0.0910 mm (5.88% of $w_{u,M}$). No significant exterior damage was recorded during the cyclic actions except for a very small crack after about 130 cycles. The main effect of the increased number of cycles was premature debonding at a load of 19 kN, about 10% less than $P_{fd,M}$ while no differences were observed in terms of P_{dm}, P_{max} and ultimate displacements w_u (see Table 3.5). Figure 3.13 and Figure 3.14 show the comparison between the P-w relationships recorded during the final monotonic reloading step of cyclic tests on plate- and sheet-reinforced specimens respectively.

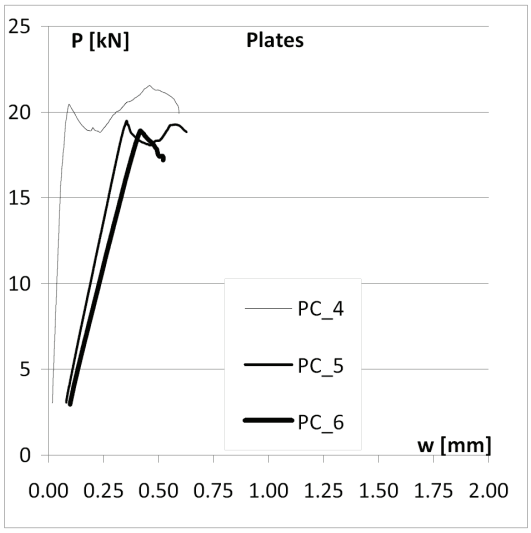

Figure 3.13 - Comparison of experimental P-w relationships: Plates lb=400mm

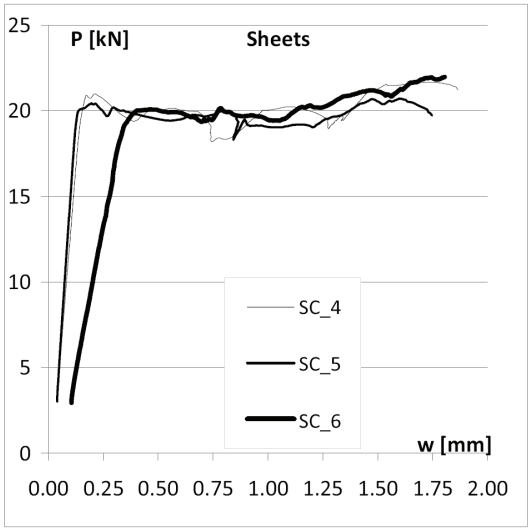

Figure 3.14 - Comparison of experimental P-w relationships: Sheet lb=400mm

The *P-w* relationship of cyclic test PC_4 shows negligible residual displacement after cyclic actions. Furthermore, the slope of the ascending branch, the first debonding P_{df} load value, the first debonding displacement w_{fd} value and ultimate displacement w_u were very close to those of their monotonic counterparts, as shown also in Table 3.3 and Table 3.5. However,

the *P-w* relationships of PC_5 and PC_6 tests showed a different trend: due to premature debonding, significant residual displacements were observed after cyclic actions of about 0.06 and 0.08 mm respectively (i.e. about 10% and 14% of $w_{u,M}$); the slope of the ascending branch was lower than that achieved in monotonic tests due to damage at the FRP-to-concrete interface. Finally, the debonding load was about 90% of $P_{max,M}$ (i.e. 19 kN).

As regards the tests performed on sheet-reinforced specimens, only on specimen SC_6 was a significant influence of the cyclic actions observed. The residual displacement recorded after the 300 cycles (about 0.10mm – 6.4% w_u, due to premature debonding) and the lower slope of the ascending branch confirmed damage at the FRP-to-concrete interface. Nevertheless, the ultimate displacement (w_u = 1.81 mm) and maximum load (P_{max} = 22.11 kN) were very close to those recorded on monotonic tests.

3.3.3 Axial strain and shear stress profiles

The behavior of the FRP-to-concrete interface was analyzed by plotting the experimental axial strains $\varepsilon_i(z)$ measured by means of strain gauges during the test along the FRP reinforcement (see Figure 3.4). The interface shear stresses $\tau_i(z)$ were evaluated by the following relationship between two strain gauges at distance Δz_i:

$$\tau_i = \frac{\varepsilon_{i+1} - \varepsilon_i}{\Delta z_i} \cdot E_f t_f \qquad (3.1)$$

where E_f and t_f are FRP Young's modulus and thickness, respectively. The most significant results related to tests performed on plates are summarized in Figure 3.15.

The strain profiles related to monotonic test PM_2 showed a maximum strain value $\varepsilon_{max} \approx 0.002$ (about 17% of ultimate strain provided by tensile flat coupon tests) at the loaded end of the CFRP plate; a decreasing trend with an approximately exponential law was recorded along the reinforcement except for the strains related to the debonding load value, P_{fd}. At this load the curvature of ε-z curve changes its sign at a shear stress peak value of about 5.5 N/mm^2 (see Figure 3.15a,b). By using the strain profile at P_{fd} an experimental effective bond length, l_{eff}, of about 150 mm may also be estimated..

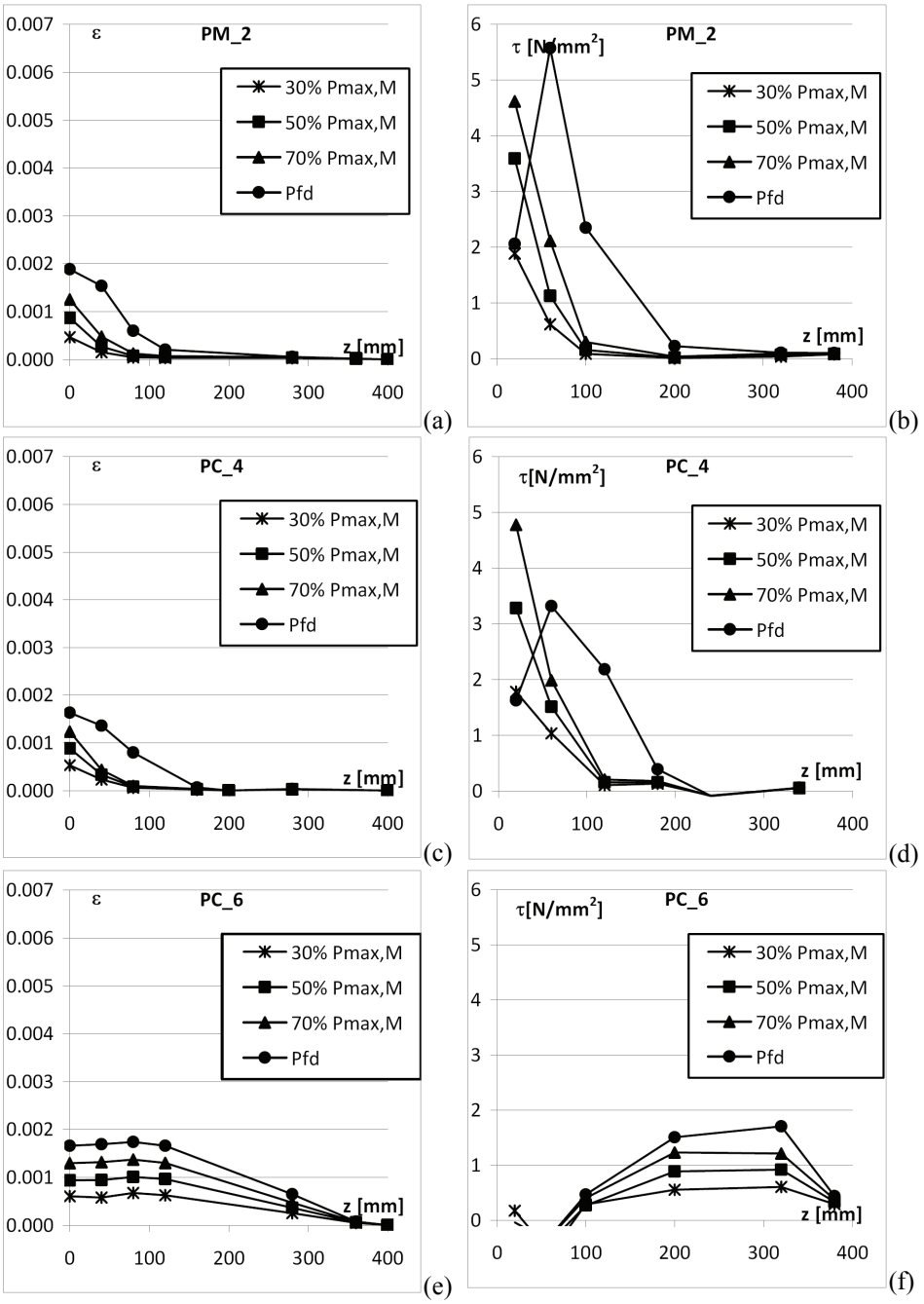

Figure 3.15 - Experimental strain and stress profiles: plates

Consistently with what observed by the *P-w* relationships, cyclic actions up to 70% of $P_{max,M}$ (test PC_4) did not particularly affect the interface behavior between concrete and the FRP plate as shown in Figure 3.15c. Indeed, we observed only a slight transfer of shear stresses along the interface with a reduction in the peak value (see Figure 3.15d). By contrast, test PC_6 clearly showed that cyclic actions up to 90% of $P_{max,M}$ caused premature debonding (see Figure 3.15e). In the wide zone of debonded FRP reinforcement the strain profiles assumed a constant trend and hence the corresponding shear stresses were equal to zero. Furthermore, the shear stress profiles in the remaining FRP-bonded zone were almost constant, lower than peak values recorded during monotonic tests (see Figure 3.15f). Moreover, Figure 3.15e,f confirms that during the cyclic phases of the test the FRP bond length l_b = 400mm, greater than the effective one, l_{eff} = 150mm, allowed the interface stresses to be transferred from initially loaded to unloaded zones.

The strain profiles recorded on sheet-reinforced specimens and the corresponding shear stress profiles are reported in Figure 3.16 on the left and right side respectively. The strain profiles of the SM_2 monotonic test (see Figure 3.16a) showed a lower experimental FRP sheet effective bond length (about 80mm) than that recorded during the counterpart PM_2 monotonic tests performed on plates (about 150mm). Furthermore, the maximum strain ($\varepsilon_{max} \approx 0.006$) was about 40% of ultimate strain provided by tensile flat coupon tests, clearly higher than that recorded during test PM_2 ($\varepsilon_{max} \approx 0.002$). Since plates are about eight times thicker than sheets and the ratio between Young moduli very close to unity (i.e. $E_{f,S}/E_{f,P}$=1.26), this result confirms that reinforcement thickness particularly affects debonding behavior. Indeed, the greater the thickness, the higher the increase in the shear and normal stresses at the FRP-to-concrete interface (Oehlers and Moran 1990, Tounsi et al. 2009). At different load levels, the shear stress profiles recorded on monotonic tests (see Figure 3.16b) followed a descending trend along the reinforcement with a maximum value at the loaded reinforcement end. With reference to the monotonic reloading step after cyclic action, Figure 3.16d clearly shows a migration of shear stresses at the interface within the effective bond length (80mm); such shear stress migration along the reinforcement increased after 300 cycles between 70% and 90% of $P_{max,M}$ (see Figure 3.16f) due to debonding propagation along the FRP-concrete interface.

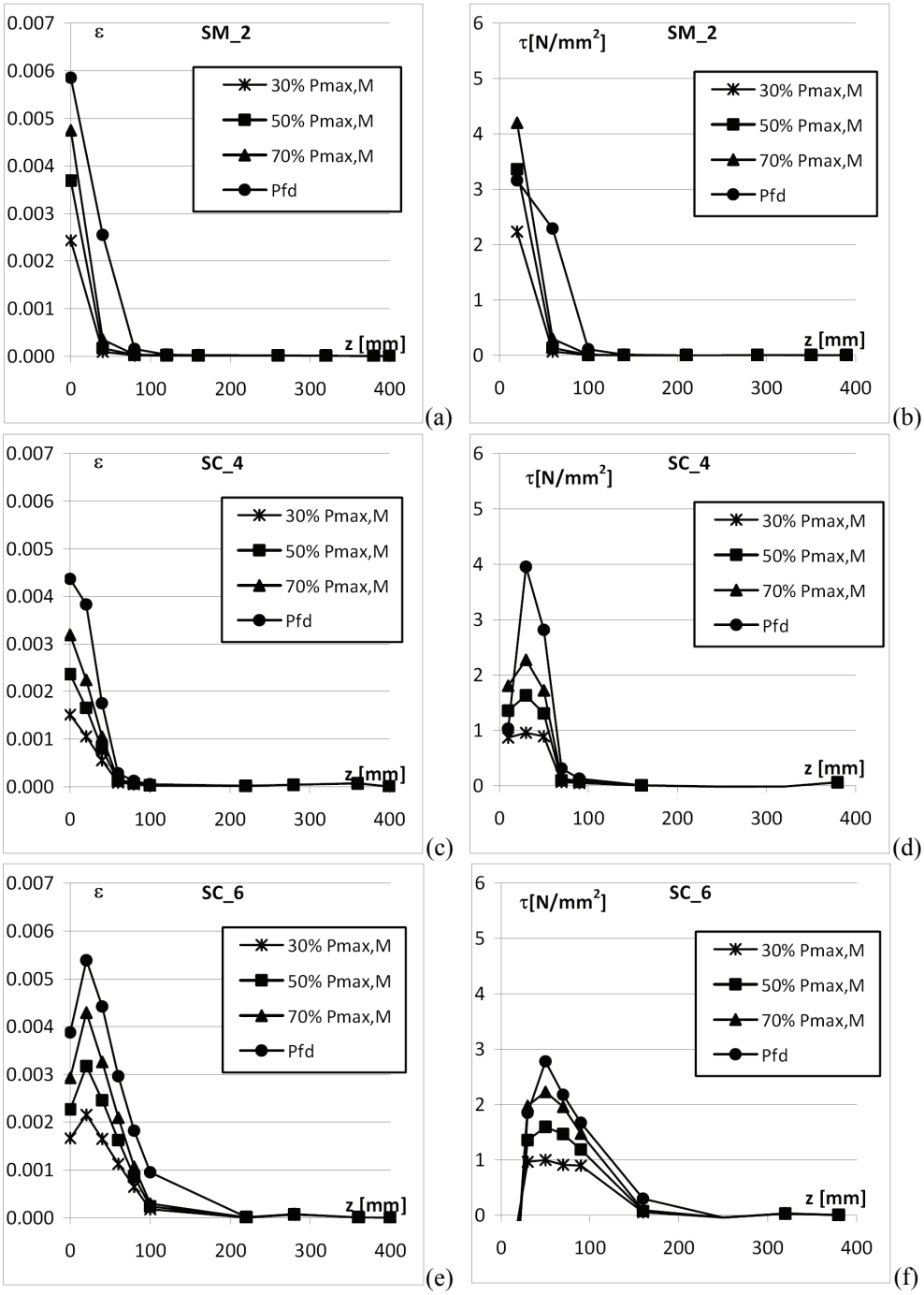

Figure 3.16 - Experimental strain and stress profiles: sheets

3.3.4 Influence of bond length

A further series of 16 SST tests (i.e. 12 monotonic and 4 cyclic tests) was performed to obtain insight into the influence of a low number of cycles (i.e. according to load path "b") on interface behavior at debonding by changing the reinforcement bond lengths, l_b. Effective bond lengths according to the relationships suggested by CNR-DT200/2004, $l_{e,CNR}$, by Teng et al. (2001), $l_{e,Teng}$ (recalled in ACI 440.2R-08,) by fib Bulletin 14, $l_{e,fib}$ as well as those adopted in the new series of tests are summarized in Table 3.6; the ratio $l_{b,Test}$ / $l_{e,CNR}$ is also reported in the right-hand column in Table 3.6.

Table 3.6 - Effective bond lengths

	$l_{e,CNR}$ (2004) [mm]	$l_{e,Teng\ (ACI)}$ (2001) [mm]	$l_{e,fib}$ (2001) [mm]	$l_{b,Test}$ [mm]	$l_{b,Test}$ / $l_{e,CNR}$ %	$l_{b,Test}$ / $l_{e,Teng\ (ACI)}$ %	$l_{b,Test}$ / $l_{e,fib}$ %
Sheet				100	95	110	78
t_f = 0.16 mm	105	91	128				
b_f = 100mm				50	47.5	55	39
Plate				250	95	110	78
t_f = 1.4 mm	262	227	320				
b_f= 50 mm				125	47.5	55	39

The first debonding load, P_{fd}, and the maximum load recorded during tests, P_{max}, are reported in Table 3.7 and Table 3.8 for monotonic and cyclic tests, respectively.

Experimental load-displacement relationships in tests performed on plate-reinforced specimens PM_7, PM_8, PM_9 (l_b = 250 mm) and PM_13, PM_14, PM_15 (l_b = 125 mm) are shown in Figure 3.17a,b, respectively. The same relationships are reported for sheet-reinforced specimens SM_7, SM_8, SM_9 (l_b = 100 mm) and SM_13, SM_14, SM_15 (l_b = 50 mm) in Figure 3.18a,b, respectively.

As shown in Table 3.7, P_{max} values recorded in tests performed on plates clearly point out that bond length l_b = 125 mm led to debonding loads very close to those recorded on 250 mm bonded plates. By contrast, P_{max} values recorded on 50-mm bonded sheet-reinforced specimens were lower than those achieved with l_b = 100mm. Moreover, Figure 3.15a and Figure 3.16a show

that the effective bond lengths (l_{eff}) experimentally evaluated in monotonic tests with l_b = 400 mm were about 150 mm and 80 mm for plates and sheets, respectively. Such values were computed with reference to the strain profiles related to the post-elastic stage of bond behavior. Thus the design equations provided by the technical literature and the main international codes for evaluating effective bond lengths proved conservative, especially for plate-reinforced specimens.

Table 3.7 - Experimental debonding load values - Monotonic tests

FRP type	l_b [mm]	f_{cm} [MPa]	Label	P_{max} kN	$P_{max,M}$ kN	P_{fd} kN	$P_{fd,M}$ kN
Plate t_f = 1.4 mm b_f= 50 mm	250	21.23	PM_7	19.02	18.77	17.28	17.36
			PM_8	19.84		18.02	
			PM_9	17.46		16.79	
	125	21.23	PM_13	19.46	19.83	19.46	19.83
			PM_14	19.30		19.30	
			PM_15	20.73		20.73	
Sheet t_f = 0.166 mm b_f = 100mm	100	21.23	SM_7	19.40	20.79	19.40	20.79
			SM_8	20.38		20.38	
			SM_9	22.60		22.60	
	50	21.23	SM_13	16.88	19.03	16.88	17.99
			SM_14	21.19		18.08	
			SM_15	19.02		19.02	

Table 3.8 - Experimental debonding load values – Cyclic tests

FRP type	l_b mm	f_{cm} [MPa]	Label	P_{fd} kN
Plates t_f = 1.4 mm b_f= 50 mm	250	21.23	PC_10	17.14
	125	21.23	PC_16	19.98
Sheets t_f = 0.16 mm b_f = 100mm	100	21.23	SC_10	20.71
	50	21.23	SC_16	18.03

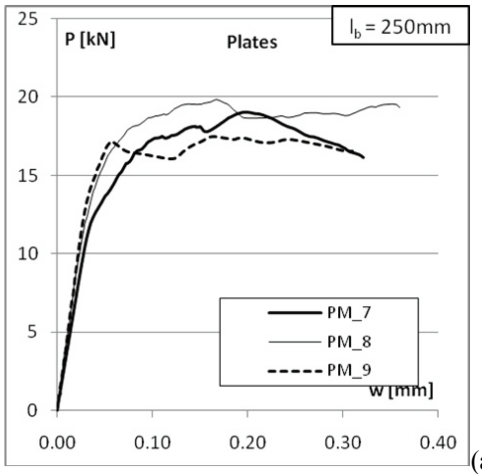

Figure 3.17 - Experimental load-displacement relationships: Plates (a) l_b=250mm (b) l_b=125mm

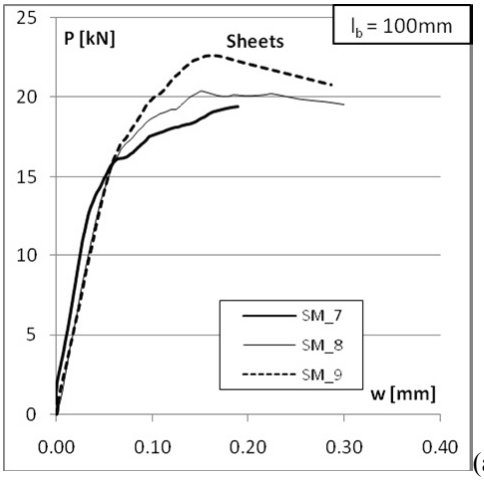

Figure 3.18 - Experimental load-displacement relationships: Sheets (a) l_b=100mm (b) l_b=50mm

The experimental load-displacement relationships related to cyclic tests performed on plate-reinforced specimens PC_10 and PC_16 and sheet-reinforced specimens SC_10 and SC_16 are reported in bold and compared with those related to equivalent monotonic tests in Figure 3.19 and Figure 3.20, respectively. After cycling, bonding behavior very similar to monotonic tests was observed during the final monotonic load path. Even if the reinforcement bond lengths were significantly low (i.e. about 50% of the theoretical effective one), cyclic test outcomes confirmed that the influence of

load-unload cycles up to 70% of $P_{max,M}$ was negligible for CFRP sheets and plates. This effect was due to the elastic behavior characterizing the FRP-concrete interface up to the above load level. Moreover, a further low number of load-unload cycles (i.e. 10 cycles) up to 90% of $P_{max,M}$ did not particularly affect the bonding capacity of CFRP reinforcement.

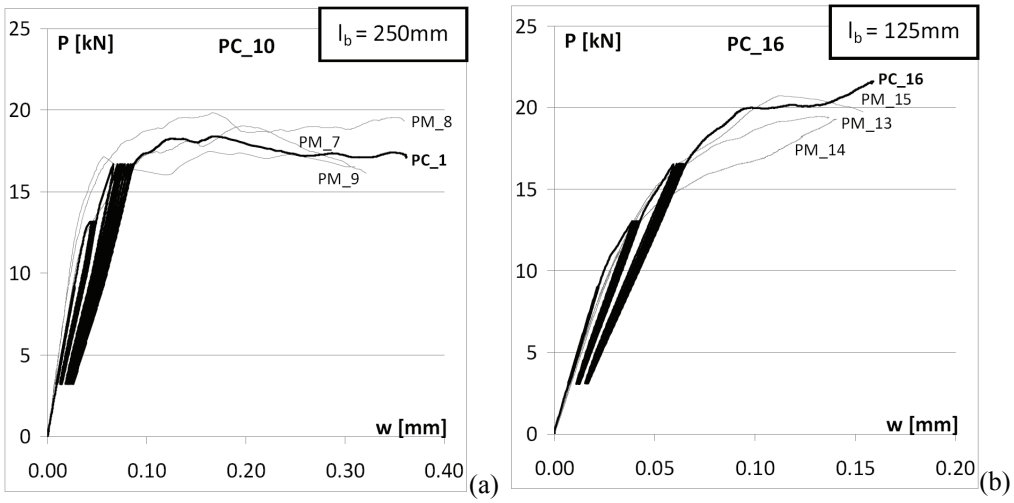

Figure 3.19 - Experimental load-displacement relationships: Plates (a) l_b=250mm (b) l_b=125mm

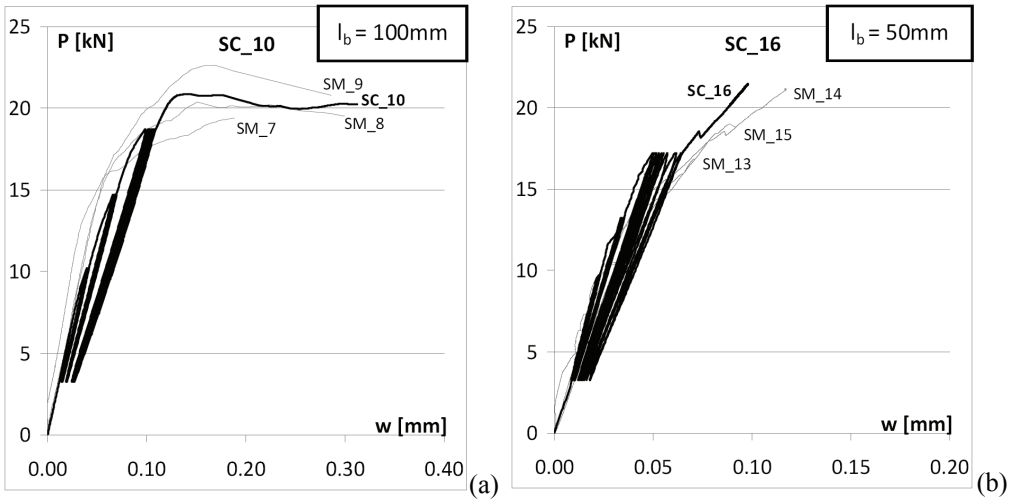

Figure 3.20 - Experimental load-displacement relationships: Sheets (a) l_b=100mm (b) l_b=50mm

3.3.5 Summary and conclusions

Compared with monotonic tests, there have been few bond tests under cyclic actions performed on CFRP sheets applied on concrete blocks. Particularly lacking are cyclic tests performed on CFRP plates and few studies are available on debonding phenomena under few cycles at high force levels, which typically occur during earthquakes. A series of cyclic SST bond tests under both monotonic and cyclic actions, without inversion of action sign, were performed to analyze both the influence of different load paths (few cycles, typical of seismic actions) and the effect of FRP bond lengths on bond behavior between FRP reinforcement and the concrete substrate. The experimental outcomes showed the following:

- the influence of few load-unload cycles up to 70% of $P_{max,M}$ was negligible in terms of bond stiffness and strength for CFRP sheets both for higher and lower bond lengths than theoretical effective ones); similar results were obtained for plates, even if experimental effective bond lengths were significantly lower than theoretical ones;
- a small number of load-unload cycles (i.e. a total of 40 cycles) up to 90% of $P_{max,M}$ induced shear stress migration along the reinforcement with a reduction in peak values due to interface damage; however, this phenomenon did not substantially affect debonding loads in the case of bond lengths exceeding the effective ones;
- the design equations provided by the main international codes to predict the effective bond lengths were in good agreement with experimental results for sheets and more conservative for plates. Indeed, experimental effective bond lengths obtained by strain readings were lower (about 150mm) than theoretical ones (between 227mm and 320mm);
- experimental tests showed that the reduction in bond length up to about 50% of the theoretical effective length induced a comparable reduction in maximum debonding load on specimens subjected to monotonic or cyclic action.

3.4 BOND TESTS ON FRP SHEETS AND PLATES

Further tests performed on concrete specimens reinforced with CFRP plates under monotonic actions, in order to significantly enrich the existing database of tests on EBR carbon plates are reported in this section.

The experimental tests were carried out in the framework of a Round Robin Tests organized by Laboratories University Network of seismic engineering (ReLUIS) supported by the Department of the Civil Protection (Reluis 2005 Grant – Task 8: Innovative materials for the vulnerability mitigation of existing structures) and a Round Robin Tests organized by the European Network for Composite Reinforcement supported by the fib Task Group 9.3.

3.4.1 Experimental program for bond tests on plates (Italian RRT)

A total of 12 SST tests were performed on CFRP plates (6) and sheets (6) applied on longitudinal faces of concrete prisms. Concrete mix was specifically designed to obtain low compressive concrete strength to simulate the FRP application on existing concrete. Compressive tests were performed at 28 days after casting: the cylinder mean strength, f_{cm}, was equal to 26.00 MPa.

CFRP Young's moduli, E_f, were obtained by means of tensile flat coupon tests on CFRP sheets and plates respectively: their mean values were about 180 GPa for plates and about 240 GPa for sheets (see Table 3.9).

Prior to FRP installation, the concrete surface was treated by sand blasting in order to eliminate the mortar till the aggregate became clear. Primer was always used to consolidate the concrete surface.

Tests were carried out under a servo-hydraulic testing machine (MTS810) with displacement control. The specimens were positioned vertically and blocked in the machine by using a steel frame: a C-shaped upper flange was connected to the reacting element by means of four steel rods. The system has been designed to minimize the eccentricity between the traction axis and the reaction element (see Figure 3.21). Metallic tabs were installed at the end of FRP reinforcement in order to guarantee an adequate clamping in the test machine grip. Several strain gauges were applied along the FRP laminates in

order to measure axial strains during the bond test (see Figure 3.21). The main parameter of experimental tests (i.e. concrete compressive strength, specimen width, FRP type and geometry) are summarized in Table 3.9

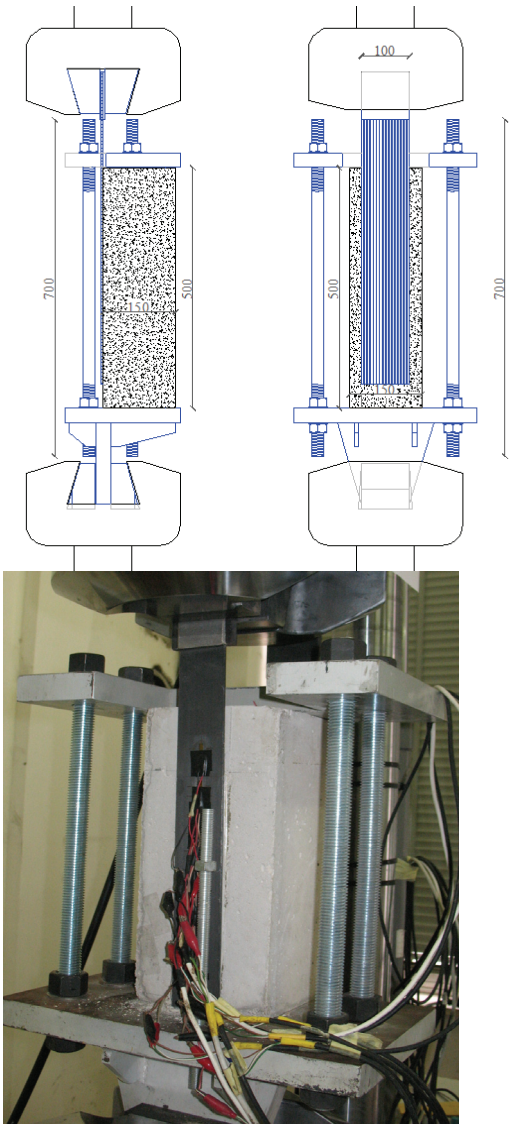

Figure 3.21 - Test Set-up

3.4.1.1 Debonding load and failure modes

The failure load, P_{test}, recorded during the tests are summarized in Table 3.9. Moreover, the experimental behavior of FRP-to-concrete interface was analyzed by plotting the experimental axial strains $\varepsilon_i(z)$ measured by means of strain gauges along the FRP reinforcement; in particular, the strain profiles recorded at the first debonding load value, P_{fd}, are reported for each test in Figure 3.22 and Figure 3.23, for sheets and plates, respectively.

Table 3.9 - Experimental debonding load values.

	Concrete cylinder mean strength	**Concrete prism width**	**FRP Young modulus**	**FRP width**	**FRP height**	**FRP bond length**	**Test failure load**	**Fiber type**
Label	f_{cm}	b_c	E_f	b_f	t_f	l_b	P_{test}	
	[MPa]	[mm]	[MPa]	[mm]	[mm]	[mm]	[kN]	
V1a	26.00	150	180000	80	1.200	400	30.14	plate
V2a			180000	80	1.200	400	33.56	plate
V3a			180000	80	1.200	400	32.47	plate
V1b			180000	80	1.200	100	28.33	plate
V2b			180000	80	1.200	100	27.58	plate
V3b			180000	80	1.200	100	30.29	plate
V18a			241000	100	0.166	400	24.00	sheet
V19a			241000	100	0.166	400	24.96	sheet
V20a			241000	100	0.166	400	23.65	sheet
V18b			241000	100	0.166	100	21.84	sheet
V19b			241000	100	0.166	100	21.49	sheet
V20b			241000	100	0.166	100	21.91	sheet

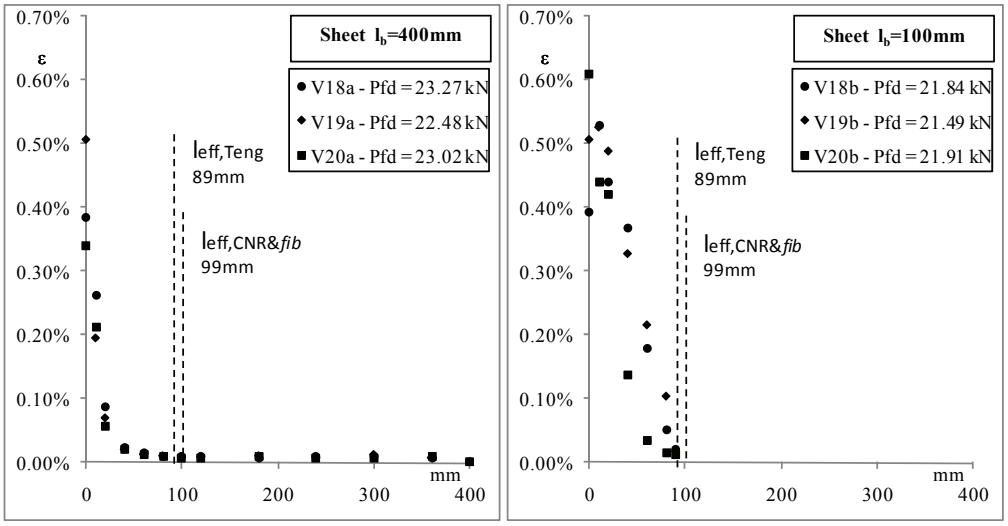

(b) (d)

Figure 3.22 - Strain profiles along FRP sheets: bond lengths 400mm (a) and 100 mm (b)

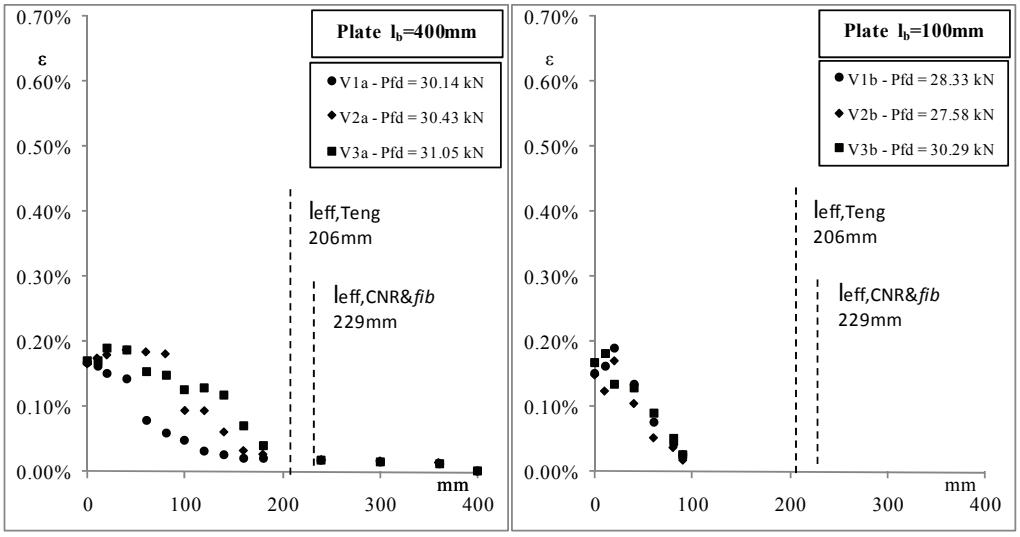

(a) (b)

Figure 3.23 - Strain profiles along FRP plates: bond lengths 400 mm (a) and 100 mm (b)

Figure 3.22a,b shows the strain profiles for sheets reinforcement characterized by bond length, l_b, equal to 400mm and 100 mm respectively. The strain profiles showed in each case a decreasing trend with an approximately exponential law along the reinforcement. The maximum strain at FRP loaded end ranged between 0.39%-0.62% and rapidly dropped to zero along the reinforcement. In particular, the distance from FRP end at which strains equal to zero are recorded represents the experimental effective bond length value, l_{eff}. This effective bond length resulted in each case lower than 100 mm. Such result is consistent with the theoretical effective bond length values computed according to the relationships suggested by CNR-DT200/2004 and *fib* bulletin 14, $l_{eff,CNR\&fib} = \sqrt{\frac{E_f \cdot t_f}{2 \cdot f_{ctm}}}$, and by Teng et al. 2001, $l_{e,Teng}$ (recalled in ACI 440.2R-08), $l_{eff,Teng} = \sqrt{\frac{E_f t_f}{\sqrt{f_{cm}}}}$) ranging between 89 mm and 99 mm.

Strain profiles recorded along FRP plates at debonding loads are reported in Figure 3.23a,b for bond length equal to 400 mm and 100 mm respectively. The maximum strain at FRP loaded end ranged between 0.10%-0.20%. They were significantly less than those recorded in the case of sheets (i.e. more than 3 times), also in the case of bond length higher than the theoretical effective ones, varying in the range of 206 mm -229 mm. Such result is clearly due to the higher stiffness of plates; indeed, the FRP stiffness, $E_f t_f$, is the main parameter influencing the effective strain reduction in the debonding phenomenon (i.e. the maximum strain due to debonding is proportional to the factor $\sqrt{1/(E_f t_f)}$). However, considering that the ratio $\left(\sqrt{1/(E_f t_f)}\right)_{sheets} / \left(\sqrt{1/(E_f t_f)}\right)_{plates}$ of FRP reinforcements investigated in the experimental tests is about 2.50, it is clear that the use of plates strongly influences the performances of reinforcement in terms of debonding strain. Indeed, the greater the thickness, the higher the increase in the normal and shear stresses at FRP to concrete interface and consequently the probability of premature debonding occurrence (Oehlers and Moran, 1990; Tounsi et al., 2009).

3.4.2 Experimental program for bond tests on plates (European RRT)

The experimental program consisted in 18 bond tests on plates. Concrete specimens were made up with the same nominal dimensions and cast in the same batch: width b_c = 160 mm, height h_c = 200 mm and length l_c = 400 mm.

A low concrete strength was used in this experimental program to simulate the application on existing RC buildings in which poor quality concrete is usually found. For 1 m^3 of concrete the following components were used: 1250 kg of gravel 4/14, 965 kg of coarse sand, 350 kg of Cem I 42.5 and 230 kg of water. Three compressive tests were performed on cylinder specimens at 28 days after casting: the cylindrical mean compressive strength was f_{cm} = 19 MPa and the mean Young's modulus was 18.6 GPa. Further compressive tests carried out on concrete cubes (side 150 mm) 200 days after casting (i.e. at test time) gave a mean cubic strength R_{cm} = 23 MPa; three-point bending tests provided a mean tensile strength equal to f_{ctm} = 2.5 MPa. Two opposite sides of each concrete specimen were strengthened, but each reinforcement was tested separately. Thus each concrete specimen was used for two tests.

The test setup is depicted in Figure 3.24a; a Single Shear Test (SST) was adopted in order to reduce the effects of detailing. Indeed, the SST is the most commonly used test (Yao et al., 2005; Ferracuti et al., 2008; Savoia et al., 2009; Dai et al., 2005;Wu et al., 2001), even if additional stresses may be induced in the FRP external reinforcements due to a possible eccentricity of the applied load. However, for FRP sheets, it was shown (Yao et al., 2005) that low rotations (about 2°) do not significantly influence the results in terms of debonding load. For laminates the influence of detailing could be greater, but lower than 10% as shown by literature bond tests (Savoia et al., 2009).

The bond tests were carried out with a servo-hydraulic testing machine; steel pipes were installed at the end of FRP reinforcement in order to ensure adequate clamping in the grips of the testing machine. The specimen was blocked at the lower base of the testing machine by a couple of steel bars embedded in the concrete prism and bolted to a system of steel plates fixed in the lower grips. According to this set-up, the concrete block was also loaded in tension too (pull-pull SST - i.e. test setup c, see 3.1). All tests were performed in displacement control with a speed of 0.003 mm/s. Several strain gauges were applied along both types of FRP reinforcements in order to measure axial strains (see Figure 3.24b).

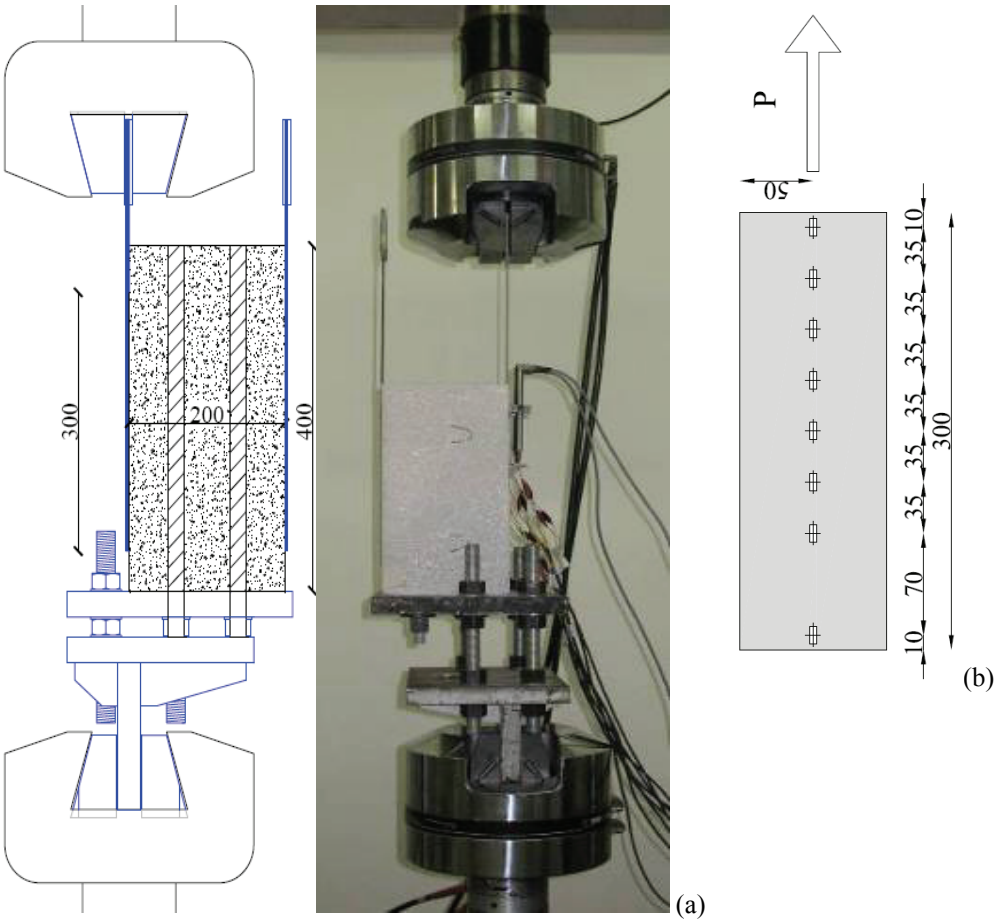

Figure 3.24 - (a) Test setup; (b) Strain gauge positions (dimensions in mm)

The bond tests on EBR systems were carried out on concrete prisms strengthened by six different types of CFRP plates (3 tests per plate type). The notation of specimens is A-x-y, where A refers to the reinforcement material ("C" for carbon), x identifies plates thickness, t_f, and width, b_f, and y distinguishes the ordinal number of tests ("1", "2" or "3"), as given in Table 3.10. The plates' bonded length was in every case l_b = 300 mm. Before the application of the FRP reinforcement, the concrete surface was first treated by bush hammering. Note that the primer installation on concrete surface was adopted only for C-1.70x100 as explicitly suggested by the manufacturer.

Table 3.10 - FRP geometrical and mechanical properties (EBR)

Label	E_f (CoV) [GPa]	t_f [mm]	$E_f \cdot A_f$ [kN]	f_{fu} (CoV) [MPa]	Adhesive Type
C-1.30x60	175 (1%)	1.30	13650	3194 (3%)	A
C-1.60x100	109 (15%)	1.60	17440	1453 (9%)	B
C-1.20x100	166 (4%)	1.20	19920	3011 (2%)	C
C-1.25x100	171 (2%)	1.25	21375	2856 (10%)	A
C-1.70x100	141 (1%)	1.70	23970	2637 (3%)	D
C-1.40x100	221 (4%)	1.40	30940	2955 (5%)	A

All plates were glued with the epoxy adhesives recommended and supplied by the manufacturers; specialized workers prepared the mixtures and applied the FRP systems. As concerns the FRP systems glued with the same resin, only one mixture was produced in order to make the bond procedure uniform. According to the manufacturers' technical sheets the tensile strength of adhesives ranged between 25-30 MPa, Young's modulus in tension between 4500-5000 MPa, and the compressive strength greater than 90 MPa.

The main geometrical and mechanical parameters of FRP plates are summarized in Table 3.10: Young's modulus, E_f, thickness t_f, axial stiffness, $E_f \cdot A_f$, and tensile strength, f_{fu}. The mechanical properties are the averages obtained by experimental tensile tests on five specimens; in particular, Young's modulus was computed referring to strains in the range of 0.1-0.3%. The variation coefficients (CoV) are also reported in brackets on Table 3.10; specimens are listed by increasing axial stiffness. The width of the reinforcement was b_f = 100 mm for all specimens except for the type C-1.30x60 for which b_f = 60 mm; this corresponds to shape ratios b_f/b_c of 0.63 or 0.38.

3.4.2.1 Debonding load and failure modes

The experimental maximum loads, P_{max}, recorded on each specimen are reported in Table 3.11 along with the mean value of the maximum load, $\overline{P_{max}}$, and the CoV of each triplet of specimens. Table 3.11 also reports the mean values of the maximum laminate tensile stress, f_{fd}, the efficiency factor defined as $\eta = f_{fd} / f_{fu}$ and the average shear stresses, $\overline{\tau_{max}}$ computed by dividing the mean failure load by the whole bonded surface ($b_f x\ l_b$) of plates.

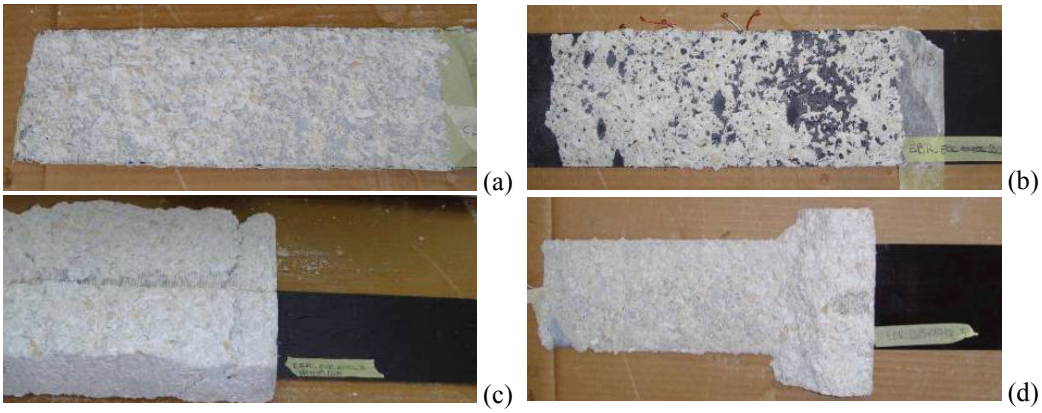

Figure 3.25 - Debonding mode of EBR specimens: a) debonding in concrete (DB/C); b) debonding at laminate adhesive interface (DB-E); c) splitting of concrete (SP); d) debonding in concrete + splitting of concrete (DB-C/SP).

Table 3.11 - Experimental debonding loads for EBR systems

Specimen	Failure mode	P_{max} [kN]	$\overline{P_{max}}$ [kN]	CoV [%]	f_{fd} [MPa]	η [%]	$\overline{\tau_{max}}$ [MPa]
C-1.30x60-1	DB-C	33.18					
C-1.30x60-2	DB-C/E	29.86	31.64	5.3	406	13	1.76
C-1.30x60-3	DB-C	31.88					
C-1.60x100-1	DB-C/E	49.41					
C-1.60x100-2	DB-C/E	39.87	44.64	15.1	279	19	1.49
C-1.60x100-3	SP	47.72*					
C-1.20x100-1	DB-C	49.85					
C-1.20x100-2	DB-C	48.05	50.17	4.6	418	14	1.67
C-1.20x100-3	DB-C/SP	52.60					
C-1.25x100-1	DB-C	41.25					
C-1.25x100-2	DB-C	38.14	39.70	5.5	318	11	1.32
C-1.25x100-3	SP	32.68*					
C-1.70x100-1	DB-C	54.79					
C-1.70x100-2	SP	51.41*	54.68	0.3	322	12	1.82
C-1.70x100-3	DB-C	54.57					
C-1.40x100-1	DB-C	48.40					
C-1.40x100-2	DB-C	35.90	45.98	19.8	328	11	1.53
C-1.40x100-3	DB-C	53.64					

DB-C = debonding in concrete, DB-E = debonding at plate/epoxy interface, SP = splitting of concrete
* not considered in the mean value of debonding strength because of splitting failure

Typical debonding failures with detachment of a thin layer of concrete were observed on most specimens (see Figure 3.25); in few cases was splitting failure in the concrete block observed. Note that the failure loads corresponding to splitting failure were not taken into account for the calculation of the average bond strength, $\overline{P_{max}}$. Low η values were attained in each case (i.e. in the range of 11%-20%).

The maximum experimental scatter is about 5% for four types of plates, while it is 15% and 20% for the C-1.60x100 and C-1.40x100 types, respectively. As concerns C-1.60x100, this scatter seems to be related to the product itself as confirmed by the scatter recorded also for Young's Modulus (see Table 3.10). As regards C-1.40x100, a similar scatter had already been found by tests performed elsewhere on identical specimens in the framework of the same RRT (personal communication by Mazzotti C., 2010).

In Figure 3.26 the effectiveness of each EBR type against plate axial stiffness ($E_f A_f$) is plotted; the graph indicates an ascending trend for values of $E_f A_f$ lower than 20,000 kN; for higher values of $E_f A_f$ the trend becomes quite constant.

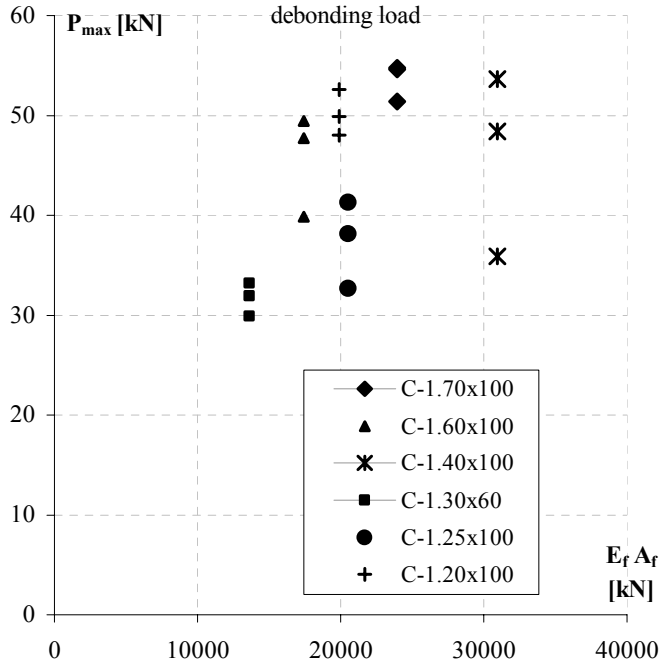

Figure 3.26 - Experimental loads vs. $E_f A_f$

The results of specimens C-1.30x60 and C-1.25x100, produced by the same manufacturer and bonded with the same adhesive, indicate that, for very similar values of E_f and t_f, the use of plates with a larger width (i.e. 100 mm vs. 60 mm) induced a load increase of only 25%. The non-proportional increase in bond strength with the area of the FRP reinforcement is related to the non-proportional growth of the concrete involved in the stress transfer. This effect in the theoretical formulation is generally taken into account by the shape factor (Yao et al., 2005).

Moreover, the failure loads of C-1.25x100 are anomalous compared with plate C-1.20x100, which is supplied by a different manufacturer and applied with a different adhesive: the latter is slightly stiffer than the former, but showed a failure load 20% larger. This anomalous behavior, clearly shown in Figure 3.26, is probably due to the different adhesive properties, as discussed in the following.

Finally, plates C-1.60x100 and C-1.40x100 attained similar debonding loads (i.e. about 45-46 kN, see Table 3.11), even if the axial stiffness of the latter is significantly higher (+75%). It is worth noting that plate C-1.40x100 is glued with the same adhesive as C-1.25x100.

3.4.2.2 Load - displacement behavior

The experimental load-slip (*P-s*) curves are reported in Figure 3.27 for each specimen; the experimental curves of specimens of each series were very low scattered. The slip is computed by integrating the experimental strains recorded by strain gauges applied on the plates.

An initial linear branch was observed on almost all the experimental curves up to about 25 kN-30 kN. At this load, except for C-1.25x100 and C-1.40x100, a sudden increase in slip is recorded probably due to initial local plate debonding.

Plates C-1.40x100, C-1.25x100, C-1.30x60 are produced by the same manufacturer and glued with the same adhesive. *P-s* curves show that plate C-1.40x100 is more deformable than C-1.60x100 despite its higher stiffness and plate C-1.25x100 is more deformable than C-1.20x100 which has comparable axial stiffness. Thus, the adhesive may well be the cause of the different behaviour of these plates compared with other similar types.

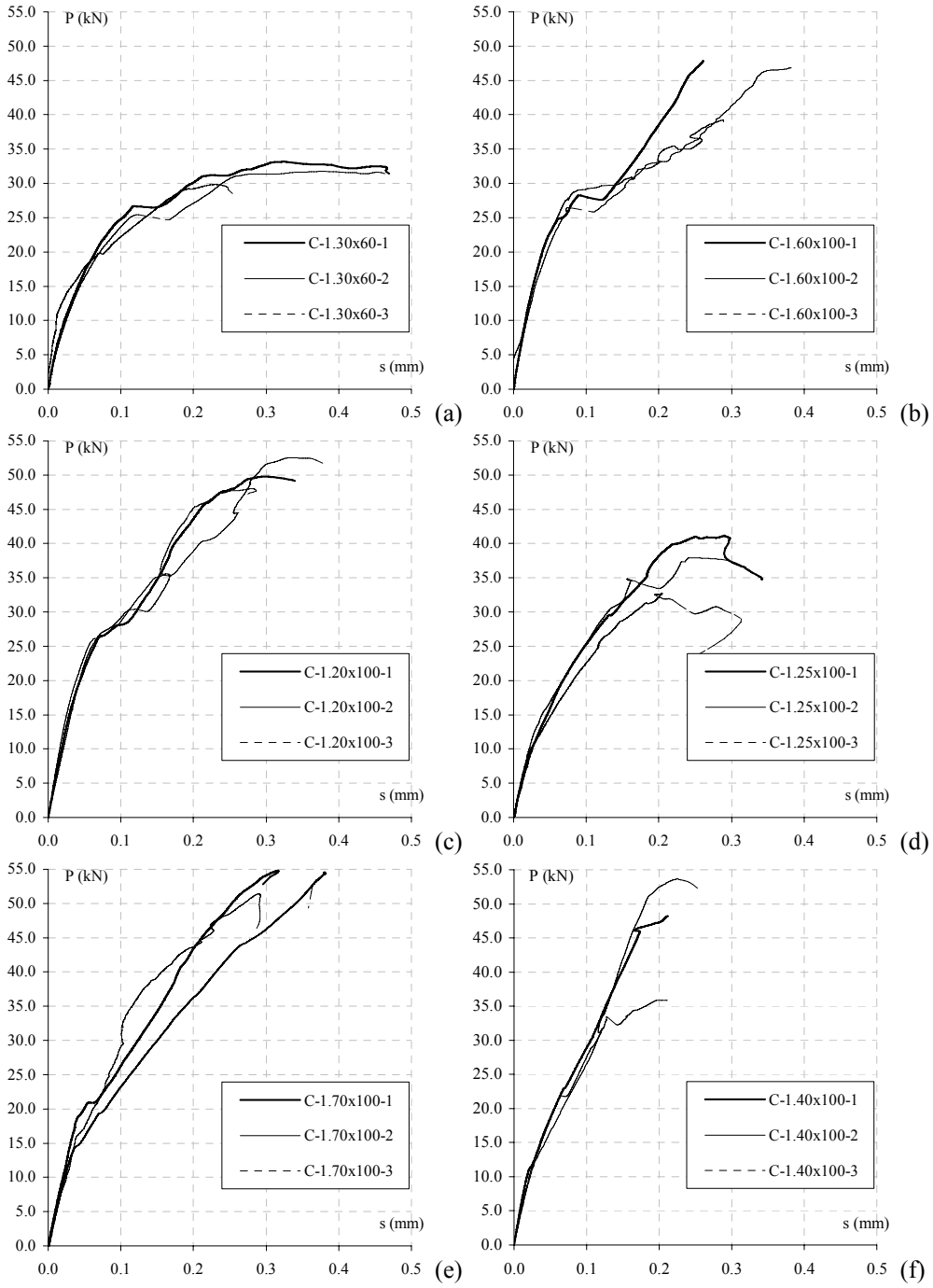

Figure 3.27 - Experimental loads plotted vs. displacements

In Figure 3.28 the mean shear stress, $\tau = P/\left(b_f \cdot L_b\right)$, is plotted versus the normalized slip, $s^* = \left(P_{\max} \cdot L_b\right)/\left(E_f \cdot A_f\right)$. This normalization allows us to annul the differences in slopes evidenced in the *P-s* curves due to the axial stiffness of the reinforcements, hence to highlight only the effect of the b_f/b_c ratio (Figure 3.28a, specimens with different widths and same adhesive) or only the adhesive (Figure 3.28b, specimens with different adhesive and same width). In particular, Figure 3.28a shows that, when the b_f/b_c ratio decreases (C-1.30x60), the concrete volume per unit of FRP width involved in the bond mechanism is greater and hence the stiffness of the whole concrete-FRP system increases. Moreover, Figure 3.28b shows that plate C-1.60x100, despite its lower axial stiffness, shows a stiffer global behaviour.

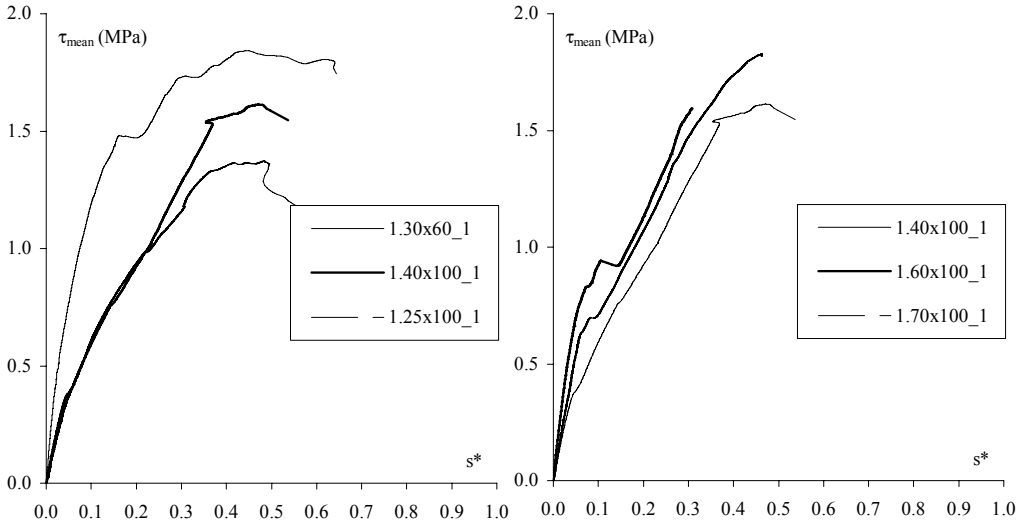

(a) (b)

Figure 3.28 - Normalized load-slip curves:
a) specimens glued with the same adhesive;
b) specimens with the same width.

3.4.2.3 Distribution of strains

The strain profiles along the reinforcement are plotted in Figure 3.29 for one specimen of each triplet and at different loads (i.e. for a load step of 5 kN up to failure). Note that the first point is not a strain gauge record but it is

computed as P/E_fA_f. Figure 3.29 shows that starting at loads of about 25-30 kN in most specimens, the first strain gauge applied on the bonded length starts providing strains very close to the P/E_fA_f ratio; this means the shear stress-slip law is at the end of the softening stage, hence the beginning of debonding in this part. Moreover, in the following 40 mm the shear stress-slip law is in the softening stage and thus the stress transfer is still active. By contrast, at the same load a significant increase in strains in the plates' central part (i.e. 50-150 mm from the loaded end) is observed. In this part the strain distribution becomes almost constant, meaning that the shear stresses are no longer transferred. Finally, the strain profile at the end (150 – 300 mm from the loaded end) shows that the bond mechanism is still in the elastic phase. Therefore, the strain distribution in the central part of the plates seems to be anomalous. This behavior could be caused by a macro-cracking in the concrete block that occurs at about 25-30 kN and between 50 and 100 mm. Indeed, macro-cracks form when the tensile strength of concrete is exceeded because of the tensile load applied to the specimen. Moreover, due to this loading condition, specimens strengthened with C-1.25x100 and C-1.40x100 show significant strains at the end as well (see Figure 3.29d and f).

However, in most specimens, at 25-30 kN the strain distribution moves along the plate up to 200-250 mm and the strains at the end of the plate are very low at the failure condition too. This means that the bonded length (300 mm) is comparable with the effective one (fib bulletin 14, 2001, Chen and Teng, 2001).

3.4.3 Summary and conclusions

The experimental bond tests presented in this section showed that the maximum efficiency of CFRP plates was only 20%. In general the increasing of stiffness leads to have higher loads, but a loss of efficiency; indeed larger transversal area do not lead to have a proportional increasing of ultimate load.

Moreover, higher values of thickness cause a larger scatter of results, the debonding load is not directly proportional with the reinforcement stiffness, and lower values of the ratio bf/bc do not determine proportional reduction of load.

Therefore the experimental results have showed that the effectiveness of the strengthening system has to be evaluated also in function of the axial stiffness: very high values of stiffness can be not useful to increase sensibly the failure load of the strengthened elements and can be uneconomical.

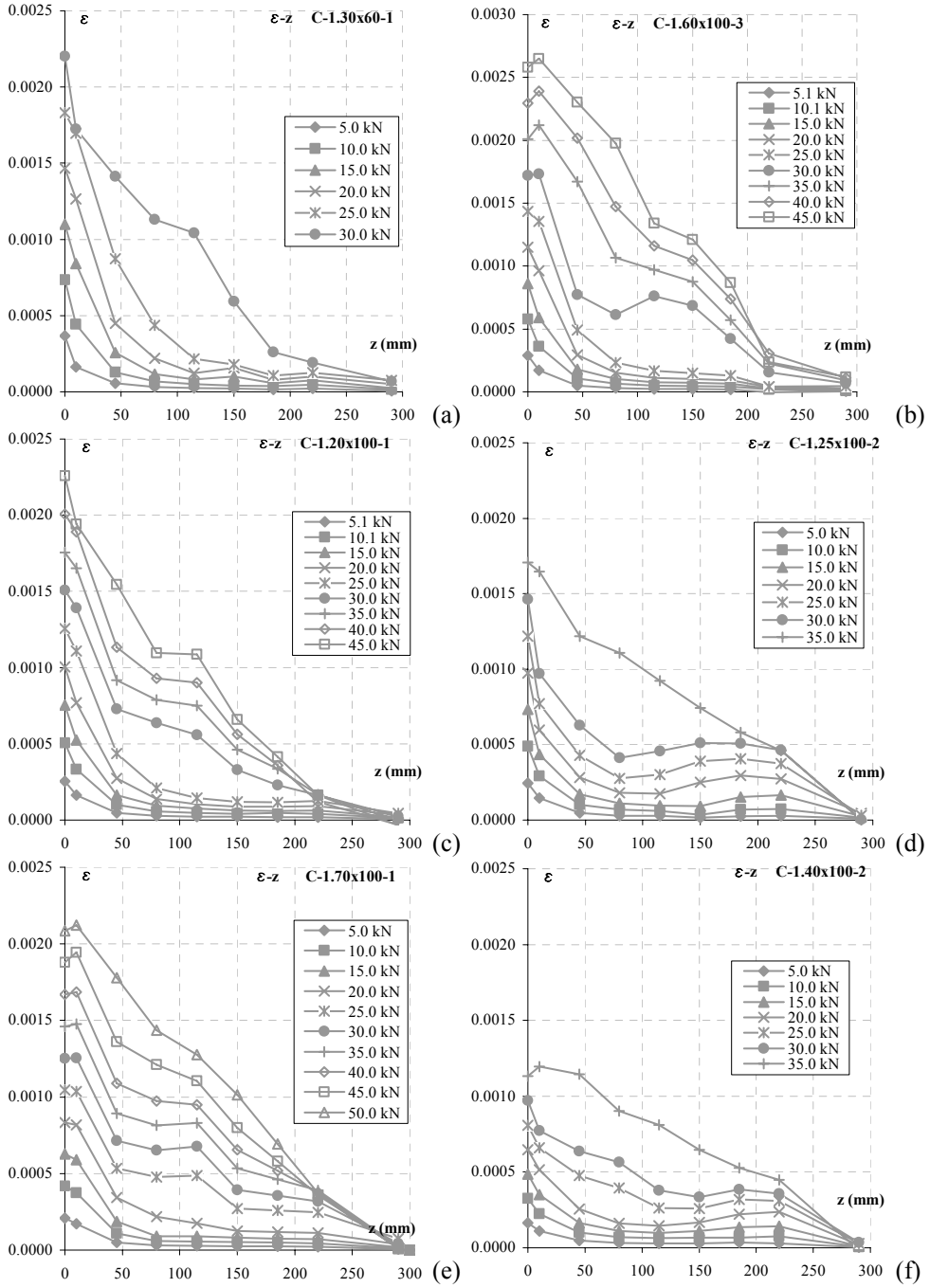

Figure 3.29 - Strain distribution along the EBR reinforcement: a) C-1.30x60; b) C-1.60x100; c) C-1.20x100; d) C-1.25x100; e) C-1.70x100; f) C-1.40x100

Chapter 4 - Analysis of the experimental results

The bond between Fiber Reinforced Polymers (FRP) and concrete substrate is a key aspect for the effectiveness of the External strengthening of Reinforced Concrete (RC) beams by FRP systems, both cured in situ (sheets) and the preformed (plates). Therefore plenty of research activities have been carried out for better understanding the debonding phenomenon and several theoretical and experimental contributions were provided. The fracture energy is a basic parameter governing the debonding problem, nevertheless assessing its value is not sufficient for reproducing the overall behavior of the FRP-to-concrete interface for modeling problems such as, for instance, intermediate debonding. Thus an accurate local bond-slip model, taking into account the different behavior of sheet and plates, is of fundamental importance in the modeling of FRP- strengthened RC structures.

The present chapter is aimed at identifying bond laws for sheets and plates through an Indirect Identification Method (IndIM - Faella et al. 2009a), based on the wide collection of results attained from the experimental tests showed and discussed in the chapter 3.

A simplified shape for the bond law (bilinear elasto-softening) was chosen on the basis of the observations of some previous studies available literary and taking into account the possibility of exploiting closed-form solutions to the problem of adhesion. The consistency of IndIM method and the robustness of the assumption on the bond law shape was showed by a comparison, in terms of axial strains throughout the bonded length, between theoretical predictions and the corresponding measured values. Finally the advisability of assessing a bond law for the plates different from that for the sheets was clearly showed.

4.1 BOND INTERFACE RELATIONSHIPS

4.1.1 Identification methods

The FRP-to-concrete interface behavior is often described by its fracture energy G_F, which the ultimate load F_{max} observed in pull-out tests is directly related to. Though, assessing the G_F value is not sufficient for reproducing the overall behavior of the FRP-to-concrete interface for modeling problems such as, for instance, intermediate debonding in RC beams externally strengthened by FRP reinforcement (Faella et al. 2008a). Thus an accurate local bond–slip model is of fundamental importance in the modeling of FRP-strengthened RC structures.

As showed in the chapter 3, the pull test delivers the ultimate load of the FRP-to-concrete interface, but also can provide useful information on the local bond–slip behavior of the interface if axial strains of the FRP reinforcement are measured with closely spaced strain gauges. Indeed, the shear-stress-relative-slip relationship, describing the FRP-to-concrete interface law, can be identified starting from the values of the strains recorded during the tests at different load levels.

Commonly, the shear stress of a particular location along the FRP-to-concrete interface can be found using a difference formula, whereas the corresponding slip can be found by a numerical integration of the measured axial strains of the FRP.

In particular the interface shear stresses $\tau_i(z)$ can be obtained by the variation of axial stresses, and thus strains, throughout the FRP by the following relationship between two strain gauges at distance Δz_i:

$$\tau_i = \frac{\varepsilon_{i+1} - \varepsilon_i}{\Delta z_i} \cdot E_f \cdot t_f \qquad (4.1)$$

where E_f and t_f are FRP Young's modulus and thickness, respectively. Typical shear stress profiles assessed for sheets and plates, respectively, are reported in Figure 4.1 -a,b. Note that, at the loaded end of the reinforcement, shear stresses assessed for loads close to the debonding of the reinforcement are lower than those assessed for lower loads. This indicates that in this zone

of the reinforcement the shear stress-slip law is in the softening stage typical of a post-elastic behaviour.

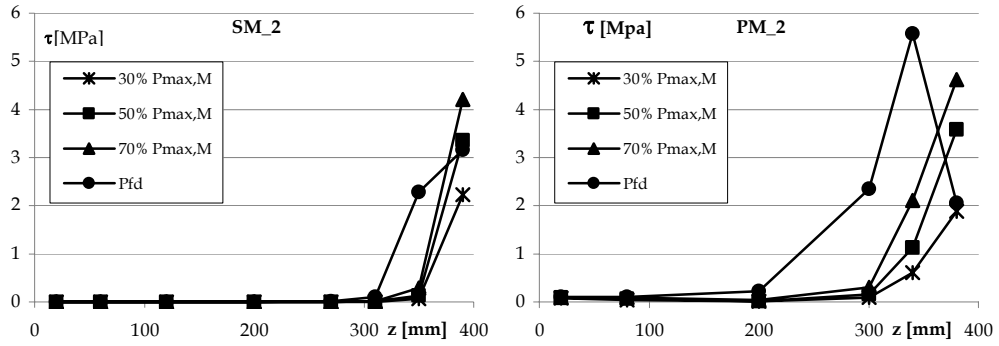

(a) (b)

Figure 4.1 - Shear stresses assessed on sheet (a) and plate (b) reinforced specimens

On the other hand, assuming for the sake of simplicity that concrete strain is negligible with respect to FRP counterpart, the slip values corresponding to the shear stress values obtained by Eq. (4.1) can be calculated by integrating the axial strains measured during the test by the following relationship:

$$s_{i,i+1} = \sum_{k=0}^{i} \frac{\left(\varepsilon_{k+1} + \varepsilon_k\right)}{2} \cdot \left(x_{k+1} - x_k\right) \tag{4.2}$$

Therefore the bond law at the FRP-to-concrete interface can be obtained by calculating the shear stresses using Eq. (4.1) (considering the strains recorded by the first two gauges - e.g. at 400mm and 380 mm in Figure 3.1) and the corresponding slips using Eq. (4.2) (considering all the strain gauges applied on the FRP reinforcement). In this way the experimental interface law is obtained directly with respect to values of shear stresses and relative slips based on experimental strains (see Figure 4.2).

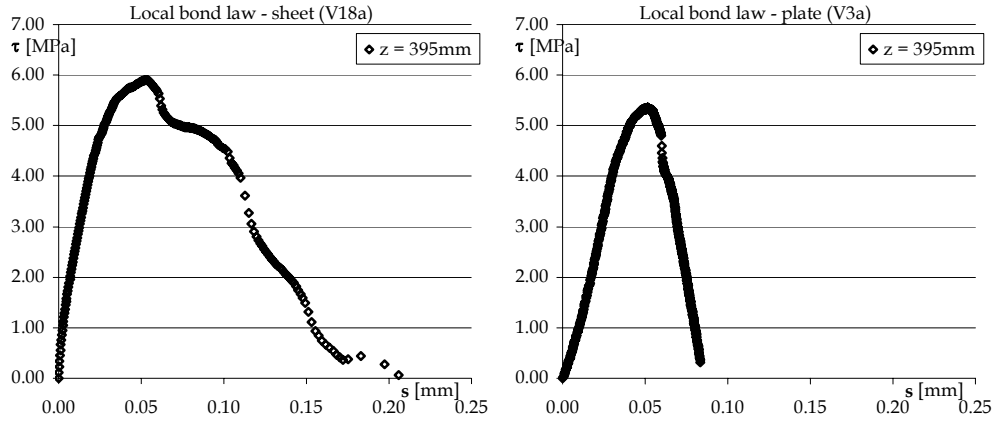

(a) (b)

Figure 4.2 - Experimental bond law at the FRP-to-concrete interface: sheet (a) and plate (b)

Moreover, the couples of values $\left(\overline{s}_j, \overline{\tau}_j\right)$ can be "directly" used to calibrate the τ-s relationship through a numerical regression, such as the least square method. This method (hereinafter called DirIM – Faella et al, 2009a) is very simple, but it does not often produce accurate local bond–slip curves. In particular the shear stress deduced from axial strains can be not reliable due to sensitivity to the distance between strain gauges in the averaging procedure needed for estimating shear stresses. Consequently the method can noticeably underestimate the values of fracture energy and provide bond–slip curves, attained from different tests, substantially diverse.

In this regard, Ferracuti et al. (2007a) presented a procedure to calibrate non-linear FRP-to-concrete interface laws from experimental results of bond tests: strains along the composite are used to obtain shear stress–slip data, whereas the maximum transmissible force is used to prescribe the value of fracture energy, G_F, of interface law. Hence, the non-linear interface law is obtained by a DirIM, taking into account of a restraint on G_F in the calibrating procedure. The interface law is then used to simulate the tests and a good agreement between numerical and experimental results are showed. Nevertheless, the distribution of shear stresses cannot be directly compared with data provided by the pull out tests, because both interface shear stresses

and local displacements cannot be directly measured during the usual pull-out tests.

In Lu et al (2005), some existing bond–slip models was presented and assessed using the results of some pull tests on simple FRP-to-concrete bonded joints, leading to the conclusion that a more accurate model, unaffected by such uncertainties, is required. For this reasons three new bond–slip models of different levels of sophistication were proposed, highlighting a novel aspect in calibrating the models on the predictions of a meso-scale finite element model. Through following comparisons with the test database, all three bond–slip models are shown to provide accurate predictions of both ultimate load and the strain distribution in the FRP reinfocement. In particular it was showed that, while a more precise bond-slip model should consist of a curved ascending branch and a curved descending branch (see also Savoia et al., 2003 and Ferracuti et al., 2007a), also other shapes such as a bilinear model can be used as a good approximation.

Among the three models proposed in Lu et al 2005, the last is just represented by a bilinear law, identified by the following relationships for determining the three parameters τ_{max}, s_e and s_u:

$$\tau_{\max} = 1.5\beta_w f_t, \tag{4.3}$$

$$s_e = 0.015\beta_w f_t, \tag{4.4}$$

$$s_u = \frac{2 \cdot G_F}{\tau_{\max}} = \frac{2 \cdot 0.308 \cdot \beta_w^2 \cdot \sqrt{f_t}}{1.5 \cdot \beta_w \cdot f_t} = 0.41 \cdot \beta_w \cdot \sqrt{f_t}, \tag{4.5}$$

where f_t is the tensile strength of the concrete and β_w is a well-known geometrical factor (as function of the ratio between the width of the FRP and the concrete member which the FRP is applied on). Slightly dissimilar expressions were suggested in literature for this factor (Lu et al 2005, Teng et al., 2002, CNR DT200, 2004, fib bulletin2001), but the difference between the expressions is however very small and all the mentioned equations are suitable for practical applications. Note that, for simplicity and uniformity, some relationships were formally rewritten.

It is worth observe that the relationships (4.3), (4.4) and (4.5) were assessed by using the experimental results of bond tests performed on sheets (i.e. wet-lay-up system characterized by thickness ranging between 0.133mm and 0.5mm for one or three layers). Very few experimental data was related to

tests performed on plates (i.e. preformed system characterized by thickness ranging between 1mm and 2mm) whereas the reinforcement thickness particularly affects debonding behavior: indeed, the greater the thickness, the higher the increase in the normal and shear stresses at FRP to concrete interface and consequently the probability of premature debonding occurrence (Oehlers and Moran, 1990; Tounsi et al., 2009). Even if the numerical analysis may take into account this parameter, the comparison performed with the experimental data appears clearly lacking from this point of view.

By contrast, recently (Bilotta et al., 2011b), in order to assess a design formulation to predict the plate end debonding load in RC elements strengthened with Externally Bonded Reinforcement (EBR) made of FRP materials by means of a statistical analysis, the experimental debonding loads of several bond tests available in literature have been collected and joined with the results of test showed in the Chapter 3. The procedure is reported and exhaustively discussed in the Chapter 6. The proposed design formulation (see also Chapter 7) is based on a detailed and consistent statistical analysis performed according to the 'design by testing' procedure suggested in the Eurocode 0 (EN1990, 2002). Cured in-situ (sheets) and preformed (plates) FRP systems have been distinguished to better exploit the performance of the former ones, as concerns the plate end debonding failure. The following relationship, widely accepted in international literature and similar in structure to that at present adopted in the Italian code CNR DT 200/2004, unified for both for sheets and plates, was calibrated for the theoretical prediction of the maximum plate end debonding load:

$$P_{f,\max} = \beta_L \cdot b_f \cdot \sqrt{2 \cdot E_f \cdot t_f \cdot \Gamma_F} = \beta_L \cdot b_f \cdot \sqrt{2 \cdot E_f \cdot t_f \cdot k_G \cdot k_b \sqrt{f_{cm} \cdot f_{ctm}}} \quad (4.6)$$

$$L_e = \sqrt{\frac{E_f \cdot t_f}{2 \cdot f_{ctm}}} \quad (4.7)$$

$$k_b = \sqrt{\frac{2 - b_f / b_c}{1 + b_f / b_c}} \quad (4.8)$$

$$\beta_l = \frac{L_b}{L_e} \cdot \left(2 - \frac{L_b}{L_e} \right) \qquad if \qquad L_b \le L_e; \qquad \beta_l = 1 \qquad otherwise \quad (4.9)$$

.

f_{cm} and f_{ctm} being the compressive (cylindrical) and tensile strengths of concrete, k_G a coefficient regarding the experimentally calibrated fracture energy, k_b is the counterpart of the well-known geometrical factor β_w discussed above, and β_L also is a familiar factor, taking into account the reduced bond strength when the bond length is lower than the effective one (Teng et al, 2002). Finally E_f and t_f are the Young modulus and the thickness of the FRP, respectively.

The calibrating procedure provided k_G values equal to 0.077 and 0.063, for sheets and plates respectively, indicating that the specific fracture energy obtained for sheets is higher than that obtained for plates (of at least 20%). Note that, in this case, the fracture energy values obtained by the calibrating procedure are independent of the bond law shape. For further details see Chapter 6.

Therefore, it is clear that Lu et al. (2005) suggested an expression for assessing the interface relationship and consequently the energy fracture value that takes into account the strength of the concrete, but completely neglects the influence of the reinforcement properties, in particular the FRP thickness. This assumption, regardless of the value of β_w, lead to same values of maximum shear stress for plates and sheets applied on the same concrete.

Considering the test data related to the sets I, II and III (for each of which both sheets and plates were applied on concrete blocks made of the same concrete - see Table 3.1), the relationships (4.3), (4.4) and (4.5) provide the values of τ_{max}, s_e, s_u and G_F reported in Table 4.1, separately for plates and sheets. The fracture energy G_F is evaluated assuming the bilinear bond law (see (4.13) for brevity)

Table 4.1 - Bond law key parameters according to Lu et al 2005 for Sets I,II,III

	sheets				**plates**			
	τ_{max} [*Mpa*]	s_e [*mm*]	s_u [*mm*]	G_F [*N/mm*]	τ_{max} [*Mpa*]	s_e [*mm*]	s_u [*mm*]	G_F [*N/mm*]
Set I	3,15	0.032	0,53	0,84	4,93	0.049	0,53	2,05
Set II	2,98	0.030	0,52	0,77	4,65	0.047	0,52	1,88
Set III	3,31	0.033	0,54	0,90	3,96	0.040	0,54	1,29

Note that for same concrete strength, the parameters obtained for the plates are higher than those obtained for the sheets only due to the higher value of the width factor β_w, which in this case is always greater for the plates.

Such a result, exactly opposite to the outcomes recalled above and better discussed in the Chapter 6, indicates the advisability of assessing a bond law for the plates different from that for the sheets.

However a simplified elasto-softening bi-linear relationship can reproduce the key aspects of the interface behaviour, as pointed out by the comparative study carried out by Lu et al. (2005), through only three mechanical parameters completely identifies such relationship (i.e. maximum shear stress τ_{max}, ultimate slip s_u, and elastic stiffness k_e). Obviously knowledge of G_F, derived by solving equations (2.63) (or (2.64) if necessary), is not sufficient for determining such parameters and a reliable calibrating procedure must be used to asses the relationship from the experimental strains measured during the test.

In order to address such question an Indirect Identification Method (hereinafter called IndIM – Faella et al, 2009a) can be pursued to calibrate an interface relationship starting from the availability of axial strain evolution in FRP plate at different load levels up to debonding failure: once a bi-linear interface relationship has been assigned, the corresponding theoretical strain distributions can be evaluated and compared with experimental data; the procedure is iterative and ends when the difference between theoretical and experimental strains is less then a prefixed tolerance (Faella et al., 2003).

On this subject, in Faella et al 2008a,b the key aspects of identifying the interface stress-strain relationship by using experimental results were presented and how best to utilize experimental data obtained through pull-out tests for calibrating the τ-s relationship at the FRP-to-concrete interface was widely discussed. In particular a comparison between the results provided by two possible approaches for completely identifying the interface law, the above-mentioned DirIM method and the IndIM method proposed in Faella et al, 2003, was showed.

With reference to the results of some experimental tests (see Chapter 3) both DirIM and IndIM have been applied in order to plot the τ-s relationship and derive the corresponding specific fracture energy G_F, computed by totalling up the area under the bi-linear curve.

Table 4.2 shows that IndIM leads to specific fracture energy G_F larger than those computed by DirIM in almost all analyzed cases. Moreover, the values of G_F obtained with IndIM are as stable as the measured failure loads P_{test}, confirming the superior accuracy of IndIM with respect to DirIM. Some of the most representative bi-linear interface relationships obtained by applying both DirIM and IndIM are reported in Figure 4.3.

Table 4.2 - Specific fracture energy GF: (DirIM) Vs (IndIM)

Label		PM_1	PM_2	PM_3	SM_1	SM_2	SM_3
G_F	(DirIM)	0.45	1.20	0.86	0.66	0.86	0.48
G_F	(IndIM)	0.73	1.75	1.03	0.66	0.67	0.72
$G_{F,(IndIM)}/G_{F,(DirIM)}$		1.61	1.46	1.20	0.99	0.78	1.50

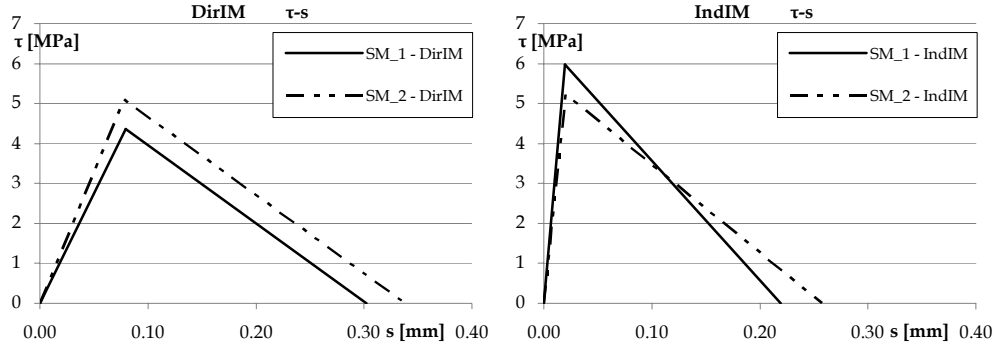

Figure 4.3 - Bi-linear interface relationship: (DirIM) Vs (IndIM).

The two methods lead to results that could be even significantly different, especially in terms of ultimate slips (Nigro et al., 2008a). Furthermore, the ascending branches of DirIM curves are characterized by a lower slope with respect to IndIM

Comparisons between the theoretical and experimental values of the axial strains throughout the FRP plate are reported, for different values of load test, in Figure 4.4. The results are referred to test SM_3. The theoretical strain values have been obtained by closed-form solutions reported in Faella et al. (2003)

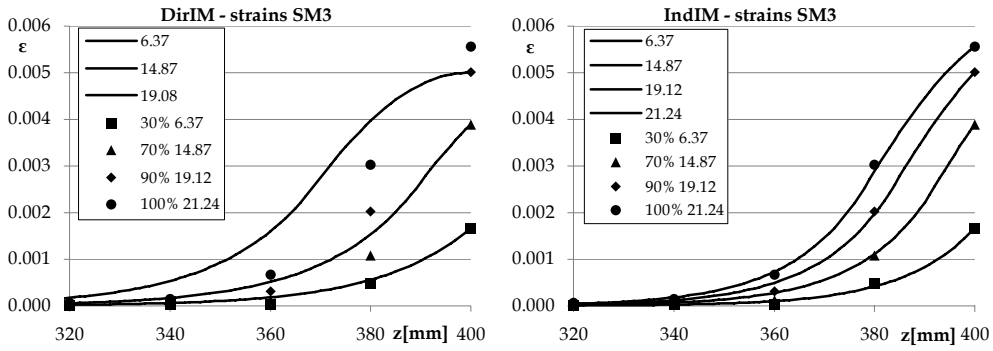

Figure 4.4 - Theoretical and experimental strains: (DirIM) Vs (IndIM)

The theoretical values of strains obtained assuming the interface relationship identified though IndIM are much closer to the observed ones than the values which can be derived assuming the τ-s relationship calibrated by means of DirIM. Thus at all as an alternative to the method DirIM, the IndIM again revealed the most accurate way of identifying nonlinear FRP-to-concrete interface laws on the basis of experimental data. Moreover, it is worth observing that the experimental data seem to be simulated with good accuracy even if a simplified adhesion law (i.e. a bilinear adhesion law) is assumed.

Thus, based on such results and the outcomes of Yao et al. (2005), Ferracuti et al. (2007a), Faella et al. (2009a) and Bilotta et al. (2011b), the IndIM procedure and the bilinear shape for the bond law will be extensively utilized with the final aim of calibrating bilinear interfaces laws, as stable as possible, and assessing their reliability for sheets and plates, separately.

4.2 APPLICATION OF THE INDIM METHOD

The IndIM method was applied therein on the results of the experimental campaign (see Chapter 3) involving both plates and sheets FRP reinforcement. Results related to tests performed with cyclic load path (see Table 3.1) were not considered for these analyses. For clarity, the general expressions of the bilinear law will briefly defined in the subsection 4.2.1 , the IndIM procedure will shortly be outlined in 4.2.2 ,and finally the results are showed and discussed in the subsection 4.2.3 .

4.2.1 Bilinear bond-law relationship

As stated above, for the analysis performed in this chapter, the simple but effective bilinear model is taken because closed-form solutions are available for a such shape of the interface law, as extensively shown in Faella et al (2003). This model is defined by the following well-known relationships (see also Figure 4.5):

$$\tau = \tau_{\max} \frac{s}{s_e} \qquad if \qquad s \le s_e , \tag{4.10}$$

$$\tau = \tau_{\max} \frac{s_u - s}{s_u - s_e} \qquad if \qquad s_e \le s \le s_u , \tag{4.11}$$

$$\tau = 0 \qquad if \qquad s > s_u , \tag{4.12}$$

defining, obviously, the following relationship for the fracture energy:

$$G_F = \frac{\tau_{\max} \cdot s_u}{2} , \tag{4.13}$$

In these relationships, three parameters identify the bond law: the maximum shear stress, τ_{max}, the corresponding slip, s_e, and the ultimate slip, s_u, which the interface shear stress can be considered null beyond.

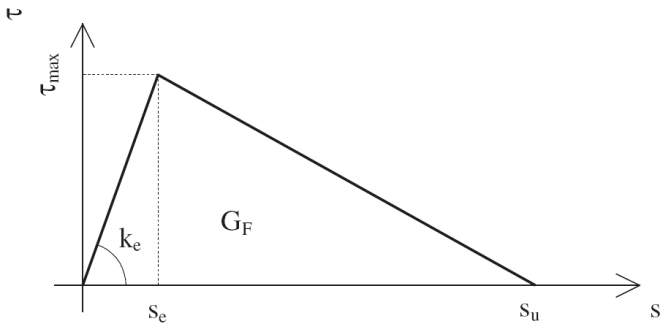

Figure 4.5 - Bilinear (elastosoftening) law at the FRP-to-concrete interface

4.2.2 Indirect Identification Method (IndIM)

Since relevant measures of shear stresses and corresponding relative strains cannot be directly drawn out by pull-out tests, an alternative procedure using the experimental measures in terms of axial strain values $\varepsilon_{f,j,i}$ recorded at distance z_j under the force F_i (see Figure 3.1) can be adopted for "indirectly" calibrating the τ-s interface relationship. In particular, for each set, q, of parameters τ_{max}, s_e and s_u a given interface law is defined, and the corresponding theoretical value $\varepsilon_{fth,j,i}$ of the axial strain developed in the FRP plate at a distance z_j under the force F_i can be evaluated. Even if numerical procedures, such as finite differences, can generally be utilized, the choice of a bilinear bond law allowed the closed-form solutions to be used (Faella et al., 2003) taking also into account, if necessary, the influence of the parameter bond length, L, in the solution of the problem. Consequently, the following constraint condition can be imposed upon the value of q to be sought for identifying the interface relationship

$$F_{\max}^{th}\left(\mathbf{q}, L\right) = F_{\max}^{\exp}, \tag{4.14}$$

where $F_{\max}^{\exp}$ is the corresponding experimental value. Moreover, once the theoretical values of the axial strains $\varepsilon_{fth,j,i}$ have been expressed for every available load step F_i and measure station at abscissa z_j, the optimal value of the vector of parameters can be evaluated through a numerical regression on the measured values $\varepsilon_{ex,j,i}$ of the axial strains developed in FRP

$$q = \arg\min_{q} \sum_{i=1}^{n} \sum_{j=1}^{m} \left[\varepsilon^{i}_{\exp,j} - \varepsilon_{th}\left(z_j, F_i; q\right) \right]^2 , \tag{4.15}$$

Consequently, the indirect identification procedure of the interface relationship can be regarded as a constrained optimization problem described by the two equations (4.14) and (4.15).

4.2.3 IndIM procedure results

Prior to show the results obtained by applying the identifying method is worth noting that all the monotonic tests mentioned above were repeated three times; this means that in Table 3.1 can be readily identified groups of three tests for which the bond law should theoretically be equal. The interface laws were assessed separately for each test and plotted for each homogeneous group in Figure 4.6 and Figure 4.7 (for sheets and plates – set I and II) and in Figure 4.8 and Figure 4.9 (for the set III).

Note that all relationships reported were based on experimental results not differently affected by the type of test set-up, because the tests (sets I, II and III) were all performed in a NES-SST scheme (i.e. test setup d, see 3.1). Moreover the identification law was not reported if it was considered not reliable, i.e. when the relationship (4.15) gave values lower than a prefixed tolerance equal to about 10^{-5} depending on the number of strain gauges and the number of the load level considered (optimal values were those lower than 10^{-6}).

For each set of three tests interface laws very similar have been obtained. This is confirmed by the mean values and the corresponding coefficients of variation (CoV) of the parameters τ_{max}, s_e and s_u reported for each group of three tests in Table 4.3. In particular the CoVs of τ_{max} and s_u are often very low (about 10% that represents a typical value of CoV for problems involving the strength of the concrete), and sometimes less than 5%. By contrast the CoVs of the elastic slip, s_e , corresponding to the maximum shear stress, τ_{max}, are quite high. This indicates that the bond behaviour in the elastic stage is not perfectly approximated by a linear branch.

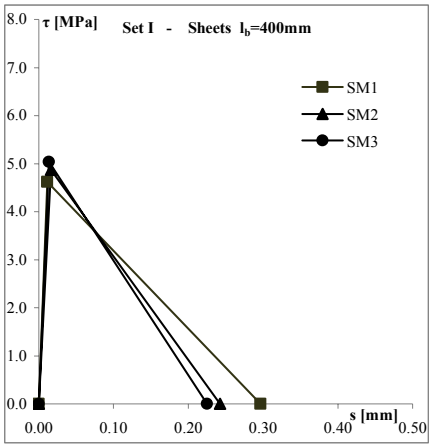

(a)

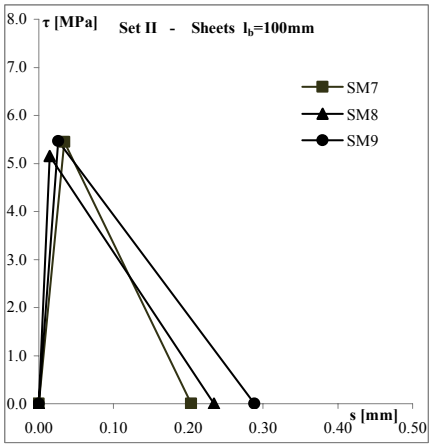

(b)

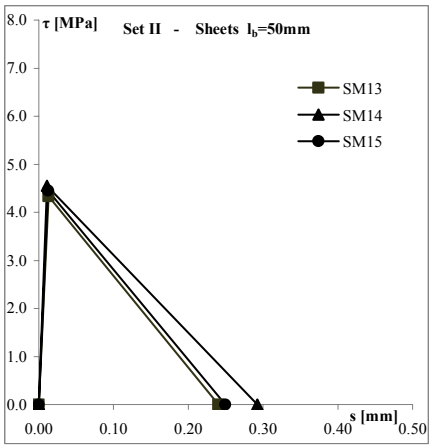

(c)

Figure 4.6 - Bilinear bond law for sheets (t_f = 0.166 mm) of set I (a) and II (b,c)

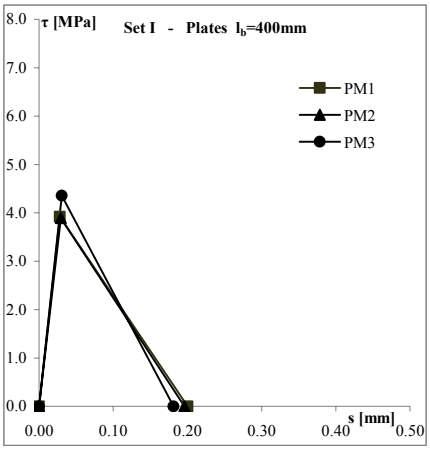

(a)

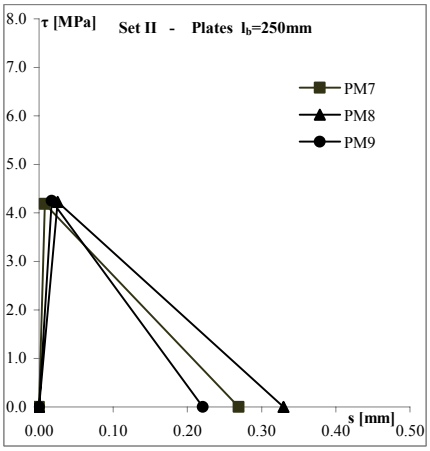

(b)

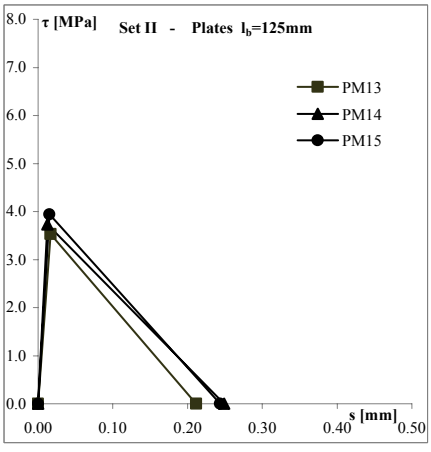

(c)

Figure 4.7 - Bilinear bond law for plates (t_f = 1.4 mm) of set I (a) and II (b,c)

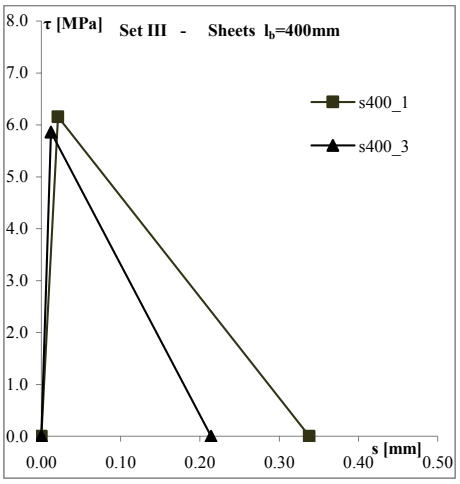

(a)

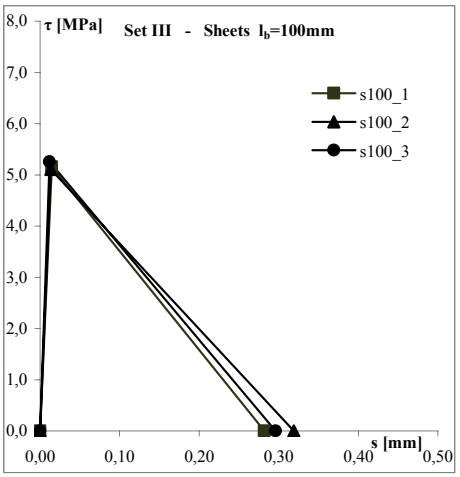

(b)

Figure 4.8 - Bilinear bond law for sheets (t_f = 0.166 mm) of set III: (a) l_b = 400 mm, (b) l_b = 100 mm

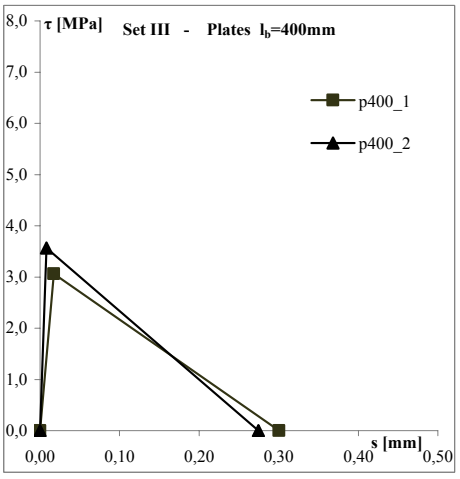

(a)

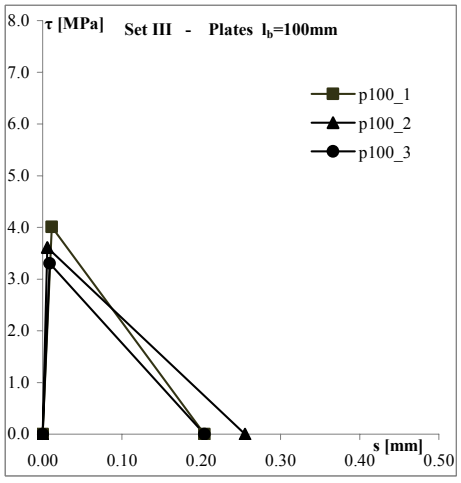

(b)

Figure 4.9 - Bilinear bond law for plates (t_f = 1.2 mm) of set III: (a) l_b = 400 mm; (b) l_b = 100 mm

The robustness of the results obtained by the IndIM method can be easily showed by a comparison, in terms of axial strains throughout the bonded length, between theoretical predictions and the corresponding measured values under the various load levels. Figure 4.10 and Figure 4.11 show the results of this comparison for sheets and plates, respectively. The axial strains evaluated assuming the interface relationships calibrated through the IndIM procedures

are very close to the experimental one for low load levels and enough precise for higher load levels due to the constraint condition (4.14), which is a key statement for the identification problem at hand. Consequently, the bond laws are showed be particularly reliable.

Table 4.3 - Bond law key parameters calibrated by the IndIM method on SST test results.

Set	sheets				plates			
	test	s_e [MPa]	s_u [mm]	τ_{max} [mm]	test	s_e [MPa]	s_u [mm]	τ_{max} [mm]
I	PM1	0.03	0.20	3.92	SM1	0.01	0.30	4.62
	PM2	0.03	0.20	3.89	SM2	0.02	0.24	4.87
	PM3	0.03	0.18	4.35	SM3	0.01	0.23	5.04
	mean	0.03	0.19	4.05	mean	0.01	0.26	4.84
	CoV	0%	6%	6%	CoV	43%	15%	4%
II	PM7	0.01	0.27	4.18	SM7	0.03	0.20	5.45
	PM8	0.03	0.33	4.23	SM8	0.01	0.23	5.16
	PM9	0.02	0.22	4.24	SM9	0.03	0.29	5.47
	mean	0.02	0.27	4.22	mean	0.02	0.24	5.36
	CoV	50%	20%	1%	CoV	49%	19%	3%
	PM13	0.02	0.21	3.53	SM13	0.01	0.24	4.34
	PM14	0.01	0.25	3.73	SM14	0.01	0.29	4.55
	PM15	0.02	0.24	3.94	SM15	0.01	0.25	4.45
	mean	0.02	0.23	3.73	mean	0.01	0.26	4.45
	CoV	35%	9%	5%	CoV	0%	10%	2%
III	V1a	0.01	0.20	4.01	V18a	0.01	0.28	5.16
	V2a	0.01	0.26	3.61	V19a	0.01	0.32	5.11
	V3a	0.01	0.20	3.30	V20a	0.01	0.30	5.26
	mean	0.01	0.22	3.64	mean	0.01	0.30	5.18
	CoV	0%	15%	10%	CoV	0%	7%	1%
	V1b	0.02	0.30	3.06	V18b	0.02	0.34	6.16
	V2b	0.01	0.27	3.56	V19b	-	-	-
	V3b	-	-	-	V20b	0.01	0.21	5.86
	mean	0.02	0.29	3.31	mean	0.02	0.28	6.01
	CoV	47%	7%	11%	CoV	47%	34%	3%

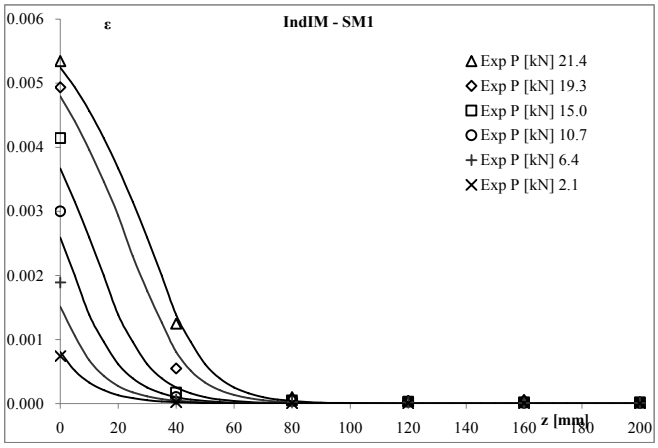

(a)

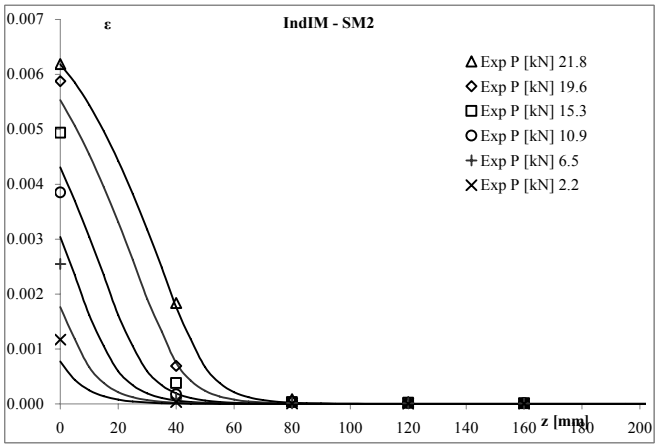

(b)

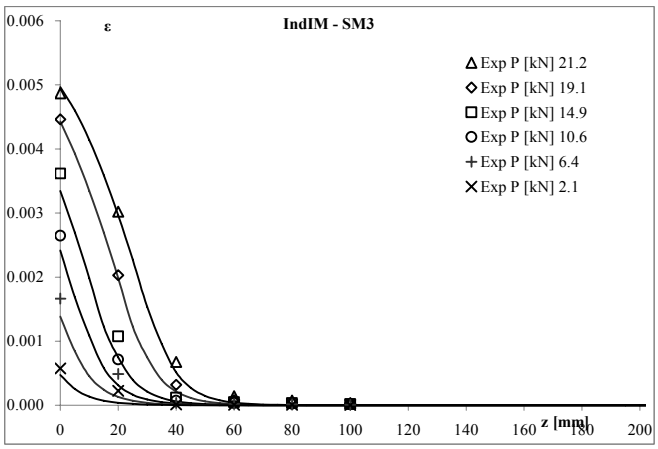

(c)

Figure 4.10 - Comparison between theoretical and experimental strains: sheets of set I

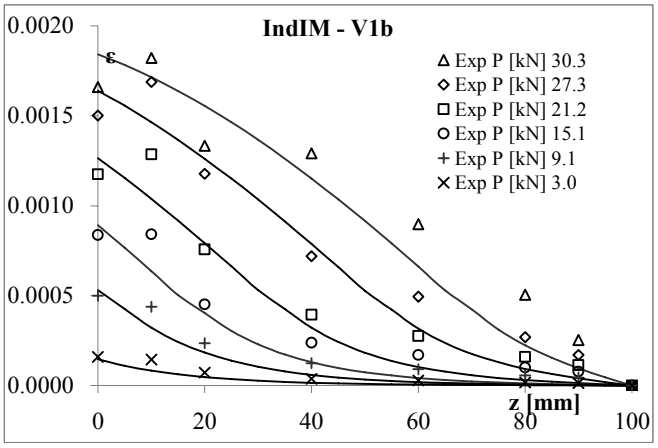

(a)

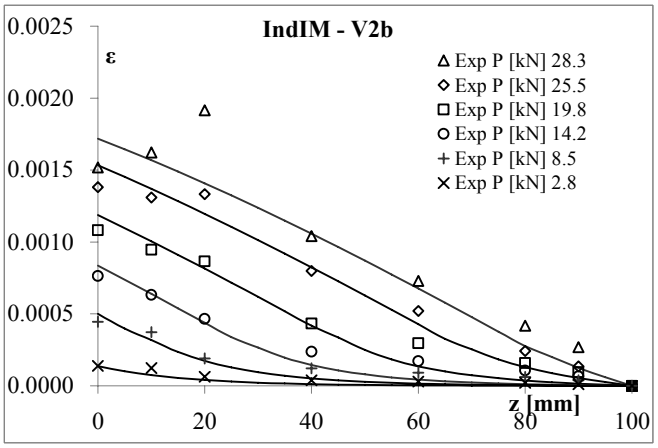

(b)

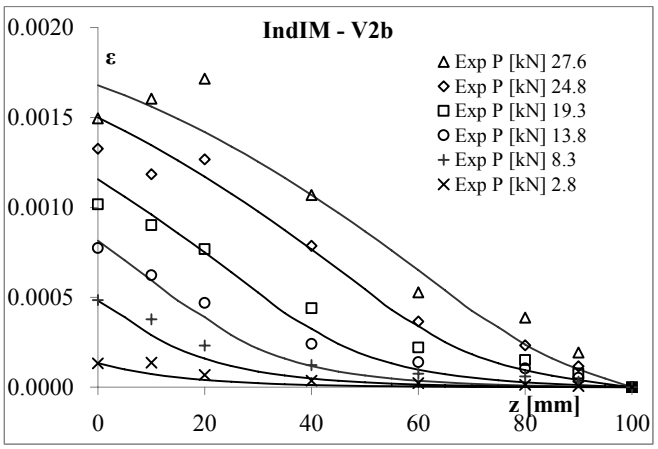

(c)

Figure 4.11 - Comparison between theoretical and experimental strains: plates of set III

In Figure 4.12 and Figure 4.13 the bond laws identified on the same material are plotted together to show that, correctly, the IndIM method provides the same interpretation of the experimental data even for different bond lengths.

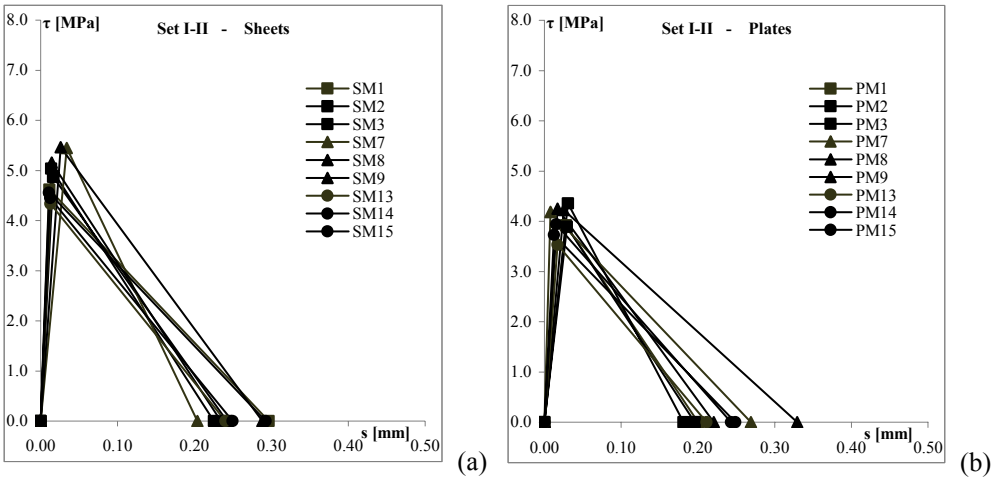

Figure 4.12 - Bilinear bond law for set I, II: (a) sheets (t_f = 0.166 mm); (b) plates (t_f = 1.4 mm)

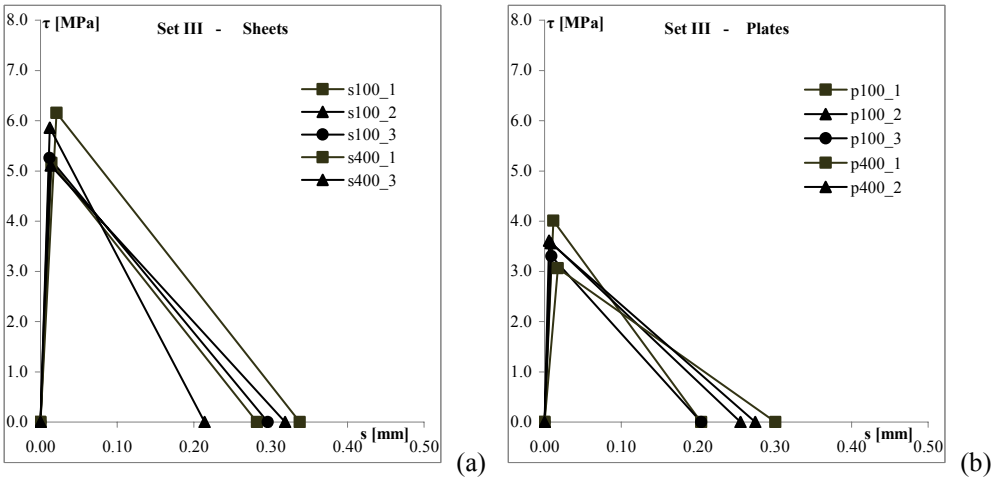

Figure 4.13 - Bilinear bond law for set III: (a) sheets (t_f = 0.166 mm); (b) plates (t_f = 1.2 mm)

Table 4.4 finally shows the average values of τ_{max}, s_e and s_u by type of material. It may firstly be noted that elastic slip, s_e, corresponding to the maximum shear stress, τ_{max}, and the ultimate slip, s_u, are on average the same for sheets and plates (although the dispersions of the values obtained by the identifying method are somewhat high). Conversely the values of maximum shear stress obtained for sheets bond laws are always higher than those obtained for plates interface relationships, of about 30% in average. Clearly the same differences are attained in terms of fracture energy. Such results are in a agreement with those shown in the Chapter 6 (see also Bilotta et al., 2011b) and confirm the unreliability of predictions provided by the relationships (4.3), (4.4) and (4.5) given in Lu et al (2005) (see Table 4.1).

Table 4.4 - Mean values of key parameters calibrated by the IndIM method on SST test results.

set		**sheets**			test	**plates**		
		s_e [Mpa]	s_u [mm]	τ_{max} [mm]		s_e [Mpa]	s_u [mm]	τ_{max} [mm]
I-II	mean	0.02	0.25	4.88	mean	0.02	0.23	4.00
	CoV	57%	13%	9%	CoV	38%	41%	7%
III	mean	0.01	0.29	5.51	mean	0.01	0.25	3.51
	CoV	37%	17%	9%	CoV	37%	18%	10%

Moreover, the bilinear bond laws obtained by using the averages of the values of τ_{max}, s_e and s_u reported Table 4.4 for the sets I and II (very similar concrete strength) are plotted in Figure 4.14a,b for sheet and plates respectively. Such laws, compared with those obtained by using the averages of the corresponding values of τ_{max}, s_e and s_u reported in Table 4.1 (Lu et al 2005), show not a very good agreement. Same comparisons are showed in Figure 4.15 with reference to the values of τ_{max}, s_e and s_u attainable by using the only bilinear law provided in CNR-DT200 (2004) for sheets and plates. This bilinear law shows a better agreement in the case of plates. Finally Figure 4.16 shows the lower difference between the bond law experimentally identified and that herein proposed, attainable by using the same relationships provided in CNR-DT200 (2004) modified to separately consider sheets and plates, according to Bilotta et al. (2011b). Note that s_u = 0.25mm (see Table

4.4) was assumed instead of s_u = 0.2mm suggested in CNR-DT200 (2004). Further details on these relationships are reported in the Chapter 7.

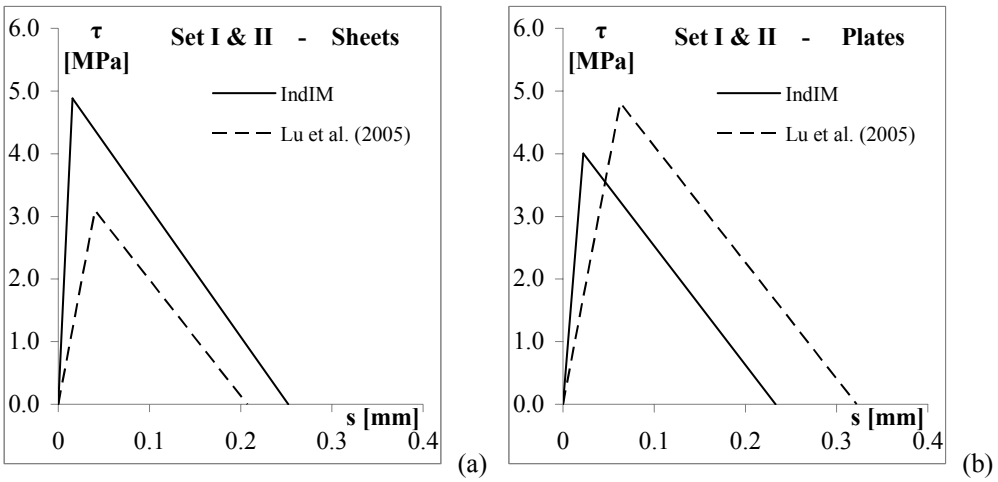

Figure 4.14 - Comparisons of bilinear bond laws: IndIM vs Lu et al (2005) for (a) sheets; (b) plates

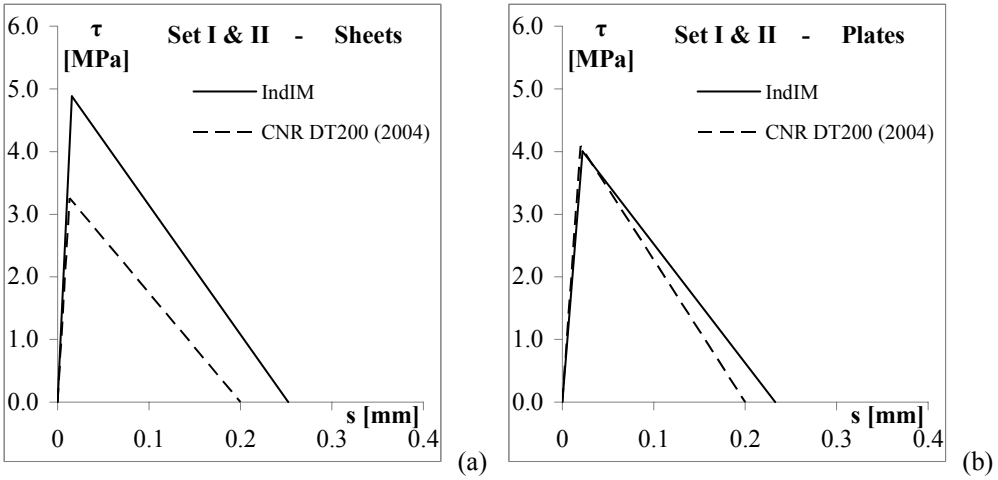

Figure 4.15 - Comparisons of bilinear bond laws: IndIM vs CNR-DT200 (2004) for (a) sheets; (b) plates

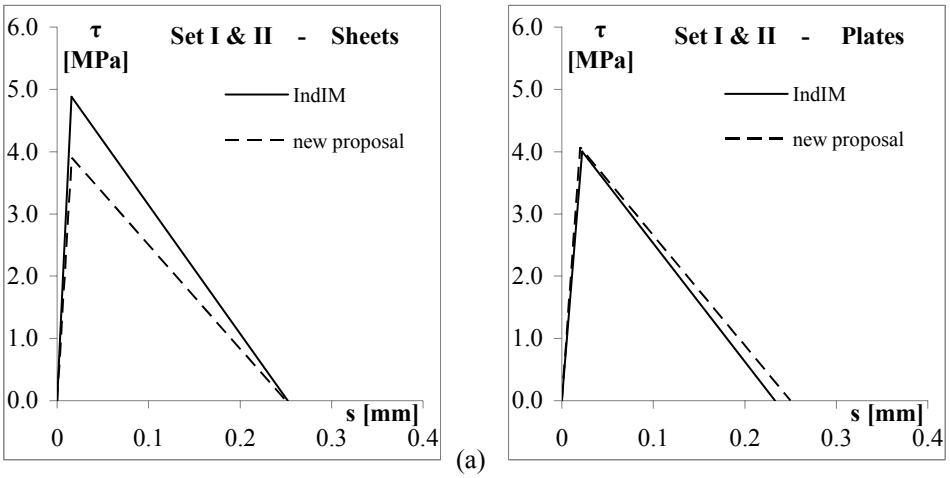

Figure 4.16 - Comparisons of bilinear bond laws: IndIM vs Bilotta et al. (2011) for (a) sheets; (b) plates

Moreover, Table 4.4 clearly show that $s_e << s_u$. Thus from (2.57)

$$k_{in} = \frac{\tau_{\max}}{\left(s_u - s_{el}\right)} \approx \frac{\tau_{\max}}{s_u} \quad . \tag{4.16}$$

Using eq (4.16) in eq. (2.60) the following relationship can be written

$$L_{eff} = \frac{\pi}{2} \cdot \sqrt{\frac{E_f t_f s_u}{\tau_{\max}}} \tag{4.17}$$

Finally using eq. (4.13) the eq. (4.17) can be expressed as:

$$L_{eff} = s_u \sqrt{\frac{\pi^2 E_f t_f}{8 G_f}} \tag{4.18}$$

providing the effective bond length.

Figure 4.17 shows the reliability of this formulation based on the experimental results of bond tests performed on both plates (Figure 4.17a) and sheets (Figure 4.17b) already reported above in Figure 3.22a and Figure 3.23a

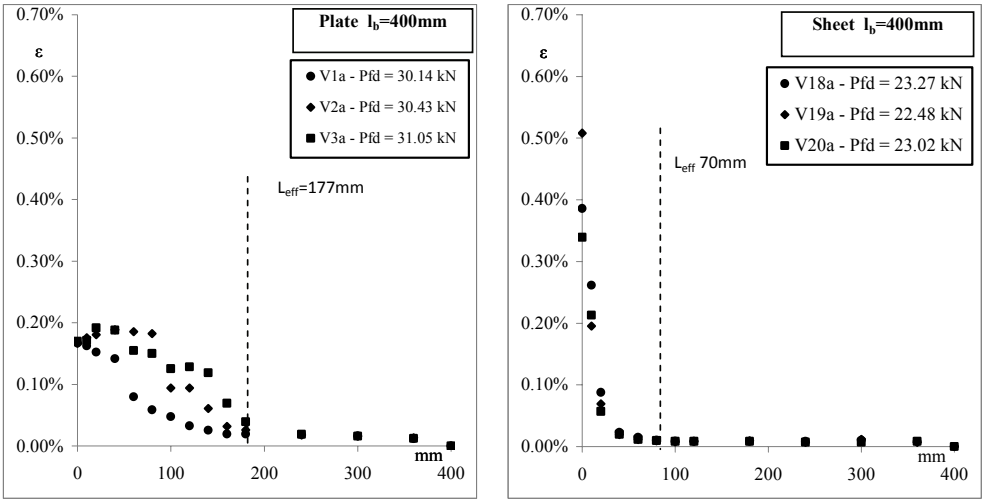

(a) (b)

Figure 4.17 - Strain profiles along FRP: (a) plates; (b) sheets

4.3 SUMMARY AND CONCLUSIONS

Theoretical strength models available in literature, predicting debonding load for two macro type of FRP systems, i.e. the cured in situ (sheets) and the preformed (plates) separately, have been considered. The comparison between the relationships showed that the specific fracture energy of the sheets can be higher than that of the plates. Anyway assessing the specific fracture energy, by this relationships, is not sufficient for reproducing the overall behavior of the FRP-to-concrete interface for modeling problems. On the other hand, simplified and accurate bond models available in literature, do not seem to take into account the different performance of sheets and plates. Thus a more accurate local bond–slip model revealed of fundamental importance to model FRP- strengthened RC structures.

Consequently bond laws for sheets and plates have been separately identified through an indirect identification method (IndIM). The identifying procedure was applied on a wide collection of experimental results attained by pull tests during which not only the load but also the corresponding axial strains of the FRP reinforcement were measured. A simplified shape for the bond law (bilinear elasto-softening) was chosen on the basis of the observations of some previous studies available literary and taking into account the possibility of exploiting closed-form solutions to the problem of adhesion.

Both the consistency of IndIM method and the robustness of the assumption on the bond law shape was showed by a comparison, in terms of axial strains throughout the bonded length, between theoretical predictions and the corresponding measured values. Even if the uncertainness in accurately identifying the parameter s_e indicated that the bond behaviour in the elastic stage was not perfectly approximated by a linear branch, the result obtained by assuming a bilinear law were satisfying.

Finally, several bond law relationships, identified by three parameter (i.e. the maximum shear stress, τ_{max}, the corresponding elastic slip, s_e, and the ultimate slip, s_u), have been compared. The elastic and ultimate slips, s_e and s_u respectively, are on average the same for sheets and plates, although the dispersions of the values obtained by the identifying method are somewhat

high. Conversely the values of maximum shear stress, τ_{max}, obtained for sheets bond laws are always higher than those obtained for plates interface relationships, of about 30% in average. Clearly the same differences are attained in terms of fracture energy. Such results are in agreement with the theoretical strength models available in literature for predicting debonding of sheets and plates separately, confirming the advisability of assessing a bond law for the plates different from that for the sheets.

Chapter 5 - Debonding failure of FRP strengthened RC members

In the introductive chapter of this thesis (Chapter 1) a detailed classification proposed by (Teng et al., 2002) has been reported to define the variety of debonding failure modes observed in tests on reinforced concrete (RC) beams strengthened by bonding fibre reinforced polymer (FRP) reinforcements to their tension face.

Anyway the failure modes can be broadly classified into two types: (a) those associated with high interfacial stresses near the ends of the bonded plate; and (b) those induced by a flexural or flexural-shear crack away from the plate ends.

The first type of failures (*plate-end debonding*) has been extensively studied by researcher in the past, as this was the most commonly observed mode of debonding failure for steel-plated RC beams, leading to many strength models also for FRP-plated RC beams.

The second type of failures (*intermediate debonding*) are more likely for FRP-plated RC beams. Thus, in the last years, several studies have been devoted to the occurrence of this failure mode, but to date definitive solutions have not been reached. However, various proposals have been derived from simplified mechanical models and calibrated by means of experimental results available in the scientific literature.

The most known plate-end debonding strength models will briefly recalled in this chapter, which will more concerned with the intermediate debonding phenomenon. Numerical simulations (Faella et al., 2008a) performed to simulate and, thus, further investigate both the debonding phenomena are also discussed.

5.1 DEBONDING FAILURE TYPES FOR RC BEAMS AND SLABS

Innovative techniques based on the external application of Fibre Reinforced Plastic (FRP) laminates (sheets or plates) are interesting alternatives to traditional solutions for strengthening Reinforced Concrete (RC) structures. Along with high structural effectiveness, composite materials are light and easy to install, their application does not entail loss of space and, in some cases, can be performed without interrupting the use of the structure. However, the high performances of FRP materials often cannot be properly exploited, since a typical failure is the debonding of the external reinforcement, namely the loss of bond at the concrete/FRP interface. This makes the bond strength at the interface a key issue in the strengthening design procedure.

Based on existing studies, a schematic representation of seven typical failure modes observed in tests is shown in Teng et al. (2002): (a) flexural failure by FRP rupture; (b) flexural failure by crushing of compressive concrete; (c) shear failure; (d) concrete cover separation; (e) plate end interfacial debonding; (f) intermediate flexural crack induced inter- facial debonding; and (g) intermediate flexural-shear crack induced interfacial debonding. For a full discussion of each of these failure modes, the reader is referred to Teng et al. (2002).

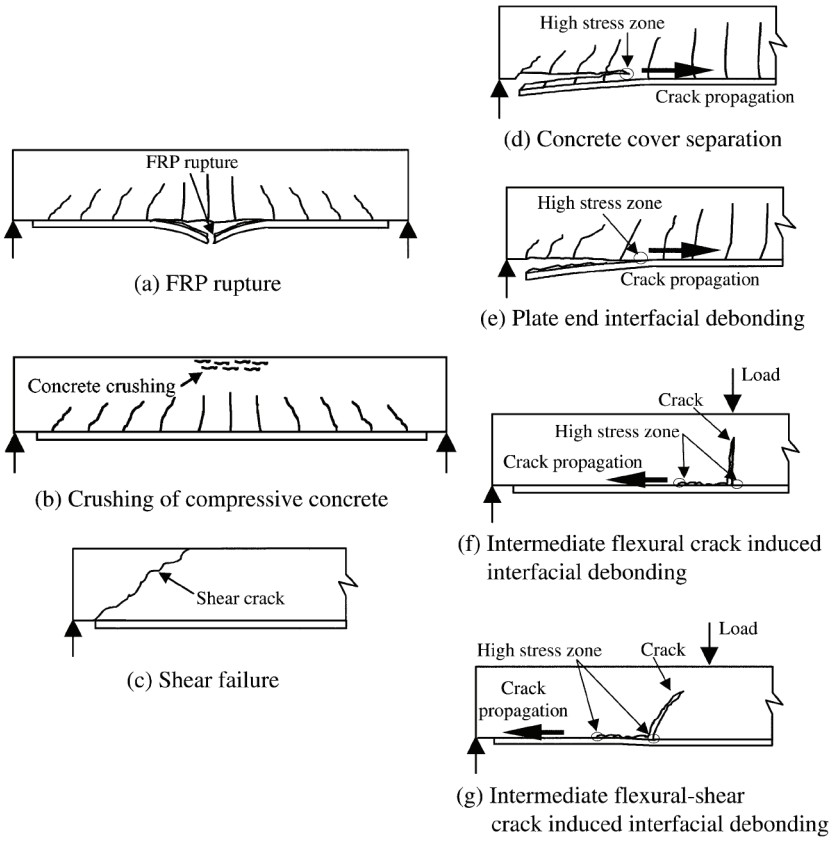

Figure 5.1 - Failure modes of RC beams flexurally-strengthened with an FRP soffit plate. (Teng et al. 2002)

Tests have shown that the load carrying capacity of RC beams flexurally-strengthened with an FRP plate bonded to the tension face is often limited by one of the debonding failure modes. The observed modes of debonding in FRP-plated beams can be broadly classified into two types: (1) those associated with high interfacial stresses near the ends of the bonded plate (failure modes (d) and (e)) which are collectively referred to as *plate end debonding*; and (2) those induced by a flexural or flexural-shear crack away from the plate ends (failure modes (f) and (g)) which are collectively referred to as *intermediate crack-induced debonding* (or simply intermediate crack debonding or IC debonding). Similarly, where a flexural crack is emphasised, intermediate flexural crack debonding is referred to as IFC debonding.

Plate end debonding failures involve the separation of the FRP plate, starting at or near a plate end. Of the two possible plate end debonding failure modes, concrete cover separation (failure mode (d)) involving the detachment of the FRP plate together with the concrete cover has been much more commonly reported.

Intermediate debonding has been observed only in a much more limited number of tests and has received much less research than plate end debonding. In particular, no reliable strength model appears to have been developed to predict such failures.

One of the reasons for this lack of attention has been due to the fact that in RC beams strengthened with a tension face steel plate, due to the much greater stiffness of the steel plate, IC debonding was not found in laboratory tests. That is, for steel plated beams, plate end debonding failures are much more likely. The situation is, however, different with FRP plates, whose strength-to-stiffness ratio is much higher than that of steel plates. As a result, the FRP plate/sheet used for a particular strengthening application is generally much thinner and /or softer than a corresponding steel plate of equivalent total tensile capacity and is much less likely to debond at plate ends.

The IC debonding failure mode is, thus, believed to be particularly important for relatively slender members and members strengthened with a relatively thin FRP plate or sheet. In this connection, it is worth noting that that the IC debonding failure mode is now attracting increasing attention as an important failure mode.

5.1.1 Plate end debonding

FRP plate end debonding has been extensively investigated and various models have been proposed (Varastehpour and Hamelin 1997; Sadadatmanesh and Malek 1998; Wang and Ling 1998; Ahmed and van Gemert 1999; Tumialan et al. 1999; Raoof and Hassanen 2000; Smith and Teng 2002a,b; Teng and Yao 2007). Some other models were initially developed for beams with bonded steel plates and used without any modification for FRP plates (Oehlers 1992; Ziraba et al. 1994; Jansze 1997; Raoof and Zhang 1997). Smith and Teng (2002a,b) classified these models and assessed some of them versus many data available from literature. In particular the plate end

debonding models were generally classified into three categories Smith and Teng (2002a):

• *Shear capacity based models*: debonding failure strength is related to the shear strength of concrete with no or only partial contribution of the steel shear reinforcement. The interfacial debonding stress between the bonded plate and the concrete are not evaluated, thus the required calculations are generally simple. The debonding strength is generally given as the shear force acting at the plate end, with or without taking into account the effect of any coexistent moment.

• *Concrete tooth models*: these models use the concept of a concrete "tooth", between two adjacent cracked surfaces, deforming like a cantilever under the action of horizontal shear stresses at the base of the beam. Debonding is deemed to occur when these shear stresses lead to tensile stresses at the root of the "tooth" that exceed the tensile strength of the concrete. An effective length for the bonded plate is defined over which the shear stress is assumed to be uniform. In these models, the contribution of the shear capacity of the beam to the failure mode is open to question because it seems that failure is controlled by the flexural crack spacing in the concrete cover. Despite this, it is acknowledged in all these models that further understanding of the shear phenomenon is required with many unresolved issues remaining. Using the value of the maximum stress in the bonded plate determined from these models and the methods of strain compatibility or non-linear finite element analysis, the external loading required to create such a stress can be determined and the beam capacity estimated.

• *Interfacial stress based models*: these models simply assume that the concrete cover separation or plate end interfacial debonding is due to high interfacial stresses at the end of the soffit plate. A concrete element adjacent to the end of a bonded plate is, thus, subjected to τ, σ_y and σ_x: shear stress, transverse normal stress perpendicular to the adhesive layer and the bonded plate (the peeling stress) and longitudinal stress, respectively. Such assumptions are logical but are labour intensive compared to the previous models.

Smith and Teng (2002b) have found all existing strength models for this type of debonding failures to be unsatisfactory for FRP-plated RC beams, so further studies should be carried out to determine the circumstances under

which plate end interfacial debonding occurs. However, Smith and Teng (2002b) stated that of the three approaches employed for developing debonding strength models, the shear capacity based models appears to be the most robust, followed by the concrete tooth models, with interfacial stress based models being the least reliable. The interfacial stress based models by Saadatmanesh and Malek (1998) and Tumialan et al. (1999) however provide safe predictions for beams with wet lay-up plates. Only Oehlers (1992) model can be used directly in design as it provides safe predictions although its predictions are overly conservative. All other models do not provide predictions of test debonding strengths with a sufficient degree of conservativeness for direct design use.

As the interaction between the shear force and the bending moment at the plate end at debonding included in Oehlers (1992) model did not appeared to exist for FRP plated beams, at least according to the test data available, Smith and Teng (2002b) proposed a simple new model which seemed superior to all existing models in providing safe and accurate predictions for design use by modifying Oehlers (1992) model. Anyway additional work is required.

In addition to the concrete cover separation discussed above, an anchorage failure due to crack propagation parallel to the bonded plate near or along the adhesive/concrete interface, starting from the critically stressed position toward the anchored end of the plate may be prematurely achieved.

Several theoretical models, based on the fracture mechanics, have been developed to estimate the debonding load of FRP reinforcement applied on concrete surface (Taljsten, 1994; Neubauer and Rostasy, 1997; Brosens and Van Gemert, 1997; fib bulletin, 2001; Chen and Teng, 2001; Smith and Teng, 2002a,b; CNR-DT200, 2004; Seracino et al., 2007; Ferracuti et al., 2007b). Main analytical relationships depend both on the stiffness, the width and the bond length of the FRP and on the width, the strength and the surface treatment of the reinforced concrete member.

In the following section a derivation of the general relationship predicting the maximum tensile force at debonding based on the fracture energy approach is briefly showed and the some of the above mentioned theoretical formulations of debonding load are recalled, paying particular attention to theoretical approaches suggested by (fib bulletin 14, 2001; Chen and Teng, 2001; CNR-DT200, 2004)

5.1.1.1 Theoretical formulations of debonding load

As showed in 2.2 , the maximum tensile force , F_{max}, at debonding in an FRP external reinforcement characterized by an infinite bonded length can be calculated as (see (2.72)):

$$F_{\max} = b_f \cdot \sqrt{2 \cdot E_f \cdot t_f \cdot \Gamma_F} \tag{5.1}$$

where t_f, b_f, E_f are the thickness, the width, and the Youngs' modulus of the FRP reinforcement.

The fracture energy, G_F, depends on both the strength properties of adherents, concrete and adhesive, and the characteristics of the concrete surface. If the FRP reinforcement is correctly applied, the debonding occurs in the concrete and the specific fracture energy of the interface law can be written in a form similar to that used for the shear fracture (mode I). Therefore, the fracture energy can be expressed as a function of the concrete shear strength: $\Gamma_f\left(\tau_{b,\max}\right)$, where $\tau_{b,max}$ depends on both tensile and compressive concrete strength.

In most formulations, the fracture energy depends directly on the concrete tensile strength and on a shape factor that is function of the FRP-to-concrete width ratio (b_f/b_c). The formulations proposed by (Neubauer and Rostasy, 1997) and (Lu et al., 2005), e.g., are:

$$G_f = 0.204 \cdot k_b{}^2 \cdot f_{ctm} \tag{5.2}$$

$$G_f = 0.308 \cdot \beta_w^2 \cdot \sqrt{f_{ctm}} \tag{5.3}$$

being f_{ctm} the mean tensile strength of concrete, k_b and β_w the shape factors defined as:

$$k_b = 1.06 \sqrt{\frac{2 - b_f / b_c}{1 + b_f / 400}} \tag{5.4}$$

$$\beta_w = \sqrt{\frac{2 - b_f / b_c}{1 + b_f / b_c}} \tag{5.5}$$

Based on both formulations of fracture energy similar to Eqns. (5.2) and (5.3) and experimental results of bond tests, several theoretical formulations to evaluate the bond strength have been proposed in the past (Taljsten, 1994; Neubauer and Rostasy, 1997; Brosens and Van Gemert, 1997; fib bulletin, 2001; Chen and Teng, 2001; Smith and Teng, 2002; CNR-DT200, 2004; Seracino et al., 2007). These expressions allow to predict the plate end debonding load. In some cases, the same expressions are suitably modified by changing some factors in order to predict the intermediate crack debonding load too in RC beams (Teng et al., 2003; Chen et al., 2007; CNR-DT200, 2004). The lay out of these formulations is often similar, while the numerical coefficients calibrated on experimental results are different. Moreover, the safety factors, which need in order to calculate design provisions as part of the Limit State approach, are not always considered. This last point is an important issue, if a safety level (mean, characteristic or design) has to be associated to the provision.

In this section, the theoretical approaches suggested by (fib bulletin 14, 2001; Chen and Teng, 2001b; CNR-DT200, 2004) have been considered to evaluate the bond strength. In particular, the bond strength expressed in terms of maximum tensile load in the FRP reinforcement, $N_{f,max}$, and the effective length, L_e, which is the minimum length required to warrant the full transfer of this load, are defined as follows by the three approaches:

1) fib bulletin 14, 2001:

$$N_{f,\max} = \alpha \cdot c_1 \cdot k_c \cdot k_b \cdot b_f \cdot \beta_L \cdot \sqrt{E_f \cdot t_f \cdot f_{ctm}} \tag{5.6}$$

$$L_e = \sqrt{\frac{E_f \cdot t_f}{2 f_{ctm}}} \tag{5.7}$$

$$\beta_L = \frac{L_b}{L_e} \cdot \left(2 - \frac{L_b}{L_e} \right) \qquad \textit{if } L_b \le L_e, \qquad \beta_L = 1 \textit{ otherwise;} \tag{5.8}$$

$$k_b = 1.06 \sqrt{\frac{2 - b_f / b_c}{1 + b_f / 400}} \ge 1 \qquad \textit{with} \qquad \frac{b_f}{b} \ge 0.33 \tag{5.9}$$

where b_f, t_f, E_f, L_b are width, thickness, Young's modulus and bonded length of the FRP reinforcement, b_c is the width of the concrete element, f_{ctm} is

the mean tensile strength of concrete, $c_1 = 0.64$ and $c_2 = 2$ are coefficients related to an experimental calibration of the fracture energy (Neubauer and Rostasy, 1997), $\alpha = 0.9$ is a reduction factor to account for the influence of inclined cracks on the bond strength, and k_c takes into account the state of compaction of concrete and usually is assumed equal to 1.00, or 0.67 for FRP bonded to concrete faces with low compaction. Finally, k_b is the shape factor

2) Chen and Teng, 2001b:

$$N_{f,\max} = \alpha \cdot \beta_w \cdot \beta_L \cdot b_f \cdot L_e \cdot \sqrt{f'_c} \tag{5.10}$$

$$L_e = \sqrt{\frac{E_f \cdot t_f}{\sqrt{f'_c}}} \tag{5.11}$$

$$\beta_L = \sin\frac{\pi L_b}{2L_e} \qquad if\ L_b \le L_e, \qquad \beta_L = 1\ otherwise \tag{5.12}$$

$$\beta_w = \sqrt{\frac{2 - b_f / b_c}{1 + b_f / b_c}} \tag{5.13}$$

f'_c being the mean cylindrical compressive strength of concrete and α a coefficient equal to 0.427 or 0.315 to calculate a mean or a design provision, respectively. β_w is the shape factor. Note that the debonding laod values of Eq. (5.10) should be divided by an appropriate safety factor $\gamma_b = 1.25$ for design purpose, according to suggestion in Section 3.4 of Teng et al. (2001).

3) CNR DT200-2004:

$$N_{f,\max} = \frac{1}{\gamma_{f,d}\sqrt{\gamma_c}} \cdot \beta_L \cdot b_f \cdot \sqrt{k_G \cdot k_b} \cdot \sqrt{2 \cdot E_f \cdot t_f \cdot \sqrt{f_{ck} \cdot f_{ctm}}} \tag{5.14}$$

$$L_e = \sqrt{\frac{E_f \cdot t_f}{2 \cdot f_{ctm}}} \tag{5.15}$$

$$\beta_L = \frac{L_b}{L_e} \cdot \left(2 - \frac{L_b}{L_e}\right) \qquad if\ L_b \le L_e, \qquad \beta_L = 1\ otherwise; \tag{5.16}$$

$$k_b = \sqrt{\frac{2 - b_f / b_c}{1 + b_f / 400}} \ge 1 \qquad with \qquad \frac{b_f}{b} \ge 0.33 \tag{5.17}$$

where f_{ck} is the characteristic value of the cylindrical compressive strength of concrete and k_G is an experimentally calibrated coefficient, which is 0.064 or 0.03 for mean or design provision, respectively. Finally k_b is the shape factor. The safety factor for debonding failure, $\gamma_{f,d}$, is usually assumed equal to 1.2 or 1.5 (non-controlled or controlled gluing application), while γ_c is the safety factor for concrete (equal to 1.5, EC2, 2004).

5.1.2 Intermediate crack-induced debonding

This section is concerned with the second type of debonding failures stated above, that one induced by a flexural or flexural-shear crack, which is referred to as intermediate crack-induced debonding. In particular, the theoretical approaches found in literature for predicting the mechanical behaviour of beams and slabs which fail by intermediate crack-induced debonding are reported and discussed.

As stated above, plate-end interfacial debonding is a common mode of failure for reinforced concrete beams with bonded steel plates. Many investigations have been performed on this mode of failure. Indeed, most of the previous models for interfacial plate-end debonding of bonded FRP laminates were based on initial models developed for steel plates. By contrast, reinforced concrete beams with bonded FRP plates commonly suffer intermediate (flexure or flexure-shear) crack-induced interfacial debonding. Therefore, only recently, experimental tests relevant for this failure mode were extensively performed to better investigate the debonding mechanism. Descriptions of this mode of failure are provided by Meier (1995), Teng et al. (2002), Bakay (2003), Teng et al. (2003), Teng et al. (2004), Yuan et al. (2007), Chen et al. (2007), Faella et al (2008a).

Crack-induced interfacial debonding phenomenon will be discussed in the following subsections: it will be evident that there is a lack of currently available models for this type of debonding; hence the suggestion provided by international codes are rightly conservative.

5.1.2.1 Experimental observation

Bakay (2003) argued that bending deformation of beams results in the creation of a flexural crack in the soffit of the beam. When shear forces also act, a vertical displacement can occur across the crack resulting in flexural

forces in the composite laminate and tensile stresses in the concrete. When these tensile stresses exceed the tensile strength of the concrete a crack will begin to propagate parallel to the length of the beam in the concrete cover. The layer of concrete remaining bonded to the laminate indicates failure is through the concrete, not the adhesive.

In a similarly manner, provided a single flexural crack dominates the process, Teng et al. (2003) summarised the mechanism of IC debonding as follows: when a major flexural crack is formed in the concrete, the tensile stresses released by the cracked concrete are transferred to the FRP plate. As a result, high local interfacial stresses between the FRP plate and the concrete are induced near the crack. As the applied loading increases further, the tensile stresses in the plate and hence the interfacial stresses between the FRP plate and the concrete near the crack also increase. When these stresses reach critical values, debonding initiates at the crack and then propagates towards one of the plate ends; Garden et al. 1998 showed that they generally propagate toward the nearer end.

Fanning and Kelly (2001) presented a research where the initial goal was to determine the relation between the length of the bonded plate within the shear span and the shear span length. Their belief was that this was an important factor in the brittle failure modes commonly witnessed with FRP strengthened beams. In their study, ten beams were constructed in pairs with varied plate lengths, and subject to 4-point bending. The compressive strength of the concrete was 80 MPa. Beams with plates bonded along their entire length were described to have failed due to the initiation of a shear crack at the soffit of the beam in line with one of the external load points. The remainder of the beams with smaller plated lengths failed as a result of ripping, initiating near the plate end. For beams failing as a result of ripping it seemed there was a relation between the failure load and the strain gradient in the bonded plate length in the shear span at failure. The failure load was higher when the mechanism of failure shifted from end peel/ripping to debonding in the region of a shear crack. Note that the plate end debonding failure was not avoided in presence of plates not bonded along the entire length of the beam. A wide State of the Art (E.Y. Sayed-Ahmed et al., 2009), shows further useful experimental observations on this issue.

5.1.2.2 Similarities between IC debonding and debonding in shear tests

The occurrence of the interfacial crack depends on the FRP-to-concrete bond-slip behaviour. If the bond slip behaviour is assumed to be rigid, the interfacial crack should be expected to occur as soon as a flexural crack appears on the tension face of the original RC beam because otherwise infinite strain is required in the plate for compatibility with the flexural crack. In reality, the bond-slip behaviour is not rigid due to elastic deformations and micro cracking of the bond (i.e. the adhesive and the adjacent concrete) (e.g. chapter 2-4), so a small crack can be accommodated through the deformation of the bond without causing the FRP-to-concrete interface to develop interfacial macro-cracking (i.e. debonding). After flexural cracks are developed, the stresses in the FRP plate are non-uniform even within the constant moment zone.

Anyway, by describing the mechanism of this type of debonding failures, some significant similarities can be highlighted between such debonding failures and those in simple shear tests of FRP-to-concrete bonded joints showed in the previous chapters.

In this regard it is worth note that intermediate crack-induced debonding occurs in two scenarios.

In the first, no significant (major) crack exists between the free end of the bonded laminates and the significant crack where debonding initiates: typical for reinforced concrete beams or slabs with low reinforcement ratios. The stress state of this first scenario is almost similar to the simple pull-off tests. Based on this similarity, the Chen and Teng (2001a) bond strength model is combined with a simple section analysis for predicting the strength of beams and slabs, which fail by intermediate crack-induced debonding. It is shown that through a simple modification of the Chen and Teng bond strength model, the proposed debonding strength model provides a good first approximation to the strengths of such beams.

On the other hand, in the second scenario, one or more significant cracks exist between the debonding initiation crack and the free end of the bonded laminates. In this situation, the stress state is different from that of the simple pull-off tests. Thus, Chen et al. (2007) proposed the following equation for the ultimate load of a bonded FRP plate between two significant cracks:

$$P_u = \frac{b_f \sqrt{2 \cdot G_f E_f t_f}}{\sqrt{1-\beta^2}} \qquad L \geq \frac{1}{\lambda} \arccos \beta \ , \tag{5.18}$$

$$P_u = \frac{b_f \sqrt{2 \cdot G_f E_f t_f} \sin(\lambda L)}{\sqrt{1-\beta \cos(\lambda L)}} \qquad L < \frac{1}{\lambda} \arccos \beta \ , \tag{5.19}$$

$$\lambda = \sqrt{\frac{\tau_f^2}{2G_f}\left(\frac{1}{E_f t_f} + \frac{b_f}{b_c E_c t_c}\right)} = \frac{\tau_f}{\delta_f E_f t_f}\left(1 + \frac{E_f b_f t_f}{E_c b_c t_c}\right) , \tag{5.20}$$

where b_f, t_f, E_f, L are width, thickness, Young's modulus and bonded length of the FRP reinforcement, E_c b_c are the Young's modulus and the width of the concrete element whereas t_c is the thickness of concrete involved in the bond mechanism. τ_f and δ_f are the local bond strength and the maximum slip of the bonded laminates between the two cracks, respectively, β is the ratio between the forces in the bonded laminates at the two cracks locations and G_F is the fracture energy which is the defined by the area under the bond-slip model adopted in the calculations for this joint. Despite their attempt to simplify it, the proposed equation of Chen et al. (2007) still contains implicit parameters which are very hard to evaluate practically.

5.1.2.3 Review of existing analytical models

Several analytical models predicting intermediate debonding are reported in technical codes: European Code (fedeération internationale du béton) fib Bulletin 14 (2001) Approaches 1 and 2; Japanese Code Japan Society of Civil Engineers JSCE (2001); British Code Concrete Society TR55 (2000), and American Code ACI (2008). Apart from these, models reported in various technical papers were also investigated: Maruyama and Ueda (2001), Teng et al. (2003, 2004), Arya and Farmer (2001), Shehata et al. I (2001), Hassanen and Raoof (2001), Wang and Ling (1998), and Zhao (2005). These models were based on the approach to limit the debonding strain in FRP to a certain value to prevent debonding in the design

Other models were based on the shear capacity of the strengthened beam and/or on an interaction between the shear and flexural capacity of the beam. These included models by Matthys (2000), Blaschko et al. (1998), Jansze (1997), Ahmed et al. (2001), Oehlers (1992), Smith and Teng (2002b), Ziraba

et al. (1994), Varastehpour and Hamelin (1996), El-Mihilmy and Tedesco (2001), Colotti and Spadea (2001), and Jones et al. (1988).

In Saxena et al (2008) several models readily available in different studies were collected and briefly described to compare the predictions in terms of bond strength of the strengthened beams. Based on the comparative study of all the models on different failure modes Saxena et al (2008) concluded that no model predicts debonding in a comprehensive way. Moreover, for models that limit the debonding strain, the results are highly conservative. These models are given by design codes and hence their objective is to prevent debonding. But in doing so, the entire capacity of the FRP strengthened beam is not utilized. Note that Saxena et al (2008) referred to ACI code 4402r-2002 and not to ACI code 440-2r-2008. The first limits the debonding strain in FRP to a values less conservative respect to those suggested by the second one. As better discussed in the following chapter, the relationships provided by ACI code 440-2r-2008 and thus also the relationships provided by ACI code 440-2r-2002, are not so conservative as Saxena et al (2008) stated. However it is clear that there is a need for balancing the efficiency of the design to the conservativeness of the approach, and thus more efficient approaches are necessary, taking into account of more key parameters ruling the debonding phenomenon.

5.1.2.4 Theoretical Models and Code Provisions

Several theoretical models have been developed in the scientific literature for checking RC beams externally strengthened by FRP against the possible premature failure due to intermediate debonding. Some of those models have been adopted by the various codes of standards. Since a wide variety of proposals are actually available, a rough classification of the various possible approaches is firstly proposed:

- models defining a maximum value for the axial strain ε_{fd} which can be developed in the FRP laminate before of the occurrence of intermediate debonding failure;
- models defining a maximum gradient of axial stresses σ_f in the FRP laminate (i.e., the maximum stress variation $\Delta\sigma_f$ between two adjacent bending-induced cracks);

– models defining a maximum shear stress τ_{db} resulting in the beam to fail in intermediate debonding.

Beyond the slight differences in the numerical details, the above alternative approached can be easily recognized in the various proposals either available in the scientific literature or adopted by the code of standards. A short review of those proposals is outlined in the following subsections.

1) ACI 440.R2 (2008)

The ACI 440 provisions are clearly inspired at the first class of models defining a maximum value of the axial strain ε_{fd} which can be developed in the FRP laminate. In particular to prevent an intermediate crack-induced debonding failure mode, the maximum strain developed in the FRP should be limited to the strain level, ε_{fd}, at which debonding may occur as defined in (5.21) (ACI 440.R2, 2008 – Eq.10-2):

$$\varepsilon_{fd} = 0.41\sqrt{\frac{f_c'}{nE_f t_f}} \le 0.9\varepsilon_{fu} \ , \tag{5.21}$$

Equation (5.21) takes a modified form of the debonding strain equation proposed by Teng et al. (2003, 2004) listed below. It was based on committee evaluation of a significant database for flexural beam tests exhibiting FRP debonding failure. The proposed equation was calibrated using average measured values of FRP strains at debonding and the database for flexural tests experiencing intermediate crack-induced debonding to determine the best fit coefficient of 0.41. Reliability of FRP contribution to flexural strength is addressed by incorporating an additional strength reduction factor ψ_f for FRP in addition to the strength reduction factor ϕ considered by ACI 318-05 (2005) for structural concrete.

2) JSCE Recommendations (2001)

The Japanese Code of Standards (2001) introduces an explicit methodology for checking the FRP strengthened beams against the premature failure due to loss of bonding. Both plate end debonding and intermediate debonding are

covered by the proposed procedure by checking that no loss of bonding occurs neither in the anchorage zone nor throughout the adhesive interface. The approach for intermediate debonding can be categorized in the second one of the classes listed at the beginning of this section.

Pull out tests and theoretical studies have pointed out that the ultimate strength of a FRP-to-concrete adhesive joint depends on the fracture energy G_f (mainly in mode II with fracture in shear) of concrete and on the Young Modulus E_f and thickness t_f of the FRP reinforcement. Based on the experimental and theoretical findings, the following check can be carried out for verifying that the FRP plate subjected to a tensile stress σ_f in correspondence of the first bending crack of the beam does not fail due to anchorage debonding (JSCE Rec., 2001 – Eq.6.4.1):

$$\sigma_f \le \sqrt{\frac{2G_f E_f}{t_f}} \ , \tag{5.22}$$

A rather similar relationship is proposed for checking the adhesive interface between two adjacent flexural cracks against the loss of bonding. In particular, the following inequality should be checked (JSCE Rec., 2001 – Eq.6.4.2)

$$\Delta\sigma_f \le \Delta\sigma_{f,\max,JSCE} = \sqrt{\frac{2G_f E_f}{t_f}} \ , \tag{5.23}$$

between the axial stress variation $\Delta\sigma_f$ throughout two subsequent cracks and the corresponding interface strength $\Delta\sigma_{f,\max,JSCE}$.

Finally, it is useful to remember that a constant value $G_f = 0.50\ N/mm$ is suggested by this code in lack of specific experimental pull-out tests. Moreover, a crack distance ranging between 150-250 mm is also proposed for estimating the stress variation $\Delta\sigma_f$ in equation (5.23)

3) *fib* bulletin 14 (2001)

fib bulletin 14 (2001) is not just a code of standard in the strict sense. It is rather a document aimed at collecting the most important contributions about designing FRP external strengthening for RC beams in bending. For this reason, more than just one approach is proposed for handling some cutting-edge problems.

In particular, three alternative approaches, each one belonging to the one of the three classes introduced at the beginning of this section, are available therein. The so-called approach #2 can be classified in the second one of those classes, providing a maximum value $\Delta\sigma_{f,\max,fib}$ for the variation $\Delta\sigma_f$ of axial stresses in FRP between two adjacent cracks:

$$\Delta\sigma_f \le \Delta\sigma_{f,\max,fib} \ , \tag{5.24}$$

conceptually defined as follows:

$$\Delta\sigma_{f,\max,fib} = \Delta\sigma_{f,\max,fib}\left(\sigma_{\min}, G_f, s_{rm}, E_f t_f\right) . \tag{5.25}$$

where σ_{min} is the minimum stress value in the two considered cracks and s_{rm} is the average spacing of those cracks.

4) Italian Code CNR DT 200 (2004)

A Code of Standards for utilizing FRP materials as a strengthening technique for both concrete and masonry members has been recently issued in Italy, covering all the main rehabilitation-related topics (flexural and shear strengthening, confinement etc.) by considering the case of strengthening against gravitational actions as well as seismic ones. Debonding failure aspects have been also covered in such a document by providing a direct limitation of the FRP strain value resulting in intermediate debonding failure. The design value ε_{fdd} of the maximum strain ε_{fd} which can be developed in the FRP laminate is defined as follows:

$$\varepsilon_{fdd} = \frac{k_{cr}}{\gamma_{f,d} \cdot \sqrt{\gamma_c}} \cdot \sqrt{\frac{2 \cdot G_{Fk}}{E_f t_f}} \ , \tag{5.26}$$

where $k_{cr} = 3.0$ is usually assumed. In equation (5.26), G_{Fk} is the characteristic value (5% percentile) of the concrete Fracture Energy (in mode II), while E_f and t_f are the FRP Young modulus and the equivalent thickness, respectively. Finally, two different partial safety factors have been introduced in equation (5.26): γ_c is the concrete partial safety factor ($\gamma_c = 1.5$ is usually assumed), while $\gamma_{f,d}$ is based on quality control on the FRP strengthening system ($\gamma_{f,d} = 1.2 - 1.5$).

5) Teng et al. (2003)

The formula proposed by Teng et al. (2003) derives by an empirical formulation formerly proposed by Chen and Teng (2001b). It was based on the analogy between IC debonding failures and debonding failures in simple shear tests and calibrated based on results of about 20 experimental tests.

The formula proposed by Teng et al. (2003) looks after the effect of the concrete compressive strength and the width ratio b_f/b, besides the usual parameters (namely, the axial stiffness $E_f t_f$ of FRP). The formula can be expressed by the following relationship:

$$\varepsilon_{deb} = 0.48 \cdot \beta_w \cdot \sqrt{\frac{\sqrt{f_c'}}{E_f t_f}} \quad , \tag{5.27}$$

where

$$\beta_w = \sqrt{\frac{2 - \frac{b_f}{b}}{1 + \frac{b_f}{b}}} \quad , \tag{5.28}$$

It is worth noting that the debonding strain values provided by (5.27) should be divided by an appropriate safety factor $\gamma_b = 1.25$ for design purpose, according to suggestion in Section 3.4 of Teng et al. (2002).

6) Teng et al. (2004)

This model adopts an approach rather close to the previous one, as both models are based on limiting the maximum strain developed in FRP. It also considers the effect of concrete strength and the width ratio b_f/b. Based on numerical simulations and regression of test data the following design relationship has been suggested:

$$\varepsilon_{deb} = 0.171 \cdot \beta_p \cdot \left(4.32 - \alpha\right) f_{ct} \sqrt{\frac{1}{E_f t_f}} \ , \tag{5.29}$$

where

$$\beta_w = \sqrt{\frac{2.25 - \frac{b_f}{b}}{1.25 + \frac{b_f}{b}}} \ , \ \alpha = \frac{1}{\frac{10.53}{\sqrt{f_{ct}^3}} - \frac{2}{3}} \tag{5.30}$$

Also in this case, values provided by (5.29) should be divided by $\gamma_b = 1.25$ for design purposes.

In the current study, the tensile concrete strength f_{ct} is calculated according to the ACI 318-89 (ACI 1989) equation:

$$f_t = 0.53 \cdot \sqrt{f_c^{'}} \ \text{(MPa)} \tag{5.31}$$

7) Said & Wu Model (2008)

Said & Wu (2008) proposed a model for predicting the ultimate capacity of RC members externally strengthened in bending by FRP. The results of about 200 experimental tests have been considered for calibrating that model and the following relationship came out from that study:

$$\varepsilon_{deb} = 0.75 \cdot \frac{0.23 \cdot \left(f_c^{'}\right)^{0.2}}{\left(E_f t_f\right)^{0.35}} \ , \tag{5.32}$$

where 0.75 is the reduction factor recommended for design purposes.

5.2 NUMERICAL MODELS INTERPRETING DEBONDING PHENOMENON

As shown above, in the last years huge research efforts have been carried out for understanding the behavior of reinforced concrete beams strengthened by externally bonded FRP. The main subject of these studies is the mechanical characterization of the FRP-to-concrete adhesive interface. The different contributions devoted to both plate end debonding and intermediate debonding occurrence have been summarized in the previous sections. However nowadays definitive solutions do not seem yet reached.

Various proposals have been derived from simplified mechanical models and calibrated making use of the experimental results available in the scientific literature (Teng et al., 2002). Alternatively numerical simulation allow to simulate and, thus, further investigate the debonding phenomenon.

Roberts et. al (1988) provided a simplified model for evaluating interface stresses in FRP (or even steel) strengthened beams; simplified equations for evaluating shear and normal stresses throughout the FRP-to-concrete interface have been provided by assuming linear elastic behavior of the adhesive interface. Similar relationships, even obtained under simplified hypotheses for the interface behavior, have been provided in Malek A. M (1998). Authors showed, even through experimental and numerical comparisons, that such simplified formulae usually result in a close approximation of the complex stress patterns which develop throughout the FRP-to-concrete interface.

The above mentioned research papers mainly deal with interface stress distribution in the elastic range, which is an aspect of concern for serviceability conditions. Premature loss of bonding between FRP and concrete needs to be studied by considering a suitable non-linear relationship between interface stresses and strains. Holzenkaempfer (1994) proposed a bi-linear relationship between shear stresses and interface slips; based on such model, Taljsten (1997) determined the expressions of the ultimate bearing capacity of FRP-to-concrete joints.

In Faella et al. (2006a,b) an interesting numerical model is implemented and validated: the study is mainly focused on debonding failure which can

occur at the FRP-cut-off section (plate end debonding) or throughout the FRP-to-concrete adhesive interface (intermediate debonding).

Interface slips between reinforced concrete beam and FRP laminates are considered and, consequently, a well-established non-linear shear stress-slip law is introduced. Moreover, non-linear stress-strain relationships are utilized for modeling the other structural materials and a completely non-linear analysis procedure is obtained by means of a secant approach; such non-linear procedure allows reproducing the whole structural behavior up to failure which can be due to FRP tearing, concrete crushing or interface debonding.

In particular non linear behavior of the materials constituting the FRP strengthened RC beams was introduced by means of fiber discretization of the beam cross section and a secant approach. Three non-linear phenomena were considered for simulating the premature failure possibly due to FRP-to-concrete debonding which can occur in an intermediate section or at the FRP cut-off section. The first one deals with the overall behavior of concrete in compression and tension; the rational formula proposed by Saenz was adopted for concrete in compression while a simple linear relationship up to the tensile stress value was considered for concrete in tension (Figure 5.2).

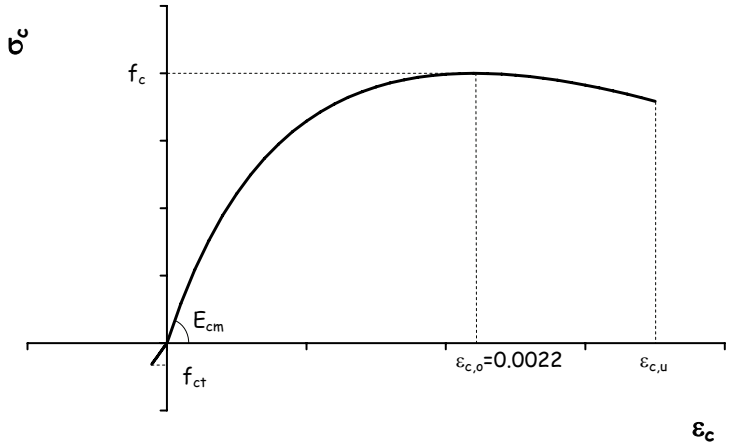

Figure 5.2 - Non-linear stress-strain law for concrete (Faella et al 2008)

Moreover, accounting for yielding in steel rebars is essential for modeling intermediate debonding phenomena in FRP-strengthened beams; the typical stress-strain relationship for steel rebars was be adopted in the numerical

analyses. Strain-hardening in steel was neglected (even if it would be introduced in the model) because strain values in FRP-strengthened beams are usually not so great for strain hardening to be developed in steel rebars.

The well-established and widely accepted elastic-brittle stress-strain relationship was assumed for FRP plate.

Finally, shear behavior of the adhesive interface connecting FRP laminate to the soffit of the beam was described by means of the well-known bi-linear elastic-softening curve introduced by Holzenkaempfer (1994).

A sensitivity analysis was performed to check that no relevant mesh-dependence existed when discretization was refined as usual in non-linear problems.

Figure 5.3 shows two cases (Spadea et. al, 1998; Pham and Al Mahaidi, 2004a) of simply supported beams externally strengthened by FRP and demonstrates how in both cases the complete evolution of the displacement-vs-force curve can be followed by the numerical procedure which provides also a good estimation of the ultimate load and displacement.

Figure 5.4 is devoted to another of the experimental cases which have been found in the scientific literature (Yao et al., 2003); a cantilever beam externally strengthened by FRP was reported in that work and the main results in terms of load-deflection curve are represented in Figure 5.4 demonstrating once more that the numerical procedure is able to reproduce the observed behavior resulting in a very refined evaluation of the ultimate load and deflection at debonding.

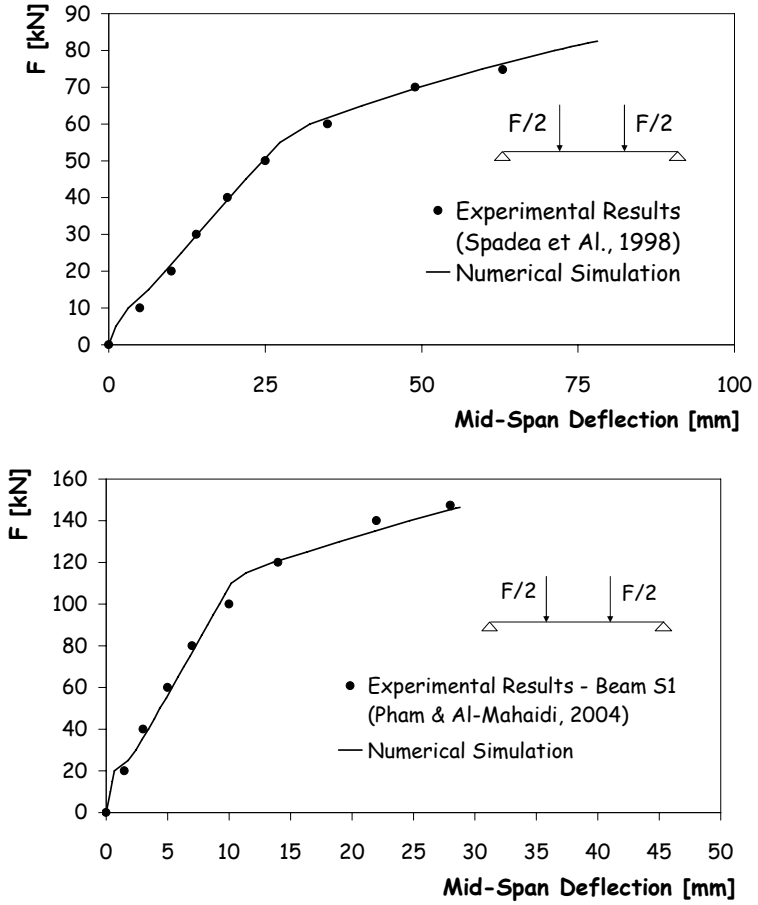

Figure 5.3 - Experimental comparison on simply supported beams: Load-Deflection curves. (Faella et al 2008a)

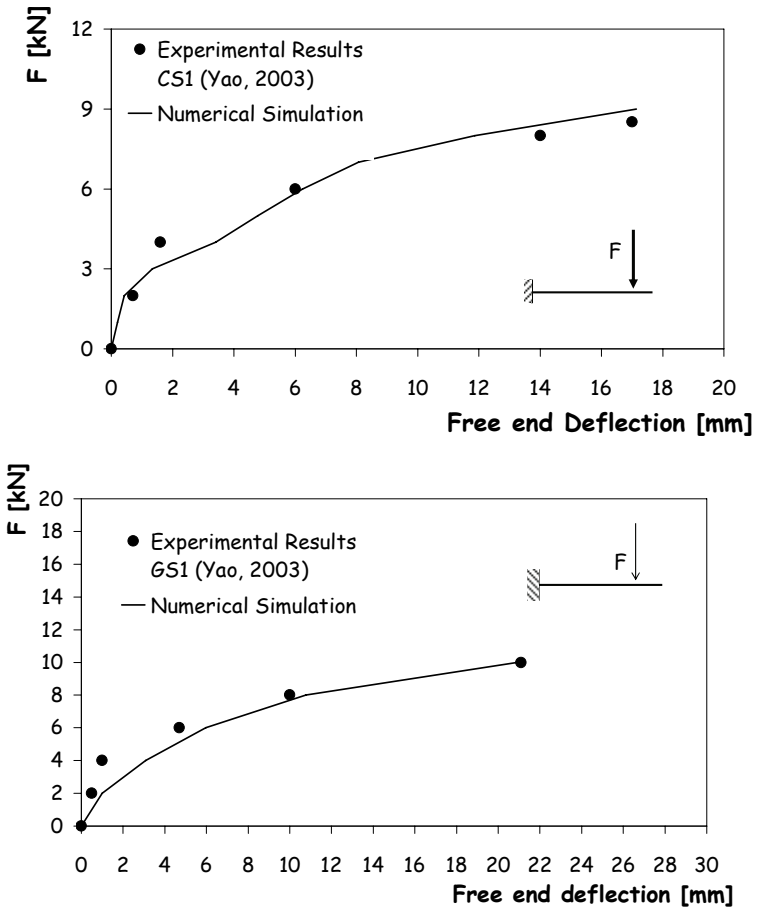

Figure 5.4 - Experimental comparison cantilever beams: Load-Deflection curves.
(Faella et al 2008a)

5.3 DEBONDING FAILURE: BEHAVIORAL OBSERVATIONS

In the present section, a short discussion is proposed for showing the two possible debonding failure modes which has been observed by various authors and can be reproduced by the model proposed in Faella et al. (2008a) mentioned above.

A beam characterized by FRP strengthening running throughout all its length and a similar beam whose FRP-strengthening is interrupted at a distance a=600 mm from the theoretical support point were analyzed.

Figure 5.5 shows the interface slip evolution under increasing load levels and Figure 5.6 represents axial stress in steel rebars and FRP plate at debonding.

Figure 5.5a and Figure 5.6a deal with the beam characterized by FRP strengthening running throughout all the beam length and show how two peak values can be recognized in interface slips. The first and most relevant one is achieved in correspondence of the steel rebar yielding: it increases sharply at the steel yielding section resulting in intermediate debonding. Such local slip growth is due to the fact that load after yielding is beard only by FRP plate as one can see in Figure 5.6a where a sudden increase in FRP strain rate can be observed starting from the above mentioned section. Another peak in slip value occurs near the support due to flexural cracking whose effects can be also observed in terms of FRP and steel axial stresses which slopes change suddenly in the section where cracking begins at about 500 mm from the theoretical support.

On the contrary, Figure 5.5b and Figure 5.6b deal with the case of incomplete FRP-strengthening. A different peak value can be observed in this case either in terms of slip concentration near the FRP cut-off section (Figure 5.5b) or in terms of FRP stress whose distribution along the beam interface is characterized by two different slope changes (Figure 5.6b). In this second case, plate end debonding failure occurs before of intermediate debonding because the ultimate slip value is achieved at FRP cut-off section under an ultimate load value slightly lesser than the one obtained for complete strengthening.

It is worth noticing that, although no emphasis has be done to plate end debonding, Figure 5.5b shows the ability of the proposed procedure to simulate both plate end debonding and intermediate interface debonding failure.

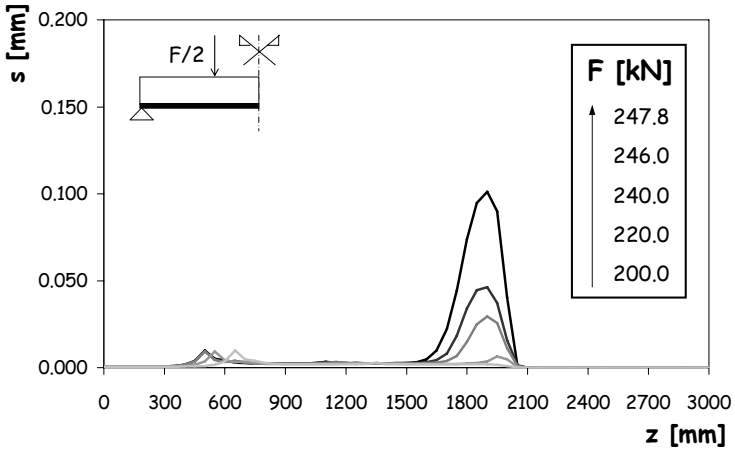

a) intermediate debonding in a case of complete strengthening

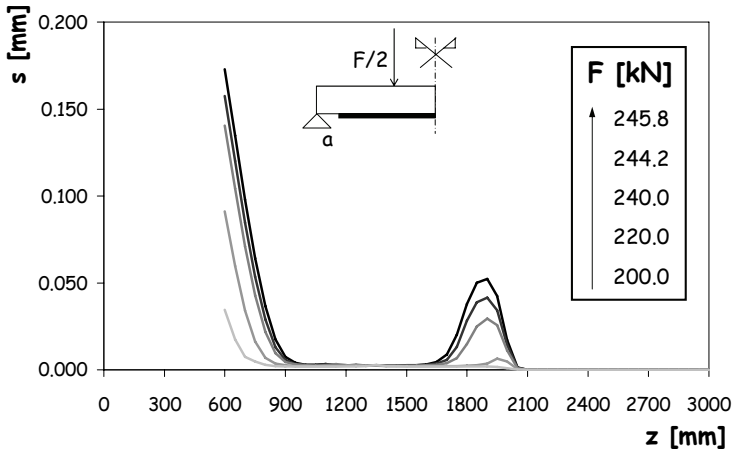

b) plate end-debonding due to partial strengthening

Figure 5.5 - Interface slip evolution due to different load levels up to debonding. (Faella et al., 2008a)

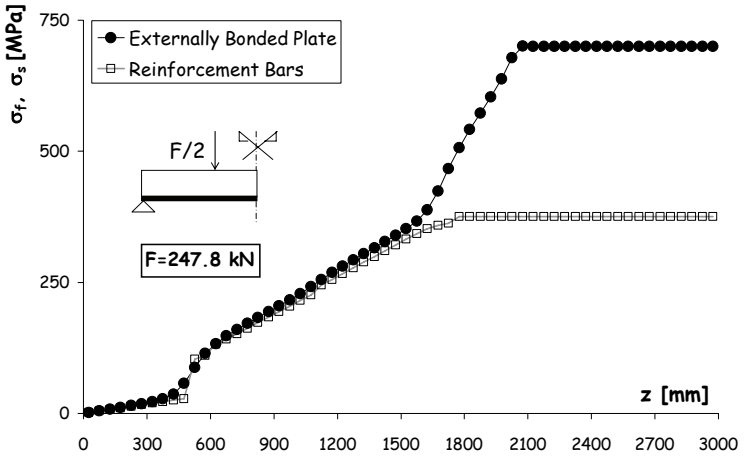

a) intermediate debonding in a case of complete strengthening

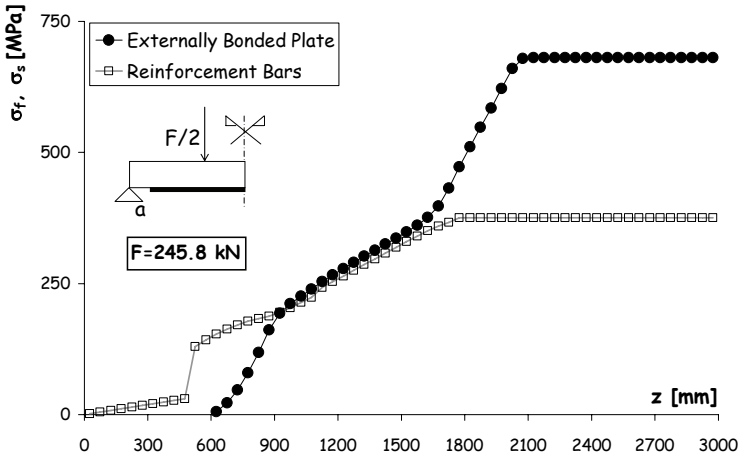

b) plate end-debonding due to partial strengthening

Figure 5.6 - Axial strain distribution in FRP and steel at failure. (Faella et al., 2008a)

A wide parametric analysis has been carried out in Faella et al. (2006b) to emphasize the role of the key parameters which control the intermediate debonding failure in FRP-strengthened RC beams.

As an example, a significant results obtained by numerical analysis is shown in Figure 5.7: $\varepsilon_{f,max}$ values obtained in the case of distributed load are usually greater than those determined under concentrated loads. In fact, being intermediate debonding failure basically controlled by interface shear stresses in correspondence of yielded sections of RC beams, concentrated load schemes, characterized by uniform values of shear force, exhibit performances worse than those obtained under uniformly distributed load.

Consequently, the effective value of FRP axial strain $\varepsilon_{f,max}$ at debonding determined through numerical simulations are usually greater than those which can be evaluated by means of other direct formulations, such as the simplified relationships suggested by some code of standards or available in the scientific literature which are generally based on considering other load conditions.

Therefore, predicting formulae should be redefined for considering the influence of the load scheme on intermediate debonding failure .

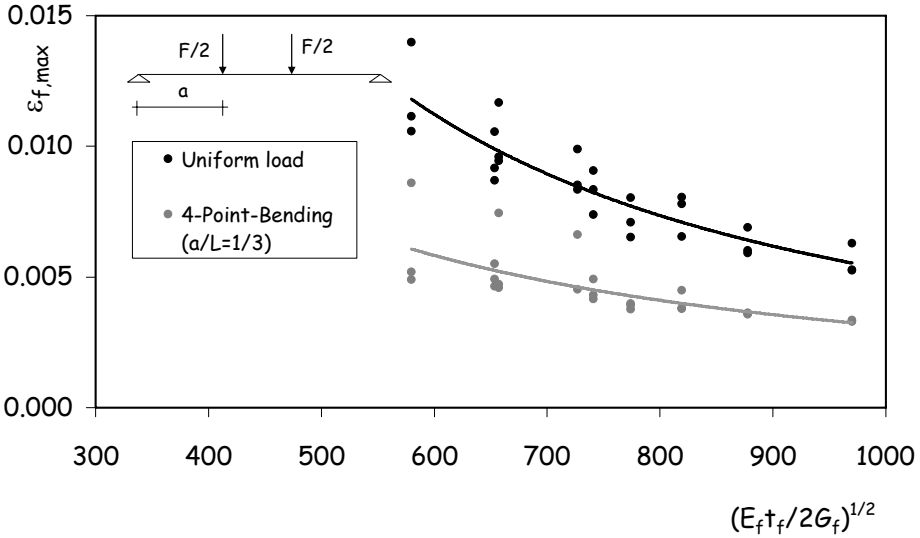

Figure 5.7 - Load scheme effect on FRP axial strain at debonding (Faella et al., 2006)

It is clear that the numerical procedure presented and validated in (Faella et al 2008a) can be utilized as a powerful tool to extend the experimental data, reaching a number of cases which is far larger than the one realizable in a laboratory for practical reasons. Consequently, the influence of the various parameters can be investigated in depth to understand their role and quantifying their importance.

Chapter 6 - Calibration of a capacity model

In this chapter a statistical procedure for the Calibration of resistance models from experimental data, in accordance with the guidelines provided in Eurocode 0 is presented.

The procedure has been implemented on the basis of the results of the bond tests carried out and analyzed in the third and fourth chapters, and based on the results of further bond tests and tests on full-scale members found in literature, briefly summarized and discussed.

The simplified analytical formulation are suggested for predicting the strength of beams and slabs in case of both *plate end debonding* and *intermediate debonding*. The application of the procedure allowed a proposal for updating the design formulae of Instructions CNR-DT200/2004 to be formulated.

6.1 PLATE END DEBONDING MODEL CALIBRATION

This section deals with the assessment of a design formulation to predict the plate end debonding load in Reinforced Concrete (RC) elements strengthened with Externally Bonded Reinforcement (EBR) made of Fiber Reinforced Polymers (FRP) materials.

Several theoretical formulations have been proposed by researchers and international codes to predict the maximum stress in the FRP reinforcement when the plate end debonding (Chen and Teng, 2001; fib bulletin, 2001; CNR DT 200, 2004; Smith and Teng, 2002a,b) or the intermediate debonding (Teng et al., 2003) occurs.

Most of these formulations, characterized by similar structures and often based on the evaluation of the fracture energy at the FRP-to-concrete interface, are calibrated by numerical factors on experimental results. The theoretical approaches have been summarized in 5.1.1.1 .

Numerous results of bond tests are now available in the technical literature, aimed both at evaluating the bond strength and at obtaining experimental bond shear stress-slip laws along the interfaces. Nevertheless, standard experimental set-ups for bond tests are not yet available, although many schemes have been proposed and tested (Yao et al., 2005).

A correct procedure to calibrate design formulations could provide the definition of a reliable test set-up and quantities to be measured, the identification of significant parameters influencing the phenomenon, the distinction between average values and other percentiles, the desegregation of the model in different parts accounting for mechanics, calibration and randomness, and, finally, the assessment of the model against the experimental results (Monti et al., 2009).

Even tough this topic has been widely dealt with by various researchers, statistical analyses are required in order to calibrate correctly the safety factors for the design bond strength model, to follow a limit state design approach and to assess clearly the structural safety associated to the strength model.

Thus, in this section a wide experimental database of bond tests is presented. In particular the experimental debonding loads of several bond tests

available in literature have been collected, examined and joined with the results of test showed in the Chapter 3.

First of all the experimental results have been compared with the predictions of the bond strength models in order to assess their reliability. The same data have been used to assess the influence on FRP debonding load of the main mechanical and geometrical parameters.

Finally a statistical analysis has been performed using the collected results in order to calibrate a bond strength model based on the fracture energy approach. The final proposed strength model is similar to other well-known models suggested in literature and codes but it is based on a detailed and consistent statistical analysis according to the 'design by testing' procedure suggested in EN1990. Different corrective factors allow different percentiles values of the debonding load to be predicted.

Moreover, as preformed and cured in-situ FRP systems have been distinguished, the performances of the latter ones, as concerns the plate end debonding failure, have been exploited.

6.1.1 Theoretical formulations of debonding load

For clarity the theoretical formulations predicting the plate end debonding load suggested by fib bulletin 14, (2001), Chen and Teng, (2001) and CNR-DT200 (2004) will briefly recalled. Further details are reported in 5.1.1.1

1) fib bulletin 14, 2001*:*

$$N_{f,\max} = \alpha \cdot c_1 \cdot k_c \cdot k_b \cdot b_f \cdot \beta_L \cdot \sqrt{E_f \cdot t_f \cdot f_{ctm}} \tag{6.1}$$

$$L_e = \sqrt{\frac{E_f \cdot t_f}{2 f_{ctm}}} \tag{6.2}$$

$$\beta_L = \frac{L_b}{L_e} \cdot \left(2 - \frac{L_b}{L_e} \right) \qquad \text{if } L_b \le L_e, \qquad \beta_L = 1 \text{ otherwise;} \tag{6.3}$$

$$k_b = 1.06 \sqrt{\frac{2 - b_f / b_c}{1 + b_f / 400}} \ge 1 \qquad \text{with} \qquad \frac{b_f}{b} \ge 0.33 \tag{6.4}$$

2) Chen and Teng, 2001:

$$N_{f,\max} = \alpha \cdot \beta_w \cdot \beta_L \cdot b_f \cdot L_e \cdot \sqrt{f'_c} \tag{6.5}$$

$$L_e = \sqrt{\frac{E_f \cdot t_f}{\sqrt{f'_c}}} \tag{6.6}$$

$$\beta_L = \sin\frac{\pi L_b}{2L_e} \qquad if\ L_b \le L_e, \qquad \beta_L = 1\ otherwise \tag{6.7}$$

$$\beta_w = \sqrt{\frac{2 - b_f / b_c}{1 + b_f / b_c}} \tag{6.8}$$

3) CNR DT200-2004:

$$N_{f,\max} = \frac{1}{\gamma_{f,d}\sqrt{\gamma_c}} \cdot \beta_L \cdot b_f \cdot \sqrt{k_G \cdot k_b} \cdot \sqrt{2 \cdot E_f \cdot t_f \cdot \sqrt{f_{ck} \cdot f_{ctm}}} \tag{6.9}$$

$$L_e = \sqrt{\frac{E_f \cdot t_f}{2 \cdot f_{ctm}}} \tag{6.10}$$

$$\beta_L = \frac{L_b}{L_e} \cdot \left(2 - \frac{L_b}{L_e}\right) \qquad if\ L_b \le L_e, \qquad \beta_L = 1\ otherwise; \tag{6.11}$$

$$k_b = \sqrt{\frac{2 - b_f / b_c}{1 + b_f / 400}} \ge 1 \qquad with \qquad \frac{b_f}{b} \ge 0.33 \tag{6.12}$$

6.1.2 The experimental database

A lot of results have been collected from the technical literature concerning bond tests on concrete elements externally strengthened with CFRP cured in situ (sheets) and preformed (plates) systems. Several set-ups (Yao et al., 2005) have been realized by the researchers and each of them can be considered more or less reliable for the right prediction of the actual loading conditions and, thus, of the plate end debonding load in existing elements. In particular, constructive detailing of specimens can influence the reliability of these results.

6.1.2.1 Description of the experimental database

The only results of push-pull bond shear tests have been considered to perform the statistical analyses; moreover, the results of cured in situ and preformed systems have been distinguished in two different groups. In the push-pull test set-up (see Figure 6.1) the concrete block is loaded by a pushing force that is applied at a certain distance, a, from the FRP reinforcement that is loaded in tension by a pulling action.

Several experimental programs have shown that the push-pull set-up can be simply realized, according to different set-ups. However, as showed in detail in chapter 3, such a set-up is less sensitive to construction details and, thus, furnishes low scattered results in terms of debonding loads. This is the reason for what it is widely used to predict the bond strength for both shear and flexural strengthening in RC beams (Yao et al., 2005).

By the contrast, the realization of bond tests where both the FRP reinforcement and the concrete block are loaded by tension forces (pull-pull scheme) requires special attention in detailing, especially if the symmetry is wanted through the application of reinforcement on both sides of the concrete specimens (Leone et al., 2009). In these schemes the set-ups are more sensitive to the geometrical inaccuracies and thus, the repeatability or the variability of the results can be strongly affected by detailing.

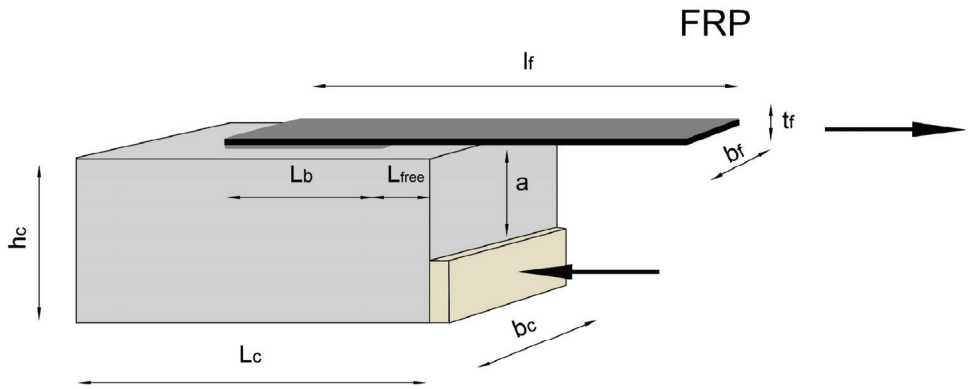

Figure 6.1 - General scheme of an asymmetrical push-pull bond test.

In existing RC element (i.e. in RC beams) the FRP external reinforcement is usually applied on the tension side, so that the pull-pull scheme seems to

replicate better the actual loading conditions. However, in the push-pull scheme, suitable values of the distance a (Figure 6.1) ensure the development of a bond failure at the concrete-FRP interface, similarly to what occurs in pull-pull scheme. By the contrast, for low values of a, the compressive stresses induced by the pushing force can limit the volume of concrete involved in the failure mechanism and, thus, furnish safe values of debonding load due to smaller values of energy fracture.

The results of specimens with bonded length, width and Youngs' modulus of the FRP reinforcement lower than 75 mm, 25 mm, and 80 GPa, respectively, were not considered.

For specimens strengthened with FRP sheets (Aiello and Leone, 2005; Yao et al., 2005; Savoia et al., 2009; Bilotta et al., 2009a,b; Ceroni and Pecce, 2010; Lu et al., 2005; McSweeney and Lopez, 2005; Takeo et al., 1997; Travassos et al., 2005; Ueda et al., 1999; Wu et al., 2001; Zhao et al., 2000) the main parameters (see Figure 6.1 for the geometrical parameters) vary in the following ranges: concrete width b_c = 100-500 mm, width of FRP reinforcement b_f = 25-100 mm, b_f/b_c = 0.17–1, thickness of FRP reinforcement t_f = 0.083-0.507 mm, bonded length of FRP reinforcement L_b = 75-500 mm, number of layers of FRP reinforcement n = 1-3, Young's modulus of FRP reinforcement E_f = 82-390 GPa, mean compressive strength of concrete f_{cm} = 17-62 MPa, and mean tensile strength of concrete f_{ctm} = 1.3-4.3 MPa.

Analogously, for specimens strengthened with FRP plates (Chajes et al., 1996; Faella et al., 2002b, Mazzotti et al., 2009; Nigro et al., 2008c; Savoia et al., 2009; Bilotta et al., 2009a,b; Bilotta et al., 2011a) the main parameters vary in the following ranges: b_c = 150-230 mm, b_f = 25-100 mm, b_f/b_c = 0.11–0.63, t_f = 1.0-1.6 mm, n = 1, L_b = 150-400 mm, E_f = 108-400 GPa, f_{cm} = 15-53 MPa, and f_{ctm} = 1.10-3.8 MPa.

Totally, 216 data of bond tests for sheets and 68 for plates have been collected. Note that data from the database presented in this thesis were 9 for sheets and 27 for plate respectively. Hence the necessity to enrich the database for plates has been enough resolved.

6.1.2.2 Comparison with existing formulations

The Eqns. (6.1), (6.5) and (6.9) have been used to calculate the theoretical debonding loads for both 216 and 68 bond tests performed on FRP cured in situ and preformed systems, respectively. In Table 6.1 and Table 6.2 the mean value, the standard deviation and the Coefficient of Variation (CoV) of the ratio N_{th}/N_{exp} are reported for each model introduced in section 6.1.1 for both FRP reinforcement typologies.

The theoretical values of Eq. (6.1) have been calculated assuming k_c =1. For Eq. (6.5) α is assumed 0.427 to calculate the mean value and 0.315 for the 0.05 percentile. In Eq. (6.9) $\gamma_{f,d} = 1$, $\gamma_c = 1$, and k_G is assumed 0.064 for the mean value and 0.030 for the 0.05 percentile.

In all cases, the tensile strength of concrete has been evaluated basing on the compressive strength provided by the experimenter by the following relationship of (EN1992, 2004):

$$f_{ctm} = 0.3 \cdot \sqrt[3]{f_{ck}^{\,2}} \qquad \text{with} \qquad f_{ck} = f_{cm} - 8 \tag{6.13}$$

For the models of (CNR DT 200, 2004 and Chen and Teng, 2001) the mean value of the ratio N_{th}/N_{exp} for the cured in situ systems is lower (about 0.9) than plates (1.02-1.07). This means that for the plates the mean provisions are not safe in some case. The same difference (about 10%) between the two systems can be observed for the 0.05 percentile too. Moreover, a similar difference is observed in the formulation of (fib bulletin 14, 2001), which gives a provision without a clear statistical significance. The values of CoV show an higher variance for the plates (+20-25%) compared with the sheets. In general, the lowest CoV is achieved by the model of (Chen and Teng , 2001) for both systems.

Table 6.1 - Statistical data for the ratio N_{th}/N_{exp} for cured in situ FRP systems (216 results).

	Mean values		5%		
N_{th}/N_{exp}	CNR DT-200 Eq (6.9)	Chen & Teng Eq. (6.5)	CNR DT-200 Eq (6.9)	Chen & Teng Eq. (6.5)	Fib bulletin 14 Eq. (6.1)
Mean	0.92	0.91	0.63	0.67	0.96
St. dev.	0.17	0.14	0.12	0.11	0.17
CoV	19.0%	15.7%	19.0%	15.7%	17.3%

Table 6.2 - Statistical data for the ratio N_{th}/N_{exp} for preformed FRP systems (68 results).

N_{th}/N_{exp}	Mean values		5%		
	CNR DT-200 Eq (6.9)	Chen & Teng Eq. (6.5)	CNR DT-200 Eq (6.9)	Chen & Teng Eq. (6.5)	Fib bulletin 14 Eq. (6.1)
Mean	1.02	1.07	0.70	0.79	1.08
St. dev.	0.26	0.20	0.18	0.15	0.24
CoV	25.0%	19.1%	25.0%	19.1%	22.5%

6.1.3 Assessment of a new formulation

A new strength model formulation has been assessed in order to calculate the plate end debonding load with an approach similar to Eqs. (6.1), (6.5) and (6.9). Moreover, the numerical coefficients have been calibrated through a probabilistic approach (Design assisted by testing, Monti et al., 2009, Bilotta et al 2009c) as suggested in (EN1990 – Annex D, EC0) and their definition is aimed to give a clear safety meaning to the provisions.

6.1.3.1 Calibration procedure

Firstly, the random variable δ is defined as the ratio of the experimental debonding load, N_{exp}, to the theoretical one representing the strength model, N_{th}:

$$\delta_i = \frac{N_{\exp,i}}{N_{th,i}} \tag{6.14}$$

The mean value, the variance, the standard deviation and the CoV of this variable are defined as:

$$\overline{\delta} = \frac{1}{n}\sum_{i=1}^{n}\delta_i \tag{6.15}$$

$$s_\delta^2 = \frac{1}{n-1}\sum_{i=1}^{n}(\delta_i - \overline{\delta})^2 \tag{6.16}$$

$$\sigma_\delta = \sqrt{s^2{}_\delta} \tag{6.17}$$

$$CoV = \frac{\sigma_\delta}{\overline{\delta}} \tag{6.18}$$

The strength model expressed by N_{th} should be fine-tuned by a least-square coefficient, which minimizes the difference between each theoretical, $N_{th,i}$, and experimental, $N_{exp,i}$, value. Usually, this can be simply carried out considering the regression line of the graph $N_{th,i}$ - $N_{exp,i}$. The slope of this line intercepting the origin furnishes the least-square coefficient, k_m.

Successively, the random variable δ_m is defined as the ratio of the experimental debonding load N_{exp}, to the theoretical one, N_{th}, adjusted by means of the fine-tuning parameter, k_m:

$$\delta_{m,i} = \frac{N_{\exp,i}}{k_m \cdot N_{th,i}} \tag{6.19}$$

The mean value, the variance, the standard deviation and the CoV of δ_m are defined as:

$$\overline{\delta_m} = \frac{1}{n}\sum_{i=1}^{n}\delta_{m,i} = \frac{1}{n}\sum_{1=1}^{n}\frac{N_{\exp,i}}{k_m \cdot N_{th,i}} = \frac{\overline{\delta}}{k_m} \tag{6.20}$$

$$s_{\delta_m}^2 = \frac{1}{n-1}\sum_{i=1}^{n}(\delta_{m,i} - \overline{\delta_m})^2 = \frac{1}{n-1}\sum_{i=1}^{n}\left(\frac{N_{\exp,i}}{k_m \cdot N_{th,i}} - \frac{\overline{\delta}}{k_m}\right) = \frac{{s_\delta}^2}{k_m} \tag{6.21}$$

Thus, the mean provision for the debonding load can be assumed as:

$$N_{th,m} = k_m \cdot \overline{\delta_m} \cdot N_{th} \tag{6.22}$$

In the Eq. (6.22) the model error is represented by the mean value of the variable δ_m, which is not 1, because the regression line was forced to intercept the origin.

In the State Limit approach, any strength is assumed as a random variable and, in general, the 0.05 percentile (named ‘characteristic value’) of its frequency distribution is used for design purposes. A very suitable distribution is the Gaussian one, but to use it the check of the normality hypothesis of the random variable is required. Several statistical tests (Shapiro-Wilk, Anderson-Darling, Martinez-Iglewicz, Kolmogorov-Smirnov, D'Agostino skewness,

D'Agostino kurtosis, D'Agostino Omnibus) can be performed (Mood et al., 1974; Shapiro and Wilk, 1965) to verify the normality or log-normality hypothesis of the experimental distributions.

If the debonding load is assumed as a random variable and the Young's modulus of the FRP reinforcement, the tensile and compressive strength of concrete are assumed as the only parameters influencing the bond strength, the general expression of the strength model adjusted by the fine-tuning coefficient, k_m, is:

$$N_{th,m} = N_{th,m}\left(E_f, f_{cm}, f_{ctm}, \overline{\delta_m}, k_m\right) \tag{6.23}$$

Moreover, under the hypothesis of Gaussian distribution, the 0.05 percentile of the variable debonding load can be calculated as:

$$N_{th,k,0.05} = N_{th,m} - 1.64 \cdot \left[Var(N_{th,m})\right]^{0.5} \tag{6.24}$$

where the variance of $N_{th,m}$ can be expressed as:

$$\begin{aligned} Var\left(N_{th,m}\right) &= C_{Efm}^2 \cdot Var\left(E_f\right) + C_{fcm}^2 \cdot Var\left(f_{cm}\right) + \\ &+ C_{fctm}^2 \cdot Var\left(f_{ctm}\right) + C_{\delta m}^2 \cdot Var\left(\delta_m\right) \end{aligned} \tag{6.25}$$

$$\begin{aligned} C_{Efm} &= \left|\frac{\partial N_{th,m}}{\partial E_f}\right|_{\overline{E_f}}, \\ C_{f_{cm}} &= \left|\frac{\partial N_{th,m}}{\partial f_{cm}}\right|_{\overline{f_{cm}}}, \\ C_{f_{ctm}} &= \left|\frac{\partial N_{th,m}}{\partial f_{ctm}}\right|_{\overline{f_{ctm}}}, \\ C_{\delta_m} &= \left|\frac{\partial N_{th,m}}{\partial \delta_m}\right|_{\overline{\delta_m}} \end{aligned} \tag{6.26}$$

If the Eqs. (6.25) and (6.26) are substituted in the Eq. (6.24), the 0.05 percentile of the debonding load becomes:

$$N_{th,k,0.05} = N_{th,m} - 1.64 \cdot N_{th,m} \cdot \left[\begin{matrix} a \cdot CoV_{E_f}{}^2 + b \cdot CoV_{f_{cm}}{}^2 + \\ + c \cdot CoV_{f_{ctm}}{}^2 + CoV_{\delta_m}{}^2 \end{matrix} \right]^{0.5} \tag{6.27}$$

where the coefficients a, b, c depend on the functional relation of N_{th} from the parameters E_f, f_{cm} and f_{ctm}. The CoVs are defined for each parameter as the ratio of its mean value to the standard deviation:

$$CoV_{E_f} = \frac{\overline{E_f}}{s_{E_f}},\ CoV_{f_{ctm}} = \frac{\overline{f_{ctm}}}{s_{f_{ctm}}},\ CoV_{f_{cm}} = \frac{\overline{f_{cm}}}{s_{f_{cm}}},\ CoV_{\delta_m} = \frac{\overline{\delta_m}}{s_{\delta_m}} \tag{6.28}$$

Note that the standard deviations of E_f, f_{cm}, and f_{ctm} have been assessed according to some literature information:

$$s_{E_f} = 0.05 \cdot \overline{E_f}\ ,\ s_{f_{ctm}} = 0.183 \cdot \overline{f_{ctm}}\ ,\ s_{f_{cm}} = 4.88\,, \tag{6.29}$$

Clearly, the coefficient of variation of the variable δ_m, $\mathrm{CoV}_{\delta m}$, depends on the data distribution.

The Eq. (6.27) can be written as:

$$N_{th,k,0.05} = k_k \cdot N_{th} \tag{6.30}$$

$$k_{k,0.05} = k_m \cdot \overline{\delta_m} \cdot \left(1 - 1.64 \cdot \left[\begin{matrix} a \cdot CoV_{E_f}{}^2 + b \cdot CoV_{f_{cm}}{}^2 + \\ + c \cdot CoV_{f_{ctm}}{}^2 + CoV_{\delta_m}{}^2 \end{matrix} \right]^{0.5} \right) \tag{6.31}$$

If the coefficients of variation of the materials were neglected, the Eq. (6.30) became the well known following one:

$$N_{th,k,0.05} = N_{th} \cdot \overline{\delta_m} \cdot k_m \cdot \left(1 - 1.64 \cdot CoV_{\delta_m}\right) = N_{th} \cdot k_m \cdot \left(\overline{\delta_m} - 1.64 \cdot s_{\delta_m}\right) \tag{6.32}$$

However, herein all coefficients of variation have been taken into account.

The percentiles 0.05 (characteristic values) are usually divided to safety factors, which take into account the model uncertainness (EN1990 – Annex D). Also, percentiles lower than 0.05 can be obtained by replacing in the Eq. (22) the coefficient 1.64 with the coefficients 2.58 and 3.08 corresponding to the 0.005 and 0.001 percentiles, respectively. These lower percentiles can be used as alternative to the characteristic values divided to the safety factors.

6.1.3.2 4.2 Application to the experimental database

The general Eq. (6.23) for debonding load can be particularized by introducing the dependence on the bond shear strength. Indeed, the bond shear strength depends on the concrete strength and can be related to the Mohr's circle representing the stress condition in the concrete at failure. Thus, different formulations for shear strength have been considered varying the dependence on the concrete strength. In particular, the following five expressions for the debonding load are examined:

$$\text{Case 1: } N_{th} = \beta_L \cdot b_f \cdot \sqrt{2 \cdot E_f \cdot t_f \cdot k_b \cdot \sqrt{f_{cm} \cdot f_{ctm}}} \tag{6.33}$$

$$\text{Case 2 : } N_{th} = \beta_L \cdot b_f \cdot \sqrt{2 \cdot E_f \cdot t_f \cdot k_b \cdot f_{cm}^{2/3}} \tag{6.34}$$

$$\text{Case 3: } N_{th} = \beta_L \cdot b_f \cdot \sqrt{2 \cdot E_f \cdot t_f \cdot k_b \cdot f_{cm}^{0.6}} \tag{6.35}$$

$$\text{Case 4: } N_{th} = \beta_L \cdot b_f \cdot \sqrt{2 \cdot E_f \cdot t_f \cdot k_b \cdot \frac{f_{cm} \cdot f_{ctm}}{f_{cm} + f_{ctm}}} \tag{6.36}$$

$$\text{Case 5: } N_{th} = \beta_L \cdot b_f \cdot \sqrt{2 \cdot E_f \cdot t_f \cdot k_b \cdot 0.9 \cdot f_{ctm}} \tag{6.37}$$

In the Eq. (6.23), if a Coulomb failure criterion is adopted, the term $\sqrt{f_{cm} \cdot f_{ctm}}$ is 2 times the cohesion associated to the Mohr's circle of an interface concrete element subjected to both shear and normal stresses. The presence of normal stresses has been often experimentally evidenced by the

visual inspection of the debonded surface configuration (Mazzotti et al., 2008). Thus, the case 1 plays better the actual physical phenomenon, because it takes into account the both presence of shear interfacial stresses and normal stresses.

Moreover, in the Eq. (6.34) the term $f_{cm}^{2/3}$ is a simplification of $\sqrt{f_{cm} \cdot f_{ctm}}$, if the concrete tensile strength is calculated by the Eq. (12).

Analogously in the Eq. (6.36), the term $\frac{f_{cm} \cdot f_{ctm}}{f_{cm} + f_{ctm}}$ is the maximum shear stress compatible with the strength f_{cm} and f_{ctm} in an interface concrete element subjected to only shear stresses (the Mohr's circle has centre in the axis origin in this case).

In the Eq. (6.37), the term $0.9 \cdot f_{ctm}$ is a simplification of the term $\frac{f_{cm} \cdot f_{ctm}}{f_{cm} + f_{ctm}}$ under the assumption that the compressive strength is about 10 times the tensile one.

Finally in Eq. (6.35), the term $f_{cm}^{0.6}$ is a further modification of $0.9 \cdot f_{ctm}$ in according to the expression for the concrete tensile strength given by (Model Code, 90)

$$f_{ctm} = 0.32 \cdot f_{cm}^{0.6} \tag{6.38}$$

For all cases the mean and the characteristic predictions of debonding load can be calculated using the previously introduced Eq. (6.22) and Eq. (6.30):

$$N_{th,m} = k_m \cdot \overline{\delta_m} \cdot N_{th} \tag{6.39}$$

$$N_{th,k,0.05} = k_{k,0.05} \cdot N_{th} \tag{6.40}$$

where k_m is the least square coefficient associated to the regression line intercepting the origin, $\overline{\delta_m}$ is given by Eq. (6.21), and $k_{k,0.05}$ is given by the Eq. (6.31).

For each equation, the best fitting coefficient k_m has been calculated considering the experimental results distinguished in two series: sheets and plates.

In Table 6.3 the coefficient k_m and the R^2 value of the corresponding least-square line, which is a measure of the reliability of the regression, are reported for all the equations. The mean value of the variable δ_m, defined by the Eqs. (6.20) and (6.21), and its *CoV* are reported too. In all cases the CoV, which is a measure of the model significance, is lower than the threshold value of 40% (Monti et al., 2009), so that all the models can be considered reliable. However, it can be observed that, while for the sheets the R^2 value is low sensitive to the model and is quite elevated (0.855-0.881), on the contrary for the plates the choice of the model can be significant considering that R^2 varies in the range 0.349 - 0.565. The higher CoV and the smaller R^2 value of the preformed FRP systems with respect to the in-situ sheets, despite of their better quality control in factory. This is justifiable by the larger sensitivity of this system to the detailing of the experimental procedure. Indeed, as increases stiffness of the FRP system more it adapts difficult to the inaccuracies of the experimental set-up, which can influence the debonding load. In particular, the case 3 results the best-fitting model because of the highest value of R^2; this relationship depends on the compressive strength of concrete with an exponent 0.6. Note that for design aim, the choice of the best-fitting model has the clear advantage to furnish characteristic values more close to the mean ones, because the theoretical loads show a smaller gap with the experimental results. In Table 6.3 the coefficients k_k to calculate different percentiles (5%, 0.5%, and 0.1%) are reported too. The coefficients $k_m \cdot \overline{\delta_m}$, which allow calculating the mean provisions, differ of about 12-15% for the sheets and the plates. The factors $k_{k,0.05}$, which allow calculating the 0.05 percentiles, differ of about 17-21%.

Table 6.3 - Statistical data for different bond strength models.

Case	FRP type	k_m	R^2	$\overline{\delta_m}$	CoV_{δ_m}	$k_m \cdot \overline{\delta_m}$	$k_{k,0.05}$	$k_{k,0.005}$	$k_{k,0.001}$
1	Sheet	0.270	0.855	1.027	17.7%	0.278	0.192	0.143	0.117
	Plate	0.236	0.349	1.064	23.2%	0.251	0.152	0.095	0.064
2	Sheet	0.258	0.878	1.010	17.6%	0.261	0.182	0.137	0.112
	Plate	0.221	0.534	1.034	20.4%	0.229	0.149	0.103	0.078
3	Sheet	0.291	0.881	1.006	17.7%	0.293	0.204	0.154	0.126
	Plate	0.248	0.565	1.030	20.0%	0.255	0.169	0.119	0.092
4	Sheet	0.535	0.862	1.022	17.6%	0.547	0.370	0.269	0.214
	Plate	0.466	0.375	1.060	23.0%	0.496	0.294	0.180	0.118
5	Sheet	0.544	0.863	1.021	17.5%	0.555	0.375	0.270	0.213
	Plate	0.473	0.379	1.059	22.9%	0.502	0.297	0.180	0.117

From the coefficients k_m and $k_{k,0.05}$ can be easily obtained the coefficients k_{Gm} and k_{Gk} calibrating the energy fracture for the different models (i.e. $k_G = (k)^2$). They are reported in Table 6.4.

Table 6.4 – k_G coefficients calibrating the energy fracture.

Case	FRP type	$k_{G,m}$	$k_{G,0.05}$
1	Sheet	0.077	0.037
	Plate	0.063	0.023
2	Sheet	0.068	0.033
	Plate	0.052	0.022
3	Sheet	0.086	0.042
	Plate	0.065	0.029
4	Sheet	0.299	0.137
	Plate	0.246	0.086
5	Sheet	0.308	0.141
	Plate	0.252	0.088

The general Eq. (6.23) for the model playing better the actual physical phenomenon (case 1) is:

$$N_{th} = \beta_L \cdot b_f \cdot \sqrt{2 \cdot E_f \cdot t_f \cdot k_b \cdot \sqrt{f_{cm} \cdot f_{ctm}}} \tag{6.41}$$

The corresponding 0.05 percentile provision given by the Eqns. (6.30) and (6.31) is:

$$N_{th,k,0.05} = N_{th,m} - 1.64 \cdot N_{th,m} \cdot \left[\begin{array}{l} 0.5^2 \cdot CoV_{E_f}{}^2 + (0.25)^2 \cdot CoV_{f_{cm}}{}^2 + \\ + (0.25)^2 \cdot CoV_{f_{ctm}}{}^2 + CoV_{\delta_m}{}^2 \end{array} \right]^{0.5} = k_k \cdot N_{th} \tag{6.42}$$

$$N_{th,k,0.05} = k_{k,0.05} \cdot N_{th} = k_m \cdot \delta_m \cdot \left[1 - 1.64 \cdot \left[\begin{array}{l} 0.5^2 \cdot CoV_{E_f}{}^2 + (0.25)^2 \cdot CoV_{f_{cm}}{}^2 + \\ + (0.25)^2 \cdot CoV_{f_{ctm}}{}^2 + CoV_{\delta_m}{}^2 \end{array} \right]^{0.5} \right] \tag{6.43}$$

with

$$C_{Efm} = \left| \frac{\partial N_{th,m}}{\partial E_f} \right|_{\overline{E_f}} = N_{th,m} \cdot \frac{0.5}{\overline{E_f}} \tag{6.44}$$

$$C_{Efm}^2 \cdot Var\left(E_f\right) = N_{th,m}{}^2 \cdot \frac{0.5^2}{\overline{E^2}_f} \cdot Var(E_f) = N_{th,m}{}^2 \cdot 0.5^2 \cdot CoV^2{}_{E_f} \tag{6.45}$$

$$C_{f_{cm}} = \left| \frac{\partial N_{th,m}}{\partial f_{cm}} \right|_{\overline{f_{cm}}} = N_{th,m} \cdot \frac{0.25}{\overline{f_{cm}}} \tag{6.46}$$

$$C_{fcm}^2 \cdot Var\left(f_{cm}\right) = N_{th,m}{}^2 \cdot \frac{(0.25)^2}{\overline{f_{cm}^2}} \cdot Var(f_{cm}) = N_{th,m}{}^2 \cdot (0.25)^2 \cdot CoV_{f_{cm}}^2 \tag{6.47}$$

$$C_{f_{ctm}} = \left| \frac{\partial N_{th,m}}{\partial f_{ctm}} \right|_{\overline{f_{ctm}}} = N_{th,m} \cdot \frac{0.25}{\overline{f_{ctm}}} \tag{6.48}$$

$$C_{fctm}^2 \cdot Var\left(f_{ctm}\right) = N_{th,m}{}^2 \cdot \frac{(0.25)^2}{\overline{f_{ctm}^2}} \cdot Var(f_{ctm}) = N_{th,m}{}^2 \cdot (0.25)^2 \cdot CoV_{f_{ctm}}^2 \tag{6.49}$$

$$C_{\delta_m} = \left| \frac{\partial N_{th,m}}{\partial \delta_m} \right|_{\overline{\delta_m}} = \frac{N_{th,m}}{\overline{\delta_m}} \tag{6.50}$$

$$C_{\delta m}^2 \cdot Var\left(\delta_m\right) = N^2{}_{th,m} \cdot \frac{Var(\delta_m)}{\overline{\delta_m}} = N^2{}_{th,m} \cdot CoV^2{}_{\delta_m} \tag{6.51}$$

Similarly, the general Eq. (6.23) for the best-fitting model (case 3) is:

$$N_{th,m} = k_m \cdot \delta_m \cdot \beta_L \cdot b_f \cdot \sqrt{2 \cdot E_f \cdot t_f \cdot k_b \cdot f_{cm}{}^{0.6}} \tag{6.52}$$

The corresponding 0.05 percentile provision given by the Eqns. (6.30) and (6.31) is:

$$N_{th,k,0.05} = N_{th,m} - 1.64 \cdot N_{th,m} \cdot \cdot \left[0.5^2 \cdot CoV_{E_f}{}^2 + \left(3/10\right)^2 \cdot CoV_{f_{cm}}{}^2 + CoV_{\delta_m}{}^2 \right]^{0.5} = k_k \cdot N_{th} \tag{6.53}$$

$$N_{th,k,0.05} = k_{k,0.05} \cdot N_{th} = k_m \cdot \delta_m \cdot \cdot \left[1 - 1.64 \cdot \left[0.5^2 \cdot CoV_{E_f}{}^2 + \left(3/10\right)^2 \cdot CoV_{f_{cm}}{}^2 + CoV_{\delta_m}{}^2 \right]^{0.5} \right] \tag{6.54}$$

with

$$C_{Efm} = \left| \frac{\partial N_{th,m}}{\partial E_f} \right|_{\overline{E_f}} = N_{th,m} \cdot \frac{0.5}{\overline{E_f}} \tag{6.55}$$

$$C_{Efm}^2 \cdot Var\left(E_f\right) = N_{th,m}{}^2 \cdot \frac{0.5^2}{\overline{E^2}_f} \cdot Var(E_f) = N_{th,m}{}^2 \cdot 0.5^2 \cdot CoV^2{}_{E_f} \tag{6.56}$$

$$C_{f_{cm}} = \left| \frac{\partial N_{th,m}}{\partial f_{cm}} \right|_{\overline{f_{cm}}} = N_{th,m} \cdot \frac{3/10}{\overline{f_{cm}}} \tag{6.57}$$

$$C_{fcm}^2 \cdot Var\left(f_{cm}\right) = N_{th,m}{}^2 \cdot \frac{(3/10)^2}{\overline{f_{cm}^2}} \cdot Var(f_{cm}) = N_{th,m}{}^2 \cdot (3/10)^2 \cdot CoV_{f_{cm}}^2 \tag{6.58}$$

$$C_{\delta_m} = \left| \frac{\partial N_{th,m}}{\partial \delta_m} \right|_{\overline{\delta_m}} = \frac{N_{th,m}}{\overline{\delta_m}} \tag{6.59}$$

$$C_{\delta m}^2 \cdot Var\left(\delta_m\right) = N^2{}_{th,m} \cdot \frac{Var(\delta_m)}{\overline{\delta_m}} = N^2{}_{th,m} \cdot CoV^2{}_{\delta_m} \tag{6.60}$$

$$C_{f_{ctm}} = \left| \frac{\partial N_{th,m}}{\partial f_{ctm}} \right|_{\overline{f_{ctm}}} = 0 \tag{6.61}$$

The last term related to the tensile strength of concrete, f_{ctm}, is clearly absent, because the debonding load in the Eq. (6.35) depends on the only compressive strength.

However, as it occurs for all other cases, the variance of the materials is less significant compared with the variance of the model. E.g., for the Case 3 the coefficient of variation of the variable δ_m for the cured in situ systems is:

$$CoV_{\delta_m} = \frac{\overline{\delta_m}}{s_{\delta_m}} = \frac{1.006}{0.178} = 0.177 \quad \rightarrow CoV^2{}_{\delta_m} = 0.031 \tag{6.62}$$

By contrast, the contributes related to the CoVs of the materials are:

$$0.5^2 \cdot CoV_{E_f}{}^2 + \left(3/10\right)^2 \cdot CoV_{f_{cm}}{}^2 = 0.0026 \approx 0.003 \approx 0.1 \cdot CoV^2{}_{\delta_m} \tag{6.63}$$

In Figure 6.2 and Figure 6.3, the experimental debonding loads are compared with the theoretical ones given by model 1 (Eq. (6.33)) and model 3 (Eq. (6.35)), respectively; the regression line intercepting the origin of axis is reported too. Figure 6.2a and Figure 6.3a refer to the cured in situ systems whereas Figure 6.2b and Figure 6.3b refer to the preformed ones.

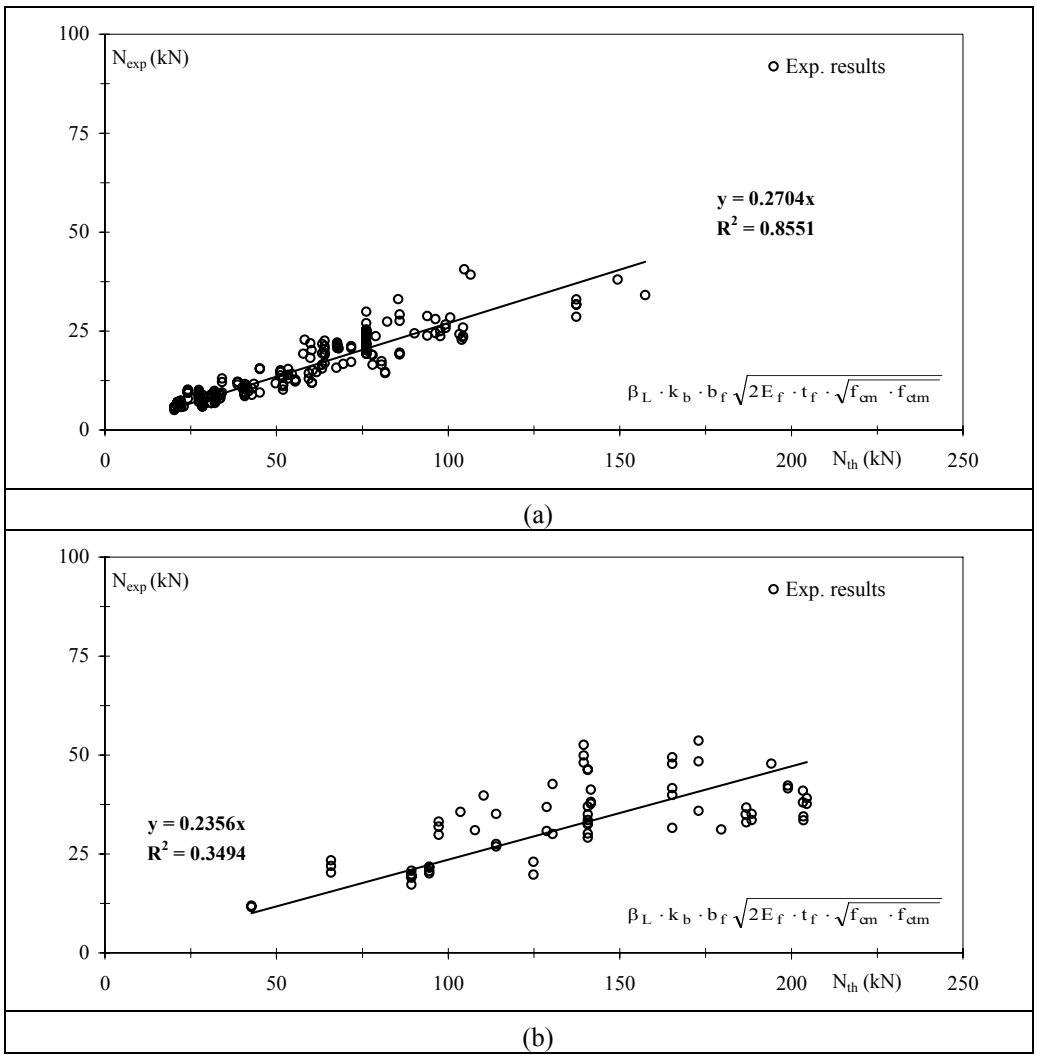

Figure 6.2 - Regression line (case 1):
a) cured in situ systems: 216 data; b) preformed systems: 68 data.

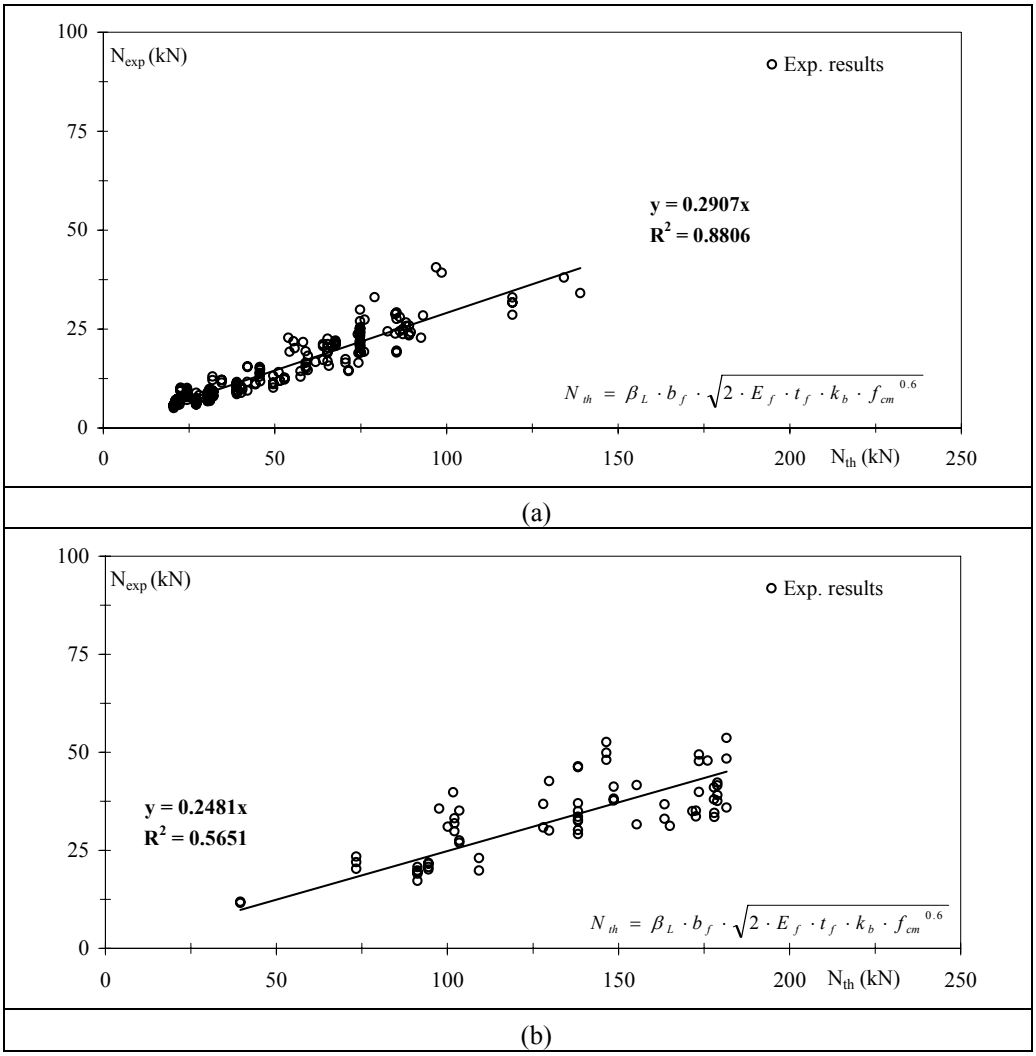

Figure 6.3 - Regression line (case 3):
a) cured in situ systems: 216 data; b) preformed systems: 68 data.

In Figure 6.4, the experimental values of strain in the FRP reinforcement at debonding are plotted together with the mean and characteristic provisions given by Eq. (6.33) using the values of k_m and k_k, for the three percentiles 5%, 0.5%, and 0.1%, listed in Table 6.3. The characteristic provision (5% percentile) divided to the safety factor γ_f = 1.2 (related to good application conditions, according to CNR-DT200, 2004) is plotted too.

Both theoretical and experimental strains are plotted vs. the term $\frac{E_f \cdot t_f}{2 \cdot \Gamma_f}$, assuming $\Gamma_f = k_b \cdot \sqrt{f_{cm} \cdot f_{ctm}}$ in compliance with Eq. (6.33). This allows graphing the theoretical curves normalized to the axial stiffness of the FRP reinforcement and the concrete strength.

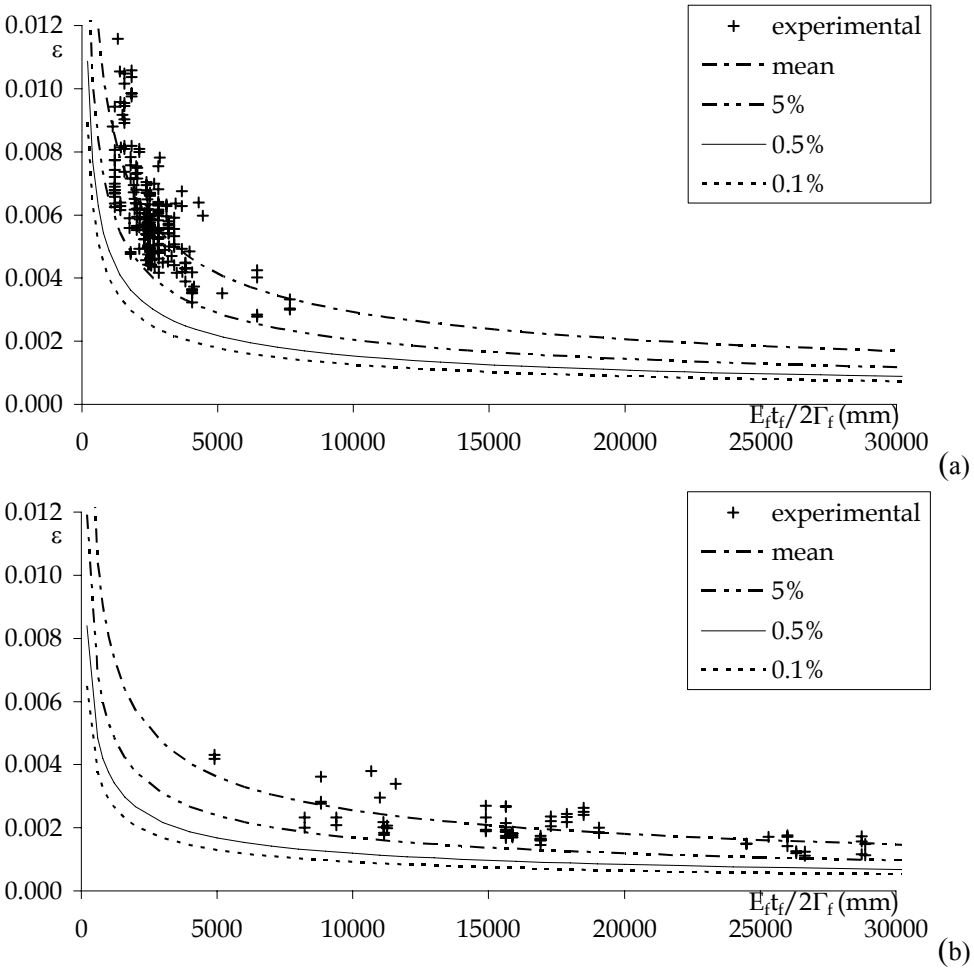

Figure 6.4 - Experimental strain at failure vs. theoretical results (case 1):
a) cured in situ systems (216 data); b) preformed systems (68 data).

The theoretical curves show that the 0.5% percentile can be a good choice to warrant a reliable safety level to the aim of furnish design provisions. Note that the assessment of the percentiles has been carried out taking into account the variance of the materials.

Another possibility, which is adopted by the Italian guidelines (CNR-DT200, 2004) and, more in general, is included in the Eurocode approach, consists into divide the characteristic provision (5% percentile) to a safety factor γ_f that depend on the quality of the application. Figure 6.4a and Figure 6.4b show that the provision corresponding to the 5% percentile divided to the factor $\gamma_f = 1.2$ are, however, less safe than the 0.5% percentile.

As concerns the percentiles provisions, it is worth noting that they have been calculated under the hypothesis of Gaussian distribution. Some statistical tests (Shapiro-Wilk, Anderson-Darling, Martinez-Iglewicz, Kolmogorov-Smirnov, D'Agostino Skewness, D'Agostino Kurtosis, D'Agostino Omnibus) have been performed to verify this assumption but the comparison between the cumulate frequency curves of N_{exp} and the Gaussian distribution, having the same mean value and standard deviation, highlighted a bad agreement, especially for the sheets. This was confirmed also by the responses of the statistical tests, which in most cases rejected the normality assumption for sheets and accepted it for plates. For the sheets, the experimental debonding loads seemed better represented by a log-normal distribution.

However, the values of percentiles calculated under the hypothesis of log-normal distributions are larger than the ones reported in Table 6.3 (Gaussian distribution). Thus, the normal distribution can be considered safe to the aim of furnishing design provisions.

Finally, in Table 6.5 and Table 6.6 the mean value, the standard deviation and the CoV of the ratio N_{th}/N_{exp} are reported for both cured in situ (sheets) and preformed systems (plates).

The theoretical values N_{th} given by the new proposal refer to both mean (Eq. (6.39)) and characteristic provisions (Eq. (6.40)); in particular the percentiles 0.05 and 0.005 have been considered. The characteristic provision (5% percentile) divided to $\gamma_f = 1.2$ is reported too. Finally, the design provisions of (CNR-DT200, 2004, Teng et al., 2001) are also listed. The characteristic provisions were divided to the safety factors: $\gamma_f = 1.2$ and $\sqrt{\gamma_c} = \sqrt{1.5}$ for CNR-DT200 (2004; $\gamma_b = 1.25$ for Teng et al. 2001.

Table 6.5 - Values of the ratio N_{th}/N_{exp} for cured in situ FRP systems (216 results).

N_{th}/N_{exp}	New proposal for debonding load				Design	
	$N_{th,m}$	$N_{th,k,0.05}$	$N_{th,k,0.05}/1.2$	$N_{th,k,0.005}$	CNR DT 200, 2004	Teng et al. 2001
Mean	1.03	0.72	0.60	0.54	0.43	0.54
St. dev.	0.173	0.121	0.101	0.091	0.083	0.08
CoV	16.8%	16.8%	16.8%	16.8%	19.4%	15.7%

Table 6.6 - Values of the ratio N_{th}/N_{exp} for preformed FRP systems (68 results).

N_{th}/N_{exp}	New proposal for debonding load				Design	
	$N_{th,m}$	$N_{th,k,0.05}$	$N_{th,k,0.05}/1.2$	$N_{th,k,0.005}$	CNR DT 200, 2004	Teng et al. 2001
Mean	1.03	0.68	0.57	0.48	0.47	0.63
St. dev.	0.20	0.13	0.11	0.09	0.12	0.120
CoV	19.1%	19.1%	19.1%	19.1%	25.1%	19.1%

The results of Table 6.5 and Table 6.6 show that the ratio $N_{th,m}/N_{exp}$ is meanly about 1 for both systems. The mean value of $N_{th,k,0.05}/N_{exp}$ for the sheets is lightly larger than the ones given by the Eq. (6.9) and the Eq. (6.5): 0.72 vs. 0.63 and 0.67 respectively (see Table 6.1). On the contrary, for the plates, the mean value of $N_{th,0.05}/N_{exp}$ is lightly lower than the one given by the Eq. (6.9) (0.68 vs. 0.70, see Table 6.1) and sensibly lower than the one given by the Eq. (6.5) (0.68 vs. 0.79, see Table 6.1). However, these differences relate to mean values of the ratio N_{th}/N_{exp} and, thus, can be misleading into compare the predictions of different models. By the contrast, the curves of Figure 6.5, where experimental and theoretical debonding strains of the only FRP sheets are plotted vs. the parameter $E_f \cdot t_f$, show the actual variations between the different formulations examined. Because of the theoretical strain depends on the concrete strength, a range of variability for this parameter has been fixed (24-30 MPa that corresponds to a mean value of about 27 MPa). The mean and the characteristic (5% percentile) provisions ($N_{th,k,0.05}$) given by the new formulation, by CNR-DT200 (2004) and by Chen and Teng (2001) are plotted in the graph. In particular, both mean and characteristic provisions (5% percentile) given by the new formulation are larger than the predictions of Chen and Teng (2001) and CNR-DT200 (2004).

Moreover, the formulation of CNR-DT200 (2004) gives the most safe results in terms of 5% percentile, while furnishes mean predictions very similar to Chen and Teng (2001). Furthermore, it can be observed that the formulation of *fib* bulletin 14 (2001), lies between the mean and the characteristic curves given by the new formulation.

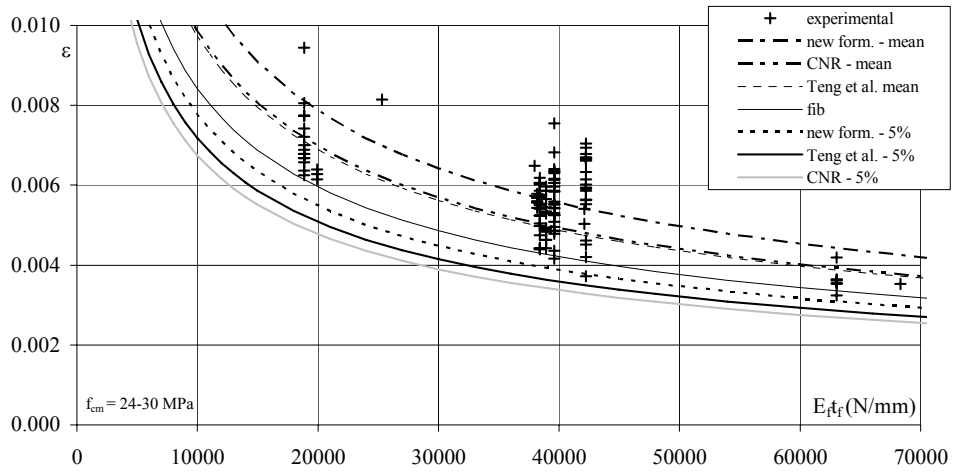

Figure 6.5 - Experimental maximum strain vs. mean and 0.05 percentile provisions for sheets.

In Figure 6.6, several design proposals coming from the new formulation (0.01%, 0.5%, and 5% percentile divided to γ_f=1.2), the model of *fib* bulletin 14 (2001), the design provisions of CNR-DT200 (2004) and Teng et al. (2001) are plotted together with the experimental debonding strains from the same tests considered in Figure 6.5. For the sheets, the graph of Figure 6.6a shows that two design proposals coming from the new formulation (5% percentile divided to 1.2 and 0.5% percentile) are less safe than the ones currently furnished by (CNR DT 200-2004). Note that the latter one introduces the additionally safety factor of concrete, $\sqrt{\gamma_c}$, for design. This coefficient has been omitted in the new formulation because the variance of the concrete has been taken into account in the calibration procedure by means of the CoV of its compressive strength (see Eq. (6.43)). Moreover, it can be observed that, the current design values of (CNR DT 200-2004) are comparable with the 0.1% percentile provisions of the new formulation. By contrast, the design formulation of Teng et al. (2001) is comparable with the 0.5% percentile of the new formulation. Finally for the cured in situ systems, if the 0.5% percentile of the new formulation is chosen as design

provision, the debonding load increases of about +25% compared with the current CNR provisions and is comparable with the design values of Teng et al. (2001). By contrast for the plates, Figure 6.6b shows that the 0.5% percentile of the new formulation is comparable with those currently furnished by CNR-DT200 (2004), while the 5% percentile divided to 1.2 is less safe (about 15%). Moreover, the design formulation of Teng et al. (2001) is less safe compared with both the 5% percentile of the new formulation divided to 1.2 and the 0.5% one.

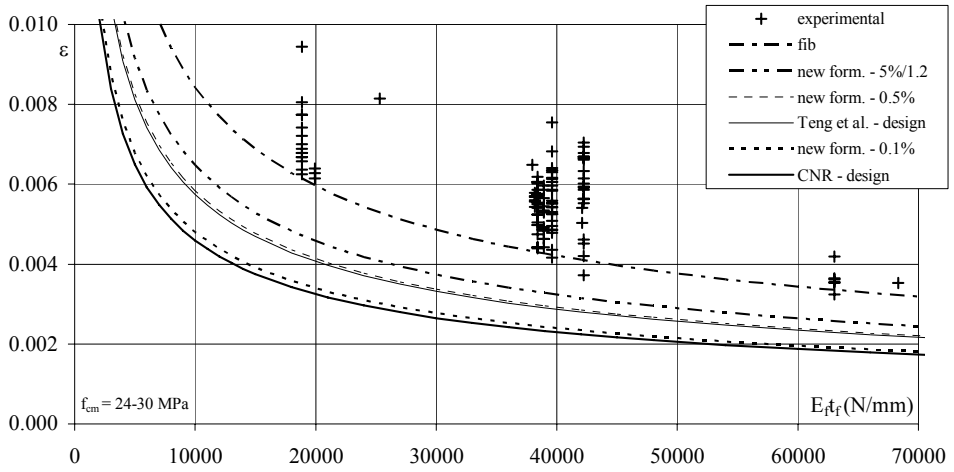

a)

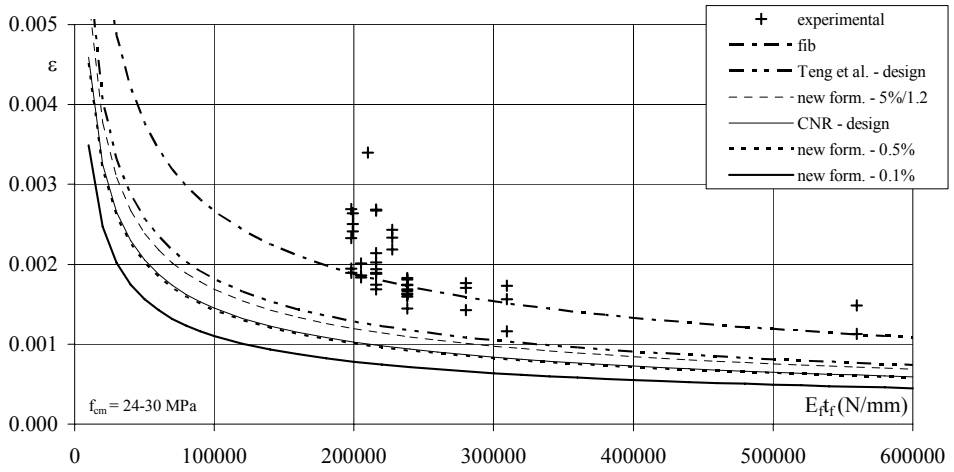

b)

Figure 6.6 - Experimental maximum strain vs. design provisions: a) sheets; b) plates.

6.1.4 Conclusions

In conclusions, the proposed formulation for the plate end debonding load has a clear statistical meaning and allows to separate the provisions for the cured in situ FRP systems and the preformed ones. This distinction is mainly due to the larger scatter of the experimental results collected for this strengthening system.

Both aspects let to better exploit the strength of the cured in situ systems; indeed the 0.5% percentile of the new formulation are larger than the design values furnished by the current Italian Guidelines and, however, allow to assess the same safety level of model of Teng et al. (2001). Moreover, it was worth to notice that the formulation of *fib* Bulletin 14 (2001) results excessively unsafe compared to the experimental results.

By contrast, the approach of Teng et al., (2001) and *fib* Bulletin 14 (2001) are found to be less safe when applied to preformed systems. Indeed, the 0.5% percentile of the proposed design formulation provides a higher safety level compared with these models, whereas it is similar to the current design provisions of CNR-DT200 (2004). Thus, these results confirm that the distinction of the two strengthening systems seem to be reliable to have suitable prediction of debonding load.

6.2 INTERMEDIATE DEBONDING MODEL CALIBRATION

As showed in 5.1.2 plenty of research activities have been carried out for better understanding intermediate debonding phenomenon, as it is one of the most common and peculiar bond-related failure modes observed in RC beams externally strengthened in bending by bonded FRP reinforcement.

A high level of uncertainty still overshadows the mechanical understanding of intermediate debonding due to the complex interactions between several phenomena, such as cracking in concrete, steel yielding in longitudinal rebars, interface adhesion properties, and so on. As a result of this incomplete understanding of the mechanical reasons leading to intermediate debonding failure of FRP-strengthened RC beams, several analytical approaches have been proposed within the scientific literature and adopted by the most common codes of standards for performing the required safety checks. A possible classification of those approaches based on the nature of the procedures utilized for checking the strengthened beam against intermediate debonding is proposed in 5.1.2.4 . Since those procedures work in rather diverse ways involving various parameters and adopting different relationships for defining interface properties, they generally lead to rather diverse predictions of the ultimate load resulting in intermediate debonding.

Moreover, such procedures actually neglect or disregard the role played by several mechanical parameters in controlling the structural response of FRP-strengthened RC beams, adopting simplified expressions for deriving formulae usually calibrated on the available experimental observations.

As a matter of principles, two different methodological paths can be followed for defining reasonably simplified design formulae based on experimental results:

- direct calibration of empirical expressions against experimental results by means of well-established mathematical procedures like least-square minimization of the overall difference between the experimental observations and the corresponding analytical values;
- validation of refined numerical models (i.e. based on finite element discretization) by means of a limited number of experimental

results and extrapolation of those results by means of the above mentioned numerical procedures.

The numerical procedure mentioned in 5.2 pointed out the role of some mechanical parameters (currently neglected in the most well-established simplified formulae) influencing the mechanical response of strengthened beams. In particular, it pointed out the key importance of yielding in steel rebars as a driving phenomenon for leading to intermediate debonding failure; moreover the role of further parameters (i.e., the load condition, the yielding strain of steel rebars, the amount of reinforcement) has been also pointed out, but it is not always easy to be assessed through the available experimental results because of the limited range of variation of those parameters actually explored in the experimental tests.

Consequently, starting by the behavioural observations derived by the parametric application of the mentioned numerical procedure, a simplified design formula will be proposed in the following by using a wide database built by collecting more than two hundred experimental results available in the scientific literature. Such database will be briefly described and analyzed in the next section. Then, the design-oriented formula will be derived, even describing the uncertainty-related issues deriving by its simplified nature.

6.2.1 The experimental database

A wide database has been assembled by collecting data of 214 experimental tests on FRP-strengthened RC beams; it has been obtained by merging the data considered by Ferracuti et Al. (2007b) with those collected by Wu and Niu (2007) and about thirty further experimental cases reported in the scientific literature (Beber, 1999, 2003; Grace et al., 1999; Khomwan et al., 2004; Pham & Al-Mahaidi, 2004a,b; Sharif et al, 1991; Triantafillou & Plevris, 1992). The resulting database collects the geometric and mechanical data describing the RC beams and their steel and composite reinforcement, the latter being made out of externally bonded composite laminates based on carbon, glass or aramid fibers.

For specimens strengthened with FRP systems cured in situ (sheets), the relevant geometric and mechanical parameters range in the following intervals: concrete width b_c = 75-960 mm, FRP width b_f = 30-480 mm, b_f/b_c = 0.17–1, FRP thickness t_f = 0.11-2.55 mm, Young modulus of FRP E_f = 21-390

GPa, mean compressive strength of concrete f_{cm} = 21-61 MPa, mean tensile strength of concrete f_{ctm} = 2.3-4.3 MPa.

For specimens strengthened with preformed FRP systems (laminates), the key parameters vary in the following ranges: concrete width b_c = 180-800 mm, FRP width b_f = 25-280 mm, b_f/b_c = 0.13–1, FRP thickness t_f = 1.0-6 mm, Young modulus of FRP E_f = 190-220 GPa, mean compressive strength of concrete, f_{cm} = 12.6-53.4 MPa, mean tensile strength of concrete, f_{ctm} = 1.62-4.25 MPa.

A total number of 214 experimental results have been collected (164 FRP cured in situ systems and 50 FRP preformed system).

Intermediate debonding failure have been observed in all those tests. As a matter of principle, the maximum bending moment M_{db} observed in the experimental tests at debonding is smaller than the ultimate one M_u, corresponding to FRP rupture. The following parameter γ could be introduced for quantifying how premature is failure with respect to the ultimate flexural strength:

$$\gamma = \frac{M_{db} - M_y}{M_u - M_y} \,, \tag{6.64}$$

being M_y the bending moment of the strengthened section at yielding of rebars: both M_u and M_y can be determined theoretically adopting the usual assumptions for RC sections at ULS. The parameter γ is as closer to zero as debonding occurs for small values of the maximum axial strain in FRP; on the contrary, it is as close to the unity as axial strain at debonding is close to the corresponding ultimate value $\varepsilon_{f,u}$. Figure 6.7 points out that the values of γ determined for the beams collected in the database generally range between zero and one; only in few cases (less than ten out of the total 214) it is slightly larger than the unity, mainly as a result of hardening in materials.

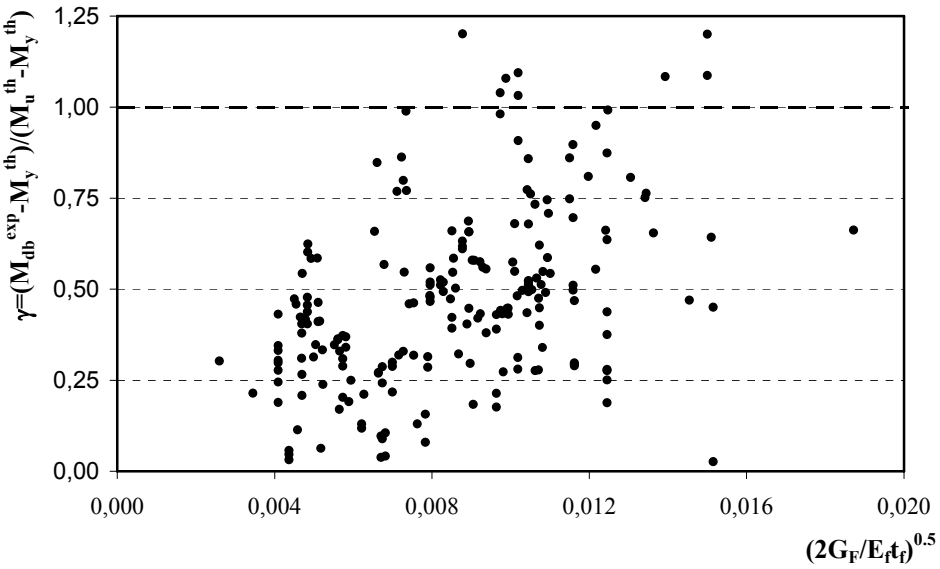

Figure 6.7 - Values of γ parameter against some mechanical parameters.

The values of γ have been represented in Figure 6.7 against the square root of the ratio between (twice) the fracture energy, G_F, and the specific axial stiffness of the FRP reinforcement, $E_f t_f$; the former parameter has been evaluated as a function of both concrete tensile, f_{ct}, and compressive, f_c, strengths through the relation proposed in the Italian Code. The ratio $2G_F/E_f t_f$ is often considered in various proposals as the key parameter for determining the value of axial strain ε_{db} developed in FRP at debonding onset. However, Figure 6.7 can only point out a general trend resulting in values of γ as large as the parameter represented on the x-axis, but it is quite hard to recognize a consistent correlation between γ (or, even, the maximum axial strain ε_{db} developed in FRP at debonding) and the quantity on the x-axis possibly depending on the two following reasons:

- fracture energy, G_F, basically depends on concrete (tensile) strength and, consequently, is hugely scattered;
- besides the one reported on the x-axis, other parameters even play an important role on the occurrence and extent of debonding failure.

For instance, the role of both the amount of steel rebars and their yielding stress/strain values have been emphasized in Faella et. al. (2008a).

Furthermore, load distribution (see 5.3) also affects the possible premature failure of FRP strengthened beams as confirmed by Figure 6.8 showing a strict correlation between the yielding moment M_y of the strengthened section and the maximum bending moment at debonding M_{db} at least in the case of three- or four-point-bending, while a completely different behaviour results in the case of uniformly distributed load.

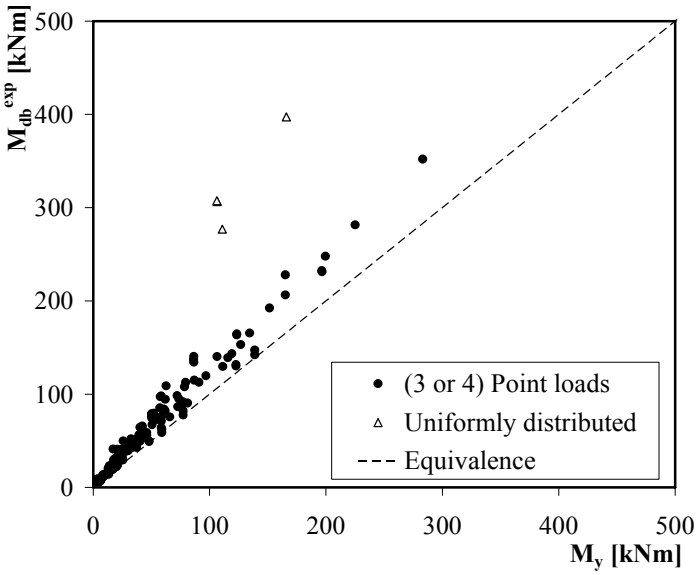

Figure 6.8 - Relation between bending moment at debonding and yielding

Figure 6.9 shows the distribution of the parameter γ for the experimental results considered within the database. It points out that such values are quite uniformly distributed since the cumulative frequency distribution is not so far from the ideally uniform straight curve, meaning that cases of very premature debonding are considered within the database as well as other cases whose failure is close to the complete development of the strength on the external reinforcement.

Finally, it is worth to precise that only the experimental results characterized by values of $\gamma \in (0,1)$ will be considered in the following, as that is a necessary condition for recognizing the cases of beams failure in intermediate debonding.

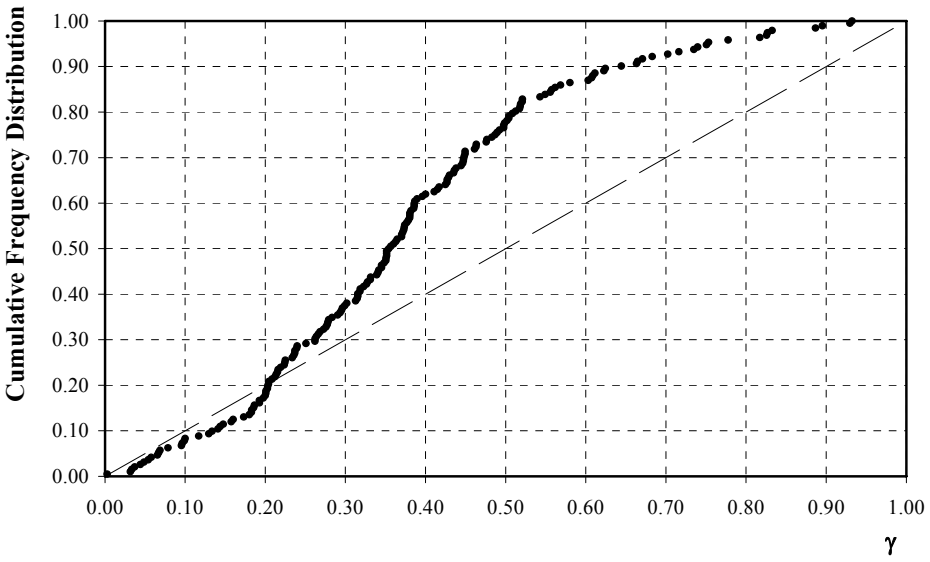

Figure 6.9 - Distribution of the parameter γ within the experimental database.

6.2.2 Calibration of a formula through Design-by-testing

The mean value of the maximum axial strain in FRP corresponding to failure in intermediate crack-induced debonding (IC debonding strain) can be expressed by means of a relationship obtained by a deterministic model and fine-tuned on experimental data by a numerical coefficient k_{IC}. A new assessment of k_{IC} is proposed through a probabilistic approach as suggested in (EN1990 – Annex D) aimed to give a clear probabilistic meaning to the provisions.

In particular, an error function δ can cover the uncertainties of the simplified model considered in the above mentioned calibration:

$$\varepsilon_{fd} = \varepsilon_{fd,m}\left(k_{IC}, f_c, f_{ct}, E_f, t_f, b_f, k_b\right)\cdot\delta \ . \tag{6.65}$$

The random variable δ is defined, for each i^{th} test, as the ratio of the experimental debonding strain, $\varepsilon_{exp,i}$, to the theoretical one, $\varepsilon_{fd,m}$ evaluated by considering the geometric and mechanical data characterizing that test:

$$\delta_i = \frac{\varepsilon_{\exp,i}}{\varepsilon_{th,i}} \ , \tag{6.66}$$

Moreover, the mean value, the variance, the standard deviation and the CoV of this variable are defined as:

$$\overline{\delta} = \frac{1}{n}\sum_{i=1}^{n}\delta_i \ ; s_\delta^2 = \frac{1}{n-1}\sum_{i=1}^{n}(\delta_i - \overline{\delta})^2 \ ; \sigma_\delta = \sqrt{s^2{}_\delta} \ ; \text{CoV} = \frac{\sigma_\delta}{\overline{\delta}} \ , \tag{6.67}$$

By assuming a formulation similar to design Eqn. (5.26) in section 5.1.2.4 , taking into account no safety partial factors the relationship (6.65) can be rewritten as follows:

$$\varepsilon_{fd,m}\left(k_{IC}, f_c, f_{ct}, E_f, t_f, b_f, k_b\right) = k_{IC} \cdot \sqrt{\frac{2 \cdot k_b \cdot \sqrt{f_c \cdot f_{ct}}}{E_f t_f}} \ , \tag{6.68}$$

The coefficient k_{IC} has been calibrated based on experimental results in terms of deformation $\varepsilon_{fd,exp}$ obtained by using the procedure in (Faella et al., 2010) as stated above. The calibration has achieved using a least-square procedure consisting in the resolution of the following minimum problem:

$$k_{IC,m} = \arg\min_{k_{IC}} \sum_{i=1}^{n}\left[\varepsilon_{fd,m}\left(k_{IC}, f^{(i)}, f_{ct}{}^{(i)}, E_f{}^{(i)}, t_f{}^{(i)}, b_f{}^{(i)}, k_b{}^{(i)}\right) - \varepsilon_{fd,\exp}{}^{(i)}\right]^2 \tag{6.69}$$

Moreover, the mean value of the intermediate debonding strain can be obtained by a coefficient $k_{IC,m}$ adjusted by means of the mean value of the error parameter $\overline{\delta}$, being in general $\overline{\delta} \neq 1$ because the regression line was imposed to intercept the origin.

$$k_{IC,m} = k_{IC,bf} \cdot \overline{\delta} \ . \tag{6.70}$$

Thus, the mean provision for the intermediate debonding strain can be assumed as:

$$\varepsilon_{th,m} = k_{IC,m} \cdot \varepsilon_{th} \ , \tag{6.71}$$

being ε_{th} the strain obtained by the deterministic model. Obviously, this strain is linearly proportional to the debonding strain being linear elastic the FRP constitutive law.

If the random variable represents a strength, its characteristic value is often defined for design purposes as the 0.05 percentile of the frequency distribution associated to the examined variable. Gauss distribution is the most generally considered for describing the errors. The so-called "hypothesis of normal distribution" for the variable δ should be checked by comparing the experimental curve of the cumulative frequency to the theoretical one corresponding to a Gaussian distribution having the same mean value and standard deviation (see Figure 6.10).

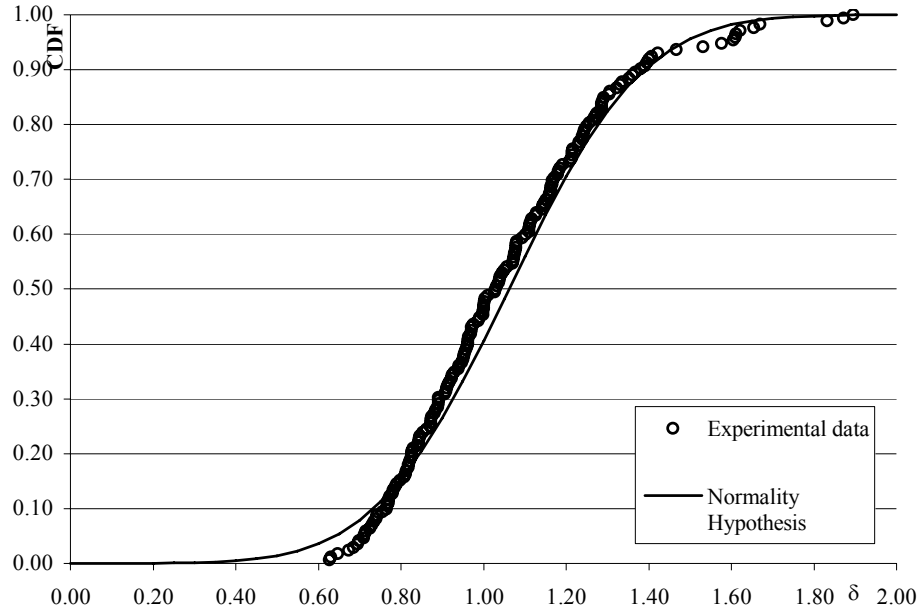

Figure 6.10 - Experimental data cumulative frequency against theoretical in normality hypothesis.

Assuming that the Young modulus E_f of the FRP reinforcement, the concrete tensile and compressive strength f_{ctm} and f_c, are the only mechanical parameters influencing the value of the maximum axial strain developed in FRP at debonding, the expressions for the both general model and the calibrated one involving the coefficient $k_{IC,bf}$ as well as $\overline{\delta}$ are:

$$\varepsilon_{th} = \varepsilon_{th}(E_f, f_{cm}, f_{ctm}) \ , \tag{6.72}$$

$$\varepsilon_{th,m} = \varepsilon_{th,m}(E_f, f_{cm}, f_{ctm}, \overline{\delta}, k_{IC,bf}) \ . \tag{6.73}$$

In the following, some assumptions already considered in defining a characteristic value for plate end debonding strength are accepted (Bilotta et al. 2011). In particular, both E_f and f_c and f_{ct} have been assumed normally and independently distributed random variables, with the following values of the coefficients of variation:

$$s_{E_f} = 0.05 \cdot \overline{E_f} \qquad s_{f_{ctm}} = 0.183 \cdot \overline{f_{ctm}} \qquad s_{f_{cm}} = 4.88 \ , \tag{6.74}$$

according to the design relationships provided by EN 1992-1-1 and literature information (Di Ludovico et al., 2009).

Hence, under the hypothesis of normal distribution for the variable δ, the provision corresponding to the 0.05 percentile of the Gaussian distribution is:

$$\varepsilon_{th,k} = \varepsilon_{th,m} - 1.64 \cdot \left[Var(\varepsilon_{th,m}) \right]^{0.5} \ , \tag{6.75}$$

where the variance of $\varepsilon_{th,m}$ can be expressed as:

$$\begin{aligned} &Var\left(\varepsilon_{th,m}\right) = C_{Efm}^2 \cdot Var\left(E_f\right) + \\ &+ C_{fcm}^2 \cdot Var\left(f_{cm}\right) + C_{fctm}^2 \cdot Var\left(f_{ctm}\right) + C_{\delta m}^2 \cdot Var\left(\delta_m\right) \end{aligned} \ , \tag{6.76}$$

$$C_{Efm} = \left| \frac{\partial \varepsilon_{th,m}}{\partial E_f} \right|_{\overline{E_f}} \tag{6.77}$$

$$C_{f_{cm}} = \left| \frac{\partial \varepsilon_{th,m}}{\partial f_{cm}} \right|_{\overline{f_{cm}}}$$

$$C_{f_{ctm}} = \left| \frac{\partial \varepsilon_{th,m}}{\partial f_{ctm}} \right|_{\overline{f_{ctm}}}$$

$$C_{f_{ctm}} = \left| \frac{\partial \varepsilon_{th,m}}{\partial \delta_m} \right|_{\overline{\delta_m}}$$

If the Eqs. (6.76) and (6.77) are substituted in the Eq. (6.75), the following general expression is obtained for the characteristic provision of the debonding load:

$$\varepsilon_{th,k} = \varepsilon_{th,m} - 1.64 \cdot \varepsilon_{th,m} \cdot \left[a \cdot CoV_{E_f}{}^2 + b \cdot CoV_{f_{cm}}{}^2 + c \cdot CoV_{f_{ctm}}{}^2 + CoV_{\delta_m}{}^2 \right]^{0.5} \quad (6.78)$$

where the coefficient a, b, c depend on the functional relationship of E_f, f_{cm} and f_{ctm} in the expression of ε_{th} and the coefficients of variation are defined for each parameter as the ratio of the mean value to its standard deviation:

$$CoV_{E_f} = \frac{\overline{E_f}}{s_{E_f}},\ CoV_{f_{ctm}} = \frac{\overline{f_{ctm}}}{s_{f_{ctm}}},\ CoV_{f_{cm}} = \frac{\overline{f_{cm}}}{s_{f_{cm}}},\ CoV_{\delta_m} = \frac{\overline{\delta_m}}{s_{\delta_m}}\ , \quad (6.79)$$

Clearly the coefficient of variation of the variable δ_m, $CoV_{\delta m}$, depends on the data distribution. The Eq. (6.78) can be written as:

$$\varepsilon_{th,k} = k_{cr,k} \cdot \varepsilon_{th}\ , \quad (6.80)$$

assuming:

$$k_{cr,k} = k_{cr,m} \cdot \left(1 - 1.64 \cdot \left[a \cdot CoV_{E_f}{}^2 + b \cdot CoV_{f_{cm}}{}^2 + c \cdot CoV_{f_{ctm}}{}^2 + CoV_{\delta_m}{}^2 \right]^{0.5}\right) \quad (6.81)$$

Lower percentiles can be obtained by substituting in the Eq. (6.81) the coefficient 1.64, related to the 0.05 percentile of the frequency distribution,

with the coefficients 2.58 and 3.08 corresponding to the 0.005 and 0.001 percentiles, respectively.

The use of percentiles lower than 0.05 can be alternative to the use of safety factors that usually have to be additionally applied to characteristic provision to take into account the model uncertainness (EN1990 – Annex D).

The following values of the coefficients defined above have been derived by considering the experimental results in a least-square procedure:

$$k_{IC,bf} = 0.53, \quad k_{IC,,m} = 0.56, \quad k_{IC,5\%} = 0.32 \quad \text{and} \quad k_{IC,0.5\%} = 0.18 \,. \tag{6.82}$$

From the coefficients $k_{IC,m}$ and $k_{IC,5\%}$ can be easily defined the following coefficients

$$\begin{aligned} k_{Gm,2} &= \left(k_{IC,m}\right)^2 = 0.32mm \\ k_{Gk,2} &= \left(k_{IC,k}\right)^2 = 0.10mm \end{aligned} \tag{6.83}$$

6.2.3 Final comparisons

Theoretical debonding strains can be expressed as a function of the parameter $E_f t_f \big/ k_b \sqrt{f_{cm} f_{ctm}}$. This parameter involves the main geometrical and mechanical properties influencing the intermediate debonding phenomenon (see (6.84)):

$$\varepsilon_{th} = k_{IC} \sqrt{\frac{2 \cdot k_b \cdot \sqrt{f_{cm} f_{ctm}}}{E_f \cdot t_f}} \,. \tag{6.84}$$

For design purpose the relationship (6.84) should be rewritten as follows:

$$\varepsilon_{th} = \frac{k_{IC}}{\gamma_{f,d} \cdot FC} \sqrt{\frac{2 \cdot k_b \cdot \sqrt{f_{cm} f_{ctm}}}{E_f \cdot t_f}} \,. \tag{6.85}$$

where $\gamma_{f,d}$ is an external safety coefficient based on quality control on the FRP strengthening system and FC is a confidence factor (in the range of 1.00-1.35) based on the level of knowledge achieved on the existing material properties and typically used for the assessment and retrofitting of buildings (European Code - UNI EN 1998-3).

Several strain versus $E_f t_f \Big/ k_b \sqrt{f_{cm} f_{ctm}}$ curves can be obtained by considering variable numerical values for the triplet (k_{IC}, $\gamma_{f,d}$, FC).

Figure 6.11 shows this curve by assuming the triplet of values ($k_{IC,m}$, 1, 1) that allows the predicted theoretical strains to be showed (k_b = 1 has been assumed for the sake of simplicity). In other words, the curve represents the mean value of the axial strain developed in FRP at debonding, as it has been calibrated by solving the least-square problem in equation (6.69).

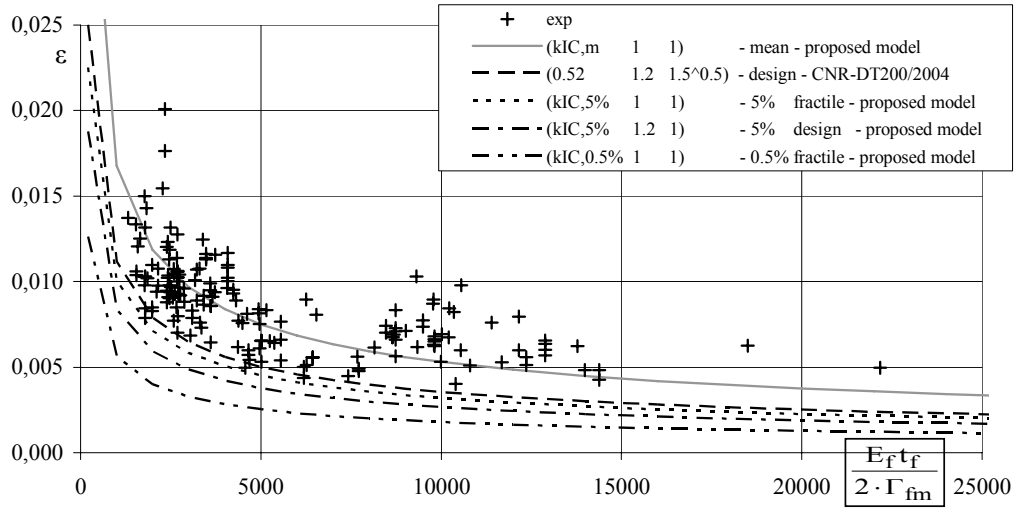

Figure 6.11 - Experimental results and theoretical prediction

Figure 6.11 confirms that this equation results in a good approximation of the experimental results. However, it cannot be directly utilized for design purposes as it is often unconservative. A reasonable level of conservativeness should be selected for design purposes. Usually, it is defined in terms of percentiles of the distribution describing the uncertainties of the calibrated formula.

Different levels of conservativeness can be achieved by adopting different values for the three parameters of the triplet (k_{IC}, $\gamma_{f,d}$, FC). For instance, the curves obtained by considering the three values ($k_{IC,5\%}$, 1, 1), ($k_{IC,5\%}$, 1.2, 1) and ($k_{IC,0.5\%}$, 1, 1) are also reported as well as the curve obtained by using the design coefficient suggested in CNR-DT200/2004 (0.52, 1.2, $\sqrt{1.5}$). Note that in CNR-DT200/2004, $FC = \sqrt{1.5}$ is used, regardless of the level of knowledge in the material properties.

Figure 6.11 shows as the design formula currently adopted by CNR-DT200/2004 is sometimes unconservative. This is not acceptable for the level of confidence and conservativeness generally required for design purposes. In fact, that formula has been obtained by means of a different calibration procedure (Ferracuti et al, 2007b) based on much less experimental data.

More conservative predictions derive by assuming the value $k_{IC,5\%}$, and a safety coefficient 1.2 or the 0.005 percentile, $k_{IC,0.5\%}$, according to Annex D - EN 1990.

Furthermore, Figure 6.12 and Figure 6.13 show a comparison between design curves obtained by assuming the coefficients calibrated through the proposed design-by-testing procedure and other curves according to some of the models outlined in section 5.1.2.4 .Since they involve the mechanical properties of concrete in rather different ways, four graphs dealing with different ranges of values of the concrete compressive strength have been plotted.

As a general trend, Figure 6.12 and Figure 6.13 show that both the model by Said and Wu (2008) and the formula adopted by ACI440-08 lead to predictions in terms of maximum axial strain in FRP at debonding which are not conservative enough to be used for design purposes. Since fractile levels generally accepted for Ultimate Limit Design are about 0.005, too many experimental points (out of the total of about 200 experimental results) fall below the two mentioned curves.

Moreover, the predictions based on the model by Teng et al. (2004) are rather close to the values obtained by the current CNR-DT200/2004 provisions. In the case of low concrete strength (namely, for f_c<40 MPa), both formulations look not conservative enough for design purposes.

Finally, the results obtained by applying the proposed formulation are also reported in Figure 6.12 and Figure 6.13 by considering the $k_{IC,5\%}$ coefficient and a further safety factor $\gamma_{f,d}$=1.2 addressing the quality of the application process is considered. The confidence factor FC = 1 is assumed as "full knowledge" is achieved about the mechanical properties of structural materials. The curves representing those results lie much below the bunch of experimental points, demonstrating the higher level of conservativeness achieved by the proposed formula.

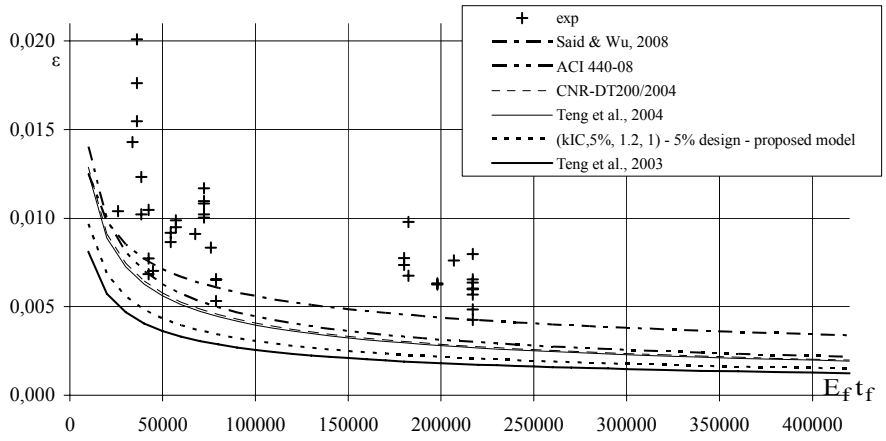

$f_{c,th}$ = 20 MPa ($f_{c,exp}$ = 20÷30)

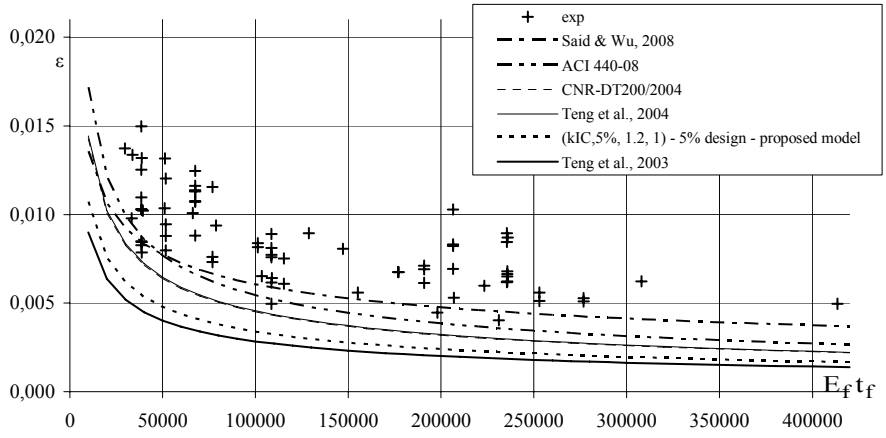

fc,th=30 (fc,exp = 30÷40)

Figure 6.12 - Experimental results and code provisions (1)

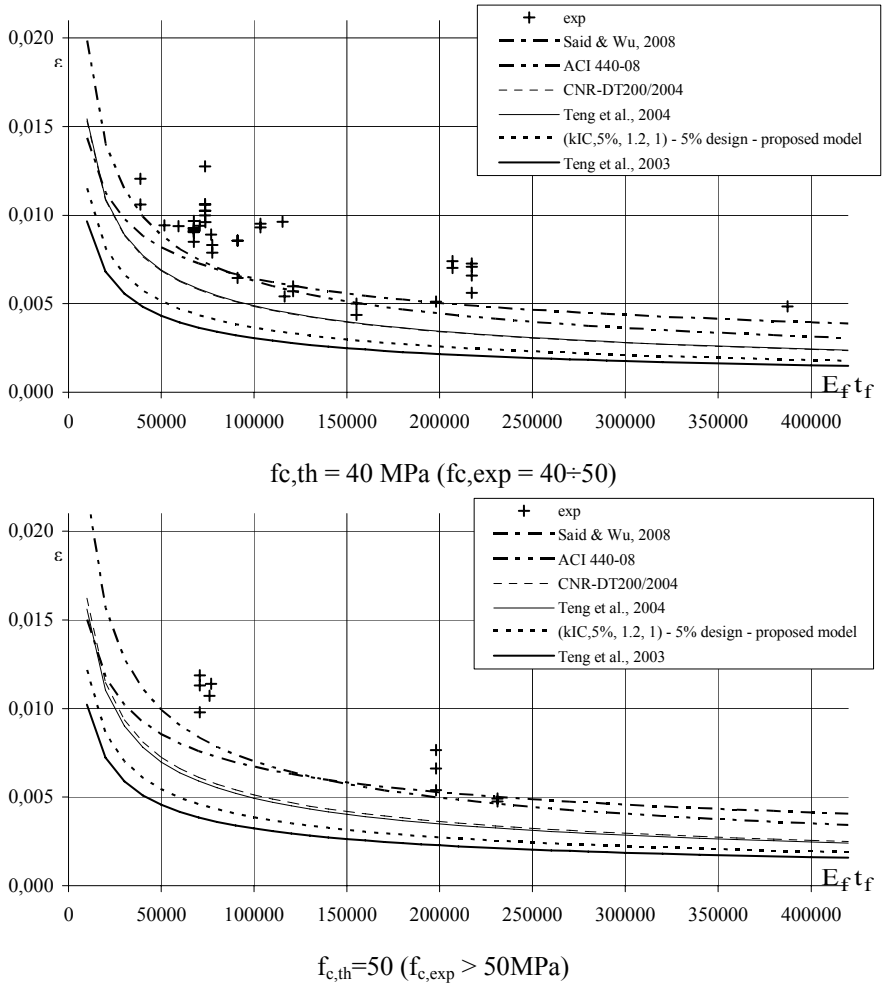

Figure 6.13 - Experimental results and code provisions (2)

Although the curves representing the results of the model by Teng et al. (2003) are generally even more conservative than those obtained by the proposed model, it could result in too strict provisions for a cost-effective application of FRP strengthening. The two curves representing the proposed formula and the model by Teng et al. (2003) are rather close one another, but the former can move upward if a unit value is also considered for $\gamma_{f,d}$, as a result of a certified application procedure allowing for higher values of the relevant mechanical properties of the adhesive-to-concrete interface.

6.2.4 Concluding remarks

The design of FRP flexural strengthening of RC beams is often controlled by intermediate debonding failure. This phenomenon involves several geometric and mechanical parameters in a rather complicated way. Consequently, validating a sound theoretical model for predicting intermediate debonding is rather impractical as both the experimental data and results are affected by high levels of uncertainties and randomness.

Consequently, a simplified empirical model for intermediate debonding has been calibrated based on the results of bending tests carried out on RC beams externally strengthened by FRP laminates. The model is based on a formula involving the key mechanical parameters such as the Young modulus E_f and the thickness t_f of the FRP reinforcement, and the concrete strength (in both compression and tension).

Although other similar models have been already presented in the scientific literature and adopted in codes of standard, the present proposal is based on a statistically consistent procedure for determining the safety levels required for defining the so-called “characteristic” and “design” values of the maximum axial strain developed in FRP at intermediate debonding. The mentioned procedure adopted for defining those values comply to the Eurocode provisions about the so-called “design-by-testing” approach.

Finally, the comparison between the proposed formula and the other ones already available in the literature point out that it is a good trade-off between the conservativeness required for design purposes and the need for efficient and cost-effective usage of materials.

Chapter 7 - Proposal of design formulae for Guidelines

In the chapter 3 the experimental program that was conducted to compare the interface behavior, under monotonic and cyclic actions, of two main types of commercial external FRP reinforcement, namely sheets and plates, was showed.

Furthermore in the chapter 4 a method of identification of interface laws defined IndIM has been used to analyze the wide collection of results attained from these tests and the advisability of assessing a bond law for the plates different from that for the sheets was clearly showed

Moreover, in the chapter 5 was showed that further investigations are necessary on the bond strength at the interface because it is a key issue in the strengthening design procedure.

Nevertheless, as showed in the chapter 6, safe design-oriented formulae can be derived from experimental data, according to a statistical procedure for the calibration of resistance models suggested in the European code.

The results obtained by applying the IndIM procedure to obtain simplified bond laws and the statistical procedure calibrating the bond strength relationships for both plate end debonding and intermediate debonding were herein summarized and integrated, in order to prepare an updating proposal for the Guidelines CNR-DT200 (2004).

7.1 SPECIFIC FRACTURE ENERGY – PLATE END DEBONDING

In the following, reference is made to Figure 7.1. Moreover, the fracture energy G_F is called Γ_F according to CNR-DT200 (2004)

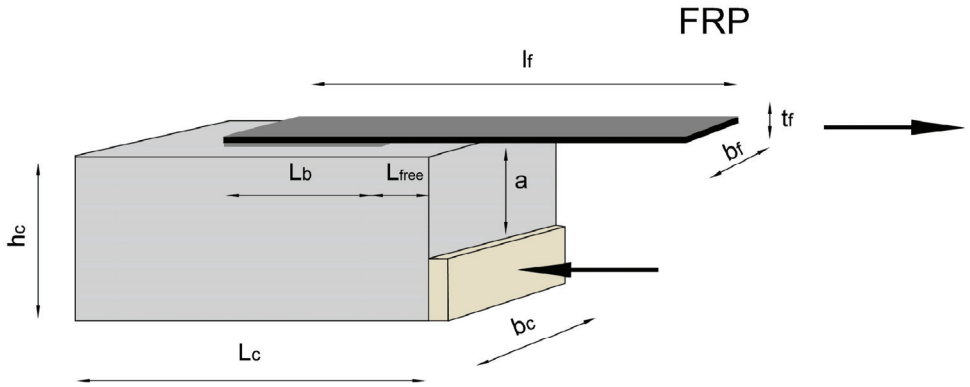

Figure 7.1. - General scheme of an asymmetrical push-pull bond test.

The maximum tensile force , F_{max}, at debonding in an FRP external reinforcement characterized by an infinite bonded length can be calculated as:

$$F_{max} = b_f \int_0^\infty \tau_b(x)\,dx, \tag{7.1}$$

being $\tau_b(x)$ the bond shear stress distribution along the concrete-FRP interface and b_f the width of the FRP reinforcement.

Moreover, the fracture energy corresponding to a generic bond shear stress-slip law, $\tau_b(s)$, can be expressed as:

$$\Gamma_F = \int_0^\infty \tau_b(s)\,ds \qquad [F/L] \tag{7.2}$$

This expression has the meaning of an energy [F L] for unit surface [L^2].

Under the hypothesis that the concrete member has a stiffness much larger than the reinforcement F_{max} can be written as follows (see (2.72)):

$$F_{max} = b_f \cdot \sqrt{2 \cdot E_f \cdot t_f \cdot \Gamma_F} \tag{7.3}$$

where t_f, b_f, E_f are the thickness, the width, and the Young modulus of the FRP reinforcement.

The fracture energy, Γ_F, depends on both the strength properties of adherents, concrete and adhesive, and the characteristics of the concrete surface. If the FRP reinforcement is correctly applied, the debonding occurs in the concrete and the specific fracture energy of the interface law can be written in a form similar to that used for the shear fracture (mode I). Therefore, the fracture energy can be expressed as a function of the concrete shear strength: $\Gamma_f\left(\tau_{b,\max}\right)$, where $\tau_{b,max}$ depends on both tensile f_{ct} and compressive f_c concrete strength.

The general Eq. (7.3) for debonding load can be particularized by introducing the dependence on the bond shear strength. Indeed, the bond shear strength depends on the concrete strength and can be related to the Mohr's circle representing the stress condition in the concrete at failure. Thus, different formulations for shear strength can be considered varying the dependence on the concrete strength.

If a Coulomb's failure criterion is adopted, the term $\sqrt{f_{cm}\cdot f_{ctm}}$ is 2 times the cohesion associated to the Mohr's circle of an interface concrete element subjected to both shear and normal stresses. The presence of normal stresses has been often experimentally evidenced by the visual inspection of the debonded surface configuration (Mazzotti et al., 2008). Thus, the case 1 plays better the actual physical phenomenon, because it takes into account the both presence of shear and normal interfacial stresses.

Hence the following relationship for the fracture energy can be assumed:

$$\Gamma_f = k_G \cdot k_b \cdot \sqrt{f_{cm}\cdot f_{ctm}} \tag{7.4}$$

where

- f_{cm} and f_{tcm} are the mean value of the cylindrical compressive strength and the tensile strength of the concrete respectively,
- k_b is the shape factor expressed as:

$$k_b = \sqrt{\frac{2-b_f/b}{1+b_f/b}} \geq 1 \qquad with \qquad \frac{b_f}{b} \geq 0.25 \tag{7.5}$$

  b_f is the width of the laminate and b is the width of the concrete member
- the coefficient k_G shall be experimentally adjusted.

The value of such coefficient has been computed over a large population of experimental results available in the literature. The database contains experimental data from bond tests carried out in the framework of the Draft "ReLUIS-DPC 2005-2008 - Task 8.2". Moreover preformed (plates) and cured in-situ (sheets) FRP systems have been distinguished.

The calibrating procedure was based on a detailed and consistent statistical analysis according to the 'design by testing' procedure suggested in the Eurocode 0 (EN1990, 2002 – Annex D). Different corrective factors allow different percentiles values of k_G to be attained. The assessment of the percentiles has been carried out taking into account the variance of the materials.

The statistical analysis of the experimental results has provided an average value of K_G equal to 0.063mm and a 5th percentile equal to 0.023mm for plates and an average value equal to 0.077mm and a 5th percentile equal to 0.037mm for sheets.

Using the mean values 0.063mm and 0.077mm Eq. (7.4) gives the mean value of the energy fracture Γ_{Fm}. When the characteristic values 0.023mm and 0.037mm are used in Eq. (7.4), the characteristic value, Γ_{Fk} , of the fracture energy is obtained.

Through Eqns (7.3) and (7.4) the plate end debonding stress can be calculated as

$$f_{fdd} = \frac{1}{\gamma_{fd}} \sqrt{\frac{2 \cdot E_f \cdot \Gamma_{Fd}}{t_f}} \tag{7.6}$$

being

- $\gamma_{f,d}$ a safety factor on gluing application uncertainness (it shall be assumed equal to 1.2 or 1.5 for controlled or not controlled gluing application)
- $\Gamma_{Fd} = \Gamma_{Fk}/FC$ where FC is a confidence factor (in the range of 1.00-1.35) based on the level of knowledge achieved on the existing material properties and typically used for the assessment and retrofitting of buildings (European Code - UNI EN 1998-3).

In Figure 7.2, the experimental values of strain, $\varepsilon_{fdd} = f_{fdd}/E_f$ in the FRP reinforcement at debonding are plotted together with the mean and characteristics curves easily calculated through Eqns (7.3) and (7.4) for the different values of k_G (for further details see section 6.1).

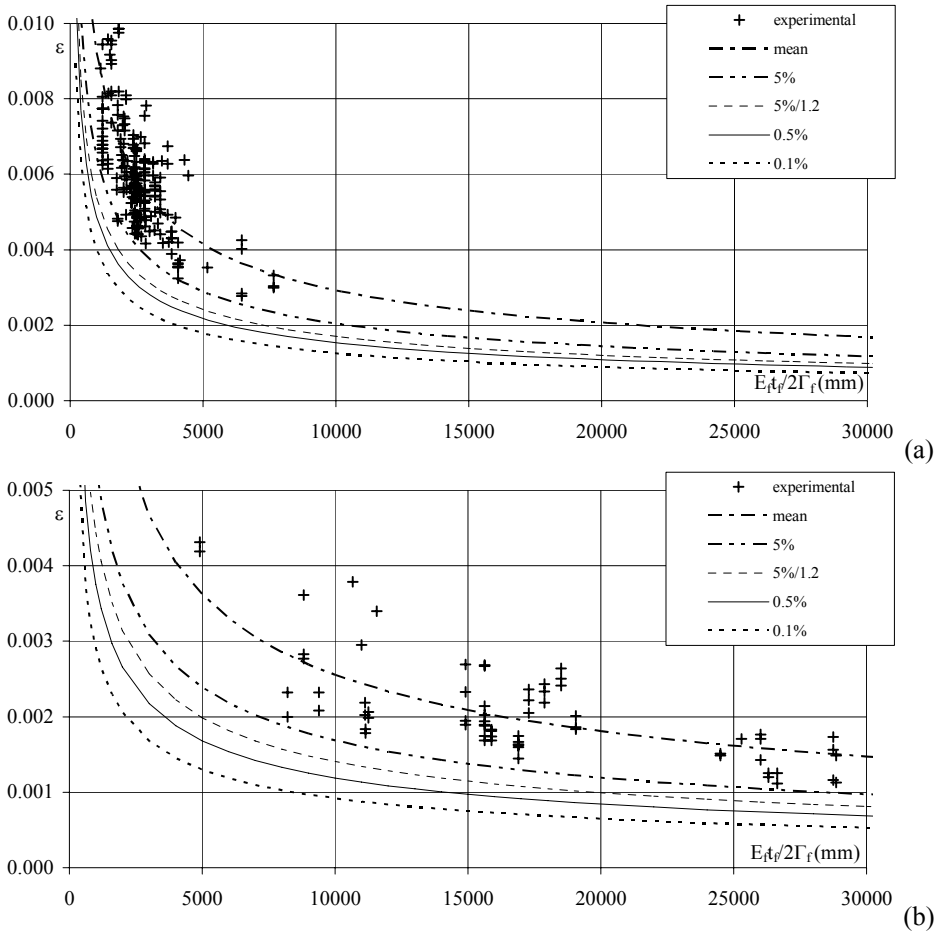

Figure 7.2. - Experimental strain at failure vs. theoretical results:
a) cured in situ systems (216 data); b) preformed systems (68 data).

The design value of the effective bond length can be derived from eq. (4.18) by using the design value of the fracture energy Γ_{Fd} mentioned above:

$$L_{eff} = s_u \sqrt{\frac{\pi^2 E_f t_f}{8\Gamma_{fd}}} \tag{7.7}$$

7.2 BOND-SLIP LAW

Bond between FRP and concrete is typically expressed with a relationship between interfacial shear stress and the corresponding slip ("τ_b-s" relationship). Both FRP and concrete mechanical characteristics as well as geometry of the FRP system and concrete support shall be considered in the analysis.

A precise bond-slip model should consist of a curved ascending branch and a curved descending branch, also other shapes such as a bilinear model can be used as a good approximation.

In particular the first ascending branch is defined by taking into account the deformability of adhesive layer and concrete support for an appropriate depth. Unless a more detailed analysis is performed, the average mechanical parameters defining the "τ_b-s" relationship, can be evaluated as follows (see Figure 7.3):

1) Interface slip corresponding to full debonding, $s_u = 0.25$mm

2) The maximum experimental average bond strength can be expressed as follows:

$$f_{fb} = \frac{2 \cdot \Gamma_{Fm}}{s_u} \tag{7.8}$$

3) The slope, K_1, of the ascending branch:

$$K_1 = \frac{c_1}{\frac{t_a}{G_a} + \frac{t_c}{G_c}} \tag{7.9}$$

where G_a , G_c represent shear modules of adhesive and concrete, respectively; t_a is the nominal thickness of the adhesive; and t_c is the effective depth of concrete (suggested values for t_c and c_1 are 20-30 *mm* and 0.5-0.7, respectively).

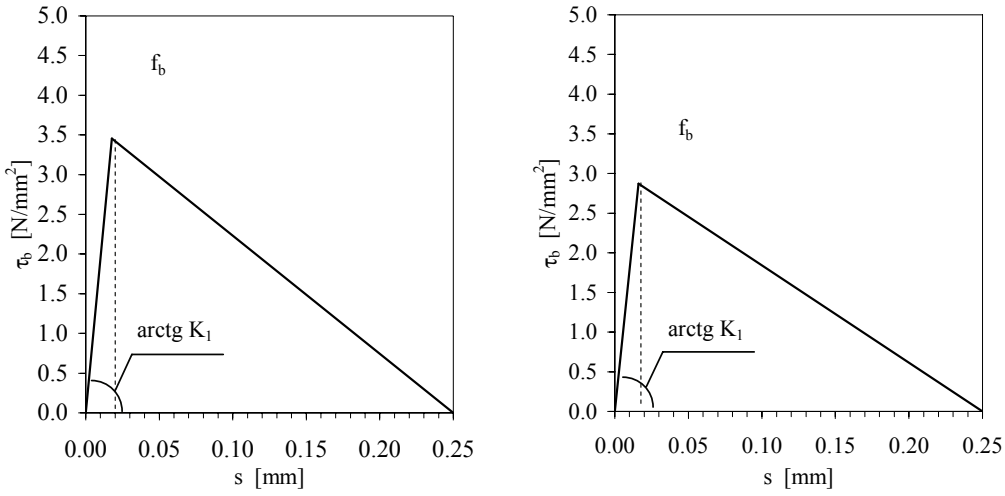

Figure 7.3. - Bi-linear "$\tau_b - s$ " relationship (f_{cm} = 20 MPa, k_b =1).

7.3 SIMPLIFIED METHOD FOR IC DEBONDING

Unless a more detailed analysis a simplified method can be used. Such method is based on the definition of a maximum value for the axial strain ε_{fd} which can be developed in the FRP laminate before of the occurrence of intermediate debonding failure.

The corresponding maximum strain can be evaluated as

$$\varepsilon_{fdd,2} = \frac{f_{fdd,2}}{E_f}\sqrt{\frac{2\cdot\frac{k_{G,2}\cdot k_b}{FC}\cdot\sqrt{f_{cm}\cdot f_{ctm}}}{E_f\cdot t_f}} \tag{7.10}$$

This relationship is similar to that proposed for the plate end debonding: the coefficient k_{G2} shall be experimentally adjusted.

The value of such coefficient has been computed over a large population of experimental results available in the literature.

The calibrating procedure was based on a detailed and consistent statistical analysis according to the 'design by testing' procedure suggested in the Eurocode 0 (EN1990, 2002 – Annex D). Different corrective factors allow different percentiles values of $k_{G,2}$ to be attained. The assessment of the percentiles has been carried out taking into account the variance of the materials.

The statistical analysis of the experimental results has provided an average value of $k_{G,2}$ equal to 0.32 mm and a 5^{th}-percentile equal to 0.10mm.

Chapter 8 - Conclusions

The strengthening of concrete structures with externally bonded reinforcement is a very powerful and effective technique to restore or enhance the bearing capacity of the structure. The basic idea of the technique is very simple. Additional reinforcement, mostly in tension, is added to the structure to increase or restore its bearing capacity.

Fiber-reinforced polymers (FRP) are more and more commonly employed for structural strengthening existing structures of both reinforced concrete (RC) and masonry. Indeed, the use of composite materials for structural strengthening of civil structures and infrastructures began with some pioneering application at the middle of the ‘80s of the past century.

Since FRP laminates are externally bonded on a concrete or masonry substrate, the issue of adhesion on those materials generally controls the effectiveness of strengthening in members stressed either in bending or shear.

Hence, a reliable design and application of this technique is only possible when the force transfer mechanism and the failure mechanism of the strengthened system is completely understood.

The PhD Thesis herein presented was aimed to contribute to the development of knowledge about such key issue. In this chapter the main findings of the performed research will be mentioned as well as recommendations for practical design and application will be summarized. Finally, some suggestions for future research are also provided.

8.1 EXPERIMENTAL OUTCOMES

From an applicative point of view and thus commercial, two main FRP systems for external strengthening of structures are distinguished in *pre-cured* systems and *wet lay-up* systems; they were briefly called *plates* and *sheets* respectively. Their mechanical behaviour may be different both when they are subjected to monotonic action and cyclic action.

In literature, compared with monotonic tests, there have been few bond tests under cyclic actions performed on CFRP sheets applied on concrete blocks. Particularly lacking are cyclic tests performed on CFRP plates and few studies are available on debonding phenomena under few cycles at high force levels, which typically occur during earthquakes.

Therefore a total of 58 single shear test (SST) tests in four sets (i.e. I-12 tests, II-16 tests, III-12 tests, IV-18 tests) were performed on CFRP plates (38) and sheets (20) applied on two opposite longitudinal faces of 29 concrete prisms. Concrete mix was specifically designed to obtain low compressive concrete strength to simulate the FRP application on existing concrete.

First two series of SST bond tests (30) under both monotonic (20) and cyclic actions (10), without inversion of action sign, were performed to analyze both the influence of different load paths (few cycles, typical of seismic actions) and the effect of FRP bond lengths on bond behavior between FRP reinforcement and the concrete substrate. The experimental outcomes showed the following:

- the influence of few load-unload cycles up to 70% of $P_{max,M}$ was negligible in terms of bond stiffness and strength for CFRP sheets both for higher and lower bond lengths than theoretical effective ones); similar results were obtained for plates, even if experimental effective bond lengths were significantly lower than theoretical ones;
- a small number of load-unload cycles (i.e. a total of 40 cycles) up to 90% of $P_{max,M}$ induced shear stress migration along the reinforcement with a reduction in peak values due to interface damage; however, this phenomenon did not substantially affect debonding loads in the case of bond lengths exceeding the effective ones;

- the design equations provided by the main international codes to predict the effective bond lengths were in good agreement with experimental results for sheets and more conservative for plates. Indeed, experimental effective bond lengths obtained by strain readings were lower (about 150mm) than theoretical ones (between 227mm and 320mm);
- experimental tests showed that the reduction in bond length up to about 50% of the theoretical effective length induced a comparable reduction in maximum debonding load on specimens subjected to monotonic or cyclic action.

Further 30 tests (set III and set IV) were performed on concrete specimens reinforced with CFRP sheets (6) and plates (24) under monotonic actions. These tests were mainly carried out to significantly enrich the existing database of the bond tests on EBR carbon plates.

These bond tests showed that the maximum efficiency of CFRP plates relevant to plate end debonding was only 20%. In general the increasing of stiffness leads to have higher loads, but a loss of efficiency; indeed larger transversal area do not lead to have a proportional increasing of ultimate load.

Moreover, higher values of thickness cause a larger scatter of results, the debonding load is not directly proportional with the reinforcement stiffness, and lower values of the ratio b_f/b_c do not determine proportional reduction of load.

Therefore the experimental results have showed that the effectiveness of the strengthening system has to be evaluated also in function of the axial stiffness: very high values of stiffness can be not useful to increase sensibly the failure load of the strengthened elements and can be uneconomical.

8.2 BOND LAW RELATIONSHIPS

An accurate local bond-slip model, taking into account the different behavior of sheets and plates, is of fundamental importance in the modeling of FRP- strengthened RC structures.

Thus, based on the wide collection of results attained from the experimental tests during which not only the load but also the corresponding axial strains of the FRP reinforcement were measured, through an Indirect Identification Method (IndIM) bond laws for sheets and plates were identified.

A simplified shape for the bond law (bilinear elasto-softening) was chosen on the basis of the observations of some previous studies available literary and taking into account the possibility of exploiting closed-form solutions to the problem of adhesion. The consistency of IndIM method and the robustness of the assumption on the bond law shape was showed by a comparison, in terms of axial strains throughout the bonded length, between theoretical predictions and the corresponding measured values. Even if the uncertainness in accurately identifying the parameter s_e indicated that the bond behaviour in the elastic stage was not perfectly approximated by a linear branch, the result obtained by assuming a bilinear law were satisfying.

Bond laws for sheets and plates have been separately identified through the IndIM method, and several bond law relationships, identified by three parameter (i.e. the maximum shear stress, τ_{max}, the corresponding elastic slip, s_e, and the ultimate slip, s_u), have been compared. The elastic and ultimate slips, s_e and s_u respectively, are on average the same for sheets and plates, although the dispersions of the values obtained by the identifying method are somewhat high. Conversely the values of maximum shear stress, τ_{max}, obtained for sheets bond laws are always higher than those obtained for plates interface relationships, of about 30% in average. Clearly the same differences are attained in terms of fracture energy. Such results are in agreement with the theoretical strength model showed in this Thesis for predicting plate end debonding of sheets and plates separately. Hence the advisability of assessing a bond law for the plates different from that for the sheets is considered appropriate.

8.3 BOND STRENGTH MODELS

A statistical procedure for the calibration of resistance models from experimental data, in accordance with the guidelines provided in Eurocode (EN1990) is presented. The procedure has been implemented on the basis of the results of the bond tests carried out and analyzed in the third and fourth chapters, and based on the results of further bond tests and tests on full-scale members found in literature, briefly summarized and discussed in the fifth and sixth chapter. The simplified analytical formulation were suggested for predicting the strength of beams and slabs in case of both *plate end debonding* and *intermediate debonding*.

In particular the proposed formulation for the plate end debonding load has a clear statistical meaning and allows to separately predict the plate end debonding for the cured in situ FRP systems and the preformed ones. Both aspects let to better exploit the strength of the cured in situ systems; indeed the 0.5% percentile of the new formulation are larger than the design values furnished by the current Italian Guidelines and, however, allow to assess the same safety level of model of Teng et al. (2001). Moreover, it was worth to notice that the formulation of *fib* Bulletin 14 (2001) results excessively unsafe compared to the experimental results.

By contrast, the approach of Teng et al., (2001) and *fib* Bulletin 14 (2001) are found to be less safe when applied to preformed systems. Indeed, the 0.5% percentile of the proposed design formulation provides a higher safety level compared with these models, whereas it is similar to the current design provisions of CNR-DT200 (2004). Thus, these results confirm that the distinction of the two strengthening systems seem to be reliable to have suitable prediction of debonding load.

Oh the other hand, as concern intermediate debonding the numerical procedure mentioned in the section 5.2 pointed out the role of some mechanical parameters (currently neglected in the most well-established simplified formulae) influencing the mechanical response of strengthened beams (i.e., the load condition, the yielding strain of steel rebars, the amount of reinforcement). Nevertheless, nowadays validating a sound theoretical model for predicting intermediate debonding is rather impractical as both the

experimental data and results are affected by high levels of uncertainties and randomness.

Consequently, a simplified empirical model for intermediate debonding has been calibrated based on the results of bending tests carried out on RC beams externally strengthened by FRP laminates. The model is based on a formula involving the key mechanical parameters such as the Young modulus E_f and the thickness t_f of the FRP reinforcement, and the concrete strength (in both compression and tension).

Although other similar models have been already presented in the scientific literature and adopted in codes of standard, the present proposal is based on a statistically consistent procedure for determining the safety levels required for defining the so-called "characteristic" and "design" values of the maximum axial strain developed in FRP at intermediate debonding. The mentioned procedure adopted for defining those values comply to the Eurocode provisions about the so-called "design-by-testing" approach.

Finally, the comparison between the proposed formula and the other ones already available in the literature point out that it is a good trade-off between the conservativeness required for design purposes and the need for efficient and cost-effective usage of materials.

8.4 FURTHER DEVELOPMENTS

The application of the IndIM procedure to obtain simplified bond laws and the statistical procedure calibrating the bond strength relationships for both plate end debonding and intermediate debonding were summarized and integrated in chapter 7, in order to prepare an updating proposal for instructions CNR-DT200 (2004). Then the first step, in a short term, is to define and present this "theoretical" update.

Anyway, it s necessary to keep in mind that the success of the technique of bonded reinforcement is closely related with the practical application of the bonded connection. Indeed, a good force transfer and a long term durability are only possible when the bonded connection is properly done according to the rules of good workmanship. Therefore the competence and the workmanship of the executing contractor are very important. This workmanship can be guaranteed by a system of guidelines and certifications and by on site inspections by the project engineer.

Finally it is clear that the numerical procedure presented and validated in the chapter 5 can be utilized as a powerful tool to extend the experimental data, reaching a number of cases which is far larger than the one realizable in a laboratory for practical reasons. Consequently, the influence of the various parameters can be investigated in depth to understand their role and quantifying their importance for both *plate end debonding* and *intermediate debonding*. Moreover the analytical formulations predicting the strength of beams and slabs could be refined by means of both numerical models (i.e. based on finite element discretization) and a limited number of experimental results and extrapolation of those results through the above mentioned numerical procedures. These new and more sound formulations could take the place of the simplified analytical formulations nowadays suggested.

Chapter 9 - References

ACI Committee 318, (2005), "Building Code Requirements for Structural Concrete (ACI 318-05) and Commentary (318R-05)," *American Concrete Institute*, Farmington Hills, MI, 430 pp.

ACI Committee 440.2 R-02 (2002): Guide for the Design and Construction of Externally Bonded FRP Systems for Strengthening Concrete Structures, Revised 28;

ACI 440.2R-08 (2008). Guide for the Design and Construction of Externally Bonded FRP Systems for Strengthening Concrete Structures. *ACI440.2R-08 American Concrete Institute, Farmington Hills, MI, 2008, 76 pp.*

Achintha P. M. M. & Burgoyne C. J. (2008). Fracture Mechanics of Plate Debonding, *ASCE Journal for Composites for Construction*, Vol. 12, No. 4, July/August 2009, 396-404, ISSN 1090-0268

Ahmed, O, van Gemert, D. (1999). Effect of longitudinal carbon fiber reinforced plastic laminates on shear capacity of reinforced concrete beams, in: Dolan CW, Rizkalla SH, Nanni A. (Eds.) Proceedings of the Fourth International Symposium on Fiber Reinforced Polymer Reinforcement for Reinforced Concrete Structures, Maryland, USA, 1999, pp. 933–943.

Ahmed, O., Gemert, D. V., and Vadewalle, L. (2001). “Improved model for plate-end shear of CFRP strengthened RC beams.” *Cement*, 23, 3–19.

Aiello, M.A. and Leone, M. (2005). Experimental bond analysis of concrete - FRP (fiber reinforced polymer) reinforced, *Proc. of fib Symposium "Keep Concrete Attractive*, Budapest, Hungary, May.

Arduini M. & Nanni A. (1997). Behavior of precracked RC beams strengthened with carbon FRP sheets, *ASCE Journal for Composites for Construction*, Vol. 1, No. 2, 63–70, ISSN 1090-0268

Arya, C., and Farmer, N. _2001_. “Design guidelines for flexural strengthening of concrete members using FRP composites.” *Proc., 5th Int. Symp. on Fiber Reinforced Concrete Structures*, Cambridge, 167–176.

Bakay, R. (2003). Midspan Shear Debonding of CFRP Laminated Reinforced Concrete Beams. MSc Thesis, Department of Civil Engineering, University of Calgary, Calgary, Alberta, Canada.

Beber A.J., Campos Filho A., Campagnolo J.L. (1999), Flexural strengthening of R\C beams with CFRP sheets, Structural Faults + Repair-99.

Beber A.J., (2003), Comportamento Estrutural de Vigas de Concreto Armado Reforçadas com Compósitos de Fibra de Carbono, tese de doutorado em Engenharia Civil da Universidade Federal do Rio Grande do Sul (in portuguese);

Bilotta A, Di Ludovico M, Nigro E. (2009a). Influence of effective bond length on FRP-concrete debonding under monotonic and cyclic actions. *Proceedings of 9th International Symposium on Fiber Reinforced Polymer Reinforcement for Concrete Structures,* Sydney (Australia), July 2009 (CD ROM).

A. Bilotta, M. Di Ludovico, E. Nigro (2009b) FRP debonding on concrete members. Part I: experimental investigation. *Proceedings of 9th International*

Symposium on Fiber Reinforced Polymer Reinforcement for Concrete Structures, Sydney (Australia), July 2009 (CD ROM).

A. Bilotta, M. Di Ludovico, E. Nigro (2009c) FRP debonding on concrete members. Part II: capacity model calibration *Proceedings of 9th International Symposium on Fiber Reinforced Polymer Reinforcement for Concrete Structures,* Sydney (Australia), July 2009 (CD ROM).

Bilotta A., Ceroni F., Di Ludovico M., Nigro E., Pecce M., Manfredi G. (2011a). Bond Tests on concrete elements strengthened with EBR and NSM FRP systems, 10th International Symposium on Fiber Reinforced Polymer Reinforcement for Reinforced Concrete Structures, April 2-4, 2011, Tampa, Florida, USA.

Bilotta A., Ceroni F., Nigro E., Pecce M. (2011b). Design by testing of debonding load in RC element strengthened with EBR FRP materials, 10th International Symposium on Fiber Reinforced Polymer Reinforcement for Reinforced Concrete Structures, April 2-4, 2011, Tampa, Florida, USA.

Bizindavyi L., Neale K. W., Erki M. A. (2003). Experimental Investigation of Bonded Fiber Reinforced Polymer-Concrete Joints under Cyclic Loading. *Journal of Composites for Construction ASCE, 7:2 127-134.*

Bizindavyi L. & Neale K. W. (1999). Transfer lengths and bond strengths for composites bonded to concrete, *ASCE Journal for Composites for Construction*, Vol. 3, No. 4, July/August 1999, 153-160, ISSN 1090-0268

Blaschko, M., Niedermeier, R., and Zilch, K. (1998). "Bond failure modes of flexural members strengthened with FRP." *Proc 2nd Int. Conf. on Composites in Infrastructure*, Ariz., 315–327.

Blontrock, H., Taerwe, L. and Vanwalleghem, H. (2002). Bond testing of externally glued FRP laminates at elevated temperature, *Proceedings of the International Symposium "Bond in Concrete: from research to standards"*, 648-654, ISBN 963-420-714-6, Budapest, November 2002, Publisher, City

Bonacci J.F. (1996). Strength, Failure Mode and Deformability of Concrete Beams Strengthened Externally with Advanced Composites, *Proceedings of the 2nd International Symposium on Advanced Composite Materials in Bridges and Structures*, ISBN, Montreal (Canada), 419-426, Publisher, City

Brosens K. (2001). Anchorage of externally bonded steel plates and CFRP laminates for the strengthening of concrete elements. *PhD thesis, K.U. Leuven, 2001, 225 pp.*

BS EN 206-1:2000. *Concrete. Specification, performance, production and conformity.*

CEB-FIP (1993). Model Code 1990, Final Draft, Bulletin d'Information n. 213/214.

Ceroni, F., Pecce, M., Matthys, S. and Taerwe, L. (2008). Bond tests on concrete elements with CFRP and anchorage systems, *Composites: Part B* - Elsevier, Vol. 39, No.3, April 2008, 429–441, ISSN 1359-8368

Ceroni F., Pecce M. (2010). Evaluation of bond strength and anchorage systems in concrete elements strengthened with CFRP sheets, *ASCE Journal of Composites in Construction*, in press, ISSN 1090-0268

Chaallal O. and Shahawy M. (2000), *Performance of fiber reinforced polymer wrapped reinforced concrete column under combined axial-flexural loading*, ACI Structural Journal, Vol. 97, no. 4, July-August 2000, pp. 659-668

Chajes M.J., Finch W.W., Januszka T.F. & Thomson T.A. (1996). Bond and force transfer of composite-material plates adhered to concrete, *ACI Structural Journal*, Vol. 93, No. 2, February 1996, 208–217, ISSN 0889-3241

Chen J.F., Yang Z.J., Holt G.D. (2001a). FRP or steel plate-to-concrete bonded joints: effect of test methods on experimental bond strength. *Steel Compos Structures 1(2), pp. 231–244.*

Chen J.F., Teng J.G. (2001b): Anchorage Strength Models for FRP and Plates Bonded to Concrete, *ASCE Journal of Structural Engineering*, Vol. 127, No. 7, July 2001, 784-791, ISSN 0733-9445

Chen, J.F., Yuan, H., and Teng, J.G. 2007. Debonding failure along a softening FRP-to-concrete interface between two adjacent cracks in concrete members. Engineering Structures, Elsevier, 29(1): 257-270.

Colotti, V., and Spadea, G. _2001_. "Shear strength of RC beams strengthened with bonded steel or FRP plates." *J. Struct. Eng.*, 127_4_, 367–373.

CNR-National Council for Research (2004). *Guide for the Design and Construction of Externally Bonded FRP Systems for Strengthening Existing Structures-Materials, RC and PC structures, masonry structures*

Czaderski C., Soudki K. & Motavalli M. (2010). Front and Side View Image Correlation Measurements on FRP to Concrete Pull-Off Bond Tests, *ASCE Journal for Composites for Construction*, Vol. 14, No. 4, July/August 2010, 451-463, ISSN 1090-0268

Dai J., Ueda T., Sato Y. (2005a). Development of Nonlinear Bond Stress-Slip Model of FRP Sheet-concrete Interfaces with a Simple Method. *Journal of Composites for Constructions, ASCE, 9(1), 52-62.*

Dai J.G., Sato Y., Ueda T., Sato Y. (2005b). Static and Fatigue Bond Characteristics of Interfaces between CFRP Sheets and Frost Damage Experienced Concrete. *Proceedings of FRPRCS-7, ACI-SP-230-86, pp.1515-1530.*

De Lorenzis L., Miller B., Nanni A. (2001). Bond of Fiber-Reinforced Polymer Laminates to Concrete. *ACI Materials Journal. 98-M29, 256-264.*

Diab H., Wu Z., Iwashita K. (2007). Experimental and numerical investigation of fatigue behavior of frp-concrete interface. *Proceeding of FRPRCS-8. Patras - Greece - July 16-18, 2007.*

Di Ludovico M, Piscitelli F, Prota A, Lavorgna M, Manfredi G, Mensitieri G. (2009). CFRP Laminates Behavior at Elevated Temperature. In: *Proceedings of the 7th International Conference on Composite Science and Technology*, January 20-22, 2009 - Sharjah, United Arab Emirates.

El-Mihilmy, M. T., and Tedesco, J. W. _2001_. "Prediction of anchorage failure for reinforced concrete beams strengthened with fiberreinforced polymer plates." *ACI Struct. J.*, 98_3_, 301–314.

Emmons P.H., Vaysburd A.M. and Thomas J. (1998a), *Strengthening concrete structures, Part I*, Concrete International, Vol. 20, no. 3, March 1998, pp. 53-58

Emmons P.H., Vaysburd A.M. and Thomas J. (1998b), *Strengthening concrete structures, Part II*, Concrete International, Vol. 20, no. 4, April 1998, pp. 56-60

European Committee for Standardization. (2002) *EN 1990 - Eurocode - Basic of Structural Design*. 2002.

European Committee for Standardization. (2004) *EN 1992* - Eurocode 2. *Design of Concrete structures – Part 1-1: General Rules and Rules for Buildings*, ENV 1992-1-1: 2004: E.

European Commitee for Standardization. (2005) EN 1998 - Eurocode 8 - Design of structures for earthquake resistance - Part 3: Assessment and retrofitting of buildings. 2005.

Faella C., Martinelli E., Nigro E., (2002a): Steel and concrete composite beams with flexible shear connection: "exact" analytical expression of the stiffness matrix and applications, Computer & Structures, Vol. 80/11, pp. 1001-1109.

Faella C., Martinelli E., Nigro E, M. Sabatino, N. Salerno, G. Mantegazza, (2002b) *Aderenza tra calcestruzzo e Lamine di FRP utilizzate come placcaggio di elementi inflessi. Parte I: Risultati sperimentali.* Proceedings of the XIV C.T.E. Conference, Mantua (Italy), 7-8 November 2002, 237-245, (in Italian);

Faella C., Martinelli E. & Nigro E. (2002c). Aderenza tra calcestruzzo e Lamine di FRP utilizzate come placcaggio di elementi inflessi. Parte II: modelli teorici ed elaborazioni numeriche, Proceedings of the XIV C.T.E. Conference, Mantua (Italy), 7-8 November 2002, 237-245, (in Italian);

Faella C., Martinelli E., Nigro E (2003). *Interface behaviour in FRP plates bonded to concrete: experimental tests and theoretical analyses*, Proceedings of the International Conference on Advanced Materials for Construction of Bridges, Buildings and other Structures - III, Davos (Svizzera), 7-12 September 2003

Faella C., Martinelli E., Nigro E (2004). *Debonding in FRP-strengthened RC beams: comparison between code provisions*, The Second International Conference on FRP Composites in Civil Engineering, Paper 074, Adelaide (Australia), 8-10 December 2004

Faella C., Martinelli E., Nigro E (2006a). *Formulation and Validation of a Theoretical Model for Intermediate Debonding in FRP Strengthened RC Beams*, Proceedings of the 2nd International *fib* Congress, Naples, Italy, 5-8 June 2006, Paper 0735

Faella C., Martinelli E., Nigro E (2006b). *Intermediate Debonding in FRP Strengthened RC Beams: A Parametric Analysis*, Proceedings of the 2nd International *fib* Congress, Naples, Italy, 5-8 June 2006, Paper 0993

Faella C., Martinelli E., Nigro E (2007a). *A Theoretical Model for Intermediate Debonding of RC Beams Strengthened in bending by FRP*, Proceedings of the 6th FramCoS Conference, Catania (Italy), 17-19 June 2007, Paper 358

Faella C., Martinelli E., Nigro E (2007b). *Intermediate Debonding of RC beams strengthened in Bending by FRP: A Theoretical Model and a Simplified Design Approach*, Proceedings of the 8th FRPRCS Conference, Patras (Greece), 16-18 July 2007

Faella C., Martinelli E., Nigro E (2007c). *Delaminazione intermedia nelle travi in c.a. rinforzate con FRP: modellazione numerica e Metodologie semplificate di progetto*, Proceedings of the Conference "Giornate AICAP 2007", Salerno (ITALY), 4-6 Ottobre 2007, Paper 074, (in Italian)

Faella C., Martinelli E., Nigro E (2007d). *Debonding failure in FRP-strengthened RC beams: a model-based approach,* Proceedings of Asia-Pacific Conference on FRP in Structures (APFIS 2007), Hong Kong (China), 12-14 December 2007, Paper 176

Faella C., Martinelli E., Nigro E (2007e). *Direct versus Indirect identification of FRP-to-concrete interface relationships,* Proceedings of Asia-Pacific Conference on FRP in Structures (APFIS 2007), Hong Kong (China), 12-14 December 2007, Paper 177

Faella C., Martinelli E. & Nigro E. (2008a). Formulation and Validation of a Theoretical Model for Intermediate Debonding in FRP Strengthened RC Beams, *Composites Part B*, Vol. 39, No. 4, 645-655, June 2008, ISSN 1359-8368

Faella C., Martinelli E., Nigro E (2008b). *Some Remarks on the Parameters affecting Debonding in FRP Strengthened RC-Beams*,

Proceedings of Fourth International Conference on FRP Composites in Civil Engineering (CICE2008), Zurich (Switzerland), 22-24 July 2008

Faella C., Martinelli E. & Nigro E. (2009a). Direct versus Indirect Method for Identifying FRP-to-Concrete Interface Relationships, *ASCE Journal for Composites for Construction*, Vol. 13, No. 3, May/June 2009, 226-233, ISSN 1090-0268

Faella C., Martinelli E., Nigro E (2009b). *Intermediate debonding in RC beams externally strengthened by FRP: mechanical remarks and simplified formulations*, 9th International Symposium on Fiber Reinforced Polymer Reinforcement for Concrete Structures (FRPRCS 9), Sydney, Australia Monday 13 – Wednesday 15 July, 2009, Paper ID: 234

Faella C., Martinelli E., Nigro E (2010). *A simplified design formula for intermediate debonding failure in RC beams externally strengthened by FRP*, 3rd *fib* International Congress, Washington, USA, May 29 – June 2, 2010, Paper ID: 672, 8 pp.

Fanning, P. J. and Kelly, O. 2001. Ultimate response of RC beams strengthened with CFRP plates. Journal of Composites for Construction, 5(2): 122-127.

Ferracuti B., Savoia M., Mazzotti C. (2007a). *Interface law for FRP–concrete delamination* Composite Structures Elsevier vol. 80 pp 523–531

Ferracuti B., Martinelli E., Nigro E., Savoia M. (2007b). *Fracture Energy and Design Rules against FRP-Concrete Debonding*, Proceedings of the 8th FRPRCS Conference, Patras (Greece), 16-18 July 2007

Ferracuti B., Mazzotti C., Savoia M. (2008). A new single-shear set-up for stable delamination tests on FRP-concrete joints, *Construction and Building Materials*, Vol. 23, No. 4, pp. 1529 – 1537.

fib Bulletin No. 14 (2001). *Externally bonded FRP reinforcement for RC structures*, Technical report prepared by the Working Party EBR of Task Group 9.3, *International Federation for Structural Concrete*, ISBN 978-2-88394-054-3, Lausanne (CH)

Gao Bo, Kim J.K., Leung C.K.Y. (2004) , Experimental study on RC beams with FRP strips bonded with rubber modified resins Catalogo Elsevier, Composites Science and Technology 64 (2004) pp. 2257-2264, July.

Garden H.N., Quantrill R.J., Hollaway L.C., Thorne A.M., Parke G.A.R. (1998), An experimental study of the anchorage length of carbon fibre composite plate used to strengthen reinforced concrete beams, Construct Build Mater, 12, 1998.

Grace N. F., Sayed G. A., Soliman A. K., Saleh K. R., (1999). "Strengthening Reinforced Concrete Beams Using Fiber Reinforced Polymer (FRP) Laminates", *ACI Struct. J.*, 96, 5, 1999, 865-875;

Guo Z. G., Cao S. Y., Sun W. M., Lin X. Y. (2005). Experimental study on bond stress-slip behaviour between FRP sheets and concrete. *Proceedings of the International Symposium on Bond Behaviour of FRP in Structures.*

Hart-Smith, L. J. (1973). Adhesive-bonded double-lap joints, NASA Technical Report, CR-112235, Hampton, Va. (USA)

Hassanen, M. A. H., and Raoof, M. (2001). "Design against premature peeling failure of RC beams with externally bonded steel or FRP plates." *Mag. Concrete Res.*, 53_4_, 251–262.

Holzenkaempfer (1994), Ingenieurmodelle des verbundes geklebter bewehrung fur betonbauteile, Dissertation, TU Braunschweig (in German);

Horii H., Kabele P., Takeuchi S., Li V.C., Matsuoka S. and Kanda T. (1998), *On the prediction method for the structural performance of*

repaired/retrofitted structures, Proceedings of FRAMCOS-3, Fracture Mechanics of Concrete structures, October 1998, Gifu, Japan, pp. 1739- 1750

Jansze, W. (1997). Strengthening of RC Members in Bending by Externally Bonded Steel Plates, PhD Thesis, Delft University of Technology, Delft, 1997.

Jones, R., Swamy, R. N., and Charif, A. _1988_. "Plate separation and anchorage of reinforced concrete beams strengthened by epoxy bonded steel plates." *Struct. Eng.*, 66_5_, 85–94.

JSCE (2001): Recommendations for upgrading of concrete structures with use of continuous fiber sheets, Concrete Engineering Series 41;

Katsumata H., Kimura K. and Kobatake Y. (1998), *Seismic retrofitting technique using carbon fibers for reinforced concrete buildings*, Proceedings of FRAMCOS-3, Fracture Mechanics of Concrete structures, October 1998, Gifu, Japan, pp. 1727-1738

Khomwan N., Foster S.J., Smith S.T. (2004), "Debonding failure in CFRP strengthened concrete beams", *Proceedings of the 2nd International Conference on FRP Composites in Civil Engineering*, CICE 2004, Adelaide (Australia), 2004, pp. 505-514.

Ko H. and Sato Y. (2007). Bond stress-slip relationship between FRP sheet and concrete under cyclic load. *Journal of Composites for Construction ASCE, 11(4): 419-426.*

Kobayashi A., Matsui S., Kishimoto, M. (2003). Fatigue Bond of Carbon Fiber Sheets and Concrete in RC Slabs Strengthened by CFRP. *Proceedings of FRPRCS-6, Edited by Tan, K. H., Vol.2, 865-874.*

Lee Y. J., Boothby T. E., Bakis C. E. & Nanni A. (1999). Slip Modulus of FRP Sheets Bonded to Concrete, *ASCE Journal of Composites for Construction*, Vol. 3, No. 4, November 1999, 161-167, ISSN 1090-0268

Leone M., Aiello M.A., Matthys S. (2009). Effect of elevated service temperature on bond between FRP EBR systems and concrete, *Composites Part B: Engineering*, Vol. 40, No. 1, pp. 85-93.

Lin X.Y., Cao S. Y., "Study on Bond Behavior between CFRP and Concrete in Beams Bonded with External Fibers", *Proceedings of the 1st APFIS Conference*, 12-14 December 2007, Hong Kong (China), vol. 2, 793-798;

Liu I., Oehlers D.J., Seracino R. (2004), Parametric study of intermediate crack (IC) debonding on adhesively plated beams, Proceedings of FRP Composites in Civil Engineering – CICE 2004, Adelaide (Australia), 8-10 December;

Lu X.Z., Teng J.G., Ye L.P. & Jiang J.J. (2005). Bond-slip models for FRP sheets/plates bonded to concrete, *Engineering Structures*, Vol. 27, No. 6, May 2005, 920-937, ISSN 0141-0296

Maalej M., Leong K.S. (2005), Effect of beam size and FRP thickness on interfacial shear stress concentration and failure of FRP strengthened beams, Catalogo Elsevier, Composites Science and Technology 65 (2005) pp. 1148-1158, January.

Malek A. M., Saadatmanesh H., Ehsani M. R. (1998). Prediction of failure load of R/C beams strengthened with FRP plate due to stress concentration at the plate end, *ACI Structural Journal*, Vol. 95, No. 2, March/April 1998, 142-152, ISSN 1090-0268

Martinelli E., Bilotta A., Faella C., Nigro E (2011). On the behaviour of FRP-to-concrete adhesive interface: theoretical models and experimental results., chapter in *Advances in Composite Materials*. Intech. ISBN: 978-953-7619-X-X. In press..

Maruyama, K., and Ueda, T. _2001_. "JSCE design recommendations for upgrading of RC member by FRP sheet." *Proc., 5th Int. Symp. On Fiber Reinforced Concrete Structures*, Cambridge, 441–446.

Matthys, S. (2000). "Structural behavior and design of concrete members strengthened with externally bonded FRP reinforcement." Dept. of Structural Engineering, Ghent Univ., Ghent, Belgium.

Mazzotti C., Savoia M. (2007) "Intermediate Debonding of FRP Strengthened Beams", *Proceedings of the 1st APFIS Conference*, Hong Kong (China), 12-14 December 2007, vol. 2, 877-884.

Mazzotti C., Savoia M., Ferracuti B. (2008). An experimental study on delamination of FRP plates bonded to concrete, *Construction and Building Materials*, Vol. 22, No. 7, 2008, pp. 1409-1421.

Mazzotti C., Savoia M., Ferracuti B. (2009). A new single-shear set-up for stable debonding of FRP–concrete joints, *Construction and Building Materials - Elsevier*, Vol. 23, No.4, April 2009, pp. 1529-1537. ISSN 0950-0618

McSweeney B.M., Lopez M.M. (2005). FRP-Concrete Bond Behavior: A Parametric Study Through Pull-Off Testing, *Proc. of 7th Int. Symp. FRP Reinforcement for Concrete Structures*, Kansas City, November, Missouri, Editors: Carol K. Shield, John P. Busel, pp. 441-460.

Meier, U. (1987). Brückensanierungen mit Hochleistungs-Faserverbundwerkstoffen, Material und Technik, Vol. 15, No 4, 125-128 ISSN

Meier U. (1995). Strengthening of structures using carbon fibre/epoxy composites, *Construction and Building Materials*, Vol. 9, No. 6, June 1995, 341–351, ISSN 0950-0618

Mood A.M., Graybill F.A., Boes D.C. (1974). *Introduction to the Theory of Statistics*, 3rd ed., McGraw-Hill, New York.

Monti G., Alessandri S., Santini S. (2009). Design by Testing: A Procedure for the Statistical Determination of Capacity Models, *Journal of Construction and Building Materials, Special Issue on FRP Composites Elsevier*, Vol. 23, 1487-1494. ISSN 0950-0618

Mutsuyoshi H., Ishibashi T., Okano M. and Fatsuki F. (1999), *New design method for seismic retrofit of bridge columns with continuous fiber sheet - Performance based design*, FRPRCS-4, 31 October - 5 November 1999, Baltimore, United Stated, pp. 229-242

Neubauer, U. and Rostasy, F.S. (1997). Design Aspects of Concrete Structures Strengthened with Externally Bonded CFRP Plates, Concrete and Composites, *Procedings of 7th International Conference On Structural Faults and Repair*, Vol. 2, 109-118, ISBN, ECS Pub. Edinburgh, Scotland.

Motavalli M. & Czaderski C. (2007). FRP Composites for Retrofitting of Existing Civil Structures in Europe: State-of-the-Art Review, *Proceedings of the American Composites Manufacturers Association 2007*, ISBN, Tampa, FL (USA), October 2007, Publisher, City

Naaman A.E., Park S.Y., Lopez M.M. & Till R.D. (2001). Parameters Influencing the Flexural Response of RC Beams Strengthened Using CFRP Sheets, *Proceedings of the Conference FRPRCS-5*, Cambridge (UK), 117-125, ISBN 0727730290

Nigro E., Savoia M. (2005). *Il fenomeno della delaminazione nel placcaggio con FRP di strutture di conglomerato cementizio armato*, L'Edilizia, n. 139, Settembre 2005

Nigro E., Di Ludovico M., Bilotta A. (2008a). Concrete interface relationships under monotonic and cyclic actions. *Fourth International*

Conference on FRP Composites in Civil Engineering (CICE2008) 22-24 July 2008, Zurich, Switzerland.

Nigro E., Di Ludovico M., Bilotta A. (2008b). FRP- Concrete Debonding: experimental Tests under Cyclic Actions, *Proceedings of 14th World Conference on Earthquake Engineering* , ISBN, Beijing (China), October 2008, Publisher, City

Nigro E., Di Ludovico M., Bilotta A. (2008c). Experimental investigation on FRP – concrete debonding under cyclic actions. Journal of Materials in Civil Engineering - ASCE. Published on line. doi: 10.1061/(ASCE)MT.1943-5533.0000173

Oehlers D.J., Moran J.P. (1990). Premature failure of externally plated reinforced-concrete beams, *Journal of Structural Engineering - ASCE,* Vol. 116, No.4, April, 1990, 978-995. ISSN 0733-9445

Oehlers DJ. (1992) Reinforced concrete beams with plates glued to their soffits. J Struct Eng ASCE 1992;118(8):2023 –2038.

Pellegrino C., Boschetto G., Tinazzi D., Modena C. (2005). Progress on under standing bond behaviour in rc elements strengthened with FRP. *Proceedings of the International Symposium on Bond Behaviour of FRP in Structures. 7-9 December 2005, Hong Kong, China.*

Pham H., Al-Mahaidi R. (2004a). Prediction models for debonding failure loads of CFRP retrofitted RC beams, *Proceedings of the 2nd International Conference on FRP Composites in Civil Engineering, CICE 2004*, Adelaide (Australia), 8-10 December 2004;

Pham H., Al-Mahaidi R. (2004b). Bond characteristics of CFRP fabrics bonded to concrete members using wet lay-up method", *Proceedings of the 2nd International Conference on FRP Composites in Civil Engineering, CICE 2004*, Adelaide (Australia), 8-10 December 2004, pp. 407-412.

Rabinovich O. & Frostig, Y. (2000). Closed-form High-order Analysis of RC Beams Strengthened with FRP Strips, *ASCE Journal of Composites for Construction*, Vol. 4, No. 2, March-April 2000, 65-74, ISSN 1090-0268

Rabinovich O. & Frostig, Y. (2001). Delamination Failure of RC Beams Strengthened with FRP Strips—A Closed-Form High-Oorder and Fracture Mechanics Approach, *Journal of Engineering Mechanics*, Vol. 127, No. 8, August 2001, ISSN 0733-9399

Raoof, M, Zhang, S. (1997) An insight into the structural behaviour of reinforced concrete beams with externally bonded plates, Proceedings of the Institution of Civil Engineers: Structures and Buildings, vol. 122, November 1997, pp. 477–492.

Raoof, M, Hassanen, MAH (2000). Peeling failure of reinforced concrete beams with fibre-reinforced plastic or steel plates glued to their soffits, Proceedings of the Institution of Civil Engineers: Structures and Buildings, vol. 140, August 2000, pp. 291–305.

Roberts T.M. (1989). Approximate analysis of shear and normal stress concentrations in the adhesive layer of plated RC beams, *The Structural Engineer*, Vol. 67, No. 12, December 1989, 229–233, ISSN 0039-2553

Saadatmanesh H., Ehsani M.R. and Limin J. (1996), *Seismic strengthening of circular bridge pier models with fiber composites*, ACI Structural Journal, Vol. 93, no. 6, November-December 1996, pp. 639-647

Saadatmanesh H., Ehsani M.R., Eeri M. and Jin L. (1997), *Seismic Retrofitting of Rectangular Bridge columns with composite straps*, Earthquake Spectra, vol. 13, no. 2, May 1997, pp. 281- 304

Saadatmanesh H, Malek AM. (1998). Design guidelines for flexural strengthening of RC beams with FRP plates. J Compos Constr ASCE 1998;2(4):158 –164.

Said and Wu, 2008 "Evaluating and proposing models of predicting IC Debonding Failure" *ASCE Journal of Composites for Construction Vol. 12, No. 3, June 1, 2008., pp. 284 - 299*

Savoia M., Ferracuti B., Mazzotti C. (2003), Non linear bond-slip law for FRP-concrete interface. *Proceedings of the conference FRPRCS-6, Singapore.*

Savoia et al. (2008). Risultati di un Round Robin sperimentale su prove di aderenza FRP-calcestruzzo. 17th *CTE Congress, 6-7-8 November 2008, Rome.*

Savoia M., Bilotta A., Ceroni F., Di Ludovico M., Fava G., Ferracuti B., Mazzotti C., Nigro E., Olivito R., Pecce M., Poggi C., (2009). Experimental round robin test on FRP concrete bonding, *Proceedings of FRPRCS9*, Sydney (Australia), July, 2009 (CD ROM).

Saxena P; Toutanji H,, Noumowe A (2008) Failure Analysis of FRP-Strengthened RC Beams *Journal of Composites for Construction*, Vol. 12, No. 1, February 1, 2008. ©ASCE, ISSN 1090-0268/2008/1

Seracino R., Saifulnaz M.R.R., Oehlers D.J. (2007), Generic Debonding Resistance of EB and NSM Plate-to-Concrete Joints, *J. of Composites for Construction*, 11 (4), 62-70.

Shahawy, M. A.; Arockiasamy, M., Beitelman, T., Sowrirajan (1996), Reinforced concrete rectangular beams strengthened with CFRP laminates Composites Structures - Part B, 27, pp. 225-233;

Sharif A., Al-Sulaimani G. J., Basunbul I. A., Baluch M. H., Ghaleb B. N., (1991) "Strengthening of Initially Loaded Reinforced Concrete Beams using FRP Plates*", ACI Structural Journal*, 91, 2, 1991, 160-168.

Shapiro S.S., Wilk M.B. (1965). *An analysis of variance test for normality (complete samples)*, Biometrika, 52, pp. 591-611.

Sharma S.K., Mohamed Ali M.S., Sikdar P.K. (2004), Investigation of debonding failure in FRP plated beams, Proceedings of FRP Composites in Civil Engineering – CICE 2004, Adelaide (Australia), 8-10 December 2004;

Shehata, I. A. E. M., Cerqueira, E. C., Pinto, C. T. M., and Shehata, L. C. D. _2001_. "Strengthening of RC beams in flexure and shear using CFRP laminates." *Proc., 5th Int. Symp. on Fiber Reinforced Concrete Structures*, Cambridge, 97–106.

Smith S.T. & Teng J.G. (2001), Strength Models for Plate End Debonding in FRP-Strengthened RC Beams, *Proceedings of the Conference FRPRCS-5*, ISBN 0727730290, Cambridge (UK), 419-428, 2001, Publisher, City

Smith S. T. & Teng J. G. (2002a). FRP-strengthened RC beams. I: review of debonding strength models, *Engineering Structures*, Vol. 24, No. 4, April 2002, 385-395, ISSN 0141-0296

Smith, S.T. and Teng J.G. (2002b). FRP strengthened RC beams – II: assessment of debonding strength models. Engineering Structures, 24(4): 397-417. ISSN 0141-0296

Spadea G., Bencardino F., Swamy R.N. (1998), Structural behavior of composite RC beams with externally bonded CFRP, J Comps Construct, ASCE, 2(3), 1998.

Swamy R.N., Jones R. & Bloxham J.W. (1987). Structural behaviour of reinforced concrete beams strengthened by epoxy-bonded steel plates, *The Structural Engineer*, Vol. 65A, No. 2 February 1987, 59–68, ISSN 0039-2553

Taheri F. & Shahin V & Widiarsa I. (2002), On the parameters influencing the performance of reinforced concrete beams strengthened with FRP plates, Catalogo Elsevier (Composites Structures), n°58, pp.217-226.

Takeo K., Matsushita H., Makizumi T., Nagashima G. (1997). Bond characteristics of CFRP sheets in the CFRP bonding technique, *Proc. of Japan Concrete Institute*, Vol. 19, No. 2., pp. 1599–1604.

Taljsten, B. (1994). Plate bonding: Strengthening of existing concrete structures with epoxy bonded plates of steel or fibre reinforced plastics, *Doctoral thesis*, Lulea, University of Technology, Sweden.

Taljsten B. (1996). Strengthening of concrete prisms using the plate bonding technique, *International Journal of Fracture*, Vol. 82, No., 253–266, ISSN 0376-9429

Taljsten B. (1997). Strengthening of beams by plate bonding, *ASCE Journal of Materials in Civil Engineering*, Vol. 9, No. 4, November 1997, 206–211, ISSN 1943-5533

Teng J. G., Smith S. T., Yao J., and Chen J. F. (2001). Intermediate Crack Induced Debonding in RC Beams and Slabs. *Construction and Building Materials, V. 17, No. 6-7, pp. 447-462*

Teng J.G., Chen J.F., Smith S.T. & Lam L. (2002). *FRP Strengthened RC Structures*, John Wiley & Sons Ltd., ISBN 0-471-48706-6, 245pp. Chichester (UK)

Teng J. G., Smith S. T., Yao J. & Chen J. F. (2003). Intermediate crack-induced debonding in RC beams and slabs, *Construction and Building Materials*, Vol. 17, No. 6-7, September-October 2003, 447-462, ISSN 0950-0618

Teng, J. G.; Lu, X. Z.; Ye, L. P.; and Jiang, J. J., 2004, "Recent Research on Intermediate Crack Induced Debonding in FRP Strengthened Beams," *Proceedings of the 4th International Conference on Advanced Composite Materials for Bridges and Structures*, Calgary, AB, Canada.

Teng, J.G., and Yao J. 2007. Plate end debonding in FRP plated RC beams-II: strength model. Structural Engineering, Elsevier, in-press.

Tounsi A., Hassaine Daouadji T., Benyoucef S., Addabedia E.A. (2009). Interfacial stresses in FRP-plated RC beams: Effect of adherend shear deformations, *International Journal of Adhesion & Adhesives – Elsevier,* Vol. 29, No. 4, June, 2009, 343-351, ISSN 0143-7496

Travassos N., Ripper T., Appleton J. (2005). Bond stresses characterization on CFRP-RC interfaces, *Proc. of 3rd Int. Conference Composites in Construction*, CCC2005, Lyon, France, July.

Triantafillou T., Plevris N. (1992). Strengthening of RC beams with epoxy-bonded FRP composite materials, *Materials and Structures*, 25, 1992, pp. 201-211;

Triantafillou T.C. (1998), *Composites: A new possibility for the shear strengthening of concrete, masonry and wood*, Composites science and technology, vol. 58, no. 8, September 1998, pp. 1285-1295

Triantafillou T., Matthys S. & Taerwe L. (2001). Design of Concrete Members Strengthened with Externally Bonded FRP Reinforcement, *Proceedings of the Conference FRPRCS-5*, Cambridge (UK), 157-166, ISBN 0727730290, Publisher, City

Tumialan, G, Belarbi, A, Nanni, A. (1999). Reinforced concrete beams strengthened with CFRP composites: failure due to concrete cover delamination, Department of Civil Engineering, Center for Infrastructure Engineering Studies, Report No. CIES-99y01, University of Missouri-Rolla, USA, 1999.

Ueda T., Sato Y., Asano, Y. (1999). Experimental study on bond strength of continuous carbon fiber sheet, *Proc. of 4th Int. Symposium on Fiber Reinforced Polymer reinforcement for Reinforced Concrete Structure*, pp. 407–16.

Ueda T. and Dai J. (2005). Interface Bond between FRP Sheets and Concrete Substrates: properties, numerical modeling and roles in member behavior. *Progress in Structural Engineering and Materials, John Wiley & Sons, Ltd., 7(1), 27-43.*

Varastehpour, H., and Hamelin, P. (1996). "Analysis and study of failure mechanism of RC beam strengthened with FRP plate." *Proc., 2nd Int. Conf. on Advanced Composites Materials in Bridges and Structures*, Canada, 527–536.

Varastehpour H, Hamelin P. (1997) Strengthening of concrete beams using fiber-reinforced plastics. Mater Struct 1997;30:160 –6.

Velazquez-Dimas J.I., Ehsani M.R. and Saadatmanesh H. (2000), *Out-of-plane behavior of brick masonry walls strengthened with fiber composites*, ACI Structural Journal, Vol. 97, no. 3, May- June 2000, pp. 377-387

Wang, CY, Ling, FS. (1998). Prediction model for the debonding failure of cracked RC beams with externally bonded FRP sheets, in: Saadatmanesh H, Ehsani MR. (Eds.), Proceedings of the Second International Conference of Composites in Infrastructure (ICCI 98), Arizona, USA, 1998, pp. 548–562.

Wu Z.S., Yuan H., Yoshizawa H., Kanakubo T. (2001), Experimental/analytical study on interfacial fracture energy and fracture propagation along FRP-concrete interface, *ACI International SP-201-8*, pp. 133–52.

Wu, Z., Yuan, H., Niu, H. (2002). Stress transfer and fracture propagation in different kinds of adhesive joints, *ASCE Journal of Engineering Mechanics*, Vol. 128, No. 5, May 2002, 562-573, ISSN: 0733-9399

Wu Z., Niu H. (2007) Prediction of Crack-Induced Debonding Failure in R/C Structures Flexurally Strengthened with Externally Bonded FRP Composite, *JSCE Journal of Materials, Concrete Structures and Pavements*, 63, 4 , 2007, pp. 620-639.

www.reluis.it "ReLUIS-Italian Civil Protection research program"

Yao J., Teng J.G., Chen J.F. (2005). Experimental study on FRP-to-concrete bonded joints, *Composites: Part B*, Elsevier, Vol. 36, No. 2, March, 2005, 99–113, ISSN 1359-8368

Yuan H., Chen J.F., Teng J.G., Lu X.Z. (2007). Interfacial stress analysis of a thin plate bonded to a rigid substrate and subjected to inclined loading, *International Journal of Solids and Structures*, Vol. 44, No. 16, August 2007, ISSN 0020-7683

Zarnic R., Gostic S., Bosiljkov V., Bokan-Bosiljkov V. (1999), Improvement of bending load-bearing capacity by externally bonded plates, Proceedings of Creating with Concrete, London, Telford, 1999.

Zhao H.D., Zhang Y., Zhao M. (2000). Research on the bond performance between CFRP plate and concrete, *Proc. of 1st Conf. on FRP Concrete Structures of China*, pp. 247–53.

Zhao, L. (2005). "Characterizations of RC beams strengthened with carbon fiber sheets." Graduation thesis, Dept. of Civil and Environmental Engineering, Univ. of Alabama in Huntsville, Huntsville, Ala.

Ziraba YN, Baluch MH, Basunbul IA, Sharif AM, Azad AK, Al-Sulaimani GJ. (1994). Guidelines towards the design of reinforced concrete beams with external plates. ACI Struct J 1994;91(6):639 –46.